VNIVERSITAT DE VALÈNCIA

FACULTAD DE MEDICINA Y ODONTOLOGÍA

DEPARTAMENTO DE FISIOLOGÍA

PROGRAMA DE DOCTORADO EN FISIOLOGÍA

DEVELOPMENT OF AN ULTRASOUND-BASED MUSCLE TEXTURE ANALYSIS AS A POTENTIAL IMAGING BIOMARKER FOR FRAILTY PHENOTYPE

Tesis doctoral presentada por:

REBECA MIRÓN MOMBIELA

Y dirigida por:

CONSUELO BORRÁS BLASCO

JUANA FORNER GINER

OCTUBRE, 2018

VNIVERSITAT DE VALÈNCIA
Facultat de Medicina i Odontologia
Departamento de Fisiología

INFORME DIRECTORAS PARA EL DEPOSITO DE TESIS

Dña. Consuelo Borrás Blasco, Catedrática/Profesor Titular del Dpto. de Fisiología de la Universitat de València. Correo electrónico: consuelo.borras@uv.es y **Dña. Juan Forner Giner**, Médico Adjunto de Ecografía del Servicio de Radiodiagnóstico del Consorcio Hospital General Universitario de Valencia. Correo electrónico: fornerjuana@hotmail.com directoras, de la tesis doctoral de **Dña. Rebeca Mirón Mombiela**, titulada "***Development of an ultrasound-based muscle texture analysis as a potential imaging biomarker for frailty phenotype*** ", emiten informe **favorable** para la realización del depósito y la defensa de la tesis y dan su visto bueno a la propuesta de expertos presentada.

Fecha 8 de octubre, 2018

Fdo.: Consuelo Borrás Blasco Fdo.: Juana Forner Giner

Director Directora

Ratificación del tutor/a con su firma:

Fdo.: Consuelo Borrás Blasco

Tutora

FOR MY BELOVED FATHER

ACKNOWLEDGEMENTS

Among the medical fields, imaging stands out for the impact and breadth of its discoveries and new technologies over the past decades. Today, there are major opportunities for innovation in health care, and in particular to radiology. However, while inspiration may be the product of a single mind, development and implementation of ideas require more than a single person to achieve it. Thus, I believe that for true innovation to be achieved, it depends more upon the organizational characteristics than it does on individual conception. I am fortunate to be a part of a research team with such characteristics, a team with a culture for innovation. I will now show my gratitude to these individuals.

To Consuelo Borrás, you have not only been my director of this work, but a true friend. I still remember when I entered the physiology department, five years ago, and you accepted to be my tutor, even when it meant going into uncharted territory. You were not afraid to explore new opportunities and allow me to develop into a better researcher and academic. You always knew how to guide me and give me the best advice. You helped me adhere to my goals, prioritize the work at hand, were always respectful and supportive of my decision-making process and always kept thoughtful communication with me thoughtful communication with me. You have been a true leader that continues to foster the conditions for an innovative field of research.

To Joaquin Barnoya, thank you for giving me the opportunity to be part of a large research group, for involving me in your work, for helping me develop my critical thinking skills, and for teaching me the basics of biomedical research. To this date, the skills you taught allow me to continue my research on my own.

To Silvia Ruiz and David Moratal, for taking a chance with my ideas, for allowing me to be part of your research group, and for always providing me with all the necessary help to carry out this work. The diversity of expertise and the effective interpersonal relations that both of you uphold, allow this to work to be easily executed. Without you, we would not have been able to import and exploit the external knowledge from my previous work and achieve this final work today.

To Jelena Vucetic, I do not have words to thank you ... you know that I would not be writing this if it were not for you. Thank you for working side by side with me for so many late afternoons and weekends, for your words of encouragement when I was down or tired, and above all, for always being there. Thank you.

To Jenny Cárdenas, for showing great interest in this work, for opening yourself to the world of research, for your constant words of encouragement and love, and always showing me the great person you are. If I am a better teacher and investigator today, is because you helped me achieve it.

To Fernando Facal, you are an example to me, both personally and professionally. It is difficult to reach where you have arrived with your humility and openness that I admire so much. Thank you for introducing me to musculoskeletal radiology, for trusting in me, despite my limited training, and for showing me that I can always count on you, as a boss and as a friend.

To Paloma Monllor, for helping me understand the amazing world of statistics, for being such a wonderful colleague during our time together in the Physiology Department, for coming to my aid whenever I needed it, and for being a constant support for me.

To my family, who have always supported me unconditionally. You have encouraged me with your love and I am very proud of having the family that I have; everything is easier with you by my side. Thank you.

To my mother, who showed me the power of passion and perseverance, and the true meaning of grit. For always being my role model of a woman and my inspiration.

I have left for the end the true architect of all this work: to my husband, for always pushing me to do better and be better.

RESUMEN TESIS DOCTORAL

INTRODUCCIÓN

En las últimas décadas, los investigadores de geriatría y gerontología han dedicado una cantidad creciente de esfuerzos en el intento de diseñar, desarrollar e implementar intervenciones preventivas contra la fragilidad, una condición de pérdida funcional asociada con la edad. El cumplimiento de dicha tarea se ha visto obstaculizada por la falta de una definición operativa estandarizada y universalmente aceptada por la comunidad médica. Estas ambigüedades de definición también se reflejan en la ausencia de biomarcadores confiables que podrían utilizarse en entornos clínicos y de investigación para identificar la fragilidad, hacer un seguimiento de su progresión a lo largo del tiempo y monitorizar su respuesta a las intervenciones. La fragilidad, con sus consecuencias económicas y de salud, así como sus dificultades de diagnóstico, confirma que existe una necesidad urgente de medidas multidisciplinarias para superar este desafío de salud. Existe la necesidad de una metodología que pueda usarse en muchas poblaciones para superar este desafío de salud y optimizar la atención al paciente. Creemos que las técnicas de imagen modernas tienen un alto potencial para ayudar a llenar este vacío y facilitar el su tamizaje y diagnóstico.

El ultrasonido es capaz de identificar cambios estructurales en el músculo causados por la degeneración muscular, específicamente el aumento del tejido conjuntivo adiposo e intramuscular, lo que resulta en un aumento en la ecointensidad del músculo evaluado. Varios estudios han demostrado la asociación negativa entre la ecointensidad, la fuerza muscular y/o la función física en los ancianos. Un estudio ha podido confirmar las relaciones publicadas anteriormente, así como encontrar una relación de mediciones de la ecointensidad basada en el estado de fragilidad, lo que demuestra que los valores de ecointensidad son más altos en individuos frágiles y pre-frágiles. Debido a que la ecointensidad determinada por el ultrasonido se puede usar para evaluar objetivamente la calidad muscular y es relativamente barata, es un candidato atractivo para explorar más a fondo como biomarcador de la fragilidad. Si los estudios demuestran exactitud, reproducibilidad, discriminación y valor predictivo, la intensidad del eco podría convertirse en una herramienta útil en el diagnóstico de fragilidad.

Las herramientas habituales para evaluar la fragilidad muestran, entre otras características, una baja sensibilidad y un bajo valor predictivo positivo. Se han identificado muchos biomarcadores

de fragilidad, pero pocos de ellos se han evaluado como marcadores clínicos y, además, hay resultados controvertidos. Teniendo en cuenta estas consideraciones, se necesita un cambio de paradigma, pasando de la búsqueda de biomarcadores únicos al desarrollo de modelos multivariados/multidimensionales de biomarcadores complementarios. La inspección única o aislada de variables puede dar como resultado una imagen parcial o incorrecta. Por otro lado, principalmente a través de la implementación de disciplinas "ómicas", los análisis multivariados han ido adquiriendo un papel cada vez más relevante en la práctica clínica y pueden extenderse fácilmente para la búsqueda de biomarcadores de fragilidad, incluidos los biomarcadores cuantitativos de imagen y la radiómica.

Los biomarcadores cuantitativos de imágenes se validan mediante la demostración de una asociación entre el valor medido del biomarcador y una respuesta fisiológica, fisiopatológica o terapéutica. Las imágenes médicas han hecho esto posible, porque refleja de alguna manera el sustrato molecular del tejido, órgano o persona sana o enferma que atraviesa las imágenes. Los estudios previos sobre biomarcadores de imagen cuantitativa en ultrasonido muscular han establecido cambios con la edad y su correlación con la fuerza y los parámetros funcionales, como la fragilidad. Lo que hace que la imagen de ultrasonido sea un candidato a biomarcador cuantitativo de la fragilidad.

Por ello, en este estudio prospectivo-retrospectivo, nos preguntamos si es posible identificar y desarrollar biomarcadores cuantitativos a partir de imágenes de ultrasonido muscular para la identificación de sujetos con riesgo de fragilidad o frágiles, utilizando el análisis de textura de ecointensidad con ayuda del aprendizaje automático (machine learning, en inglés) como enfoque experimental para responder a esta pregunta.

OBJETIVOS

1. *Objectivo general:*

El objetivo general es identificar posibles biomarcadores cuantitativos a partir de imágenes de ultrasonido muscular para la identificación de sujetos con riesgo de fragilidad (pre-frágiles) o frágiles con la ayuda del análisis de textura de aprendizaje automático.

2. *Objetivos específicos:*

[Objetivo 1] Identificar y priorizar los biomarcadores de imágenes cuantitativas potencialmente útiles.

[Objetivo 2] Desarrollar biomarcadores de imágenes cuantitativas simples, reproducibles y rentables en el contexto clínico del fenotipo de fragilidad.

[Objetivo 3] Estimar el rendimiento de biomarcadores cuantitativos clínicos de imagen y evaluar su capacidad para distinguir a los sujetos con fragilidad (pre-frágiles y frágiles) de los sujetos que no son frágiles.

[Objetivo 4] Evaluar las propiedades intrínsecas (por ejemplo, precisión, repetibilidad, sensibilidad y especificidad) en sus características específicas (por ejemplo, mecanismos, procesos, parámetros) de cada biomarcador cuantitativo de imágenes desarrollado e impulsar su potencial de implementación en la detección, evaluación de referencia y / o definición de resultados.

[Objetivo 5] Determinar las aplicaciones clínicas de biomarcadores cuantitativos de imágenes para resultados secundarios (morbilidad y mortalidad) y otras covariables de interés (datos demográficos, antropométricos, función física y factores de riesgo, frecuencia de hospitalización, consultas de atención primaria y consultas a urgencias).

METODOLOGÍA

Sujetos del Estudio

El estudio se realizó en seres humanos y se adhirió a los principios de bioética incluidos en la Declaración de Helsinki y la legislación española pertinente. Se obtuvo la aprobación del comité de investigación y del comité de ética de investigación clínica del Consorcio Hospital General Universitario de Valencia (CHGUV). Todos los participantes fueron informados de los procedimientos experimentales y el propósito del estudio. Cada paciente dio su consentimiento informado por escrito antes de ingresar al estudio.

Los **criterios de inclusión** fueron los siguientes:

- Para el grupo experimental: personas mayores de 60 años o más, capaces de caminar de forma independiente, incluida la ayuda de un bastón, un caminador o un dispositivo de asistencia similar. Hombres y mujeres fueron incluidos por igual.
- Además, se reclutaron hombres y mujeres, de entre 20 y 59 años de edad, para el grupo de control, dado que existe un pico de desarrollo muscular dentro de este grupo de edad, medido por el grosor del músculo por ultrasonido.

Los **criterios de exclusión** fueron los siguientes:

- Pacientes con trastornos neuromusculares, enfermedades agudas o crónicas que evitan la medición de la fuerza con un dinamómetro o alteran la arquitectura muscular.
- Pacientes oncológicos sometidos a quimioterapia o radioterapia en el momento de la exploración. Se incluyeron pacientes con cáncer previo, estables o curados.
- Pacientes institucionalizados o que no puedan ir al centro de investigación utilizando sus propios medios de transporte.
- Demencia grave que impide o influye en la capacidad del paciente para comprender el consentimiento informado y/o el cuestionario del estudio.

Se invitó a participar a pacientes referidos de atención primaria, que asistieron consecutivamente a una cita de ultrasonido en la Sección de ecografías del Departamento de radiología del CHGUV. Ciento cuarenta y dos pacientes fueron invitados al estudio y 121 aceptaron participar. De ellos, solo 112 individuos cumplieron todos los criterios de inclusión y ningún criterio de exclusión. Mediciones de ultrasonido cegadas, evaluación de fragilidad y cuestionario de calidad de vida se realizaron en todos los 112 de ellos. Once sujetos de control se excluyeron del análisis estadístico debido a que la evaluación de fragilidad y / o las imágenes de ultrasonido los clasificaron como frágiles, dejando 101 participantes para este estudio. Durante el período de seguimiento, determinamos que estos individuos tenían enfermedades asociadas que probablemente alteraron su estructura muscular y su intensidad de eco, o síntomas secundarios que dieron lugar a criterios de fragilidad positivos, que no conocían al momento del examen de ultrasonido. Entre las enfermedades asociadas, hubo hepatopatía severa, obesidad, depresión, enfermedad pulmonar obstructiva crónica, artritis reumatoide, polimiositis y cardiopatía con hiperlipidemia.

Diseño del Estudio

Este fue un estudio experimental de corte transversal que se realizó en un entorno de consulta externa. Los pacientes fueron remitidos de atención primaria desde el 1 de noviembre de 2014 hasta el 28 de febrero de 2015. Las comorbilidades iniciales se evaluaron después del examen de ultrasonido, y hubo un seguimiento de los pacientes para otras comorbilidades o muerte hasta por dos años (hasta el 31 de marzo de 2017).

El proyecto se desarrolló en el Departamento de Radiología del “Consorcio Hospital General Universitario de Valencia”, donde se realizó la ecografía muscular. Al final de la adquisición de las imágenes de ultrasonido, se realizó una medición de la fuerza muscular con un dinamómetro

y se completó un cuestionario electrónico con los datos epidemiológicos, los criterios del fenotipo de fragilidad y calidad de vida de los adultos mayores. Los sujetos de 60 años o más participaron en el grupo experimental. Este grupo fue subdividido de acuerdo al fenotipo de fragilidad. El fenotipo de fragilidad consiste en la acumulación de déficits en cinco dominios: pérdida de peso involuntaria, mayor cansancio o agotamiento, baja actividad física, velocidad lenta para caminar y debilidad muscular. Los pacientes se dividieron en robustos, prefrágiles o frágiles según sus respuestas a las tres preguntas, la velocidad de la marcha y la fuerza medida por un dinamómetro de mano digital. También incluimos un grupo control con sujetos de 20 a 59 años de edad.

La comorbilidad de cada sujeto, factores de riesgo y número de visitas a atención primaria, servicio de urgencias y hospitalizaciones en el momento de la evaluación con ultrasonido, se obtuvieron de su historial médico electrónico y se registraron en la base de datos. Dos años después de la ecografía inicial, este proceso se repitió para determinar si desarrollaron nuevas comorbilidades y si estaban vivos o muertos.

A esto le siguió el post-procesado de las imágenes bidimensionales de ultrasonido con el análisis de textura de 43 características. El análisis de textura proporciona una evaluación objetiva y cuantitativa de la heterogeneidad muscular mediante el análisis de la distribución y la relación de los niveles de píxeles grises en la imagen. Los valores de ecointensidad se obtuvieron utilizando el programa MatLab (R2017b; The MathWorks Inc., Natick, MA, EE. UU.). El análisis de la textura se realizó en la región muscular de interés seleccionada (*cuádriceps muscular*). Se utilizaron métodos estadísticos para extraer las características predeterminadas y se desarrollaron modelos predictivos para determinar las mejores características para el diagnóstico de fragilidad con la ayuda de la tecnología de aprendizaje automático (Machine learning, en inglés), una rama de la inteligencia artificial.

En el análisis de textura, el poder discriminativo del modelo predictivo depende de tener suficientes datos. El análisis de textura se puede realizar con tan solo 100 pacientes. Nuestra muestra de estudio fue calculada para cumplir con este criterio. No se realizaron otros cálculos de la muestra.

Métodos de medición

1. Ecografía muscular y sus mediciones

El grosor de los tejidos del compartimento anterior del muslo se midió mediante ecografía (Modelo LOGIC S7 Expert, General Electric, EE. UU.) en el modo B, obteniendo imágenes transversales con un transductor lineal de 6-15Hz. Durante la exploración del paciente, la ganancia se mantuvo constante en 54dB y la frecuencia en 12Hz. Esta es la ganancia y la frecuencia de elección para los estudios musculares, que proporcionan una buena resolución de la estructura muscular en la imagen. Ambos parámetros no se modificaron entre los pacientes ni durante la exploración de los pacientes. LA zona focal es el parámetro que le dice al ultrasonido la profundidad a la que desea la resolución más alta. La zona focal generalmente se ubica en o justo debajo del objeto que está evaluando, en este estudio se ajustó a la profundidad del recto femoral de cada paciente.

El procedimiento se realizó con el paciente en posición supina, con las piernas extendidas y relajadas. Se exploró el compartimento anterior del muslo derecho (elegido arbitrariamente para la exploración) aplicando suficiente gel y evitando la presión excesiva durante las mediciones, evitando así la interferencia con el grosor real del músculo evaluado. El sitio medido fue el punto medio entre el borde superior de la rótula y la espina ilíaca anterosuperior, con el transductor colocado perpendicular al eje longitudinal del cuádriceps femoral. En esta posición, las imágenes se congelaron y se midió el grosor muscular y el grosor del tejido adiposo subcutáneo. El grosor muscular correspondió a la suma del grosor del *rectus femoris* y el músculo *vastos intermedius*; mientras que el tejido adiposo subcutáneo correspondió a la distancia entre la fascia del recto femoral y la dermis. Se obtuvieron tres mediciones para cada paciente y se utilizó el promedio en el análisis de los datos. Para evaluar la fiabilidad de las mediciones de la persona que escanea a los pacientes, se evaluaron los coeficientes de correlación intraclase (ICC) para determinar el grosor muscular y el tejido adiposo subcutáneo. Los valores ICC fueron 0,969 (95% CI: 0,957-0,992) para el grosor muscular y 0,992 (95% CI: 0,984-0,998) para el tejido adiposo subcutáneo.

Las imágenes realizadas durante la exploración con ultrasonido se almacenaron en el Sistema de comunicación y archivo de imágenes (PACS, por sus siglas en inglés) del hospital. Cada examen de ultrasonido muscular consistió en siete imágenes. Había tres imágenes transversales que correspondían a las medidas, como ya se ha descrito. También adquirimos tres imágenes transversales más y una imagen longitudinal, para realizar un análisis de la textura de la intensidad del eco de una ROI seleccionada en el músculo. Un único investigador

con una experiencia de un año en ecografía realizó las mediciones de ultrasonido y que estaba cegado al estado de fragilidad de los pacientes.

Al final de cada exploración, se escribió un informe radiológico y se guardó en el historial médico de cada paciente.

2. Datos epidemiológicos y antropométricos

La primera sección del cuestionario electrónico incluyo preguntas sobre información epidemiológica general (fecha de nacimiento, edad, sexo, etc). El peso y la altura de los sujetos se midieron para calcular el índice de masa corporal (IMC). El peso se determinó después de la exploración con ultrasonido en la misma cabina, indicando a los sujetos que pisaran la báscula descalzos. El peso fue medido en kilogramos. Se colocó un talímetro de pared en la cabina de ultrasonidos para medir todos los sujetos. La altura se midió primero colocando a los sujetos correctamente. Explicamos a los sujetos que se pararan con los pies juntos, descalzos y con la espalda contra la pared. Se usó una regla para la medición y se bajó hasta que toco la cabeza. Registramos entonces la altura. El IMC se calculó dividiendo el peso del paciente (en kilogramos) por la altura (en metros) al cuadrado (IMC = peso/altura^2).

3. Criterios fenotipo de fragilidad

La segunda sección del cuestionario electrónico del paciente fueron los criterios para la evaluación del fenotipo de fragilidad. Se utilizaron los criterios propuestos por Linda Fried y sus colaboradores en el año 2001. Esto incluye pérdida de peso involuntaria, sensación de agotamiento general, bajo nivel de actividad física, velocidad lenta para la marcha y debilidad muscular. Se asignó un punto a cada criterio positivo, construyendo una puntuación final formada por la suma de los cinco criterios. Según este puntaje, los sujetos fueron clasificados de la siguiente manera:

- Robusto: 0 puntos.
- Pre-frágil: 1 o 2 puntos.
- Frágil: 3 o más puntos

4. Evaluación de la calidad de vida de las personas mayores

La evaluación de la calidad de vida se basó en el uso del cuestionario genérico para ancianos, conocido como OPQOL-35 (Calidad de vida de las personas mayores). El cuestionario consistió en 35 preguntas que evaluaron ocho dominios: vida en general (4 ítems), salud (4 ítems), relaciones y participación social (5 ítems), independencia, control sobre sus vidas y

libertad (4 ítems), hogar y comunidad (4 ítems), estado emocional y psicológico (4 ítems), circunstancias financieras (4 ítems) y actividades recreativas y religión (6 ítems). Se utilizó una escala de Likert para cada pregunta, el valor mínimo del cuestionario es 35 (malo, no puede ser peor) y un máximo de 175 (bueno, no puede ser mejor). El cuestionario fue traducido del inglés al español por la doctoranda.

5. Historia clínica del paciente, comorbilidades y mortalidad

De la historia clínica electrónica de cada paciente se extrajo la siguiente información. La presencia o ausencia de hipertensión, hiperlipidemia, diabetes mellitus, enfermedad pulmonar obstructiva crónica, discapacidad auditiva o visual desarrollada en los últimos 6 meses, enfermedad de Parkinson, accidente cerebrovascular previo, insuficiencia cardíaca congestiva, enfermedad cardíaca (que no es insuficiencia cardíaca ni infarto de miocardio), infarto de miocardio, insuficiencia renal de moderada a grave, cáncer previo, artritis/osteoartritis, síndrome de ansiedad, depresión, fracturas previas/osteoporosis, enfermedad hepática o hepatopatía, demencia/pérdida de memoria, enfermedad del tejido conectivo, hemiplejia, neoplasia leucemia, linfoma maligno, metástasis sólida, síndrome de inmunodeficiencia adquirida y enfermedad vascular periférica. También buscamos factores de riesgo, como fumar, consumir alcohol, caídas y obesidad. Además, se calculó un índice de comorbilidades de acuerdo con el índice de comorbilidad de Charlson (CCI). Por último, registramos el número de visitas a la atención primaria, al servicio de urgencias y el número de ingresos hospitalarios en los últimos 6 meses.

Dos años después del examen de ultrasonido, revisamos nuevamente los registros médicos del sujeto e hicimos un seguimiento de las mismas variables descritas anteriormente. También determinamos si el paciente estaba vivo o muerto y lo grabamos. Se registró la fecha del último contacto dentro de la red del hospital o la fecha de la muerte.

6. Proceso para el análisis de texturas

El análisis de textura puede proporcionar una evaluación cuantitativa y objetiva del fenotipo de fragilidad al analizar la distribución y la relación entre los niveles de gris de las imágenes de ultrasonido. La aplicación implica un proceso que consta de seis pasos: adquisición de imagen, segmentación de la región de interés, pre-procesamiento de la región de interés, extracción de características, selección de características y clasificación. El resultado de la textura puede verse considerablemente afectado según la metodología utilizada en todo el proceso; En las siguientes secciones, describiremos el proceso en detalle.

6.1 Datos de la imagen por ultrasonido

Se realizó un análisis de adquisición posterior a la imagen. Las imágenes DICOM (Digital Imaging and Communications in Medicine, en inglés) de la ecografía muscular se descargaron del PACS del hospital y se guardaron en la computadora portátil de la doctoranda. El protocolo de ultrasonido para la adquisición de imágenes se ha descrito en una sección anterior (Ecografía muscular y sus mediciones).

6.2 Segmentación de la Región de Interés

Las imágenes de ultrasonido del *rectus femoris* y *vastus intermedius* se segmentaron en 2D utilizando una herramienta de software desarrollada en MATLAB (R2017b; The MathWorks Inc., Natick, MA, EE. UU.) específicamente para este estudio. El software carga las siete imágenes correspondientes a un tema en formato DICOM. Antes de seleccionar la región de interés, se seleccionó el plano de exploración (axial o sagital), el músculo (recto femoral o vasto intermedio) y el grupo de pacientes (control, robusto, pre-frágil y frágil).

El proceso de segmentación fue realizado por la doctoranda. Cada región de interés del músculo se segmentó manualmente a partir de las imágenes axial y sagital de ambos músculos. La región de interés segmentada excluyo el hueso, el tejido adiposo y la fascia muscular. Todas las regiones de interés se midieron para determinar su área en milímetros cuadrados (mm2) y determinar si el tamaño era consistente entre los cuatro grupos (frágil, prefrágil, robusto y de control). Dado que los sujetos robustos y controles comparten características similares, se analizaron como un solo grupo. Lo mismo se hizo para los sujetos pre-frágiles y frágiles. Se usó la prueba de Wilcoxon Rank para determinar el valor p entre los grupos. Esto es importante porque grandes diferencias entre los tamaños de las regiones de interés de los grupos pueden influir en el análisis de la textura. Pudimos determinar que los tamaños de las regiones de interés eran consistentes entre los grupos para continuar con el siguiente paso del análisis de textura.

6.3 Pre-procesado de la región de interés

Se han propuesto varias técnicas de pre-procesamiento para minimizar los efectos de los protocolos de adquisición. El propósito principal de estas técnicas de pre-procesamiento es poner todas las regiones de interés en la misma condición, por lo que las características extraídas de ellas representan esencialmente la textura que se está examinando y mejoran la discriminación. El pre-procesamiento de imagen aplicado depende de la

modalidad de imagen utilizada. Por lo general, incluye la interpolación, la normalización y la reducción de los niveles de gris.

Se ha informado que la resolución de la imagen es un factor influyente para la discriminación del análisis de textura. La resolución en imágenes de ultrasonido se ve afectada por varios factores (ganancia, frecuencia, enfoque, etc.) antes de que se almacene la imagen final. Estos parámetros se modifican en el momento del escaneo, con el objetivo de mejorar la resolución de la imagen. La información de resolución espacial se extrajo del encabezado del archivo DICOM. Las imágenes de ultrasonido utilizadas en este estudio tuvieron resoluciones entre $0.07x0.07mm^2$ y $0.16x0.16mm^2$ con 256 niveles de gris. En base a estos datos determinamos que la resolución de las imágenes era aceptable para la extracción y el análisis de características. Por lo tanto, la interpolación de las imágenes no fue necesaria.

También concluimos que la reducción del nivel de gris no era necesaria para las imágenes de ultrasonido. Las imágenes de ultrasonido tienen 256 niveles de gris. Esto es principalmente necesario en la resonancia magnética, ya que hay entre 1024 y 4096 niveles de gris. Sin embargo, antes del cálculo de las características de textura, el rango de intensidad de la región de interés se cuantificó de 256 niveles de gris a un número menor de niveles de gris (16, 32, 64 y 128) porque esto mejora la relación señal/ruido. Todos los cálculos se realizaron con estos cuatro niveles de gris. El propósito fue determinar si algún nivel de gris supera al otro, ya que no hay literatura publicada sobre análisis de textura de ultrasonido en este tema.

6.4 Extracción de características

La extracción de características implica el cálculo de las características de textura a partir de las regiones de interés de los músculos predefinidas. Para extraer características, utilizamos la caja de herramientas MATLAB Radiomics implementada por Vallières y colegas. La caja de herramientas utiliza métodos estadísticos para la extracción de 43 características de textura para el análisis de texturas. Se extrajeron tres características del histograma de intensidad (estadísticas de primer orden) y las otras 40 se extrajeron de métodos estadísticos de segundo orden incluyendo: matriz de co-ocurrencia de niveles de gris (GLCM, por sus siglas en inglés) se derivaron 9 características, matriz de secuencias de niveles de grises (GLRLM, por sus siglas en inglés) 13, matriz por zona de tamaño de

niveles de gris (GLSZM, por sus siglas en inglés) 13, y de la matriz de diferencia de tonos de gris según su vecindario (NGTDM, por sus siglas en inglés) solo 5.

6.5 Selección y clasificación de las características del análisis de texturas

Se estudiaron seis modelos predictivos diferentes para evaluar el poder de discriminación de las características de textura 2D: clasificador Bayes (NB), vecinos más cercanos a k (k-NN), perceptrón multicapa (MLP), bosques aleatorios (RF), máquina de vectores de soporte con Kernel lineal (SVM_L) y kernel radial (SVM_R). Elegimos seis clasificadores comunes de diferentes familias predictivas para ver cuál de ellos proporciona la mejor precisión de clasificación y para verificar si hay diferencias notables entre el análisis de textura 2D que utiliza diferentes enfoques.

Se utilizó una estructura de validación cruzada (CV) anidada para evaluar el rendimiento de cada modelo sin mantener algunas de las muestras como un conjunto de prueba independiente. Utilizamos este enfoque porque el tamaño de la muestra de nuestro conjunto de datos es relativamente pequeño y, en esta situación, se recomienda utilizar cada muestra para la construcción del modelo. Se pueden lograr estimaciones adecuadas del rendimiento del modelo utilizando métodos de remuestreo cuando el número de muestras no es grande.

Leave-group-out CV (LGOCV) se aplicó en el bucle externo. Este método de remuestreo divide aleatoriamente el conjunto de datos en entrenamiento y prueba, y establece un total de N veces, formando N grupos. Cada grupo se examina de forma independiente: el conjunto de entrenamiento de un grupo se utiliza para construir el modelo y luego este modelo se evalúa utilizando el conjunto de pruebas del mismo grupo. Al final, se promedian los resultados de clasificación proporcionados por las estimaciones de todos los grupos. En este estudio, se eligió un valor de N = 100 grupos para obtener resultados con una varianza baja y, en consecuencia, para disminuir la incertidumbre de las estimaciones de rendimiento. En cada grupo, el 25% del conjunto de datos se seleccionó al azar como conjunto de pruebas y el 75% restante se utilizó como conjunto de entrenamiento. El rendimiento del modelo se evaluó utilizando el área bajo la curva de características operativas del receptor (ROC).

El paso de selección de características se calculó dentro del proceso de construcción del modelo utilizando el conjunto de capacitación de cada grupo. Este proceso se computó

como un paso independiente para evitar el sobreajuste. Los dos métodos se utilizaron para la selección de características, uno método de filtro y el otro método de ajuste. El método de selección de características de filtro basado en el valor p proporcionado por una prueba de rango con signo de Wilcoxon (P-ranking), se empleó para generar una clasificación de las características con el poder más discriminativo. Este método evalúa la importancia estadística de cada característica de forma independiente, sin analizar la relación entre las características y sin involucrar ningún modelo predictivo. El principal inconveniente de los métodos de filtro es que la selección de características se basa en la información intrínseca de los datos de entrenamiento y no considera la capacidad predictiva de un cierto subconjunto de características. Los métodos de envoltura aprovechan un algoritmo de clasificación y buscan el subconjunto de características que proporciona un rendimiento de clasificación óptimo. La eliminación de características recursivas (RFE), una envoltura, clasifica las características mediante el entrenamiento recursivo de un clasificador y la eliminación de la característica con la puntuación de clasificación más pequeña. En este exhaustivo método de búsqueda, se probaron posibles combinaciones de características y se seleccionan aquellas que producen la mejor discriminación. En este estudio, usamos la técnica de envoltura de selección de características conocida como máquina de vectores de eliminación de características recursivas (RFE-SVM).

El ajuste de parámetros se calculó utilizando el conjunto de entrenamiento de cada grupo realizando un bucle interno de CV de 10 veces. Este paso se realizó F = 43 veces en cada estimación de grupo: las características clasificadas proporcionadas por el paso de selección de características se agregaron progresivamente una por una, de la más importante a la menos importante, y luego se usó cada subconjunto de características para entrenar el modelo predictivo y calcular el AUC En las muestras de prueba del mismo grupo. Al final, se proporciona un total de F = 43 valores AUC en cada evaluación de grupo, uno por cada subconjunto de características. El número de vecinos (k) en k-NN se seleccionó de $k \in \{1, 3, 5, ..., 15\}$. El número de variables muestreadas aleatoriamente como candidatas en cada división (mtry) en RF se eligió de $mtry \in \{2, 4, 6, 8, 10, 12, 14\}$. El número de unidades en la capa oculta (l) de la MLP se seleccionó de $l \in \{3, 5, 7, ..., 15\}$. El parámetro de costo SVM (C) fue elegido de $C \in \{2\text{-}4,\ldots, 20,\ldots, 24\}$.

Este proceso de evaluación del modelo se implementó con el paquete Caret en la versión R 3.2.5 (R Core Development Team, Viena, Austria).

Análisis estadístico

Los datos descriptivos se presentan con la media ± desviación estándar con la distribución de los datos verificada por la prueba de normalidad de Kolmogorov-Smirnov. Para evaluar las diferencias en las características físicas y las variables del estudio según el sexo, se usó t-Student para variables paramétricas y Mann-Whitney para las variables no paramétricas. La evaluación de las diferentes variables del estudio según el fenotipo de fragilidad y el grupo control se determinó mediante ANOVA para las variables paramétricas (seguidas de la prueba post hoc de Bonferroni) y para la prueba no paramétrica de Kruskal-Wallis. Las correlaciones se realizaron para investigar la relación entre las características físicas, las mediciones de ultrasonido, la calidad de vida, el fenotipo de fragilidad, las comorbilidades, los factores de riesgo y las características de la textura. Utilizamos el coeficiente de Pearson (r) para datos paramétricos, el rango de Spearman para datos no paramétricos y Tau B de Kendal para las variables ordinales. Las correlaciones se consideraron débiles para el coeficiente de correlación de ± 0,01 a 0,35, moderadas para ± 0,36 a 0,67 y fuertes para ± 0,68 a 1,00. Para determinar la precisión de las características de las texturas de ecointensidad muscular, se evaluó el área bajo la curva ROC (acrónimo de Receiver Operating Characteristic). Se realizó un análisis de regresión múltiple en pasos con las características de textura de los mejores modelos predictivos de fragilidad, ajustados con las características de ultrasonido y las características físicas. Se aplicó un modelo logístico múltiple para las variables de morbilidad y mortalidad. Para comparar la confiabilidad de todas las características de las texturas de ecointensidad en ambos músculos y en ambos planos; realizamos el coeficiente de correlación intraclase (ICC) y los límites de concordancia del 95% de Bland-Altman. Los valores ICC se clasificaron como malos para valores ≤0,20, justos para 0,21-0,40, moderados para 0,41-0,60, buenos para 0,61-0,80 y muy buenos para 0,81- 1,00. La significación estadística se definió como $p < 0,05$. Aplicamos el método de descubrimiento falso de Benjamini & Hochberg ya que se realizaron comparaciones múltiples durante el estudio. Todos los análisis estadísticos, incluyeron el grupo de control, se realizaron con SPSS versión 24.0 para Windows (IBM SPSS, Inc., Chicago, IL).

RESULTADOS

La muestra estuvo compuesta por 101 pacientes, 46 eran mujeres y 55 hombres. La muestra del estudio es homogénea con respecto a la edad, el IMC, la velocidad de la marcha, la fuerza muscular y los valores de la calidad de vida según el sexo. Hay que tener en cuenta que el fenotipo de fragilidad también fue independiente del sexo en esta muestra; mientras que el

peso, la altura, el grosor tejido adiposo subcutáneo y el grosor muscular tuvieron diferencias estadísticamente significativas entre hombres y mujeres.

La muestra según fenotipo de fragilidad, esta compuesta de 24 controles, 22 pacientes robustos, 30 pre-frágiles y 25 frágiles. Los datos muestran que existen diferencias estadísticamente significativas entre la edad, la altura, el IMC, la velocidad de la marcha, el grosor muscular y la calidad de vida. El peso y el grosor del tejido adiposo subcutáneo se distribuyeron homogéneamente dentro de estos grupos. Además, el género se distribuyo homogéneamente entre los grupos.

Se determinó la frecuencia de comorbilidades en el momento en que se realizó la ecografía muscular y después de dos años de seguimiento. El análisis de las comorbilidades según el sexo mostró que la mayoría son homogéneas, a excepción de las fracturas/osteoporosis y caídas, que fueron más comunes en las mujeres. El consumo de alcohol fue más común en los hombres. El análisis de las comorbilidades según el fenotipo de fragilidad, muestra cómo la distribución cambia entre los grupos y aumenta en frecuencia durante el seguimiento. Entre las comorbilidades que fueron estadísticamente significativas según el fenotipo de fragilidad en el momento de la ecografía y el seguimiento están: hipertensión, hiperlipidemia, diabetes mellitus, deterioro visual, accidente cerebrovascular, enfermedad cardíaca, enfermedad renal, cáncer previo, artritis/osteoartritis, depresión, caídas, obesidad, índice de comorbilidad de Charlson, número de visitas a atención primaria, número de visitas al servicio de urgencias, hospitalizaciones y muerte.

Se analizó las 43 características de texturas de ecointensidad según sexo y fenotipo de fragilidad. Las características de la textura son diferentes según el fenotipo de fragilidad en ambos músculos (*rectus femoris* o *vastus Intermidius*) utilizados en este estudio. La mayoría de estas características también son independientes del sexo.

Utilizamos múltiples correlaciones de todas las variables en este estudio con el propósito de realizar minería de datos (data mining, en inglés), para un análisis más detallado y para extraer las características más relevantes para los próximos análisis. El fenotipo de fragilidad se correlacionó fuertemente con la edad (r = 0,696**) y la velocidad de la marcha (r = 0,764**); se correlaciona moderadamente con el grosor muscular (r = -0,528**); y débilmente a la altura (r = -0,321**), IMC (r = 0.264**), fuerza muscular (r = -0,213*) y calidad de vida (r = -0,261**). La edad se asoció moderadamente con la velocidad de la marcha (r = 0.613**) y el grosor muscular

(r = -0.556**); y hubo una asociación débil con la altura (r = -0,200*). No se encontró asociación entre la edad y la fuerza muscular, o la edad y la calidad de vida. La velocidad de la marcha tuvo una asociación moderada con el grosor muscular (r = -0,556**) y débil con la calidad de vida (r = -0,262**), pero no con la fuerza muscular.

El fenotipo de fragilidad tuvo correlaciones estadísticamente significativas con el desarrollo de accidente cerebrovascular (r = 0,250**), infarto de miocardio (r = 0,267**), índice de comorbilidad de Charlson (r = 0,306**), mayor número de visitas a atención primaria (r = 0,177*), y muerte (r = 0,370**) durante el seguimiento. Todas las correlaciones fueron débiles, excepto el fenotipo de fragilidad y la muerte, que fue moderada. La velocidad de la marcha y el grosor muscular tenían correlaciones similares a la del fenotipo de fragilidad. No encontramos asociaciones significativas para la fuerza muscular.

Las características del análisis de textura tenían correlaciones estadísticamente significativas con el fenotipo de fragilidad, la edad, la velocidad de la marcha y el grosor muscular. El peso, el IMC y el grosor de tejido adiposo subcutáneo tuvieron una asociación débil a moderada, pero solo fue significativo en algunos de los músculos o planos, sin ningún patrón claro. La fuerza muscular y la calidad de vida no tuvieron una correlación significativa con las características del análisis de textura.

Se encontraron asociaciones estadísticamente significativas entre las características de la textura y los resultados de comorbilidades. Esto incluye el desarrollo de deficiencia auditiva (35/43 características), accidente cerebrovascular (37/43 características), infarto de miocardio (37/43 características), demencia/pérdida de memoria (30/43 características), índice de comorbilidad de Charlson (30/43 características), caídas (29/43), aumento de visitas a atención primaria (25/43 características) y muerte (40/43 características). Todas estas asociaciones eran débiles. El resto de comorbilidades y variables clínicas de interés no mostraron asociaciones estadísticamente significativas con las características del análisis de textura.

Utilizamos el enfoque de aprendizaje automático (machine learning, en inglés) descrito en la sección de materiales y métodos para la selección y clasificación de las características de la textura. El rendimiento predictivo de los diferentes métodos de selección y clasificación de características se evaluó utilizando el área bajo la curva característica del operador (AUC). Se lograron mayores AUC con el método de P-ranking que con la máquina de vectores de eliminación de características recursivas (RFE-SVM) para el proceso de selección de

características. Para los métodos de clasificación, el perceptrón multicapa (MLP) y la máquina de vectores de soporte con núcleo lineal (SVM_L) tuvieron el mayor rendimiento predictivo.

Encontramos que los múltiples modelos predictivos desarrollados tenían buenas áreas bajo la curva para la identificación de sujetos con riesgo de fragilidad o debilidad. El análisis de regresión logística múltiple paso a paso de los mejores modelos demostró que los biomarcadores de imagen cuantitativa desarrollados clasificaron correctamente 70 a 87% de los casos, y explicaron entre 23% y 80% de la varianza en la identificación del fenotipo de fragilidad con los modelos predictivos de análisis de textura por sí solos. Además, estos modelos mejoran si el grosor de los músculos o la velocidad de la marcha se ingresan en los modelos predictivos. Al hacer esto se logró clasificar correctamente del 87% al 100% de los casos. Después del ajuste, los modelos predictivos fueron independientes de la edad, el sexo, el IMC, el tejido adiposo subcutáneo y la fuerza muscular. Los biomarcadores cuantitativos de imágenes también se asociaron con una mayor morbilidad y fueron altamente predictivos de muerte a los 2 años de seguimiento.

DISCUSIÓN

Estos resultados indican que es posible identificar sujetos con riesgo de fragilidad (pre-frágiles) o frágiles con la ayuda de modelos predictivos de análisis de textura, ayudados por el aprendizaje automático, como biomarcadores de imágenes cuantitativas obtenidos de imágenes de ultrasonido muscular. Creemos que la heterogeneidad de las características de la textura muscular capta la calidad muscular y/o la disfunción muscular de los sujetos. Estas características hacen que las imágenes de ultrasonido con la ayuda del análisis de textura de aprendizaje automático sean un buen biomarcador cuantitativo de imágenes.

En el núcleo de la descripción del fenotipo de fragilidad que Fried y sus colegas describieron, se encuentra la disfunción muscular. Probablemente esta sea la razón por la que encontramos una correlación entre el análisis de la textura del músculo cuádriceps y el fenotipo de fragilidad. El envejecimiento afecta en gran medida la calidad muscular, incluyendo la disminución de la función mitocondrial para la síntesis de proteínas, el aumento del estrés oxidativo, la activación neuromuscular alterada, la velocidad de contracción más lenta, la mayor infiltración de grasa y la transformación fibrótica de los tejidos. Esto es particularmente importante cuando se considera que el músculo esquelético es el segundo depósito más grande de energía en el cuerpo. Estas alteraciones en la célula muscular y el entorno celular se traducen en una arquitectura muscular anormal, explicando en parte por qué las características de la textura de

la ecointensidad tienen una mayor heterogeneidad del músculo en sujetos frágiles y en riesgo de fragilidad o prefrágiles.

El vínculo entre la disfunción musculoesquelética y el aumento de morbilidad/mortalidad implica que un vínculo importante entre los dos y el posible uso de la calidad muscular en las imágenes radiológicas para su diagnóstico. El músculo esquelético es el tejido más abundante en el cuerpo (aproximadamente 40% de la masa corporal) y secreta cientos de péptidos que influyen en la sensibilidad a la insulina, la inflamación, la función inmunológica y regulan el anabolismo y el catabolismo. La disminución de masa muscular en los ancianos frágiles no solo se trata de la pérdida de la función mecánica, si no también es una causa importante del deterioro metabólico de todo el cuerpo, a su vez responsable de la asociación en morbilidad y mortalidad. Como la fragilidad denota un síndrome con poca capacidad para responder a los factores estresantes y mantener la homeostasis, y por lo tanto pone a esto individuados a riesgo de una variedad de resultados adversos (caídas, fracturas, discapacidad, muerte), la capacidad de identificar quién está en riesgo de estos eventos adversos es invaluable.

El impacto clínico de nuestros resultados se ilustra por el hecho de que avanza el conocimiento en el análisis y la caracterización de la fragilidad en imágenes médicas, que anteriormente no se ha realizado; y proporciona conocimiento actualmente no utilizado en la clínica. Mostramos el rendimiento complementario del análisis de texturas con las comorbilidades y el aumento de riesgo de mortalidad, lo que ilustra la importancia clínica de nuestros hallazgos. También demostramos que el método mejora cuando la información sobre el grosor muscular y la velocidad de la marcha se ingresan en los modelos predictivos. En los futuros ensayos clínicos, este método podría utilizarse para la estratificación del riesgo (frágil y no frágil). Será particularmente útil reconocer a las personas con alto riesgo de desarrollar deterioro funcional y pérdida de las actividades de la vida diaria. Sería un logro que los biomarcadores de imágenes cuantitativas se incluyeran como parte de los algoritmos clínicos que utilizan los médicos y los geriatras para seleccionar y dirigir el manejo de los individuos frágiles, a través del desarrollo de guías clínicas para su diagnóstico. Aunque el impacto a largo plazo del tratamiento y/o la prevención de la fragilidad aún se desconoce, es necesario un diagnóstico temprano, simple y objetivo para evaluar los programas de prevención y desarrollar una terapia adecuada.

Creemos que los biomarcadores de imagen en la fragilidad pueden tener éxito donde otros biomarcadores han fallado. La utilización de las imágenes médicas para la toma de decisiones clínicas ha aumentado en las últimas cuatro décadas. Hay ejemplos muy bien establecidos de

uso exitoso de imágenes médicas para la toma de decisiones preclínicas, como el uso de mamografías para detección de cáncer o ultrasonido para la detección de líquido libre en el abdomen en el contexto del trauma agudo. Las imágenes médicas brindan la capacidad de detectar y localizar muchos cambios que son importantes para determinar si una enfermedad está presente, si ha habido progresión de la enfermedad o si la terapia es efectiva. Al describir alteraciones en procesos anatómicos, fisiológicos, bioquímicos o moleculares. Los biomarcadores de imagen cuantitativas son medidas sensibles, específicas, precisas y reproducibles de estos cambios, y, como lo sugieren los resultados de este estudio, se pueden usar en la detección o diagnóstico de fragilidad. Los candidatos a biomarcadores circulantes conocidos tienen asociaciones débiles con resultados clínicos relevantes, esto resalta la idea de que podría no haber un solo marcador biológico que pueda rastrear de manera confiable la fragilidad y que existe un margen de mejora con el uso de nuevas herramientas. El análisis de ROC de 40 biomarcadores de envejecimiento celular, inflamación, hematología e inmunosenescencia mostró una capacidad discriminativa moderada para la mortalidad, sin que el AUC de los biomarcadores individuales superara 0,61, mientras que todos los modelos predictivos desarrollados aquí alcanzaron un AUC superior a 0,70. Los biomarcadores de imagen cuantitativa desarrollados de este estudio tuvieron fuertes asociaciones y valor predictivo con los resultados clínicos del estudio. Esto es importante, ya que el uso de biomarcadores en cualquier estudio también debe ser "adecuado para su propósito" y “clínicamente significativo”; creemos que hemos logrado este objetivo también.

Un hallazgo interesante, pero inesperado, fue que los modelos predictivos desarrollados identificaron un fenotipo de carácter pronóstico en los sujetos frágiles y pre-frágiles del estudio. Este fenotipo de función muscular y arquitectura muscular alterada determinada por la heterogeneidad de las características de la textura se asocia con un grupo distintivo de enfermedades. La disfunción muscular en el contexto de la fragilidad en este estudio tuvo una mayor incidencia de deficiencias auditivas, accidentes cerebrovasculares, infarto de miocardio, demencia/pérdida de memoria y caídas durante el seguimiento. Creemos que este grupo de enfermedades que identificamos comparten un vínculo mitocondrial. La patogenia de la disfunción muscular en el individuo envejecido es multifacética y abarca hábitos de estilo de vida, factores sistémicos, perturbaciones del entorno local y procesos específicos intramusculares. En este escenario, los trastornos en la función mitocondrial en los miocitos esqueléticos también se reconocen como factores que contribuyen a la disfunción muscular dependiente de la edad.

Las enfermedades mitocondriales son causadas por una función anormal de las mitocondrias. Pueden ser el resultado de mutaciones espontáneas o heredadas en el genoma mitocondrial o en genes nucleares que codifican componentes mitocondriales, pero también pueden adquirirse como consecuencia de efectos adversos de medicamentos, infecciones u otras causas ambientales. Estas disfunciones parecen ser más prevalentes en las enfermedades hereditarias de lo que se anticipó anteriormente y también se han atribuido a la patogenia de las afecciones comunes asociadas con el envejecimiento, incluidas las enfermedades neurodegenerativas, los trastornos cardiovasculares, la diabetes mellitus y varios tipos de cáncer. Los trastornos mitocondriales deben considerarse siempre que se sospeche un trastorno multisistémico progresivo y, en ocasiones, para síntomas aislados, como atrofia óptica, sordera neurosensorial, cardiomiopatía, diabetes, seudoobstrucción, neuropatía, miopatía, enfermedad hepática, accidentes cerebrovasculares precoces o convulsiones. El fenotipo que describimos comparte cuatro enfermedades de esta lista. Aunque los defectos mitocondriales afectan a muchos procesos celulares, los patrones de fenotipo representan predominantemente deficiencias en el metabolismo energético y el sistema nervioso es el más susceptible. La distribución de los fenotipos dentro de las categorías clínicas es en gran medida consistente con la distribución tisular del gasto de energía en el estado de reposo. Las mitocondrias proporcionan la mayor parte de la energía del cuerpo, y las mediciones de la respiración mitocondrial han demostrado que el tejido cerebral contiene más complejos de cadenas respiratorias activas que el hígado, el corazón o los músculos. Por lo tanto, nuestros resultados que muestran una mayor proporción de características neurológicas (p. Ej., Apoplejía y audición), cardiológicas (p. Ej., Infarto de miocardio) y musculoesqueléticas se correlacionan positivamente con la tasa metabólica basal y las actividades de la cadena respiratoria.

Todavía necesitamos una mejor comprensión de la implicación clínica del uso de estos biomarcadores cuantitativos de imágenes desarrollados. El impacto de estos resultados será importante no solo para comprender las conexiones potenciales entre el ámbito clínico y radiológico de la disminución de la fuerza, la resistencia y la masa muscular dentro del sistema musculoesquelético, sino también la fisiología y biología que subyace a estos cambios clínicos y radiológicos en el adulto mayor frágil.

Los biomarcadores de imágenes cuantitativas desarrollados proporcionan una forma no invasiva, rápida, de bajo costo y precisa de investigar información fenotípica. Analizar imágenes médicas es un ajuste natural para el "aprendizaje automático", una forma de inteligencia artificial. Una variedad de individuos y entidades en el campo médico esperan que incluir la

inteligencia artificial a la clínica hará que el diagnóstico sea más rápido y más barato. Los modelos predictivos desarrollados serán capaces de detectar matices que los humanos no pueden detectar. Evaluar el riesgo de fragilidad en los pacientes simplemente al mirar una imagen, abre nuevas aplicaciones para las imágenes médicas. Incluso en el mundo desarrollado, la radiología no es barata. Si la inteligencia artificial puede hacerlo más eficiente, el precio debería bajar, permitiendo que sus beneficios se distribuyan más ampliamente.

En resumen, existe la necesidad de desarrollar herramientas innovadoras para evaluar la disfunción muscular en los ancianos frágiles; creemos que los biomarcadores de imagen cuantitativa desarrollados podrían convertirse en una evaluación precisa de la calidad muscular de un individuo. Estos biomarcadores cuantitativos de imágenes podrían transformar la forma en que los médicos tratan a los pacientes. El desarrollo de herramientas y software (por ejemplo, aprendizaje automático, app´s de inteligencia artificial, dispositivos portátiles, etc), no solo ayudará al desarrollo y uso de técnicas y tecnologías de imágenes, sino también a su difusión e implementación. Es una característica del análisis de texturas ser independientes de la plataforma de la modalidad de la imagen, por lo que el modelo predictivo desarrollado aquí puede aplicarse potencialmente a otras modalidades, como la tomografía o la resonancia magnética. En el futuro, los fabricantes de ultrasonido, tomografía computarizada y resonancia magnética podrían agregar biomarcadores de imagen cuantitativa de fragilidad a su cartera como respuesta a la creciente solicitud clínica.

CONCLUSIONES

A la luz de los resultados obtenidos, podemos extraer las siguientes conclusiones:

1. Los biomarcadores de imágenes cuantitativas desarrollados a partir de ultrasonido muscular pueden identificar sujetos con riesgo de fragilidad (pre-frágiles) o frágiles con buena precisión, con la ayuda del análisis de textura de aprendizaje automático.
2. La heterogeneidad de las características de la textura muscular captura la calidad muscular y / o la disfunción muscular de los sujetos. Estas características hacen que las imágenes de ultrasonido con la ayuda del análisis de textura de aprendizaje automático sean un buen biomarcador cuantitativo de imágenes.
3. Los modelos predictivos desarrollados para imágenes de ultrasonido proporcionan un biomarcador de imágenes cuantitativo no invasivo, rápido y de bajo costo, así como repetible.

4. La precisión diagnóstica de los biomarcadores de imágenes cuantitativas desarrollados puede mejorarse si el grosor muscular y la velocidad de la marcha se introducen en los modelos.
5. Los modelos de biomarcadores de imágenes cuantitativas funcionan mejor cuando se usan para el músculo *Vastus Intermedius* que para el músculo *Rectus Femoris*, ya sea en el plano axial o sagital.
6. Los biomarcadores de imagen cuantitativa desarrollados fueron fuertemente pronóstico de muerte y se asociaron con una mayor morbilidad.
7. Los biomarcadores de imágenes cuantitativas desarrollados identifican un fenotipo de pronóstico general que se identificó en los sujetos frágiles y pre-frágiles del estudio, que se caracteriza por un aumento en la incidencia de deficiencias auditivas, accidentes cerebrovasculares, infarto de miocardio, demencia/pérdida de memoria y caídas en los dos siguientes años, en el contexto de disfunción muscular identificada.

INDEX

INDEX OF FIGURES, TABLES AND GRAPHICS

A. FIGURES:

B. TABLES

C. GRAPHICS

INDEX OF ABBREVIATIONS

2D: Two-dimension

30SS: 30s sit-to-stand test

AI: artificial intelligence

AIDS: Acquired Immune Deficiency Syndrome

AU: Arbitrary Units

AUC: Area under the curve

ATP: adenosine triphosphate

BMI: Body Mass Index

CCI: Charlson Comorbidity Index

CHGUV: Consorcio Hospital General Universitario de Valencia

CI: confidence intervals

COPD: Chronic Obstructive Pulmonary Disease

CV: cross-validation

CT: computed tomography

dB: decibels

DICOM: Digital Imaging and Communications in Medicine

DM: Diabetes Mellitus

DBSCAN: density-based spatial clustering of applications with noise

DXA: dual-energy X-ray absorber

ED: Emergency Department

EI: Echo Intensity

FOV: field of view

GLCM: Gray-Level Co-occurrence Matrix

GLRLM: Gray-Level run-Length Matrix

GLSZM: Gray-Level Size Zone Matrix

Hz: Hertz

ICC: intra-class correlation coefficients

IHF: Intensity Histogram Feature

ISODATA: iterative self-organizing data

Kgs: Kilograms

k-NN: k-nearest neighbours

LDA: Linear discriminant analysis

LGOCV: Leave-group-out CV

m: meters

MLP: multilayer perceptron

MRI: magnetic resonance imaging

MS: muscle strength

MT: muscle thickness

mtDNA: mitochondrial genome

NB: naïve Bayes classifier

Ng: Number of gray levels

NGTDM: Neighborhood Gray-Tone Difference Matrix.

OPQOL: Older's People Quality of Life

PACS: Picture Archiving and Communication System

PC: Primary Care

PCA: Principal component analysis

QIB: quantitative imaging biomarker

RF: random forests

RFE: recursive feature elimination

RFE-SVM: recursive feature elimination-support vector machine

ROC: Receiver Operating Characteristic

ROI: Region of Interest

s: seconds

SD: Standard Deviation

SFT: Subcutaneous Fat Tissue

SVM: support vector machine

SVM_L: support vector machine with linear kernel

SVM_R: support vector machine with radial kernel

1. INTRODUCTION

1.1 Aging

The worldwide epidemic of chronic disease is strongly linked to population aging, and to the epidemiological transition from the age of pestilence and famine, to the age of degenerative and man-made diseases (Prince et al., 2015). According to data from World Population Prospects (United Nations, 2015), the number of older people—those aged 60 years or over—has increased substantially in recent years in most countries and regions, and that trend is projected to accelerate in the coming decades. Between 2015 and 2030, the number of people in the world aged 60 years or over is projected to grow by 56%, from 901 million to 1.4 billion, and by 2050 the global population of older persons is projected to double its size, reaching nearly 2.1 billion (Bouillon et al., 2013). Due to the increase in life expectancy and the decline in the fertility rate, the proportion of people over 60 is increasing more rapidly than any other age group in almost all countries. In Spain, according to data collected from the observatory of sustainability of Spain (OSE), life expectancy at birth has been increasing progressively over the years, for both men and women. In the case of men, 76.3 years in 2002 to 78.9 years in 2010 and, in the case of women, from 83.2 years in 2002 to 84.8 years in 2010 (OSE, 2010).

The aging of the population can be considered a success of public health policies and socioeconomic development; but it also constitutes a challenge for society, which must adapt to this in order to optimize the health and the functional capacity of the elderly, as well as their social participation and their safety (Beard et al., 2016). This implies a realigning of health systems to better address the unmet needs of older people, independent of socioeconomic background. Age-related conditions and disabilities are burdening for the person, their family and public health care systems. A close relationship between the percentage of older persons in the population and health care expenditure has been clearly described in high-income countries. Health care expenses for the older population have been increasing more rapidly than those for younger adults; mainly due to an inadequacy of systems at meeting multiple and complex needs of the elderly. Such scenarios obviously endanger the sustainability of health and social care systems (Cesari et al., 2016). In this context, the concept of “frailty phenotype” is of special interest.

1.2 Frailty Phenotype

In an attempt to find terms to describe the progressive decrease in functional capacity inherent to aging, and subsequently, the increase in the likelihood of dependence of the elderly person, concepts of "frailty" and "frail elder" emerge. Etymologically, the fragile term comes from the

French "frêle", which means "little resistance", and from the Latin *fragilis*, which means, "that breaks easily" (Afilalo, 2011).

There is no universal definition of frailty. Currently the most accepted is coined by Linda Fried et al. in 2001, according to which frailty is a "physiological state characterized by an increase in vulnerability to external aggressions, as a result of a decrease or dysregulation of the physiological reserves of multiple systems, which causes difficulties in maintaining homeostasis" (Cruz-Jentoft et al., 2010; Fried et al., 2001). This definition provides a more precise quantification of the vulnerability of an individual which allows the consideration of their health state rather than one that only attends to chronological age. Frailty identifies a high-risk subgroup of people and offers information of great clinical importance: a higher reversibility at early stages than disability, and higher predictive value than chronic diseases for adverse outcomes at older ages (Rodriguez-Mañas & Fried, 2015).

Frailty is a syndrome of the elderly, the reported prevalence varies substantially across studies, ranging from 4% to 59% according to the adopted operational definition of frailty and the characteristics of the studied sample. Nevertheless, when the analysis is restricted to studies using the phenotype model proposed by Fried and colleagues, the weighted average prevalence was 9.9% and 44% for frail and pre-frail, respectively. Similar findings have been reported for the prevalence of frailty among participants aged 65 years and older in Europe, with pre-frail having a 42% prevalence with a range by country of 34-50% and frail 17% with a range of 6-27% (Cesari et al., 2016).

Frailty has a negative impact on European economies with physical disability, falls and injuries, prolonged hospitalization and the associated health care costs estimated to be more than one billion euros in costs for patients in rehabilitation per year (Cesari et al., 2016). People with chronic illnesses and activity limitations caused by frailty have more physician visits and fill more prescriptions than those individuals with no activity limitations, all of which presents a greater burden on the health care system (Prince et al., 2015). Though frailty contributes to numerous other health problems and accounts for a similar percentage of healthcare costs as osteoporosis for example (Blume & Curtis, 2011; Ensrud et al., 2018; Hajek et al., 2018), no public health campaigns are directly aimed at reducing the prevalence of frailty or treating it, yet.

With a growing population of older adults, there is an interest in research of the frailty phenotype and the development of instruments or tools for its identification (Rodriguez-Mañas

& Fried, 2015). These frail patients experience an increased risk of disability and institutionalization, higher hospitalization cost, lower quality of life, increased morbidity and mortality, showing the importance of identifying seniors at risk who could benefit from certain socio-health interventions, mainly preventive (exercise programs, hormonal or pharmacological treatments) (Cesari et al., 2016; Chumlea et al., 2011). A significant body of research in recent years suggests that both behavioural and pharmacologic interventions have the potential to slow declines associated with frailty and may be able to improve physical performance declined due to multiple disease and conditions (Prince et al., 2015).

The previously mentioned aspects point to the need of establishing intervention programs. Much of the potential to reduce disease burden will come from more effective primary, secondary and tertiary prevention programs targeting older people (Prince et al., 2015). For this, it is necessary to delimit the target subjects, for which we should know what are the physiological bases of frailty and possible biomarkers for its early identification. Research also needs to identify the clinical severity of frailty beyond which an intervention might not be beneficial (Rodriguez-Mañas & Fried, 2015).

1.3 Biomarkers of Frailty

The term “biomarker” is defined as a characteristic that is measured objectively and assessed to be an indicator of a biological physiological process, pathogenic processes and/or pharmacological process including therapeutic interventions (Cesari et al., 2012). Therefore, biomarkers favour a diagnosis, facilitate the monitoring of changes over time, and help clinical and therapeutic decisions.

If we look at the definition of frailty, characterized by a decrease or loss of homeostasis, we can deduce that it originates from the alteration of multiple and interrelated systems. Several studies have tried to explain the physiological basis of frailty and establish possible biomarkers. Thus, several alterations in the neuroendocrine system have been associated to frailty: a decrease in testosterone (Hyde et al., 2010), a decrease in dehydroepiandrosterone sulfate, androgen, and estrogen pre-hormone prohormone (Baylis et al., 2013), alterations of the axis of the growth factor similar to insulin type 1 (Leng et al., 2004), and an increase in cortisol (Holanda, Cristina Marques de Almeida et al., 2012) have also been described.

Regarding the immune and cardiovascular system, Walston et al. showed a positive relationship between the state of frailty, markers of inflammation and activation of the coagulation cascade (Walston et al., 2002). These authors demonstrated that there is a significant increase in levels of proinflammatory cytokines, such as C-reactive protein, in frail patients compared with non-frail patients, after excluding diabetics and heart disease patients. Higher levels of interleukin 6 have also been observed, which have been associated with lower muscle strength and slower gait (Ferrucci et al., 2002; Puts, Visser, Twisk, Deeg, & Lips, 2005). Regarding the markers of the coagulation pathway, high levels of coagulation factor VIII, fibrinogen, D-dimer and alpha-1 antitrypsin have been associated with frailty (Reuben et al., 2000; Walston et al., 2002).

Metabolic markers such as insulin, glycaemia, lipids and proteins have been studied too. With respect to glycaemia and insulin, frail non-diabetic individuals show significantly higher values than non-frail individuals at fasting and two hours after oral ingestion of 75g of glucose (Walston et al., 2002). In addition, in cross-sectional and longitudinal studies (Alvarado, Zunzunegui, Béland, & Bamvita, 2008; Hubbard, Lang, Llewellyn, & Rockwood, 2010; Woods et al., 2005) it has been observed that obesity is associated with frailty, especially abdominal obesity. Likewise, a situation related to obesity, insulin resistance, is considered as a determinant of sarcopenia and a risk factor for frailty (Barzilay et al., 2007). Regarding lipids and proteins, the relationship between frailty and decrease in albumin and total cholesterol levels has been postulated (Schalk, Visser, Deeg, & Bouter, 2004), as well as lower levels of low density lipoproteins (Walston et al., 2002). These and other authors (Ranieri, Rozzini, Franzoni, Barbisoni, & Trabucchi, 1998), state that the decrease in the risk of frailty is associated with the increase in cholesterol levels of low-density lipoproteins, high-density lipoproteins and total cholesterol. Indeed, when diabetics and heart patients are excluded, those with higher levels of total cholesterol and low-density lipoproteins are less likely to be frail. The decrease in serum albumin levels is associated with an increase in the relative risk of death (Reuben et al., 2000). On the other hand, the deficiency of a micronutrient, vitamin D, has been related to frailty (Wilhelm-Leen, Hall, Deboer, & Chertow, 2010), and it has even been proposed that individuals considered as pre-frail with higher levels of vitamin D are more likely to recover and become non-frail than those with lower levels (Shardell et al., 2012). Other possible biochemical markers related to frailty are certain markers of oxidative stress and brain-derived neurotrophic factors (Inglés et al., 2014; Inglés et al., 2017)

Regarding alterations in the musculoskeletal system, sarcopenia is considered as the key component of frailty (Roubenoff, 2000), characterized by a loss of strength and muscle mass. The pathophysiology of sarcopenia involves a denervation of the motor units, the conversion of

rapid muscle fibers (type II) into slow fibers (type I) and the deposition of lipids in muscle tissue (Lang et al., 2010). Several working groups for sarcopenia recommend using the presence of both low muscle strength or physical function and low muscle mass to diagnose sarcopenia (Chen et al., 2014; Cruz-Jentoft et al., 2010):

- *Muscle mass*: For the measurement of muscle mass, dual-energy x-ray absorptiometry (DXA) is considered the standard method. Other methods to quantify muscle mass include bioelectrical impedance, computed tomography, magnetic resonance imaging, urinary creatinine excretion or anthropometric measurements (Cooper et al., 2013).
- *Muscular strength*: For its determination, the grip force is measured by means of a dynamometer or the evaluation of knee flexion-extension. Low levels of grip strength predict better the risk of suffering clinical complications than low levels of muscle mass. In addition, there is a clear linear relationship between low levels of grip strength and the incidence of difficulties in carrying out activities of daily living (Cooper et al., 2013).
- *Physical performance*: Measured with the "Short Physical Performance Battery" which includes the 8-foot walk test, usual gait speed, 6-minute walk test, the "timed get up and go" test and the "stair climb" power test" (Cooper et al., 2013).

Despite all the knowledge about the physiopathology of the process, it continues to be a challenge for geriatric medicine to recognize this condition especially in its earliest phases and to establish appropriate treatment, hence the interest in search for frailty biomarkers. The syndromic nature of frailty as well as the wide range of pathogenic processes that contribute to its development and progression, poses major challenges for the identification of specific biological markers. Indeed, currently available biomarkers for frailty are typically related to specific pathogenic mechanisms and/or phenotypes. As such, they only describe single aspects of the conditions and are weakly associated with clinically relevant outcomes (Calvani et al., 2015). It would be particularly relevant for a biomarker (or several) to be sensitive and specific enough to identify frail individuals that could be subsidiary of primary prevention interventions (Rodriguez-Mañas & Fried, 2015).

1.4 Muscle Dysfunction and Sarcopenia with Frailty

An important component of the frailty phenotype is the increase in muscle dysfunction and the presence of sarcopenia, as mention previously. It is a part of the aging process to have changes in the quality and quantity of the muscle. These changes specifically include an increase in the amount of adipose tissue and connective tissue, a reduction in the number and size of muscle fibers, a reduction in maximum voluntary agonist activity, and an increase in antagonist co-

activation (Cesari et al., 2012; Lambert & Evans, 2002). These physiological factors result in the loss of strength and functional capacity of the muscle in the elderly.

Sarcopenia, or age-related decline in skeletal muscle mass and strength, is a major public health concern, affecting up to 29% of community-dwelling older adults. The Asian Consensus on the definition and diagnosis of sarcopenia defines it as a syndrome characterized by the generalized and progressive loss of strength and muscle mass (Chen et al., 2014). This decline is commonly coupled with declines in muscle function and performance, a major component of the frailty phenotype (Bartley & Studenski, 2017). When Fried et al. developed the phenotypic definition of frailty based on physical aspects; she coined five aspects to make a diagnosis: unintentional weight loss, fatigue or exhaustion, weakness, slow gait and decreased physical activity (Fried et al., 2001).

Multiple components of the frailty phenotype involve muscle dysfunction at its core. Indeed, many of the adverse outcomes of frailty are believed to be mediated by muscle decline and dysfunction (Calvani et al., 2015). Because of the overlapping paradigms, sarcopenia and frailty are commonly studied in parallel and often present concurrently in the clinical setting (Bartley & Studenski, 2017). The majority of frail individuals exhibit sarcopenia, and older individuals who present sarcopenia are also frail (Davies et al., 2018; Morley, 2016). Sarcopenia may be considered both the biological substrate for the development of frailty and the pathway through which the negative health outcomes of frailty ensue (Calvani et al., 2015). However, the concept of frailty goes beyond physical factors and includes psychological and social factors as well, including mental or cognitive state, social support and environmental factors (Chen et al., 2014; Chumlea et al., 2011).

1.5 Current Methods for Measuring Muscle Dysfunction

Since frailty is associated with decreased muscle mass, and therefore with decreased strength in older adults, several procedures and imaging methods have been used in order to identify the loss of muscle mass and muscle strength. To estimate muscle mass, computed tomography (CT), magnetic resonance imaging (MRI) and dual-energy X-ray absorptiometry (DXA) were used as mentioned in the previous section. CT and MRI are very precise imaging techniques, which can discriminate the fat of other tissues, and are considered the Gold Standard to estimate muscle mass (Cooper et al., 2013). These techniques require specialized equipment, are expensive and complicated to perform on people with a certain degree of disability, limiting their clinical use.

In addition, none have proven its usefulness in assessing strength and muscle mass in the clinical setting. However, the quality and quantity of skeletal muscle can be assessed by an ultrasound; it is a non-invasive and safe technique because it does not expose the patient to radiation (Cadore et al., 2012; Pillen et al., 2009). Few studies have compared muscle ultrasound to other techniques of muscle measurement, including DXA, CT or MRI, but all of these studies agreed that the sonographic measurement of muscle thickness, obtained either at multiple sites or at the thigh, have a high concordance with these techniques for muscle mass assessment (Ticinesi, Meschi, Narici, Lauretani, & Maggio, 2017).

Ultrasound is able to identify structural changes in the muscle caused by muscle degeneration, specifically the increase of adipose and intramuscular connective tissue, which results in an increase in the echogenicity of the assessed muscle (Wilhelm et al., 2014). It is believed that this change in muscle composition is caused mostly by the deposition of intramuscular lipids, which may be due to an increase in the expression of the protein related to lipid differentiation contained in the muscles of older adults. It has also been demonstrated that populations of older adults have high values of echo intensity in the grey scale compared to populations of young people (I. M. P. Arts, Pillen, Schelhaas, Overeem, & Zwarts, 2010; Strasser, Draskovits, Praschak, Quittan, & Graf, 2013). A recent study demonstrated that ultrasonographic echo intensity was significantly related to intra-muscular adipose tissue content as determined by MRI in thirty young and older individuals ($r = 0.485–0.648$, $P < 0.05–0.01$), suggesting that ultrasonography can provide similar information about the adipose-to-muscle ratio as MRI (Akima et al., 2016).

1.6 Echo Intensity and its Relation to Muscle Quality

There are few studies that investigate the relationship between echo intensity and physical parameters in the elderly. It is believed that the most important consideration of an older person is likely to be his/her physical function. Comprehensive assessment of physical function in older age is also much better predictors of survival and other outcomes than the presence of disease or even the extent of comorbidities (Beard et al., 2016). This makes these few studies very interesting in terms of possible tools for the identification of frail elderly and its association with how they function.

The first studies reported in the literature showed that echo intensity of the femoral quadriceps is associated with knee extension force in a sample of older adults (Sipila & Suominen, 1991; Sipila & Suominen, 1994). Unfortunately, the echo intensity values were generated visually by the researchers, introducing an operator dependent bias. In another study based on the analysis

of greys by computer, they observed a negative correlation between echo intensity and isometric strength in older men (Cadore et al., 2012), suggesting that those subjects with higher adipose tissue and connective tissue with high echo intensity values showed less muscle strength. A similar study also concluded that there is a negative correlation between the echo intensity of the *rectus femoris* and the isometric and isokinetic torsion peak force of the lower limbs (Fukumoto et al., 2012). Both studies were performed only in healthy elderly subjects and with relatively small samples. A group of Japanese researchers have verified the relationship of echo intensity with muscle quality and muscle strength independently, including variables such as age, weight, height and thickness of subcutaneous adipose tissue in 189 older men (Y. Watanabe et al., 2013). These results have been replicated by other researchers as well, but they also evaluated the functional capacity of the subjects with the use of the 30-s sit-to-stand test, which had a moderate correlation with echo intensity (Akazawa, Okawa, Tamura, & Moriyama, 2017; Akima et al., 2017; Rech et al., 2014; Wilhelm et al., 2014). They concluded that muscle echo intensity could be an important predictor of functional performance as well as strength in the elderly.

More recently, two studies aimed to determine whether morphological and qualitative characteristics classified by quadriceps are associated with muscle strength, physical function and sarcopenia in community-dwelling older adults (Kawai et al., 2018; Yamada et al., 2017) have become the most extensive samples carried out to date. According to the receiver-operating characteristic analysis, quadriceps muscle thickness and thigh muscle volume were better indicators of muscle mass, whereas the quadriceps muscle echo intensity was a more robust indicator of muscle function (Yamada et al., 2017). Kawai and colleagues, using the quadriceps muscle thickness and echo intensity, classified 1,290 participants with latent class analyses in normal, obesity, sarcopenic obesity, and sarcopenia (Kawai et al., 2018). Therefore, obtaining muscle quality and quantity indicators for sarcopenia diagnosis by ultrasonography is possible, based on these preliminary results.

The evidence from cross-sectional studies supporting an association between sonographic echo intensity, strength, and functional parameters is summarized in Table 1.1.

Table 1.1 Summary of Studies Comparing Muscle Ultrasound EI with Muscle Strength and Functional Parameters in Elderly Patients								
First Author, Year, Country	***Setting / Health Status***	***Sample Size***	***Male (%) / Female (%)***	***Mean age +/- SD (Range)***	***Measured Ultrasound Parameters***	***Reference Technique of Muscle Strength***	***Functional Parameters Measured***	***Correlation Coefficients or AUC (where available)***
Mirón Mombiela et al., 2017, Spain	Voluntary outpatients from a ultrasound clinic.	112	61(55% / 51(45%)	63 ± 15.8 (20-90)	MT of quadriceps muscle and EI of the femoris rectus	Handgrip strength of dominant hand	-	Men: rMT = 0.58 rEI = -0.355 / Women: rMT = 0.45 rEI = -0.522
Yamada et al., 2017, Japan	Community-dwelling older adults in the Tokyo prefecture	347	100 (29%) / 247 (71%)	Men: 81.6 ± 7.4 / Woman: 79.7 ± 6.9	EI of quadriceps femoris	Handgrip strentgh, maximal isometric knee extension and knee extension torque	Measurements of Physical Performances were obtained: 5-m walking speed, the timed up and go test, the 1-leg stand test, and the 5 chair stand test.	Men: AUC 0.66 (95% CI 0.54-0.77) / Women: AUC 0.66 (95% CI 0.59-0.73)
Kawai et al., 2017, Japan	Community-dwelling elderly who participated in the health check-up in the Itabashi ward, Tokyo.	1239	511 (41%) / 728 (59%)	72.8 ± 5.3	MT and EI of the femoris rectus	Knee extension strength measured by dynamometer	-	Men: r MT = 0.297 r EI = -0.312 / Women: r MT = 0.257 r EI = -0.268
Akima et al., 2017, Japan	The participants were healthy; habitually physically active; and free of neurological, cardiovascular, and lower-extremity diseases.	64	27 (42%) / 37(58%)	Men: 72.9 ± 4.5 (65-82) / Women: 71.5 ± 5.3 (65-88).	EI of quadriceps femoris	-	Sit-to-stand test: subjects were timed performing, as quickly as possible, 10 repetitions of standing from a sitting position with arms crossed on the chest	Men: r = 0.492 / Women: r = 0.385

Akazawa et al., 2016, Japan	Community-dwelling female subjects. 25 were unable to walk independently (dependent group), 22 frail older women (frail group) and 22 were healthy (healthy group).	48	-	Dependent group = 83.4 ± 7.8, Frail gorup = 81.4 ± 5.0, Healthy group = 81.9 ± 2.2	EI of quadriceps femoris	Maximal isometric strength of the right quadriceps was measured using a handheld dynamometer	Sit-to-stand test: subjects were timed performing, as quickly as possible, 10 repetitions of standing from a sitting position with arms crossed on the chest	r = -0.635
Rech et al., 2014, Brazil	Healthy, physically active elderly women	45	Female	70.28±6.2 (60-83)	EI and MT of quadriceps femoris muscle	Knee extension isometric peak torque, rate of torque development (RTD)	30s sit-to-stand test and usual gait speed	EI vs RTD r=-0.386. MT vs RTD r=0.545, p<0.01
Wilhelm et al., 2014, Brazil	Healthy older men not engaged within any systematic physical exercise program.	50	Male	66 ± 4.5	MT and EI of quadriceps muscle	Isometric peak torque, rate of torque development and knee extension force	30s sit-to-stand test (30SS) and vertical jump power	EI r = -0.498 / MT r = 0.592 / EI vs 30SS = -0.502 / MT vs 30SS = 0.409
Watanabe et al., 2013, Japan.	Elderly men who lived independently who are able to walk without an assistive device	184	Male	74,4 ± 5.9 (65-91)	MT and EI of rectus femoris muscle	The maximum isometric torque of knee extension at an angle of 90° was measured in a sitting position on a custom-made dynamometer chair.		EI r=-0,333, MT r=0,411

Cadore et al., 2012 Brazil	Elderly volunteers without any history of neuromuscular, metabolic, hormonal and cardiovascular diseases.	31	Male	64.7 ± 4.1 stated in text. 65.5 ± 5 showed in Table 1.	EI of rectus femoris and MT of all four heads of quadriceps femoris	Maximal isometric and isokinetic peak torques were obtained using an isokinetic dynamometer	Cardiovascular performance - incremental test on a cycle ergometer to determine the peak oxygen uptake, ventilatory thresholds and maximal work load	RF EI vs isometric and isokinetic peak torques r=-048 to r=-0.64, p<0.05. RF EI vs workload at VT1 r=-0.46, p=0.01, at VT2 r=-0.50, p=0.09
Fukumoto et al., 2012, Japan	Community-dwelling elderly women able to walk without assistive devices, no trauma, no dementia, no neuromuscular disorders.	92	Female	70.4 ± 6.6 (51-87)	EI and muscle thickness of quadriceps femoris muscle	Maximal isometric strength of the knee extensors	-	EI r=-0.40, MT r=0.47, both p<0.01

Abbreviations: EI: echo intensity; MT: muscle thickness; RTD: rate of torque development; 30SS: 30s sit-to-stand test; AUC: area under the curve; r: Pearson correlation.

The ability of muscle ultrasound parameters, including echo intensity, to prospectively predict clinical outcome for adult and elderly patients has been even less investigated (Ticinesi et al., 2017). Mirón Mombiela and colleagues recently demonstrated that echo intensity was negatively correlated with muscle strength and was significantly greater in frail individuals, even after adjustment for sex and BMI (Mirón Mombiela, Facal de Castro, Moreno, & Borras, 2017). In addition, the ultrasonographic measurement of rectus femoris cross sectional area was demonstrated as an independent predictor of hospital length of stay, mortality, and nursing home discharge in a group of adults admitted in an intensive care unit (Mueller et al., 2016a). A similar study found that loss of muscle mass shows a negative correlation with length of stay, and seem to be higher during the first 2-3 weeks of immobilization in the intensive care unit stay (Gruther et al., 2008). Despite these reports, the relevance of muscle ultrasound measures in term of clinical outcomes needs further investigation (See Table 1.2).

Table 1.2 Association of Ultrasonic Muscle structure Parameters with Clinical Outcomes in Elderly Patients										
First Author, Year, Country	***Setting / Health Status***	***Sample Size***	***Male (%) / Female (%)***	***Age Mean age +/- SD (Range)***	***Measured Ultrasound Parameters and Site***	***Outcomes measured***	***CC, AUC or OR (where available)***	***Other Clinical Parameter***	***CC, AUC or OR (where available)***	***Results***
Mirón Mombiela et al., 2017, Spain	Voluntary outpatients from ultrasound clinic.	112	61(55% / 51(45%)	64 +/- 15.8 (20-90)	MT and EI of the femoris rectus	Frailty	rEI = 0.49 rMT = 0.57	Quality of Life	rEI = -0.29 rMT = 0.11	EI according to ultrasound was found to be negatively correlated with muscle strength and was significantly greater in frail individuals, even after adjustment for sex and BMI.
Mueller et al., 2015, Germany	ICU patients from two large academic medical center	102	62 (61%) / 40 (39%)	61.9 +/- 15.8 (21-89)	Cross-sectional area of the rectus femoris (RF CSA)	Adverse discharge disposition defined as discharge to a skilled nursing facility or in-hospital mortality.	RF CSA OR 0.30; 95%CI 0.14–0.66	Frailty	r = -0.48, p <0.001	17.6% of patients had an adverse discharge disposition (13 to a skilled nursing facility and 5 in-hospital deaths). All patients who died in the hospital were sarcopenic. After including the covariates in a multivariable regression model, sarcopenia was found to be an independent predictor of adverse discharge disposition.
Gruther et al., 2008, Austria	ICU patients who had a LOS longer than 7 days and survived their critical illness.	118	88 (75%)/ 30(25%)	55 +/- 16	MT of quadriceps muscle	LOS	R2 = 0.527	-	-	Loss of muscle mass shows a negative correlation with length of stay, and seem to be higher during the first 2-3 weeks of immobilization/intensive care unit stay.

Abbreviations: EI: echo intensity; MT: muscle thickness; ICU: intensive care unit; LOS: length of stay; RF CSA: Cross-sectional area of the rectus femoris; CC: correlation coefficient; AUC: area under the curve; OR: odds ratio; r: Pearson correlation.

Our previously published work focused on the importance of muscle quality reflected by the composition of the muscle rather than the mass-force relationship for the identification of the frailty syndrome (Mirón Mombiela et al., 2017). Others have shown the negative association between echo intensity, muscle strength and/or physical function in the elderly (Akazawa et al., 2017; Akima et al., 2017; Cadore et al., 2012; Fukumoto et al., 2012; Rech et al., 2014; Y. Watanabe et al., 2013; Wilhelm et al., 2014; Yamada et al., 2017). We were able to confirm the previously published relationships, as well as to find a relation of echo intensity measurements based on the state of frailty, demonstrating that the values of echo intensity are higher in frail and pre-frail individuals. These findings are supported by the fact that echo intensity was also associated with muscle strength, muscle thickness and quality of life in relation to the state of frailty markers with strong relationships with frailty status in previous research (Bartley & Studenski, 2017).

There is no question that innovative tools for measuring muscle and its quality are needed in elderly adults, and although the ultrasonic measurement of echo intensity is a promising and potentially effective imaging biomarker, it needs further assessment and validation. It is, however, necessary to consider some limitations. The ultrasound waves are attenuated through the tissues and the value of echo intensity is affected by the thickness of tissues, this being a factor inherent in the technique. It is also necessary to consider that the absolute values of echo intensity are not comparable between studies since these vary between ultrasound equipment and parameters used. This technicality is a limiting factor for absolute comparison of the values of echo intensity between studies and research centers. It is therefore necessary to establish a method of calibration and analysis to determine the value of echo intensity and the muscle changes in ultrasound images; we believe that other methods of imaging processes should be applied (Ticinesi et al., 2017). Muscles in the body, like many other anatomical structures, have repeating subunits and therefore fractal properties. It is theorized that, in part, progressive loss of complexity in the fractal architecture of muscle could characterize both aging and frailty (Lipsitz, 2004; Lipsitz, 2008). This makes muscle ultrasound images suitable for fractal analysis.

Together with the tutor of this project, we carried out a pilot study utilizing fractal analysis, a type of texture analysis. The intention was to overcome some of the limitations of the technique from the previous study. The fractal dimension parameter of the muscle correlates with echo intensity ($r = 0.537$, $P < 0.01$) and shows different pattern according to frailty criteria. Correlation for Pearson was $R2 = 0.303$ for non-frail subjects, and $R2 = 0.427$ for pre-fail and frail subjects. The diagnostic accuracy for echo intensity was good according to the area under the curve (AUC) of the receiver operating characteristic (ROC) (AUC of 0.722 ± 0.09 (SD), $P = 0.022$). However, fractal dimension did

not improve the AUC when we combined both parameters. The fact that we only studied one texture parameter may have contributed to this finding (Sogawa et al., 2017). We believe that combinations of different texture features may be required for prediction of diagnosis, monitoring, and prognosis of frailty in the elderly (Molinari, Caresio, Acharya, Mookiah, & Minetto, 2015). As the union of these two factors explains only 77% of the total variance of the sample, it is possible that the AUC could be increased by the utilization of other texture features or the combination of several of them. We concluded that fractal analysis was useful to characterize echo intensity, since it gives us information about the texture of the muscle and its heterogeneity in the context of frailty. it also supports echo intensity as a biomarker for the frailty phenotype given that the increase in echo intensity reflects muscle dysfunction related to frailty (unpublished results).

1.7 Progress Beyond the State-of-the-Art

Over the last few decades, geriatrics and gerontology researchers have devoted an increasing amount of efforts in the attempt of designing, developing, and implementing preventive interventions against this age-associated functional loss condition. The accomplishment of such task has been hampered by the lack of a unique, standardized, and universally agreed operational definition for frailty (Rodríguez-Mañas et al., 2013). These definitional ambiguities are also reflected by the absence of reliable biomarkers that could be utilized in clinical and research settings to identify frailty, track their progression over time, and monitor their response to interventions (Calvani et al., 2015). Frailty, with its health and economic consequences as well as its diagnostic difficulties, confirms that there is an urgent need for multidisciplinary action to overcome this health challenge. Available opportunities are not fully exploited, and modern imaging techniques have a high potential to help fill this gap and facilitate diagnostic screening. We need a methodology that could be used across many populations to overcome this health challenge and optimize patient care. Because echo intensity determined by ultrasound can be used to objectively evaluate muscle quality, and is relatively cheap, it is an attractive candidate to explore further as a biomarker of frailty. If the studies demonstrate accuracy, reproducibility, discrimination and predictive value, echo intensity could become a useful aid in the diagnosis of frailty phenotype.

The usual tools to assess frailty show, among other characteristics, a low sensitivity and a low positive predictive value. Many biomarkers of frailty have been identified but few of them have been assessed as clinical markers and moreover there are controversial results (Rodríguez-Mañas, 2015). Bearing these considerations in mind, a shift of paradigm is needed, moving from the quest for single biomarker to the development of multivariate/multidimensional modelling of a panel of complementary biomarkers. Single or isolated inspection of variables can result in a partial or

incorrect picture. On the other hand, mainly through the implementation of “omics” disciplines, multivariate analyses have been gaining a more and more relevant role in clinical practice and may easily be extended for the search for frailty biomarkers (Calvani et al., 2015), including quantitative imaging biomarkers (QIBs) and radiomics.

That is why, in this prospective-retrospective study, we asked whether it is possible to identify and develop QIBs from muscle ultrasound images for the identification of subjects at risk of frailty or already frail with the aid of machine learning texture analysis as the experimental approach to answer this question.

1.8 Quantitative Imaging Biomarkers and Radiomics

Extending the definition of a biomarker from above, a QIB can be defined as “the extraction of quantifiable features from medical images for the assessment of normal (findings) or the severity, degree of change or status of a disease, injury or chronic condition relative to normal (findings)” (Sullivan et al., 2015). Medical imaging provides the ability to detect and localize many changes that are important to determine whether a disease is present or a therapy is effective, by depicting alterations in anatomic, physiologic, biochemical or molecular processes. In addition, most of the current imaging technologies available can provide quantitative information about some properties of the tissue from which the imaging signal has emanated (Aerts, Hugo J W L et al., 2014; Sullivan et al., 2015). QIBs are sensitive, specific, accurate and reproducible imaging measures of these changes, and the use of computer-assisted image processing and analysis (machine learning) is extremely important for the discovery, characterization, validation, and application of these QIBs (Prescott, 2013).

QIBs are validated by demonstrating an association between the measured biomarker value and a physiologic, pathophysiologic or therapeutic response (Prescott, 2013; Sullivan et al., 2015). Medical imaging has made this possible because it reflects in some way the molecular substrate of the healthy or diseased tissue, organ or person going through imaging (Sullivan et al., 2015). For example, the previous studies on muscle quantitative imaging biomarkers changes with age, and its correlation with strength and functional parameters makes quantitative imaging biomarkers a frailty biomarker candidate (Akima et al., 2017; Cadore et al., 2012; Fukumoto et al., 2012; Mirón Mombiela et al., 2017; Rech et al., 2014; Y. Watanabe et al., 2013; Wilhelm et al., 2014; Yamada et al., 2017).

The field of image analysis has grown exponentially, with increased number of pattern recognition tools and an increase in data set sizes. These advances have facilitated the development of processes for high-throughput extraction of quantitative features that result in the conversion of images into mineable data and the subsequent analysis of these data for decision support; this is the practice of "Radiomics"(Aerts, Hugo J W L et al., 2014; Gillies, Kinahan, & Hricak, 2016; Lambin et al., 2012). This is in contrast to the traditional practice of treating medical images as pictures intended solely for visual interpretation (Gillies et al., 2016). Importantly, the data are designed to be extracted from standard-of-care images, leading to a very large potential subject pool (Kumar et al., 2012).

Since radiomics is motivated by the concept that biomedical images contain information that reflect underlying pathophysiology, these relationships can be revealed via quantitative image analysis (Lambin et al., 2012). Quantitative image features based on intensity, shape, size or volume and texture offer information on disease phenotype and microenvironment that is distinct from that provided by clinical reports, laboratory test results and genomic/proteomic assays (Gillies et al., 2016). Associations between these changes and disease state can be analysed using statistical models or classifiers. Radiomics data is in a mineable form and can be used to build descriptive or predictive models relating image features to phenotypes. This is call data mining, which refers to the process of discovering patterns in large data sets and is used for evidence-based clinical decision support (Calvani et al., 2015; Gillies et al., 2016; Kumar et al., 2012).

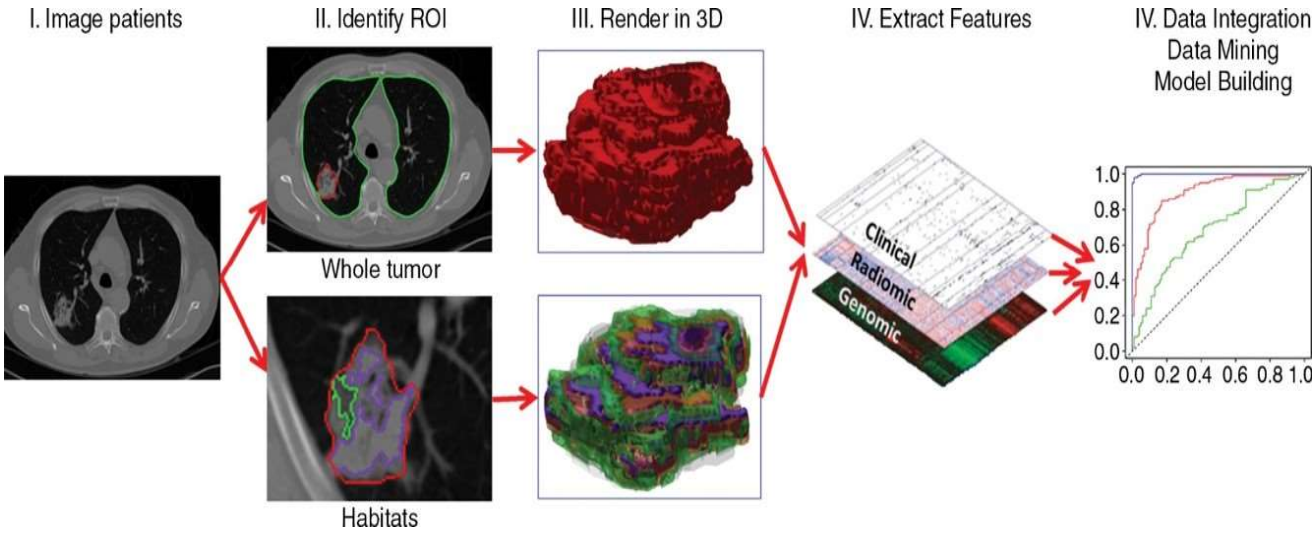

Figure 1.1 Flowchart shows the process of radiomics and its use in decision support (Gillies et al., 2016)

(Reprinted with permission of Radiological Society of North America)

Patient work-up requires information from disparate sources to be combined into a coherent model to describe where the lesion is, what it is, and what it is doing. Radiomics begins with acquisition of high-quality images. From these images, a region of interest (ROI) is identified and segmented. Quantitative features are extracted from this ROI to generate a report, which is placed in a database along with other data, such as clinical and genomic data. These data are then mined to develop diagnostic, predictive, or prognostic models for outcomes of interest (Figure 1.1). In summary, the radiomics processes includes: (1) image acquisition, (2) image segmentation, (3) feature extraction, (4) feature selection and classification (model building), and (5) statistical and radio-informatics analyses (Gillies et al., 2016).

1.8.1 Image acquisition

During the past decades, medical imaging innovation allowed the field to move towards quantitative imaging. Digital imaging is one of these innovations. Digital image acquisition is the creation of a digitally encoded representation of the visual characteristics of the body or its parts. Digital imaging can be classified by the type of electromagnetic radiation, ultrasound waves, or other waves whose variable attenuation, as they pass through or reflect off objects, conveys the information that constitutes the image.

Routine clinical image acquisition has a wide variation in imaging parameters such as image resolution (pixel size or matrix size), patient position, scanner parameters and the variations introduced by different reconstruction algorithms and slice thickness, which are different for each scanner vendor (Kumar et al., 2012). Even this simple set of imaging issues can create difficulty in comparing results obtained across institutions with different scanners and patient populations, reason way a standardized protocol of image acquisition is needed. The lack of standardization in imaging makes it difficult to determine the effectiveness of image features being developed and prediction models built to work on those feature values.

1.8.2 Image segmentation

Segmentation of images into ROI such as diseased tissue, normal tissue and other anatomical structures is a crucial step for subsequent informatics analyses. Texture features are computed inside a predefined ROI, and the size of the ROI should be sufficiently large to capture the texture information thereby eliciting statistical significance (Larroza, Bodí, & Moratal, 2016). Many automatic and semi-automatic segmentation methods have been developed across various image modalities (Kumar et al., 2012). Nevertheless, manual definition of ROIs is still considered

the gold standard in many applications (Larroza et al., 2016), even when it suffers from inter-reader variability and is labour intensive.

Accuracy, reproducibility and consistency are the most important factors to evaluate segmentation process for medical images. Conventional evaluation metrics normally utilize the manual segmentation provided by radiologists, which is subjective and error-prone. In the majority of cases, manual segmentation tends to overestimate the lesion volume to ensure the entire lesion is identified and the process is highly variable. In other words, "gold standard" segmentation does not really exist. Hence, it is believed that reproducibility and consistency are more important than accuracy for the evaluation of segmentation process (Kumar et al., 2012).

It is clear from Section 1.8.1 that acquisition protocols are highly relevant for texture analysis. Several pre-processing techniques have been proposed in order to minimize the effects of acquisition protocols. The main purpose of these pre-processing techniques is to put all ROIs in the same condition, so features extracted from them represent essentially the texture being examined (Larroza et al., 2016). Some of these techniques are interpolation, normalization, inhomogeneity correction, and quantization of gray-levels.

1.8.3 Feature extraction

Once ROIs are defined, imaging features can be extracted. These features describe characteristics of the ROIs including size or volume, tumor intensity histogram (e.g. high or low contrast), tumor shape (e.g. round or spiculated), texture patterns (e.g. homogeneous or heterogeneous), as well as descriptors of ROI location and relations with the surrounding tissues (e.g. near the heart). Here we will focus on texture analysis only.

1.8.3.1 Texture analysis

Muscular heterogeneity can be difficult to assess and quantify with traditional tools or subjective image evaluation. Therefore, although texture analysis it is not a new tool, there is a renewed interest in the extraction of texture features from medical images. Echo intensity is a potentially useful biomarker that allows the evaluation and quantification of the spatial heterogeneity of the muscle in the context of frailty. In previous studies, only the mean of echo intensity has been explored, in this study we explored its texture.

Texture analysis refers to the branch of imaging science that is concerned with the description of characteristics imaged by textural features. Meanwhile, advances in image

analysis, aided by improvements in computer software, can provide important information about the structural arrangement of surfaces and their relationship to the surrounding environment known as texture analysis. Texture analysis is only one part of the growing field of radiomics. Texture analysis provides an objective, quantitative assessment of disease heterogeneity by analysing the distribution and relationship of pixel gray levels in the image. Different methods of texture analysis have been applied, including statistical-, model-, and transform-based method (Lubner, Smith, Sandrasegaran, Sahani, & Pickhardt, 2017).

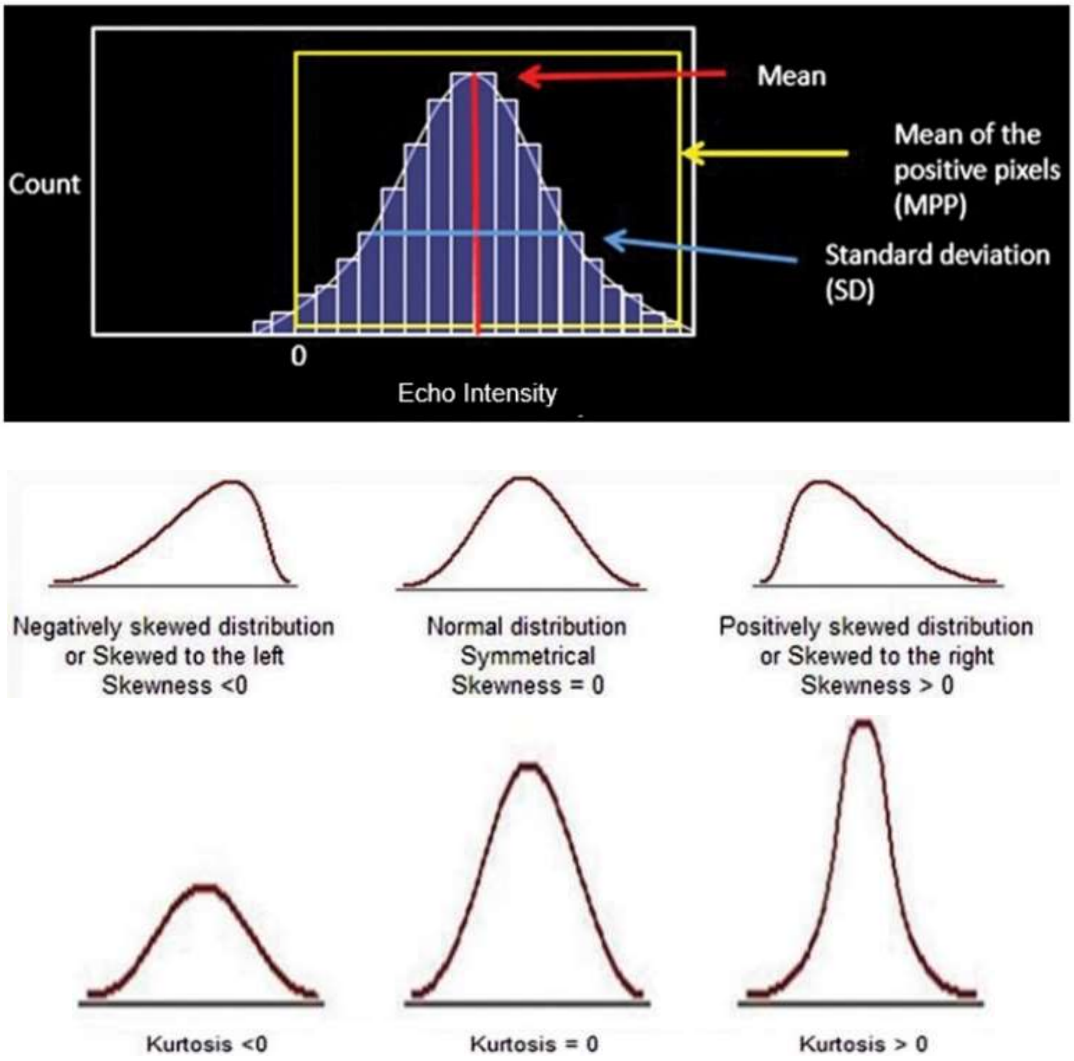

Figure 1.2 First-order statistical-based sonographic texture parameters (Lubner et al., 2017)

(Reprinted with permission of Radiological Society of North America (RSNA))

Statistical-based techniques have been most commonly applied, either through commercially available or in-house software tools, to describe the relationship of gray-level values in the image (Lubner et al., 2017). In a statistical-based model, first-order statistics evaluate the gray-level frequency distribution from the pixel intensity histogram in a given area of interest, including mean intensity, threshold (percentage of pixels within a specified range), entropy (irregularity), standard deviation, skewness (asymmetry), and kurtosis (peakedness/flatness of pixel histogram), for example (Figure 1.2). The main advantage of this approach is its simplicity through the use of standard descriptors to characterise the data. However, the power of the approach for discriminating between unique textures is limited in certain applications because the method does not consider the spatial relationship, and correlation between pixels (Larroza et al., 2016; Lubner et al., 2017).

In second-order statistical texture analysis, information on texture is based on the probability of finding a pair of gray-levels at random distances and orientations over an entire image. Second-order statistics can be based on a co-occurrence matrix and include things like second-order entropy, energy, homogeneity, dissimilarity, and correlation. Second-order statistics can also be derived using a run-length matrix, which analyses texture in a specific direction. Extension to higher-order statistics involves increasing the number of variables studied. Some examples of higher-order statistics, such as contrast, coarseness, and busyness, can be calculated using neighbourhood gray-tone difference matrices, which examine location and relationships between three or more pixels (Lubner et al., 2017).

In Figure 1.3 we can observe each of the circles contains the same number of light gray, medium gray, dark gray and black “pixels,” so the first-order texture features and pixel histograms are nearly identical for these two images. However, higher-order texture features that take into account pixel location and relationship to adjacent pixels, such as grey-level co-occurrence matrix or run-length matrix, would be different between these two images. For example, a light gray pixel occurs horizontally adjacent to and to the left of a black pixel four times in the left circle but only twice in the right circle. The gray-level co-occurrence matrix measures the frequency with which each type of pixel occurs in the horizontal, vertical, and oblique planes adjacent to all other pixels. This frequency is then mapped, representing the spatial relationship between the pixels, not just the pixels present (Lubner et al., 2017).

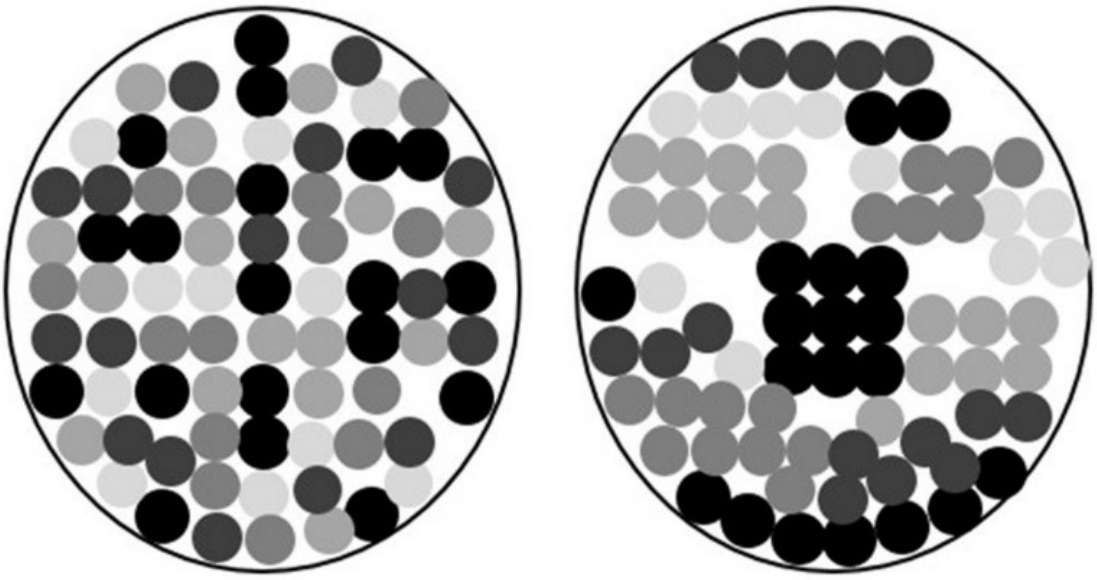

Figure 1.3 Diagrams of two different gray-scale images (Lubner et al., 2017)

(Reprinted with permission of RSNA)

1.8.4 Feature selection and classification:

As described above, a large number of image features may be computed. However, all these extracted features may not be useful for a particular task. In addition, the numbers of extracted features can be higher than the number of samples in a study, reducing power and increasing the probability of over-fitting the data. Therefore, dimensionality reduction and selection of task-specific features for best performance is a necessary step. Different feature selection methods can be used for this purpose and may exploit machine learning or statistical approaches. In addition to feature selection for informative and non-redundant features, high reproducibility of the features is important in the development of clinical biomarkers, which requires the availability of a test-retest data set (Kumar et al., 2012). Here it will be reviewed feature selection and classification with the aid of machine-based learning.

1.8.4.1 Machine-based learning

Machine learning is an exciting field of research in computer science and engineering. It is considered a branch of artificial intelligence because it enables the extraction of meaningful patterns from examples, which is a component of human intelligence. More recently, machines have demonstrated the capability to learn and even master tasks, showing that machine learning algorithms are potentially useful components of computer-aided diagnosis and decision support systems. This discovery has led to substantial and increased interest in

the field of machine learning, specifically how it might be applied to medical images (Erickson et al., 2018).

The following is one broadly accepted definition of machine learning. If a machine learning algorithm is applied to a set of data (tumor images), and some knowledge about this data (benign or malignant tumors), then the algorithm system can learn from the training data and apply what it has learned to make a prediction (in our example, whether a different image is depicting benign or malignant tumor tissue). If the algorithm system optimizes its parameters such that its performance improves, that is, more test cases are diagnosed correctly then it is considered to be learning that task (Erickson, Korfiatis, Akkus, & Kline, 2017). In other words, for training, the machine learning algorithm system uses a set of input images to identify the image properties that, when used, will result in the correct classification of the image—that is, depicting benign or malignant tumor—as compared with the supplied labels for these input images. For predicting or testing, once the system has learned how to classify images, the learned model is applied to new images to assist radiologists in identifying the tumor type (Figure 1.4).

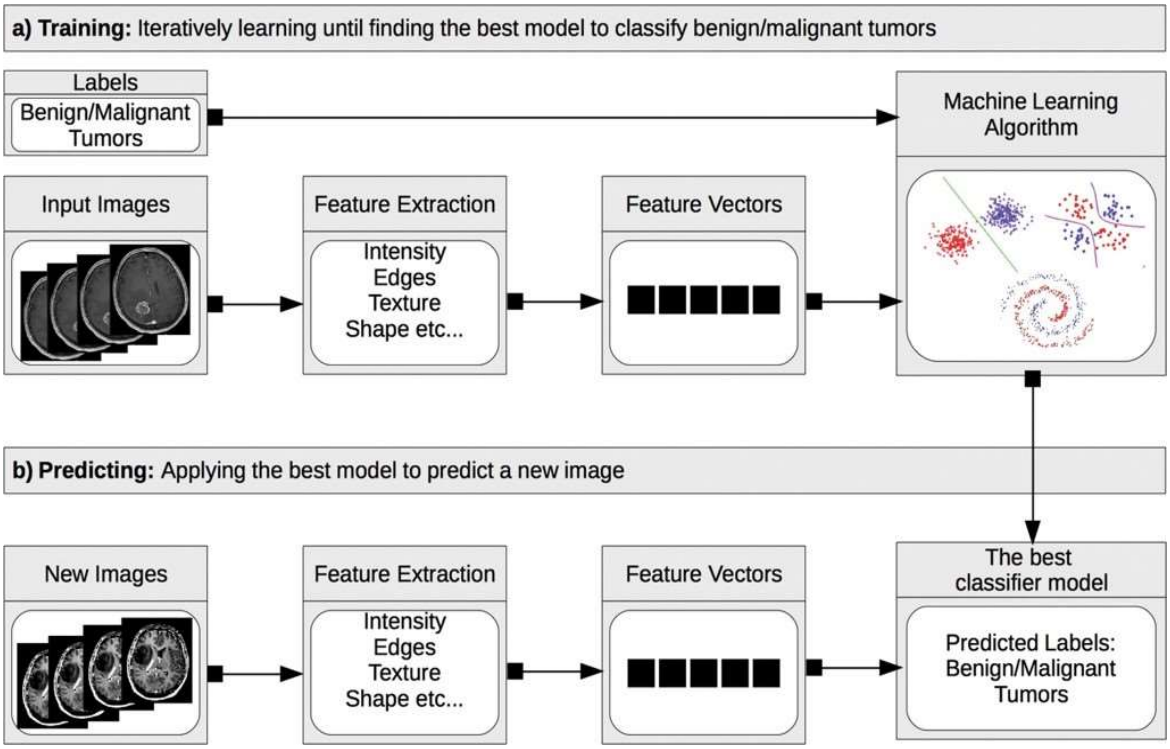

Figure 1.4 Machine learning model development and application model for medical image classification tasks (Erickson et al., 2017) (Reprinted with permission of Radiological Society of North America)

1.8.4.2 Feature Selection

The first step in machine learning is to extract the features that contain the information that is used to make decisions (Section 1.8.3). The vast variety of feature extraction methods for texture analysis allows us to obtain a myriad of features. This generates a problem, because the more features we have, the more complex the classification model becomes (Larroza et al., 2016). Although it is possible to compute many features from an image, having too many features can lead to overfitting rather than learning the true basis of a decision. The process of selecting the subset of features that should be used to make the best predictions is known as feature selection. (Erickson et al., 2017).

Feature selection is the process of choosing the most relevant features for a specific application. Reducing the number of features speeds up the testing of new data and makes the classification problem easier to understand, but the main benefit is the increase of classification performance. While methods like principal component analysis (PCA) or linear discriminant analysis (LDA) are used for feature reduction, they are not considered as feature selection methods since they still require computation of all the original features (Larroza et al., 2016).

A straightforward approach to find the most discriminative features, or the combination of features that yields the best classification, is to perform an exhaustive search as done by filter methods. In these methods, all possible combinations of features are tested as input to a classifier and those that yield the best discrimination are selected. The problem with this method is that it becomes tremendously expensive to compute when the feature space is very high. Filter feature selection methods make use of a certain parameter to measure the discriminatory power. For example, typical statistical methods, such as the Mann-Whitney U-test or Wilcoxon signed rank test can be used to find and select features with statistical significance.

The main drawback of the filter methods is that feature selection is based on the intrinsic information of the training data and does not consider the predictive capability of a certain subset of features. Wrapper methods take advantage of a classification algorithm and search the subset of features that provides optimal classification performance. The quality of the selected subset of features depends fundamentally on the search algorithm used. We mentioned earlier that an exhaustive search is not feasible for high dimensional datasets, so an algorithm that uses some type of search strategy has to be chosen. The recursive feature

elimination (RFE) ranks the features by recursively training a classifier and removing the feature with the smallest ranking score and selecting the subset of features that yields the best classification. Any classifier can be used in conjunction with the RFE to compute the feature scores. The feature selection technique known as recursive feature elimination-support vector machine (RFE-SVM), first proposed for gene selection in cancer classification, has gained major attention for selecting texture features due to its good performance over other methods (Larroza et al., 2016).

1.8.4.3 Feature Classification

The main goal in texture analysis applications is the classification of different tissues and lesions to automate or aid the diagnosis decision. Simple statistical methods can be used to determine the texture features with statistical significance for discrimination of two or more classes. However, following the feature selection step described in the previous section, we focus on more complex classification algorithms that make use of proper combination of features to achieve the highest discrimination. Machine learning classification algorithms can be classified on the basis of training styles: supervised, unsupervised, and reinforcement learning. To explain these training styles, consider the task of separating the regions on a brain image into tumor (malignant or benign) versus normal tissue.

In our example (Figure 1.4), supervised learning involves gaining experience by using images of brain tumor examples that contain important information specifically, “benign” and “malignant” labels and applying the gained expertise to predict benign and malignant neoplasia on unseen new brain tumor images (test data). In this example case, the algorithm system would be given several brain tumor images on which the tumors were labelled as benign or malignant. Later, the system would be tested by having it try to assign benign and malignant labels to findings on the new images, which would be the test dataset. Examples of supervised learning algorithms include support vector machine, decision tree, linear regression, logistic regression, naive Bayes, k-nearest neighbour, random forest, AdaBoost, and neural network methods (Erickson et al., 2017).

With unsupervised learning, data (eg, brain tumor images) are processed with a goal of separating the images into groups for example, those depicting benign tumors and those depicting malignant tumors. The key difference is that this is done without the algorithm system being provided with information regarding what the groups are. The algorithm system determines how many groups there are and how to separate them. Examples of

unsupervised learning algorithm systems include K-means, mean shift, affinity propagation, hierarchical clustering, DBSCAN (density-based spatial clustering of applications with noise), Gaussian mixture modeling, Markov random fields, ISODATA (iterative self-organizing data), and fuzzy C-means systems (Erickson et al., 2017).

Like supervised learning, reinforcement learning begins with a classifier that was built by using labelled data. However, the system is then given unlabelled data, and it tries to further improve the classification by better characterizing these data, similar to how it behaves with unsupervised learning. Examples of reinforcement learning algorithm systems include Maja and Teaching-Box systems (Erickson et al., 2017).

Important considerations have to be made when reporting classification results. To avoid overestimated values, it is always recommended to separate the data into training and validation sets so that results on new data can be reported. When the dataset is sparse, resampling approaches like cross-validation or bootstrapping are recommended (Larroza et al., 2016). With cross validation, one first selects a subset of examples for training and designates the remaining examples to be used for testing. Training proceeds and the learned state is tested. This process is then repeated, but with a different set of training and testing examples selected from the full set of training examples (Erickson et al., 2017). For unbalanced data, i.e., data containing more normal than abnormal tissues, it is suggested to report results using the AUC of the ROC instead of the overall accuracy or misclassification rate (Larroza et al., 2016).

1.8.5 Statistical and Radio-informatics Analyses

Analysis within radiomics must involve appropriate approaches for identifying reliable, reproducible findings that could potentially be employed within a clinical context. Applying the existing bioinformatics “toolbox” to radiomic data is an efficient first step since it eliminates the necessity to develop new analytical methods and advantages accepted and validated methodologies. Radiomics-specific analysis issues still exist. Some of the more significant methods or developments from the bioinformatics toolbox include: 1) multiple testing issues 2) supervised and unsupervised analysis, and 3) validating biomarker classifiers.

Another important analytical consideration is the incorporation of clinical and patient risk factor data since they may have a causal effect or correlation with image features or they may

confound statistical associations. Thus, synergizing biostatistics, epidemiology, and bioinformatics approaches is necessary to build robust and clinically relevant predictive models relating image features to phenotypes or endpoints (Kumar et al., 2012).

2. HYPOTHESIS AND OBJECTIVES

2.1 Work Hypothesis

The hypothesis of the present work is the following:

- It is possible to identify and develop quantitative imaging biomarkers from muscle ultrasound images for the identification of subjects at risk of frailty (pre-frail) or frail with the aid of machine learning texture analysis.

2.2 Objectives

2.2.1 General Objective:

The general objective is to identify possible quantitative imaging biomarkers from muscle ultrasound images for the identification of subjects at risk of frailty (pre-frail) or frail with the aid of machine learning texture analysis.

2.2.2 Specific Objectives:

[Objective 1] To identify and prioritize potentially useful Quantitative Imaging Biomarkers.

[Objective 2] To develop simple, reproducible, and cost-effective quantitative imaging biomarkers in the clinical context of frailty phenotype.

[Objective 3] To estimate performance of clinical quantitative imaging biomarkers and asses its ability to distinguish subjects with frailty or at risk of frailty from subjects that are non-frail.

[Objective 4] To assess the intrinsic (e.g. precision, accuracy, sensibility and specificity) properties on its specific characteristic (e.g. mechanisms, processes, parameters) of each quantitative imaging biomarkers developed and drive their potential for implementation in screening, baseline evaluation, and/or definition of outcomes.

[Objective 5] To determine the clinical applications of quantitative imaging biomarkers for secondary outcomes (morbidity and mortality), and mayor covariates (demographics, anthropometrics, health behaviour and risks, hospitalization, emergency and primary care visits).

3. MATERIALS AND METHODS

3.1 Materials

The clinical phase of the present study was carried out in the Consorcio Hospital General Universitario de Valencia (CHGUV). In this phase, the following materials were used:

3.1.1 Provided by the Research Center:

- Ultrasound Machine (Model LOGIC S7 Expert, General Electric, USA), located in booth 32, 1st floor, Pavilion A. Clinical section of Ultrasound, Department of Radiology, CHGUV (Figure 3.1).
- Gel/lubricant for performing ultrasounds.
- Napkins for cleaning the patient after applying the gel.
- Examination bed, exterior corridor of ultrasound booth, and ultrasound booth (Figure 3.2).
- Nursing service to assist patients before and after the ultrasounds, to clean them, help them dress, clean the booth, and the ultrasound machine after each patient.
- Administration staff (secretary) and computer program for the citation of patients.
- Electronic programs for image archiving (PACS) and patient control (Connect Hall).

Figure 3.1 Ultrasound machine

3.1.2 Acquired by the Researcher:

- Informed consent form (Annex 1).
- Samsung 22 inches laptop.
- Handheld digital dynamometer (Trailite Steiner, TL-LSC100 Coesfeld, Germany; Figure 3.3).
- SECA digital precision balance, model 803, 150Kg capacity, to determine the patients' weight.
- SECA wall height measuring device for determining the height. Measuring range: 0-220cm, weight: 202g.
- Chronometer Casio Unisex HS-3V-1RET.
- Marked distance of 4.6 meters (m) in length (exterior corridor of ultrasound booth, Figure 3.2).

Figure 3.2 Exterior corridor of the ultrasound booth and examination bed

- Rating scales:
  - Fried frailty phenotype scale (Annex 2).
  - Older People Quality of Life Questionnaire (Annex 3).

- Folders: to archive documents from each patient in the study including informed consent, questionnaires, copy of the report of the muscle ultrasound, among others.
- Paper sheets: for photocopies and printed inform consents.
- Pencils and felt pens.

Figure 3.3 Handheld digital dynamometer

3.2 Study Subjects

The study was conducted on humans and adhered to the principles of bioethics included in the Declaration of Helsinki and the relevant Spanish legislation. The approval of the research committee (CI by its Spanish acronym) and the clinical research ethics committee (CEIC by its Spanish acronym) of the CHGUV were obtained (Annex 4). All participants were informed of the experimental procedures and the purpose of the study. Each patient gave written informed consent before entering the study (Annex 1).

The **inclusion criteria** were the following:

- For the experimental group - Individuals aged equal to or greater than 60 years-old, able to walk independently, including the help of a cane, walker or similar assistance device. Men and women were included alike.
- In addition, men and women, between 20 and 59 years-old were recruited for the control group, given that there is a peak of muscular development within this age group, measured by the thickness of the muscle by ultrasound (I. M. Arts, Pillen, Overeem, Schelhaas, & Zwarts, 2007).

The **exclusion criteria** were the following:

- Patients suffering from neuromuscular disorders, acute or chronic disease that prevents the measurement of force with a dynamometer or would alter the muscle architecture.
- Oncological patients undergoing chemotherapy or radiotherapy; patients with previous cancer, either stable or cured were included.

- Institutionalized patients or unable to go to the research center using their own means of transportation.
- Severe dementia that impedes or influences the patient's ability to understand the informed consent and/or the study questionnaire.

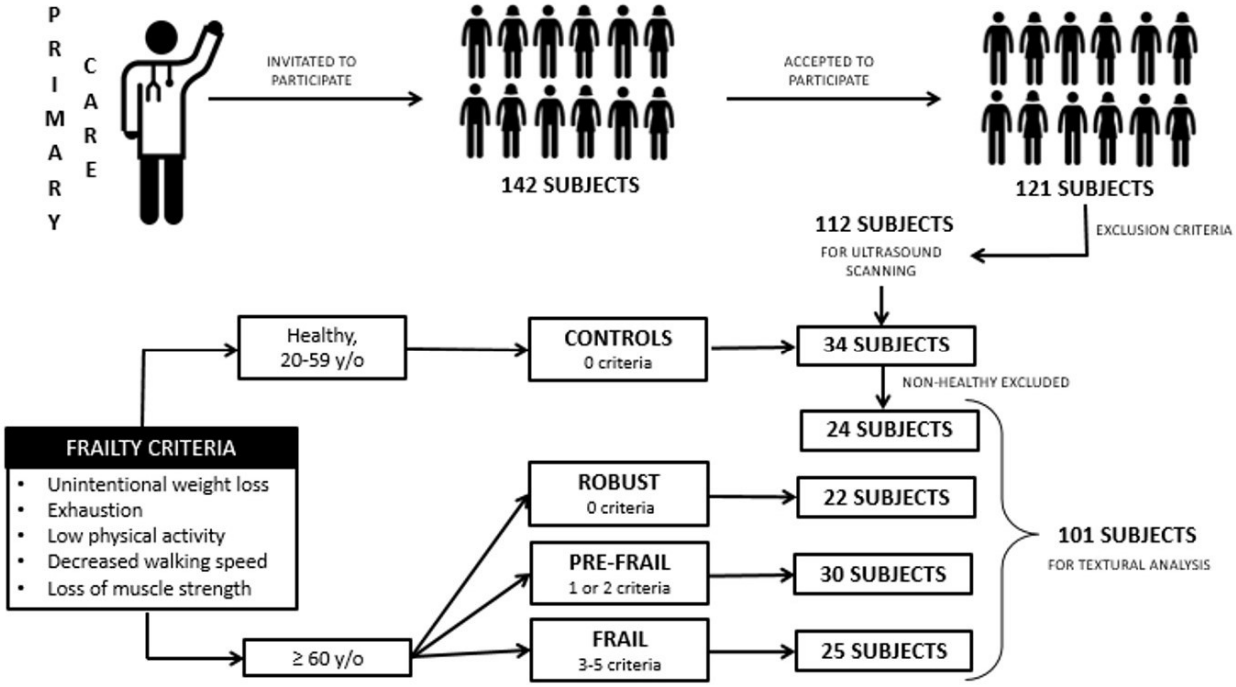

Figure 3.4 Report flow of participants through the study

Patients referred from primary care, who consecutively attended to an ultrasound appointment in the Ultrasound Section of the Radiology Department of the **CHGUV**, were invited to participate. One hundred forty-two patients were invited to the study and 121 accepted to participate. Of those, only 112 individuals fulfilled all inclusion criteria and no exclusion criteria. Blinded ultrasound measurements, frailty evaluation and quality of life questionnaire were performed in on all 112 of them. Eleven control subjects were excluded from the statistical analysis because frailty evaluation and/or ultrasound images classified them as frail, leaving 101 participants for this study (Figure 3.4). During the follow-up period, we determined that these individuals had associated diseases that probably altered their muscle structure and echo intensity, or secondary symptoms that resulted in positive frailty criteria, not known by them at the time of the ultrasound examination. Figure 3.5 shows a typical image of a control subject and of two subjects with altered echo intensity and muscle structured that were excluded from the study. Among the associated diseases, there were

severe hepatopathy, obesity, depression, chronic obstructive pulmonary disease (COPD), rheumatoid arthritis, polymyositis, and cardiopathy with hyperlipidemia.

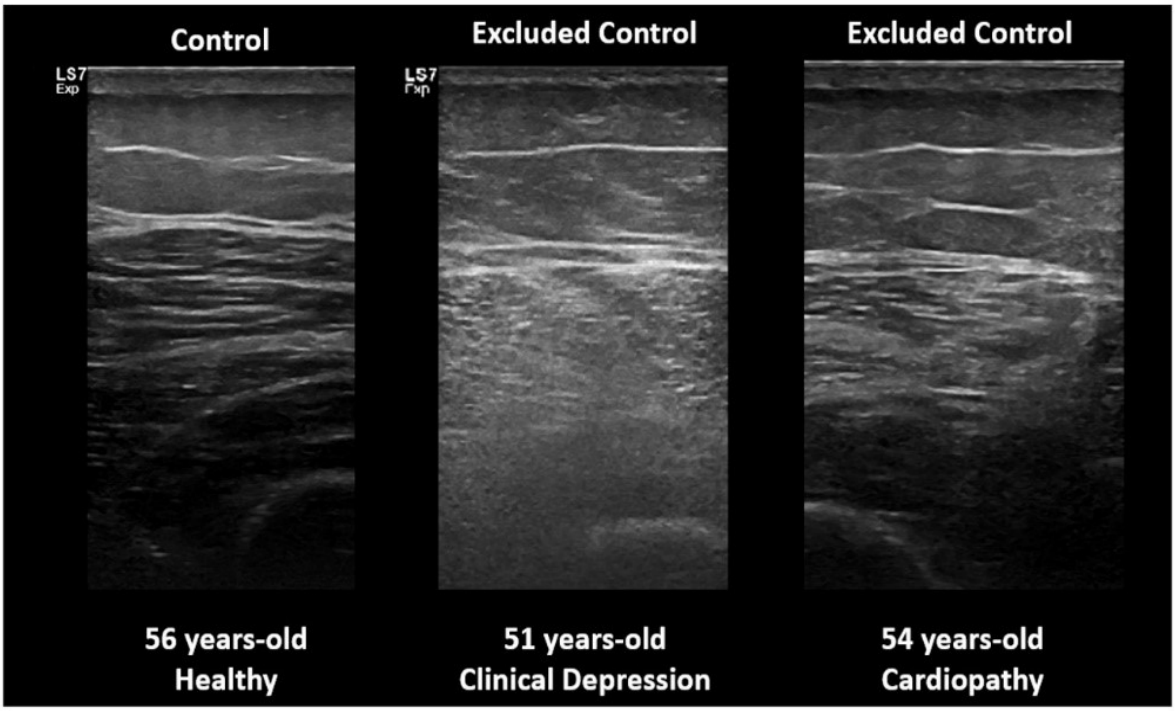

Figure 3.5 Examples of ultrasound images of controls and excluded controls

3.3 Study Design and Setting

This was an experimental prospective-retrospective study that was performed in an outpatient clinic setting. Patients were referred from primary care from November 1st of 2014 to February 28th of 2015. Baseline comorbidities were assessed after the ultrasound examination and there was a follow-up for development of other comorbidities or death for up to two years (until March 31st of 2017).

The project was developed in the Radiology Department of the CHGUV, where the experimental muscle ultrasound was performed. At the conclusion of the ultrasound image acquisition, a muscle strength measurement was performed with a dynamometer and then the main researcher filled in an electronic questionnaire with the epidemiological data, the frailty phenotype criteria, and the quality of life for older people questionnaire. We decided to add the section on quality of life of the patient to assess the benefits of the proposed intervention and show evidence in terms of the patient's health status, which in the future can serve to guide prevention and treatment decisions

in the elderly population (Rizzoli et al., 2013). We believe this to be of interest to assess public health measures.

Subjects 60 years-old or older referred from primary care participated in the experimental group. This group was subdivided according to their frailty phenotype, following the Fried criteria (Fried et al., 2001). The frailty phenotype consists of the accumulation of deficits in five domains: unintentional weight loss, increased tiredness or exhaustion, low physical activity, slow walking speed and muscle weakness. Patients were divided into robust, pre-frail or frail based on their responses to three questions, gait speed, and handgrip strength measured by a digital hand dynamometer (Trailite Steiner, TL-LSC100 Coesfeld, Germany). We also included a control group with subjects from 20 to 59 years of age to be able to have true comparison of healthy individuals for the robust group and to add rigor to the study.

Each subject's comorbidity, risk factors and number of visits to primary care, emergency department and hospitalizations at the time of the ultrasound evaluation (baseline), were searched in their electronic medical history and recorded. Two years after the baseline this process was repeated to determine if they developed new comorbidities and if they were alive or dead.

This was followed by the post-processing of the ultrasound images with a two-dimensional (2D) texture analysis of 43 features. Texture analysis provides an objective and quantitative assessment of muscle heterogeneity by analysing the distribution and relationship of pixel gray levels in the image (Lubner et al., 2017). The values of echo intensity were obtained using the MatLab program (R2017b; The MathWorks Inc., Natick, MA, USA). Texture analysis was performed in the selected muscle ROI. Statistically based methods were used to extract the predetermined features and predictive models were developed to determine the best features for the diagnosis of frailty.

In texture analysis, the discriminative power of the predictive model is dependent on having sufficient data. Texture analysis can be performed with as few as 100 patients (Gillies et al., 2016). Our study sample was calculated to meet this criterion. No other sample calculations were performed.

Table 3.1 summarizes the different activities of the study, the content of each of them, and when they were performed.

Table 3.1 Summary of the Activities of the Study		
ACTIVITY	**DESCRIPTION**	**PERIOD**
Phase 1	Drafting of the protocol, including the preparation of the documents requested by the Foundation of the CHGUV and its Ethics Committee.	June to August 2014.
Phase 2	Evaluation and approval of the protocol by the Foundation of the CHGUV and its Ethics Committee.	September to October 2014
Phase 3	Performing muscle ultrasound scans, and carry out patient's questionnaires. Recording the information obtained in an electronic database.	November 2014 to February 2015.
Phase 4	Patient's follow-up for comorbidities and death.	March 2015 to March 2017.
Phase 5	Post-processing of ultrasound images and data collection on texture analysis.	April 2017 to November 2017.
Phase 6	Statistical analysis and drafting of the main results.	December 2017 to April 2018
Phase 7	Writing final doctorate work and conclusion of the project.	May to September 2018.

We proceeded to develop each activity, with its corresponding methods in the following section.

3.4 Methods of Measurement

3.4.1 Muscle Ultrasound Scanning and Measurements

The thickness of the tissues of the anterior compartment of the thigh was measured by ultrasonography (Model LOGIC S7 Expert, General Electric, USA) in mode B obtaining transverse images with a 6-15Hz linear transducer. During the scanning of the patient, the gain remained constant at 54dB and the frequency at 12Hz. This is the gain and frequency of choice for muscle studies, which provide good image resolution of muscle structure. Both parameters were not modified between patients nor during the scanning of the patients. The focal point or zone is the parameter that tells the ultrasound the depth at which you would like the highest resolution (Lutz & Elisabetta Buscarini, 2011). The focal zone is typically positioned at or just below the object being evaluated, in this study was adjusted to each patient *rectus femoris* depth.

The procedure was carried out with the patient in supine, legs extended and relaxed. It was specified that the musculature being explored should not be tense during the scanning. The anterior compartment of the right thigh (arbitrarily chosen for the exploration), was scanned applying enough contact gel and avoiding excessive pressure during the measurements, thus avoiding the interference with the actual thickness of the assessed muscle. The measured site was the midpoint between the superior border of the *patella* and the anterosuperior *iliac spine*,

with the transducer positioned perpendicular to the longitudinal axis of the femoral quadriceps (Figure 3.6). In this position, the images were frozen and the muscle thickness and the thickness of the subcutaneous fat tissue were measured using the caliper. The muscle thickness corresponded to the sum of the thickness of the *rectus femoris* and the *vastus intermedius* muscles (Figure 3.7); while the subcutaneous fat thickness corresponded to the distance between the femoral rectus fascia and the dermis (Y. Watanabe et al., 2013). Three measurements were obtained for each patient and the average was used in the data analysis. To assess test–retest reliabilities of the person scanning the patients, intra-class correlation coefficients (ICC) were evaluated for muscle thickness and subcutaneous fat thickness. The ICC values were 0,969 (95%CI: 0,957 -0,992) for muscle thickness and 0,992 (95%CI: 0,984 -0,998) for subcutaneous fat thickness.

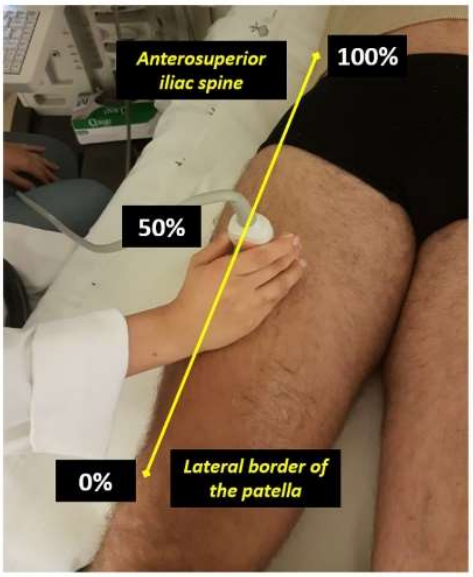

Figure 3.6 Transducer placement in the right leg of the patient

The images made during the ultrasound scanning were stored in the Picture Archiving and Communication System (PACS) of the hospital. Each muscle ultrasound examination consisted of seven images. There were three cross-sectional images that corresponded to the measurements, as already described. We also acquired three more cross-sectional images and one longitudinal image, all corresponding to the anterior compartment of the right thigh at the level specified in figure 3.6, in order to perform texture analysis of the echo intensity of a ROI selected in the muscle. A single researcher with a year experience in

ultrasound scanning made the ultrasound measurements and was blinded to the frailty status of the patients.

At the conclusion of each exploration, a radiological report was written and saved to each patient medical history. The ultrasound measurement template was used with the objective to have an uniform report and improve the efficiency of the ultrasound scanning (Annex 5).

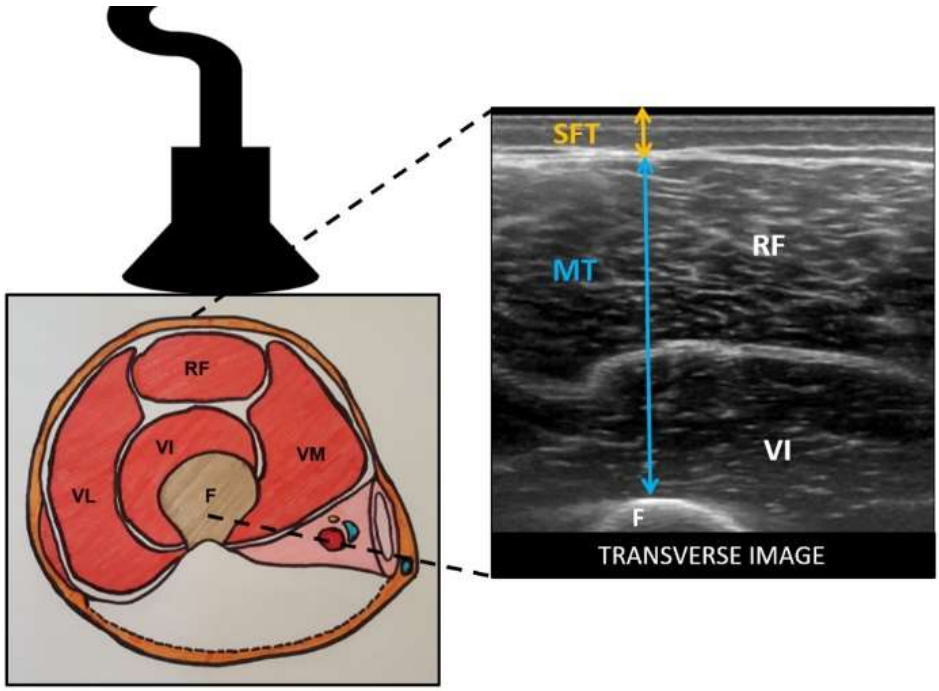

Figure 3.7 Measurement of muscle and subcutaneous fat thickness

3.4.2 Epidemiological and Anthropometric Data

The first section of the electronic questionnaire included questions on general epidemiological information (date of birth, age, gender, etc) which can be seen in annex 6. Weight and height of the subjects were measured to calculate body mass index (BMI).

The weight was determined after the ultrasound scanning in the same booth, indicating the subjects to step on the scale barefoot. The weight was measured in kilograms. The scale was calibrated before the first patient each time ultrasound scanning was scheduled.

A measuring rod was placed in one of the walls of the ultrasound booth to measure all subjects. The height was measured first by positioning the subjects correctly. We explained subjects to

stand with their feet together, barefoot and with their back to the wall (there must be contact with it at the following points: head, dorsal area of the back, and gluteus). A ruler was use for the measurement and lower it until it touches the head. We then recorded the height.

The BMI was calculated by dividing the patient's weight (in kilograms) by height (in meters) squared.

$$BMI = weight/height^2$$

3.4.3 Frailty Phenotype Criteria

The second section of the patient's electronic questionnaire was the frailty phenotype criteria (Annex 6). For the assessment of frailty phenotype, the criteria proposed by Linda Fried and collaborators in 2001 were used (Fried et al., 2001). This includes unintentional weight loss, feeling of general exhaustion, low level of physical activity, slow walking speed, and muscular weakness. The criteria are detailed in Annex 2; however, the methods used to evaluate each criterion are described below:

- *Unintentional weight loss*: It was defined as an unintentional weight loss of 4.5 Kg or more during the past year. This information was obtained through the question, "In the last year, have you lost more than 4.5 Kg unintentionally (not due to diet or exercise)?"
- *Increased tiredness or exhaustion*: This was self-reported by the subject, answering affirmatively the following questions: "I feel that everything I did was a great effort in the last 3 or 4 days" and/or "In the last month, I have too little energy to do things I like to do".
- *Low level of physical activity:* A positive response to either two statements: "I do not do physical activity" or "I do no more than one or two walks per week".
- *Slow walking speed*: Defined as a speed lower than predetermined values according to the sex and height of the subject (Annex 2) in the speed test of the march at a distance of 4.6 meters, in accordance with the provisions of the "Short Physical Performance Battery" (Guralnik, Seeman, Tinetti, Nevitt, & Berkman, 1994). Aids like cane, walker or crutches were allowed for walking. Since the goal was to determine their usual walking speed, subjects were not encouraged to go fast. To avoid the biases of the reaction time, the initial acceleration, and the possible final deceleration, both at the exit of the test and at its arrival, the exit and arrival signals were located 0.50 m away from the start and the end of the footage tested (4.6 m). These signals were marked with adhesive tapes on the ground. It was explained to the subjects what the test consists of: that they "walk as he normally does on the street", "naturally" and that they do not

stop until crossing the marks. A test demonstration was made and subsequently, the subjects performed once and the principal investigator timed with a chronometer in seconds.

- *Muscle weakness:* The contraction force or muscle grip of the dominant hand of the patients was measured (Cooper et al., 2013; Cruz-Jentoft et al., 2010) with a hand-held digital dynamometer (Trailite Steiner, TL-LSC100 Coesfeld, Germany) in kilograms (Kg). The patients were seated with the elbow flexed at a right angle along the body, the wrist in the neutral position and the hand on the handle of the dynamometer (Massy-Westropp, Gill, Taylor, Bohannon, & Hill, 2011). In the initial position, the subject took the dynamometer and after explaining what the test consists of (it was explained that it is not about keeping it as long as possible, but making as much pressure as possible), it is instructed to perform a test. Submaximal pre-test was performed to familiarize patients with the device. Then each subject was asked to make three attempts with their maximum sustained effort for 15 seconds, with 30 seconds of recovery between each measurement. During the test patients were encouraged to do their best effort. Cases in which the patient did not have dominant laterality, the measurement was made in the right hand. For data analysis, the average of the three attempts was used, and muscle weakness was defined as a value in Kgs below predetermined values, adjusted for sex and BMI (Kg/m^2), as shown in Annex 2. The ICC for the muscle strength measurement was 0,989 (CI95%: 0,982 - 0,993).

A point was assigned to each positive criterion, constructing a final score formed by the sum of the five criteria. According to this score, subjects were classified as follows:

- Robust: 0 points
- Pre-frail: 1 or 2 points
- Frail: 3 or more points

Although there are several scales to measure frailty, and still none is recognized as the Gold Standard to diagnose this clinical syndrome, the phenotype developed by Fried is the most widely used and accepted in the literature (Bouillon et al., 2013). The reason why this scale was chosen for the study was so that our results can be comparable with those of other studies.

3.4.4 Quality of Life for Older People Assessment

The assessment of quality of life was based on the use of the generic questionnaire for the elderly, known as OPQOL-35 (Older's People Quality of Life). This was the last section of the

patient´s electronic questionnaire (Annex 6). The questionnaire consisted of 35 questions that evaluated eight domains: life in general (4 items), health (4 items), relationships and social participation (5 items), independence, control over their lives and freedom (4 items), home and community (4 items), emotional and psychological state (4 items), financial circumstances (4 items), and recreational activities and religion (6 items) (Bowling, 2009). A Likert scale was used for each question, the minimum value of the questionnaire being 35 (bad, it cannot be worse) and a maximum of 175 (well, it cannot be better). The questionnaire was translated from English to Spanish by the main researcher. A full copy of the original document in English can be seen in Annex 3 (Spanish version in Annex 6).

There is no widely accepted standard measure of quality of life for use with older populations. The OPQOL is a measure of quality of life that covers the domains nominated by, and initially piloted with, a sample of people aged 65+. It is the first multidimensional measure of quality of life, which was directly derived from people's views of what gives their lives quality and what takes quality away (Bowling, 2009). The reason why we decided to employ this survey over others like the WHOQOL- OLD or CASP-19 was that overall, the OPQOL meets the thresholds for acceptability, internal consistency, and construct validity in population samples of older people (Bowling, 2009).

3.4.5 Collection of Data and Coding

The above information corresponds to the patient's electronic questionnaire that can be read in full in the Annex 6. This information was registered electronically through the free program Magpi (Magpi, Version 4.0.3, USA http://home.magpi.com/). The program allowed us to develop a digital database in the cloud. This database was synchronized via the app of the mobile phone of the principal investigator. The principal investigator collected this data via interview with the patients after the ultrasound scanning. This allowed us to collect and code the information at the same time while the patients were being interviewed.

3.4.6 Patient's Medical history, Comorbidities and Mortality:

From each patient´s electronic medical history the following information was extracted. The presence or absence of hypertension, hyperlipidemia, diabetes mellitus, COPD, hearing or visual impairment developed in the last 6 months, Parkinson disease, previous stroke, congestive heart failure according to Framingham criteria (McKee, Castelli, McNamara, & Kannel, 1971), heart disease (that is not heart failure nor myocardial infarction), myocardial infarction, renal disease (moderate to severe renal failure), previous cancer, arthritis or osteoarthritis, anxiety syndrome,

depression, previous fractures or osteoporosis, liver disease or hepatopathy, dementia or memory loss, connective tissue disease, hemiplegia, neoplasm, leukemia, malignant lymphoma, solid metastasis, acquired-immuno deficiency syndrome (AIDS), and peripheral vascular disease. We also searched for risk factors, including smoking, alcohol consumption, falls and obesity. The last one was confirmed or excluded based on patients´ BMI obtained previously. In addition, an index of comorbidities was calculated according to the Charlson Comorbidity index (CCI) (Charlson, Pompei, Ales, & MacKenzie, 1987; Quan et al., 2011; Radovanovic et al., 2014) using an online calculator (https://www.mdcalc.com/charlson-comorbidity-index-cci). This index shows estimated 10-year survival, expressed in %. Finally, we recorded the number of visits to a primary care physician, to the emergency department, and of hospital admissions in the last six months.

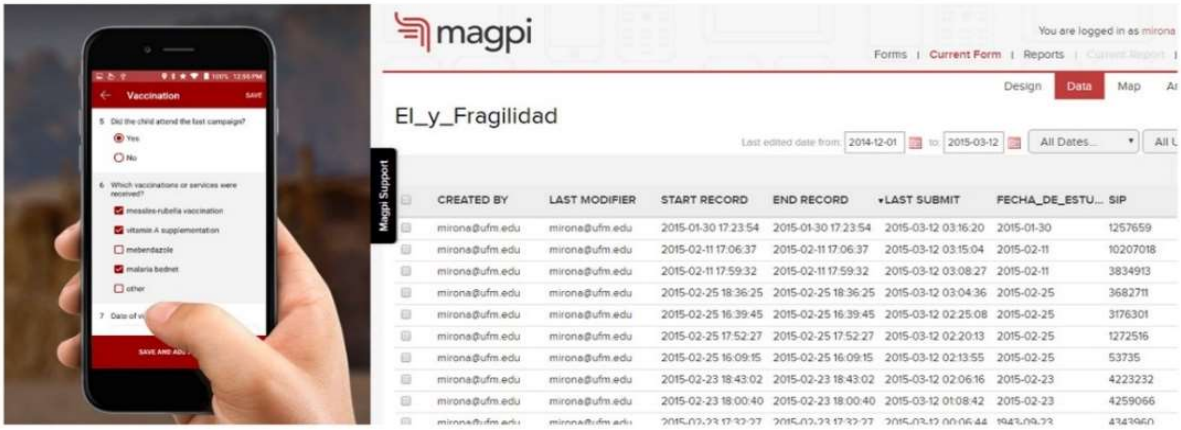

Figure 3.8 Mobile data collection and screenshot of the program

Two years after the ultrasound examination, we reviewed the subject's medical records again and did a follow-up on the same variables described earlier. We also determined if the patient was still alive or dead and recorded the information. Finally, the date of last contact within the hospital network or the date of death was recorded.

3.4.7 Texture Analysis Process

Texture analysis can provide an objective quantitative assessment of frailty phenotype by analysing the distribution and relationship between the gray levels of the ultrasound images. The application involves a process that consists of six steps: image acquisition, ROI segmentation, ROI pre-processing, feature extraction, feature selection, and classification Figure 2.9). The texture outcome can be considerably affected depending on the methodology used throughout the whole process; the next section will describe the process in detail.

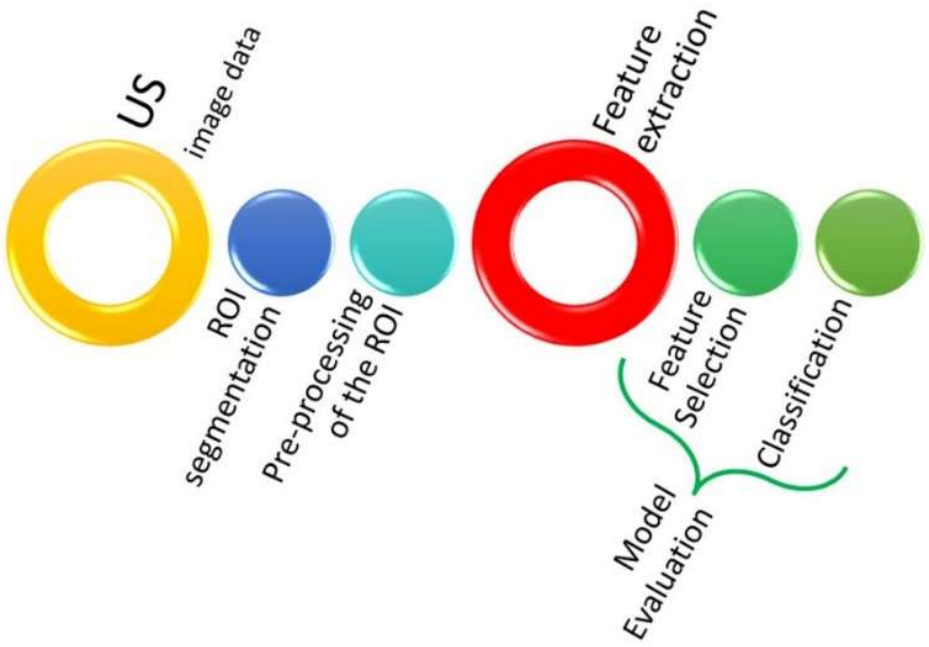

Figure 3.9 Main steps for ultrasound classification using texture analysis

3.4.7.1 Ultrasound Image Data

A post-image acquisition analysis was undertaken. DICOM (Digital Imaging and Communications in Medicine) images of the muscle ultrasound scanning were downloaded from the hospital PACS and saved into the principal investigator laptop. The ultrasound protocol for image acquisition has been described in a previous section (see 3.4.1 Muscle ultrasound scanning and measurements).

3.4.7.2 ROI Segmentation

The ultrasound images of *rectus femoris* and *vastus intermedius* muscles were segmented in 2D using a software tool developed in MATLAB (R2017b; The MathWorks Inc., Natick, MA, USA) specifically for this study (Figure 3.9). The software loads all the seven images corresponding to a subject in DICOM format. Before drawing the ROI, the scanning plane (axial or sagittal), the muscle (*rectus femoris* or *vastus intermedius*) and patient group (control, robust, pre-frail and frail) were selected.

The segmentation process was performed by a radiologist with three years-experience in muscle ultrasound. Each muscle ROI was manually segmented in 2D from the axial and sagittal images of both muscles. The segmented ROI excluded bone, fatty tissue, and muscle fascia, and for the *rectus femoris* muscle, its internal tendon when possible too. An example

of ROI muscle segmentation can be seen in figure 3.10. All ROIs were measured to determine their area in square millimetres (mm^2) and determine if the size was consistent between the four groups (frail, pre-frail, robust and control). Since robust and control subjects share similar characteristics they were analysed as one group. The same was done for pre-frail and frail subjects. This was based on a previous published article on the subject (Mirón Mombiela et al., 2017). Wilcoxon signed rank test was used to determine the p-value between the groups. The average size of the ROIs of each muscle in both planes can be seen in the table 3.2, as well as the p-values. This is important because large differences between the ROI sizes of the groups can influence the texture analysis. The ROI sizes were consistent between groups and the study could proceed on to the next step of textural analysis.

Figure 3.10 Screenshot of software tool for segmentation

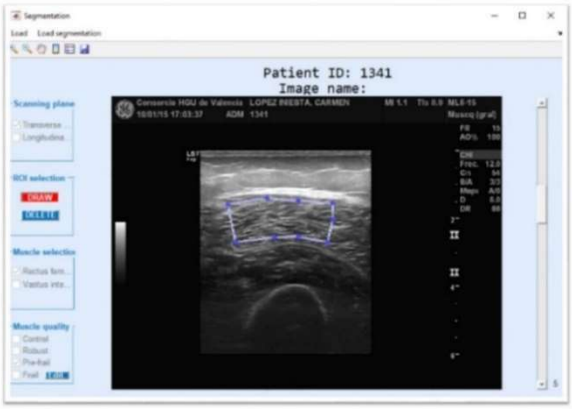

Figure 3.11 Example of a ROI segmentation

3.4.7.3 Pre-processing of the ROI

Several pre-processing techniques have been proposed in order to minimize the effects of acquisition protocols. The main purpose of these pre-processing techniques is to put all ROIs in the same condition so features extracted from them represent essentially the texture being examined and improve discrimination (Larroza et al., 2016). The image pre-processing applied depends on the imaging modality used. It usually includes interpolation, normalization and quantization/reduction of gray-levels.

Image resolution has been reported to be an influential factor for the discrimination of texture analysis (Jirák, Dezortová, & Hájek, 2004; Larroza et al., 2016; Mayerhoefer, Szomolanyi, Jirak, Materka, & Trattnig, 2009). Resolution in ultrasound imaging is affected by several factors (gain, frequency, focusing, etc) before the final image is stored. These

parameters are modified at the moment of scanning with the objective of improving the image resolution (see section 3.4.1 Muscle ultrasound scanning and measurements). The spatial resolution information was extracted from the DICOM file header. The ultrasound images used in this study had resolutions between 0.07 x 0.07mm^2 to 0.16 x 0.16mm^2 (0.07mm, 0.08mm, 0.09mm, 0.10mm, 0.12mm, 0.14mm y 0.16mm), with 256 gray levels. From previous experience, we concluded that the resolution of the images was acceptable for feature extraction and analysis. Therefore, interpolation of the images was not necessary.

Table 3.2 Regions of Interest Area Size in mm^2			
RF AXIAL (p = 0.06)		**VI AXIAL (p = 0.08)**	
Control/Robust mean (SD)	*Pre-frail/Frail* mean (SD)	*Control/Robust* mean (SD)	*Pre-frail/Frail* mean (SD)
285.76 (88.00)	256.79 (105.94)	240.03 (67.84)	288.03 (81.40)
RF SAGITTAL (p = 0.06)		**VI SAGITTAL (p = 0.34)**	
Control/Robust mean (SD)	*Pre-frail/Frail* mean (SD)	*Control/Robust* mean (SD)	*Pre-frail/Frail* mean (SD)
289.36 (101.56)	256.76 (101.06)	281.13 (104.5)	258.08 (91.89)

Abbreviations: RF: *Rectus femoris*; VI: *Vastus Intermedius*; SD: Standard Deviation.
Wilcoxon signed rank test use for the statistical analysis of this sample.

We also concluded that the quantization or reduction of gray-level was not necessary for the ultrasound images. Ultrasound images have 256 levels of gray. This is mostly necessary in the MRI, since there are between 1024 and 4096 levels of gray. However, prior to the computation of texture features, the intensity range of the ROIs was quantized from 256 gray levels to a lower number of gray levels (16, 32, 64 and 128) because this improves the signal-to-noise-ratio (Gibbs & Turnbull, 2003). All computations were done with these four gray levels. The purpose was to determine if any gray level outperforms the other, as there is no published literature on ultrasound texture analysis on this subject.

3.4.7.4 Feature Extraction

Feature extraction implies the computation of texture features from the predefined muscle ROIs. To extract features we used the MATLAB toolbox *Radiomics* implemented by Vallières and colleagues (Vallières, Freeman, Skamene, & El Naqa, 2015). The toolbox utilizes statistical-methods for the feature extraction and it allows extracting 43 texture features for the 2D texture analysis. Three features were extracted from the intensity histogram (first-order statistics) and the other 40 features were extracted from second-order statistical methods: from the gray-level co-occurrence matrix (GLCM) 9 features were derived, from the gray-level run-length matrix (GLRLM) 13 features, from the gray-level size zone matrix

(GLSZM) 13 features and from the neighbourhood gray-tone difference matrix (NGTDM) only 5. The second-order statistical features applied in the study met the criterion of rotation invariability. To this end, only one GLCM, GLRLM, GLSZM, and NGTDM per muscle was computed (Ortiz-Ramon, Larroza, Arana, & Moratal, 2017). Finally, all texture features were standardized to zero mean and unit variance to avoid model computation being affected by differences in the feature scales (Kuhn & Johnson, 2013). The full list of the texture features used in this study can be found in table 3.3. Information of each method and the corresponding features can be seen in Annex 7.

Table 3.3 List of Texture Features Used in the Texture Analysis

GROUP	NUMBER	*TEXTURE ANALYSIS VARIABLES*
Intensity histogram or first-order statistics	3	Variance
		Skewness
		Kurtosis
Gray-level co-occurrence matrix (GLCM)	9	Energy
		Contrast
		Entropy
		Homogeneity
		Correlation
		Sum Average
		Variance
		Dissimilarity
		Auto-Correlation
Gray-level run-length matrix (GLRLM)	13	Short Run Emphasis
		Long Run Emphasis
		Gray-Level Nonuniformity
		Run Length Nonuniformity
		Run Percentage
		Low Gray-Level Run Emphasis
		High Gray-Level Run Emphasis
		Short Run Low Gray-Level
		Short Run High Gray-Level
		Long Run Low Gray-Level
		Long Run High Gray-Level
		Gray-Level Variance
		Run-Length Variance
Gray-level size zone matrix (GLSZM)	13	Small Zone Emphasis
		Large Zone Emphasis
		Gray-Level Nonuniformity
		Zone-Size Nonuniformity
		Zone Percentage
		Low Gray-Level Zone Emphasis
		High Gray-Level Zone Emphasis
		Small Zone Low Gray-Level Zone Emphasis
		Small Zone High Gray-Level Zone Emphasis
		Large Zone Low Gray-Level Zone Emphasis
		Large Zone High Gray-Level Zone Emphasis
		Grey-Level Variance
		Zone-Size Variance

Neighbourhood gray-tone difference matrix (NGTDM)	5	Coarseness
		Contrast
		Busyness
		Complexity
		Strength

3.4.7.5 Feature Selection and Classification: Predictive Models of Evaluation

Six different predictive models were studied to evaluate the discrimination power of the 2D texture features: naïve Bayes classifier (NB), k-nearest neighbours (k-NN), multilayer perceptron (MLP), random forests (RF), support vector machine with linear kernel (SVM_L) and radial kernel (SVM_R). We chose six common classifiers from different predictive families to see which of them provides the best classification accuracy and to verify if there are noteworthy differences between 2D texture analysis using different approaches.

A nested cross-validation (CV) structure was used to evaluate the performance of each model (Figure 3.12) without holding out some of the samples as an independent test set. We used this approach because the sample size of our dataset is relatively small and, in this situation, it is recommended to use every sample for model building. Proper estimates of model performance can be achieved using resampling methods when the number of samples is not large (Kuhn & Johnson, 2013).

Leave-group-out CV (LGOCV) was applied in the outer loop. This resampling method randomly divides the data set into a training and a test set a total on N times, forming N groups. Each group is examined independently: the training set of a group is used to build the model and then this model is evaluated using the test set of the same group. At the end, the classification results provided by the estimates of all groups are averaged. In this study, a value of N = 100 groups was chosen to obtain results with low variance and consequently to decrease the uncertainty of the performance estimates (Kuhn & Johnson, 2013). In each group, 25% of the dataset was randomly selected as the test set and the remaining 75% was used as the training set. Model performance was evaluated using the area under the receiver operating characteristic (ROC) curve averaged over groups´ estimates (mean ± SD).

The feature selection step was computed within the model building process using the training set of each group. This process was not computed as an independent step to avoid over fitting. The two methods were used for the feature selection, one a filter method and the

other one a wrapper method. The filter feature selection method based on the p-value provided by a Wilcoxon signed rank test, was employed to generate a ranking of the features with the most discriminative power. This method evaluates the statistical significance of each feature independently, without analysing the relation between features and without involving any predictive model (Kuhn & Johnson, 2013). The main drawback of the filter methods is that the feature selection is based on the intrinsic information of the training data and does not consider the predictive capability of a certain subset of features. Wrapper methods take advantage of a classification algorithm and search the subset of features that provides optimal classification performance (Larroza et al., 2016). The recursive feature elimination (RFE), a wrapper, ranks the features by recursively training a classifier and removing the feature with the smallest ranking score. In this exhaustive search method, possible combinations of features were tested and those that yield the best discrimination are selected. In this study, we used the feature selection wrapper technique known as recursive feature elimination-support vector machine (RFE-SVM).

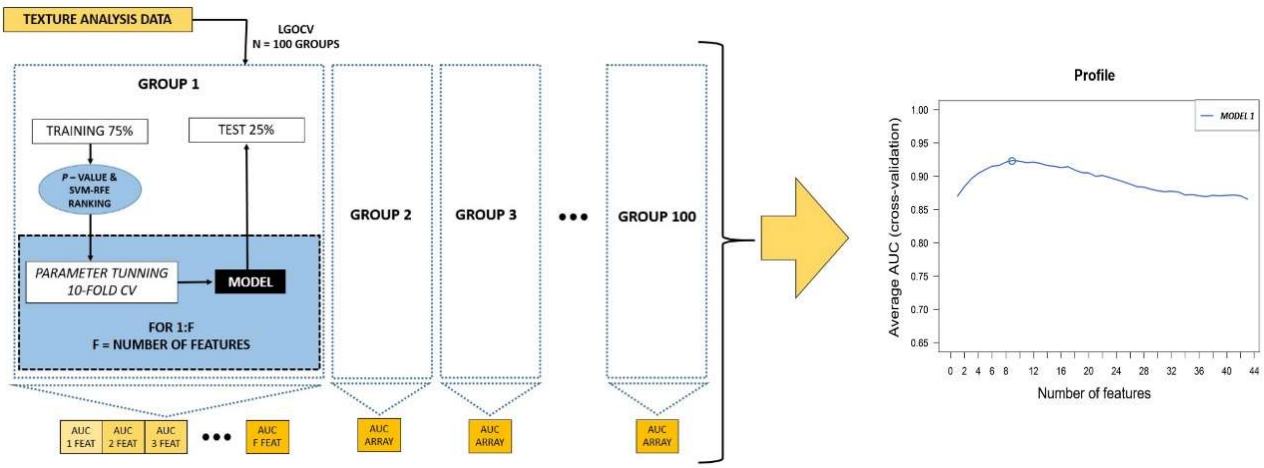

Figure 3.12 Structure of the nested CV process used to evaluate the different predictive models

Parameter tuning was computed using the training set of each group by performing an inner 10-fold CV loop. This step was performed F = 43 times in each group estimate: the ranked features provided by the feature selection step were progressively added one by one from most to least important. Then each feature subset was used to train the predictive model and to compute the AUC on the test samples of the same group. At the end, a total of F = 43 AUC values are provided in each group evaluation, one per each feature subset. The number of neighbors (*k*) in k-NN was selected from k ϵ {1, 3, 5, …, 15}. The number of variables

randomly sampled as candidates at each split (*mtry*) in RF was chosen from *mtry* ϵ {2, 4, 6, 8, 10, 12, 14}. The number of units in the hidden layer (*l*) of the MLP was selected from *l* ϵ {3, 5, 7, …, 15}. SVM cost parameter (C) was chosen from C ϵ $\{2^{-4}, \ldots, 2^{0}, \ldots, 2^{4}\}$.

This model evaluation process was implemented with the Caret package (Kuhn Max, 2008) in R version 3.2.5 (R Development Core Team, Vienna, Austria).

3.5 Statistical Analysis of the Data

Descriptive data is presented with mean ± standard deviation (SD) with the distribution of the data verified by the Kolmogorov-Smirnov normality test. To assess the differences in physical characteristics and the study variables according to sex, t-Student was used for parametric variables and Mann-Whitney for the non-parametric variables. The evaluation of the different variables of the study according to frailty phenotype and control group were determined using ANOVA for the parametric variables (followed by Bonferroni post-hoc test) and for the non-parametric Kruskal-Wallis test were used. Correlations were performed to investigate the relation between physical characteristics, ultrasound measurements, quality of life, frailty phenotype, comorbidities, risk factors, and texture features. We used coefficient of Pearson (r) for parametric data, Spearman's Rank for non-parametric data and Tau B of Kendal used for ordinal variables. The correlations were considered weak for the correlation coefficient of ± 0,01 to 0,35, moderate for ± 0,36 to 0,67, and strong for ± 0,68 to 1,00. To test the accuracy of muscle EI texture features the area under the ROC curve were assed. Frailty phenotype was dichotomized into non-frail (controls and robust group) and at risk of frailty or frail (pre-frail and frail groups) for the analysis. Stepwise multiple regression analysis was performed with the texture features of the best frailty predictive models, adjusted for the ultrasound characteristics, and the physical characteristics. A multiple logistic model was applied for outcome variables. To compare the reliability of all EI texture features in both muscles and in both planes, we performed intraclass correlation coefficient (ICC) and the Bland-Altman 95% limits of agreement. The ICC values were classified poor for values ≤0,20, fair for 0,21-0,40, moderate for 0,41-0,60, good for 0,61-0,80 and very good for 0,81-1,00. Statistical significance was defined as $P < 0,05$. We applied false discovery method by Benjamini & Hochberg as multiple comparisons were perform during the study. All statistical analysis, including the control group, were performed with SPSS version 24.0 for Windows (IBM SPSS, Inc., Chicago, IL).

4. RESULTS

4.1 Baseline Characteristics

The sample was composed of 101 patients, 46 were females and 55 males. Table 4.1 summarizes the physical characteristics (age, weight, height, BMI, gait speed and muscle strength), ultrasound measurements (muscle thickness and subcutaneous fat thickness), quality of life, and frailty phenotype according to sex. Each variable is shown with the mean and SD. The study sample is homogeneous regarding age, BMI, gait speed, muscle strength, and the values of quality of life according to sex. Note that frailty phenotype is also sex independent in this sample. Weight, height, subcutaneous fat tissue, and muscle thickness had statistically significant differences between men and women.

Table 4.1 Baseline Characteristics of the Sample According to Sex

Group	***Female (n = 46)***	***Male (n = 55)***	***Total (n = 101)***	***Statistical Test***
Variable	***Mean ± SD***	***Mean ± SD***	***Mean ± SD***	***P***
Physical Characteristics				
Age (years)	66 ± 16	64 ± 15	65 ± 15,14	0,665*
Weight (Kg)	70,7 ± 14,2	77,6 ± 13,0	74,4 ± 14,0	0,012*
Height (m)	1,58 ± 0,06	1,69 ± 0,07	1,64 ± 0,09	<0.001
BMI (kg/m ^{2})	28,4 ± 5,1	27,3 ± 4,1	27,8 ± 4,6	0,239
Gait Speed (s)	3,7 ± 1,0	3,5 ± 1,4	3,6 ± 1,2	0,076*
MS (Kg)	27,93 ± 11,76	25,95 ± 11,62	26,86 ± 11,67	0,375
Ultrasound Measurements				
SFT (cm)	1,53 ± 0,50	0,71 ± 0,23	1,08 ± 0,55	<0,001*
MT (cm)	2,36 ± 0,73	2,68 ± 0,67	2,53 ± 0,71	0,027
Quality of Life (A.U.)	119,09 ± 6,17	118,80 ± 7,00	118,93 ± 6,61	0,829
Frailty Phenotype	***N (%)***	***N (%)***	***N (%)***	0,222*
Control	11 (23.9)	13 (23.6)	24 (23.8)	
Robust	6 (13)	16 (29)	22 (21.7)	
Pre-frail	15 (32.6)	15 (27.3)	30 (29.7)	
Frail	14 (30.4)	11 (23.9)	25 (24.8)	

Abbreviations: SD: standard deviation; BMI: body mass index; MS: muscle strength; MT: muscle thickness; SFT: subcutaneous fat thickness; AU: arbitrary units.

* Variables without normal distribution, nonparametric tests used for the analysis.

There were 24 controls, 22 robust, 30 pre-frail and 25 frail patients. Table 4.2 shows physical characteristics (age, weight, height, BMI, gait speed and muscle strength), ultrasound

measurements (muscle thickness and subcutaneous fat thickness), quality of life, sex and frailty criteria distributed by the frailty phenotype and the control group. The data shows that there are statistically significant differences between age, height, BMI, gait speed, muscle thickness, and quality of life, depending on frailty phenotype. The weight and subcutaneous fat thickness were distributed homogeneously within the groups. In addition, females and males were homogenously distributed among the groups.

Table 4.2 also shows the number of positive criteria subjects had in each group, explaining how patients were classified in the study. For comparison reasons, we also applied the criteria to controls.

Table 4.2 Baseline Characteristics of the Sample According to Frailty Phenotype

Group	*Controls (n = 24)*	*Robust (n = 22)*	*Pre-frail (n = 30)*	*Frail (n = 25)*	*Total (n = 101)*	*Statistical Test*
Variable	***Mean ± SD***	***Mean ± SD***	***Mean ± SD***	***Mean ± SD***	***Mean ± SD***	***P value***
Physical Characteristics						
Age (years)	43 ± 12	68 ± 6	73 ± 7	74 ± 8	65 ± 15	<0,001*
Weight (Kg)	72,6 ± 13,5	74,2 ± 11,0	75,8 ± 15,5	74,8 ± 15,5	74,4 ± 14,0	0,826*
Height (m)	1,67 ± 0,08	1,66 ± 0,08	1,64 ± 0,09	1,58 ± 0,09	1,64 ± 0,09	0,002
BMI (kg/m ^{2})	26,1 ± 3,8	26,8 ± 3,5	28,1 ± 4,2	29,8 ± 5,7	27,8 ± 4,6	0,022
Gait Speed (s)	2,7 ± 0,6	2,9 ± 0,5	3,7 ± 0,7	5,0 ± 1,2	3,6 ± 1,2	<0,001*
MS (Kg)	30,49 ± 12,46	29,12 ± 13,78	25,24 ± 10,48	23,31 ± 9,25	26,86 ± 11,67	0,204*
Ultrasound Measurements						
SFT (cm)	1,2 ± 0,5	0,9 ± 0,5	1,1 ± 0,5	1,1 ± 0,7	1,1 ± 0,6	0,372*
MT (cm)	3,25 ± 0,59	2,44 ± 0,54	2,41 ± 0,64	2,08 ± 0,54	2,53 ± 0,71	<0,001
Quality of Life (A.U.)	119 ± 5,4	122 ± 6,6	120 ± 4,8	115 ± 7,6	119 ± 6,6	0,001
Sex	***N (%)***	***N (%)***	***N (%)***	***N (%)***	***N (%)***	0,235*
Female	11 (45,8)	6 (27,3)	15 (50)	14 (56)	46 (45,5)	
Male	13 (54,2)	16 (72,7)	15 (50)	11 (44)	55 (54,4)	
Frailty Criteria						<0.001*
No positive criterion	17 (70,1)	22 (100)	0	0	39 (38,6)	
1 positive criterion	5 (20,8)	0	13 (43,3)	0	18 (17,8)	
2 positive criteria	2 (8,3)	0	17 (56,6)	0	19 (18,8)	
3 positive criteria	0	0	0	11(44)	11 (10,9)	
4 positive criteria	0	0	0	7 (28)	7 (6,9)	
5 positive criteria	0	0	0	7 (28)	7 (6,9)	

Abbreviations: SD: standard deviation; BMI: body mass index; MS: muscle strength; MT: muscle thickness; SFT: subcutaneous fat thickness; AU: arbitrary units.

* Variables without normal distribution, nonparametric tests used for the analysis.

A post-hoc analysis (Table 4.3) of statistically significant variables with normal distribution showed that:

- There were differences in height between frail, controls, and robust group, but not between frail and pre-frail subjects.
- BMI only showed difference between controls and frail individuals.
- There were differences in muscle thickness between controls and the rest of the groups. No differences were detected between robust, pre-frail, and frail individuals.
- The quality of life was significantly different between frail and the rest of the groups, but no differences were found between control, robust, and pre-frail groups.

Table 4.3 Post-hoc Analysis of Baseline Characteristics by Frailty Phenotype (N = 101)

Variables	*Group*	*Control (n = 24)*	*Robust (n = 22)*	*Pre-frail (n = 30)*	*Frail (n = 25)*
Physical Characteristics					
Height	Control	-	1,000	1,000	0,005*
	Robust	1,000	-	1,000	0,008*
	Pre-frail	1,000	1,000	-	0,122
	Frail	0,005*	0,008*	0,122	-
BMI(kg/m ^{2})	Control	-	1,000	0,588	0,024*
	Robust	1,000	-	1,000	0,132
	Pre-frail	0,588	1,000	-	0,936
	Frail	0,024*	0,132	0,936	-
Ultrasound Measurements					
MT (cm)	Control	-	<0,001*	<0,001*	<0,001*
	Robust	<0,001*	-	1,000	0,228
	Pre-frail	<0,001*	1,000	-	0,212
	Frail	<0,001*	0,228	0,212	-
Quality of Life (A.U.)	Control	-	1,000	1,000	0,047*
	Robust	1,000	-	1,000	0,001*
	Pre-frail	1,000	1,000	-	0,008*
	Frail	0,047*	0,001*	0,008*	-

Abbreviations: BMI: body mass index; MT: muscle thickness; AU: arbitrary units.

* <0,05 represent significant differences between the groups

Figure 4.1 demonstrates visually the same ultrasound characteristics described in the previous tables. It shows typical examples of the ultrasound images for different phases of frailty (robust, pre-frail and frail) and the control group. Since there are significant sex differences regarding subcutaneous fat thickness and muscle thickness variables, the examples are shown for men and

women alike. Progressive increase of the echo intensity (increased whiteness) in the *rectus femoris* and *vastus intermedius* muscle can be observed; as well as change in muscle structure, from well-defined striated muscle to less defined, blurry structure. In addition, progressive decrease in muscle thickness with the advance of frailty phenotype can be observed in both sexes. Subcutaneous fat thickness remains mostly constant between groups and sexes.

Figure 4.1 Typical images of Ultrasound Measurements by Sex and Frailty Phenotype

By Frailty Phenotype	*By Sex*	
	Female	*Male*
Control	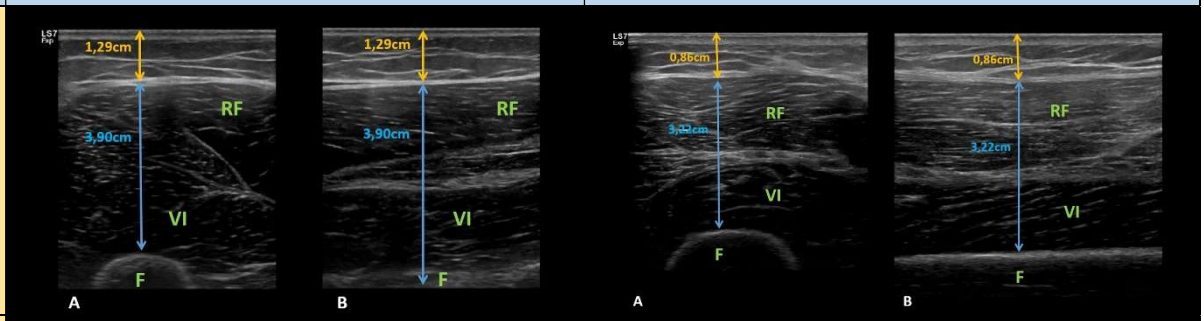	
Robust	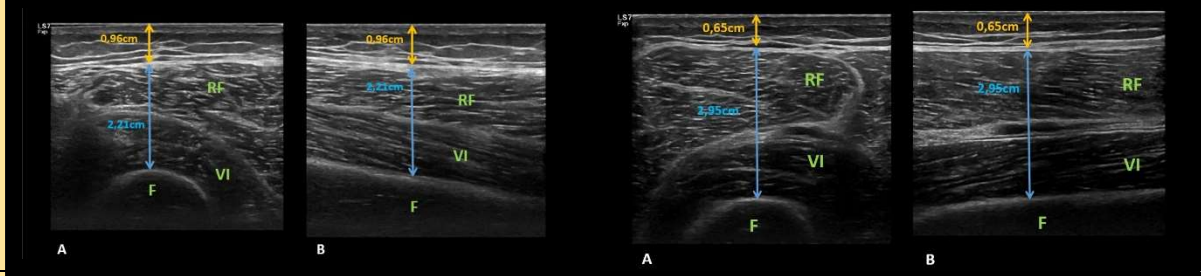	
Pre-Frail	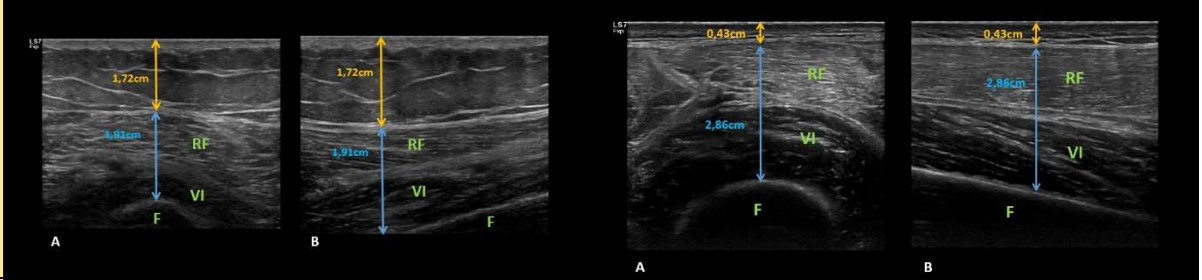	
Frail	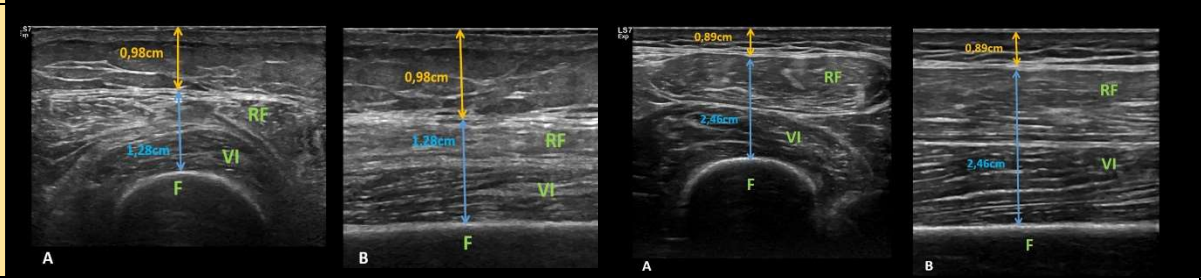	

Abbreviations: RF: rectus femoris; VI: vastus intermedius; F: femur.

Description: (A) Axial images of subjects anterior mid- thigh; (B) Sagittal images of subject's anterior mid-thigh; Yellow arrows correspond to subcutaneous fat thickness and blue arrows to muscle thickness.

4.2 Patients Comorbidities

We determined the frequency of comorbidities at the moment the muscle ultrasound was performed (baseline) and after two years of follow-up. In the following tables comorbidities were subdivided by associated diseases, risk factors, variables associated with frailty, and death.

The analysis of comorbidities according to sex (Table 4.4), showed that most are homogenous, except for previous fractures/osteoporosis and falls which were more common in females, and alcohol consumption, more common in males. In the follow-up, arthritis/osteoarthritis and previous strokes were more common in females and myocardial infarction was more common in males. After two-years, there is a trend of increased morbidity as the frequency of most diseases increased and the estimated survival went from 60% to 40%, although most of the variables remained homogenous regarding sex.

Table 4.4 Comorbidities at Baseline and at Two-Year Follow-up According to Sex

Group	**Comorbidities at baseline**			***Statistical Test***	**Comorbidities at follow-up**			***Statistical Test***
Variable	Female (n=46)	Male (n=55)	***Total (n=101)***	***P***	Female (n=46)	Male (n=55)	***Total (n=101)***	***P***
Associated Diseases	***N (%)***	***N (%)***	***N (%)***		***N (%)***	***N (%)***	***N (%)***	
Hypertension	23 (50)	17 (30,9)	40 (39,6)	0,052*	30 (65,2)	26 (46,4)	56 (554)	0,072*
Hyperlipidemia	26 (56,5)	31 (56,3)	57 (56,4)	0,987*	31 (67,3)	36 (65,5)	67 (66,3)	0,838*
DM	14 (30,4)	12 (21,8)	26 (25,7)	0,326*	15 (32,6)	15 (27,3)	30 (29,7)	0,561*
COPD	4 (8,7)	8 (14,5)	12 (11,8)	0,368*	4 (8,7)	10 (18,2)	14 (13,8)	0,172*
Hearing Impairment	9 (19,7)	11 (20)	20 (19,8)	0,957*	10 (21,7)	12 (21,8)	22 (21,7)	0,992*
Visual Impairment	23 (50)	22 (40)	45 (44,5)	0,316*	25 (54,3)	25 (45,5)	50 (49,5)	0,376*
Parkinson Disease	1 (2,1)	1 (1,8)	2 (1,9)	0,899*	1 (2,1)	2 (3,6)	3 (2,9)	0,668*
Previous Stroke	4 (8,7)	1 (1,8)	5 (4,9)	0,114*	7 (15,2)	2 (3,6)	9 (8,9)	0,043*
Congestive Heart Failure	2 (4,3)	3 (5,4)	5 (4,9)	0,799*	3 (6,5)	4 (7,2)	7 (6,9)	0,883*
Heart Disease	7 (15,2)	11 (20)	18 (17,8)	0,534*	12 (26)	16 (29,1)	28 (27,7)	0,738*
Myocardial Infarction	0	2 (3,6)	2 (1,9)	0,194*	1 (2,1)	8 (14,5)	9 (8,9)	0,031*
Renal Disease	9 (19,6)	8 (14,5)	17 (16,8)	0,504*	16 (34,7)	13 (23,6)	29 (28,7)	0,220*
Previous Cancer	8 (17,4)	9 (16,3)	17 (16,8)	0,891*	10 (21,7)	9 (16,4)	19 (18,8)	0,493*
Arthritis / Osteoarthritis	28 (60,9)	23 (41,8)	51 (50,5)	0,058*	31 (67,4)	26 (47,3)	57 (56,5)	0,043*
Anxiety / Depression	19 (41,3)	16 (29)	35 (34,6)	0,201*	22 (47,8)	17 (30,1)	39 (38,6)	0,084*
Previous fractures / Osteoporosis	14 (30,4)	5 (22,7)	19 (18,8)	0,007*	20 (43,5)	6 (10,9)	26 (25,7)	<0,001*

Liver Disease / Hepatopathy	4 (8,7)	3 (5,4)	7 (6,9)	0,525*	5 (10,9)	3 (5,4)	8 (7,9)	0,318*
Dementia / Memory Loss	0	1 (1,8)	1 (0,9)	0,360*	5 (10,9)	7 (12,7)	12 (11,8)	0,775*
Connective Tissue Disease	0	0	0	1,000*	1 (2,1)	2 (3,6)	3 (2,9)	0,668*
Hemiplegia	0	0	0	1,000*	1 (2,1)	0	1 (0,9)	0,274*
Neoplasm	0	0	0	1,000*	3 (6,5)	7 (12,7)	10 (9,9)	0,301*
Leukemia/Malignant Lymphoma	0	0	0	1,000*	1 (2,1)	1 (1,8)	2 (1,9)	0,899*
Solid Metastasis	0	0	0	1,000*	0	1 (1.8)	1 (0,9)	0,360*
AIDS	0	0	0	1,000*	0	0	0	1,000*
Peripheral Vascular Disease	0	2 (3,6)	2 (1,9)	0,194*	1 (2,1)	2 (2,9)	3 (2,9)	0,668*
Risk Factors								
Smoker	11 (23,9)	19 (34,5)	30 (29,7)	0,247*	11 (23,9)	18 (32,7)	29 (28,7)	0,332*
Alcohol	0	5 (22,7)	5 (4,9)	0,037*	0	5 (22,7)	5 (4,9)	0,037*
Falls	6 (13)	0	6 (5,9)	0,006*	9 (19,6)	2 (3,6)	11 (10,8)	0,011*
Obesity	5 (10,9)	4 (7,2)	9 (8,9)	0,530*	7 (15,2)	5 (22,7)	12 (11,8)	0,346*
Associated with Frailty								
CCI	3 (6,5)	3 (5,4)	3 (2,9)	0,715*	5 (10,9)	4 (7,2)	4 (3,9)	0,492*
Estimated 10-year survival	60,89%	65,91%	63,62%	0,691*	41,43%	47,22%	44,58%	0,542*
# of visits to PC	6 (13)	5 (9)	5 (4,9)	0,127*	6 (13)	6 (10,9)	6 (5,9)	0,899*
# of visits to ED	1 (2,1)	1 (1,8)	1 (0,9)	0,108*	1 (2,1)	1 (1,8)	1 (0,9)	0,679*
# of Hospitalizations	0	0	0	0,473*	0	1 (1,8)	1 (0.9)	0,493*
Death	0	0	0	NA	5 (10,9)	7 (12,7)	12 (11,8)	0,775*

Abbreviations: N: number of positive cases; SD: standard deviation; DM: diabetes mellitus; COPD: chronic obstructive pulmonary disease; AIDS: acquired immune deficiency syndrome; CCI: Charlson comorbidity index; PC: primary care; ED: emergency department, #: number.

* Variables without normal distribution, nonparametric tests used for the analysis.

The analysis of comorbidities according to frailty phenotype (Table 4.5), shows how the distribution changes among groups and increases in frequency at follow-up. At baseline, 11 out of 34 comorbidities surveyed were heterogeneous between the groups (control, robust, pre-frail and frail) and at follow-up 19 out of 35. Among the comorbidities that were statistically significant according to frailty phenotype at baseline and follow-up are: hypertension, hyperlipidemia, diabetes mellitus, visual impairment, previous stroke, congestive heart failure, heart disease, renal disease, previous cancer, arthritis/osteoarthritis, anxiety/depression, falls, obesity, CCI, estimated survival at 10 years, number of visits to primary care, number of visits to emergency department, hospitalizations and death.

Table 4.5 Comorbidities at Baseline and at Two-Year Follow-up According to Frailty Phenotype												
Group	***Controls***	***Robust***	***Pre-frail***	***Frail***	***Total***	***Statistical***	***Controls***	***Robust***	***Pre-frail***	***Frail***	***Total***	***Statistical***
	(n = 24)	***(n = 22)***	***(n = 30)***	***(n =25)***	***(n=101)***	***Test***	***(n = 24)***	***(n = 22)***	***(n = 30)***	***(n =25)***	***(n=101)***	***Test***
Variable	***N (%)***	***N (%)***	***N (%)***	***N (%)***	***N (%)***	***P***	***N (%)***	***N (%)***	***N (%)***	***N (%)***	***N (%)***	***P***
Associated Diseases												
Hypertension	4 (16,6)	8 (36,3)	13 (43,3)	15 (60)	40 (39,6)	0,020*	7 (29,2)	9 (40,9)	20 (66,7)	20 (80)	56 (55,4)	0,001*
Hyperlipidemia	9 (37,5)	10 (45,4)	22 (73,3)	16 (64)	57 (56,4)	0,036*	10 (41,6)	15 (68,1)	22 (73,3)	20 (80)	67 (66,3)	0,026*
DM	0	6 (27,3)	10 (33)	10 (40)	26 (25,7)	0,008*	1 (4,2)	7 (31,8)	12 (40)	10 (48)	30 (29,7)	0,017*
COPD	0	2 (9)	5 (16,7)	5 (20)	12 (11,8)	0,134*	0	2 (9)	5 (16,7)	7 (28)	14 (13,8)	0,035*
Hearing Impairment	3 (12,5)	4 (18,2)	7 (23,3)	6 (24)	20 (19,8)	0,719*	3 (12,5)	4 (18,1)	8 (26,7)	7 (28)	22 (21,7)	0,504*
Visual Impairment	5 (20,8)	11 (50)	14 (46,7)	15 (60)	45 (44,5)	0,044*	3 (12,5)	14 (63,6)	17 (56,7)	16 (64)	50 (49,5)	0,001*
Parkinson Disease	0	0	2 (6,7)	0	2 (1,9)	0,189*	0	0	2 (6,7)	1 (4)	3 (2,9)	0,408*
Previous Stroke	0	0	2 (6,7)	3 (12)	5 (4,9)	0,160*	0	0	2 (6,7)	7 (28)	9 (8,9)	0,001*
Congestive Heart Failure	1 (4,2)	1 (4,5)	0	3 (12)	5 (4,9)	0,241*	1 (4,2)	1 (4,5)	0	5 (20)	7 (6,9)	0,026*
Heart Disease	3 (12,5)	3 (13,6)	5 (16,7)	7 (28)	18 (17,8)	0,476*	3 (12,5)	5 (22,7)	8 (26,7)	12 (48)	28 (27,7)	0,044*
Myocardial Infarction	1 (4,2)	1 (4,5)	0	0	2 (1,9)	0,489*	1 (4,2)	1 (4,5)	2 (6,7)	5 (20)	9 (8,9)	0,164*
Renal Disease	1 (4,2)	2 (9)	5 (16,7)	9 (36)	17 (16,8)	0,017*	1 (4,2)	7 (31,8)	9 (40,9)	12 (48)	29 (28,7)	0,009*
Previous Cancer	0	5 (22,7)	7 (23,3)	5 (20)	17 (16,8)	0,093*	0	5 (22,7)	6 (20)	8 (32)	19 (18,8)	0,036*
Arthritis / Osteoarthritis	2 (1,9)	12 (54,5)	21 (70)	16 (64)	51 (50,4)	<0,001*	3 (12,5)	13 (59)	24 (80)	17 (68)	57 (56,4)	<0,001*
Anxiety / Depression	3 (12,5)	7 (31,8)	10 (33,3)	15 (60)	35 (34,6)	0,007*	4 (16,7)	7 (31,8)	12 (40)	16 (64)	39 (38,6)	0,007*
Previous fractures / Osteoporosis	1 (4,2)	3 (13,6)	7 (23,3)	8 (32)	19 (18,8)	0,074*	2 (8,3)	5 (22,7)	10 (33,3)	9 (36)	26 (25,7)	0,106*
Liver Disease / Hepatopathy	1 (4,2)	0	1 (3,3)	5 (20)	7 (6,9)	0,029*	1 (4,2)	0	2 (6,7)	5 (20)	8 (7,9)	0,062*
Dementia / Memory Loss	0	0	0	1 (4)	1 (0,9)	0,385*	0	2 (9,1)	5 (16,7)	5 (20)	12 (11,8)	0,134*
Connective Tissue Disease	0	0	0	0	0	1,000*	1 (4,2)	2 (9,1)	0	0	3 (2,9)	0,202*
Hemiplegia	0	0	0	0	0	1,000*	0	0	0	1 (4)	1 (0,9)	0,385*
Neoplasm	0	0	0	0	0	0,385*	1 (4,2)	2 (9,1)	4 (13,3)	3 (12)	10 (9,9)	0,704*

Leukemia/Malignant Lymphoma	0	0	0	0	0	1,000*	0	0	1 (3,3)	1 (4)	2 (1,9)	0,632*
Solid Metastasis	0	0	0	0	0	1,000*	0	1 (4,5)	0	0	1 (0,9)	0,309*
AIDS	0	0	0	0	0	1,000*	0	0	0	0	0	1,000*
Peripheral Vascular Disease	0	0	1 (3,3)	1 (4)	2 (1,9)	0,632*	0	1 (4,5)	0	2 (8)	3 (2,9)	0,262*
Risk Factors												
Smoker	8 (33,3)	4 (18,2)	10 (33)	8 (32)	30 (29,7)	0,618*	8 (33,3)	4 (18,1)	9 (30)	8 (32)	29 (28,7)	0,663*
Alcohol	2 (8,3)	1 (4,5)	0	2 (8)	5 (4,9)	0,454*	2 (8,3)	1 (4,5)	0	2 (8)	5 (4,9)	0,454*
Falls	0	0	3 (10)	3 (12)	6 (5,9)	0,146*	0	0	6 (20)	5 (20)	11 (10,8)	0,017*
Obesity	0	2 (9)	1 (3,3)	6 (24)	9 (8,9)	0,015*	1 (4,2)	2 (9,1)	2 (6,7)	7 (28)	12 (11,8)	0,038*
Associated with Frailty												
CCI	1 (4,2)	3 (13,6)	4 (13,3)	5 (20)	3 (2,9)	<0,001*	1 (4,2)	5 (22,7)	5 (16,7)	7 (28)	4 (3,9)	<0,001*
Estimated 10-year survival	95,54%	70,09%	56,80%	35,48%	63,62%	<0,001*	91,21%	42,50%	33,03%	15,52%	44,58%	<0,001*
# of visits to PC	4 (16,7)	5 (22,7)	5 (16,7)	7 (28)	5 (4,9)	0,077*	4 (16,7)	5 (22,7)	6 (20)	9 (45)	6 (5,6)	0,001*
# of visits to ED	1 (4,2)	1 (4,5)	1 (3,3)	1 (4)	1 (0,9)	0,177*	1 (4,2)	1 (4,5)	1 (3,3)	2 (8)	1 (0,9)	0,001*
# of Hospitalizations	0	0	0	1 (4)	1 (0,9)	0,243*	0	0	0	1 (4)	1 (0,9)	0,085*
Death	0	0	0	0	0	1,000*	0	0	3 (10)	9 (45)	12 (11,8)	<0,001*

Abbreviations: N: number of positive cases; SD: standard deviation; DM: diabetes mellitus; COPD: chronic obstructive pulmonary disease; AIDS: acquired immune deficiency syndrome; CCI: Charlson comorbidity index; PC: primary care; ED: emergency department, #: number.

* Variables without normal distribution, nonparametric tests used for the analysis.

4.3 Texture Features

We analysed 43 texture features according to sex and frailty phenotype. Table 4.6 is a summary of the p-values obtained from this analysis.

Table 4.6 Summary of P-values of Texture Features

According to:		Sex				Frailty			
Muscle and Plane		*Axial RF*	*Axial VI*	*Sagittal RF*	*Sagittal VI*	*Axial RF*	*Axial VI*	*Sagittal RF*	*Sagittal VI*
Texture Feature		*P value*	*P value*	*P value*	*P value*	*P value*	*P value*	*P value*	*P value*
IHF	Variance	0,324	0,967*	0,998	0,261*	0,550	0,025*	0,499	0,216*
	Skewness	0,877	0,144*	0,894	0,390*	<0,001	<0,001*	0,235	<0,001*
	Kurtosis	0,526*	0,350*	0,956*	0,723*	<0,001*	<0,001	0,090*	<0,001*
GLCM	Energy	0,429*	0,179*	0,682*	0,801*	0,008*	<0,001*	0,043*	<0,001*
	Contrast	0,733*	0,303*	0,713*	0,120*	0,933*	0,006*	0,469*	0,119*
	Entropy	0,251	0,738*	0,764	0,522*	0,180	<0,001*	0,189	<0,001*
	Homogeneity	0,717	0,222*	0,281	0,838*	0,190	<0,001*	0,087	<0,001*
	Correlation	0,037	0,008*	0,151	0,064	0,584	0,004*	0,049	0,021
	Sum Average	0,082	0,934	0,786	0,553	0,004	<0,001	0,032	<0,001
	Variance	0,055	0,595*	0,728*	0,024*	0,840	<0,001*	0,513*	0,004*
	Dissimilarity	0,792	0,777	0,615	0,153	0,834	<0,001	0,379	0,015
	Auto-Correlation	0,096	0,709	0,658*	0,357*	0,031	<0,001	0,050*	<0,001*
GLRLM	Short Run Emphasis	0,865*	0,398*	0,319	0,658*	0,054*	<0,001*	0,016	<0,001*
	Long Run Emphasis	0,648*	0,044*	0,421*	0,619*	0,008*	<0,001*	0,001*	<0,001*
	Gray-Level Nonuniformity	0,036*	0,249*	0,965	0,222*	0,088*	<0,001*	0,275	<0,001*
	Run Length Nonuniformity	0,870*	0,429*	0,322	0,614*	0,054*	<0,001*	0,016	<0,001*
	Run Percentage	0,754*	0,084*	0,377	0,849*	0,016*	<0,001*	0,004	<0,001*
	Low Gray-Level Run Emphasis	0,070*	0,202*	0,946*	0,718*	<0,001*	<0,001*	0,008*	<0,001*
	High Gray-Level Run Emphasis	0,091	0,343*	0,614*	0,207*	0,043	<0,001*	0,056*	<0,001*
	Short Run Low Gray-Level	0,045*	0,425*	0,929*	0,854*	<0,001*	<0,001*	0,010*	<0,001*
	Short Run High Gray-Level	0,098	0,340*	0,648*	0,190*	0,044	<0,001*	0,054*	<0,001*
	Long Run Low Gray-Level	0,210*	0,046*	0,354*	0,263*	0,008*	<0,001*	0,067*	<0,001*
	Long Run High Gray-Level	0,059	0,310*	0,553*	0,266*	0,054	<0,001*	0,082*	<0,001*
	Gray-Level Variance	0,908*	0,108*	0,553*	0,790*	<0,001*	<0,001*	0,217*	<0,001*
	Run-Length Variance	0,150*	0,001*	0,647	0,019*	0,050*	0,089	0,693	0,062*
GLSZM	Small Zone Emphasis	0,995*	0,043*	0,414	0,003	0,387*	0,514	0,142	0,248
	Large Zone Emphasis	0,687*	0,024*	0,394*	0,495*	0,009*	<0,001*	<0,000*	<0,001*
	Gray-Level Nonuniformity	0,020*	0,134*	0,796*	0,134*	0,263*	<0,001*	0,171*	<0,001*
	Zone-Size Nonuniformity	0,968	0,045*	0,428	0,003	0,410	0,517	0,13	0,285
	Zone Percentage	0,697	0,405*	0,299	0,562	0,049	<0,001*	0,015	<0,001*
	Low Gray-Level Zone Emphasis	0,052*	0,558*	0,535*	0,908*	<0,001*	<0,001*	0,001*	<0,001*
	High Gray-Level Zone Emphasis	0,074	0,238*	0,576*	0,173*	0,055	<0,001*	0,070*	<0,001*
	Small Zone Low Gray-Level Zone Emphasis	0,029*	0,517*	0,336*	0,967*	<0,001*	<0,001*	0,003*	<0,001*
	Small Zone High Gray-Level Zone Emphasis	0,052	0,190*	0,623*	0,135*	0,067	<0,001*	0,064*	<0,001*
	Large Zone Low Gray-Level Zone Emphasis	0,035*	0,035*	0,350*	0,212*	0,079*	<0,001*	0,102*	<0,001*
	Large Zone High Gray-Level Zone Emphasis	0,001*	0,019*	0,367	0,235*	0,093*	0,640*	0,123	0,440*
	Grey-Level Variance	0,609*	0,095*	0,302	0,567*	0,005*	<0,001*	0,008	<0,001*
	Zone-Size Variance	0,061*	0,036*	0,406	0,207*	0,168*	0,247	0,065	0,115*
NGTDM	Coarseness	0,859*	0,390*	0,157	0,310*	0,142*	<0,001*	0,188	<0,001*
	Contrast	0,924*	0,051	0,343*	0,062	0,678	0,005	0,665*	0,256
	Busyness	0,333*	0,817*	0,609*	0,956*	0,007*	<0,001*	0,110*	<0,001*
	Complexity	0,254	0,266*	0,849*	0,122*	0,749*	<0,001*	0,353*	0,003*
	Strength	0,186*	0,007*	0,822*	0,054*	0,384*	0,032*	0,519*	0,012*

Abbreviations: IHS: Intensity Histogram Features; GLCM: Gray-Level Co-occurrence Matrix; GLRLM: Gray-Level run-Length Matrix; GLSZM: Gray-Level Size Zone Matrix; NGTDM: Neighborhood Gray-Tone Difference Matrix.

* Variables without normal distribution, nonparametric tests used for the analysis.

Texture features are different by frailty phenotype in both muscles (*Rectus Femoris* or V*astus Intermidius*) and planes (axial or sagittal) used in this study, and most of them are sex independent, although there were some exceptions. In axial *Rectus Femoris*, 7 out of 43 features were statistically significant according to sex, while 21 out of 43 according to frailty phenotype. In the case of axial *Vastus Intermidius,* it was 12 out of 43 for sex and 38 for frailty phenotype; in sagittal *Rectus Femoris,* none were statistically significant for sex, and 13 out of 43 were for frailty phenotype; and for sagittal *Vastus Intermidius* 4 out 43 were statistically significant for sex, 35 out 43 were significant for frailty phenotype. Full details of the analysis for texture features for both muscles and planes can be found in Annex 8.

4.4 Correlations

We used multiple correlations of all the variables in this study with the purpose to perform data mining, which refers to the process of discovering patterns or phenotypes in large data sets (Gillies et al., 2016) associated with imaging for further analysis.

4.4.1 Correlations of Baseline Characteristics

Table 4.7 shows the correlations of the physical characteristics (age, weight, height, BMI, gait speed and muscle strength), ultrasound characteristics (subcutaneous fat tissue and muscle thickness), frailty phenotype and quality of life of the participants.

Table 4.7 Correlations of Baseline Characteristics (n = 101)

Variables	*Age (years)*	*Weight (kg)*	*Height (m)*	*BMI (kg/m²)*	*Gait Speed (s)*	*Frailty Phenotype*	*SFT (cm)*	*MT (cm)*	*MS (kg)*	*OPQoL (A.U.)*
Age (years)	1	0,047	-,200*	0,181	,613**	,696**	-0,071	-,556**	-0,186	-0,053
Weight (kg)	-	1	,484**	,808**	-0,065	0,05	0,06	,352**	0,071	0,078
Height (m)	-	-	1	-0,066	-,374**	-,321**	-,369**	,281**	0,062	0,107
BMI (kg/m²)	-	-	-	1	0,159	,264**	,277**	0,184	0,073	0,006
Gait Speed (s)	-	-	-	-	1	,764**	0,006	-,502**	-0,145	-,262**
Frailty Phenotype	-	-	-	-	-	1	-0,024	-,528**	-,213*	-,261**
SFT (cm)	-	-	-	-	-	-	1	-0,07	0,153	0,09
MT (cm)	-	-	-	-	-	-	-	1	-0,064	0,117
MS (kg)	-	-	-	-	-	-	-	-	1	0,089
OPQoL (A.U.)	-	-	-	-	-	-	-	-	-	1

Abbreviations: BMI: body mass index; MS: muscle strength; MT: muscle thickness; SFT: subcutaneous fat thickness; OPQoL: Older´s People Quality of Life; AU: arbitrary units.

Rho of Spearman used for the statistical analysis

* The correlation is significant at the 0.05 level (bilateral).

** The correlation is significant at the 0.01 level (bilateral).

Frailty phenotype was strongly correlated with age (r = 0,696**) and gait speed (r = 0,764**), moderately correlated with muscle thickness (r = -0,528**), and weakly to height (r = -0,321**), BMI (r = 0.264**), muscle strength (r = -0,213*) and quality of life (r = -0,261**). Age was moderately associated with gait speed (r = 0.613**) and muscle thickness (r = -0.556**) and there was a weak association with height (r = -0,200*). No association was found between age and muscle strength, or age and quality of life. Gait speed had a moderate association with muscle thickness (r = -0,556**) and weak with quality of life (r = -0,262**), but not with muscle strength.

4.4.2 Correlations with Comorbidities

In this study, quality depends not only on the image acquisition and processing conditions, but also on the availability of the covariates and outcomes. For this reason, we incorporated multiple clinical variables. Since it is difficult to process large data sets and multiple variables, we subtracted the positive comorbidities at baseline from positive comorbidities at two years' follow-up. The result of this was the incidence of comorbidities measured in the cohort during the 2 years' follow-up. This was the information used in this analysis to determine the most significant outcomes of the study in relation to frailty phenotype, baseline characteristics and the analysis of the texture features.

Frailty phenotype had statistically significant correlations with the development of stroke (r = 0,250**), myocardial infarction (r = 0,267**), increased CCI (r = 0,306**), increased number of visits to primary care (r = 0,177*), and death (0,370**) during the follow-up. All correlations were weak, except for frailty phenotype and death, which was moderate. Gait speed and muscle thickness had similar correlations as frailty phenotype. Gait speed correlated with stroke (r = 0.167*), congestive failure (r = 0,166*), myocardial infarction (r = 0,263*), CCI (r = 0,269**), and death (r = 0.349**), while muscle thickness correlated with stroke (r = 0,202*), myocardial infarction (r = 0.188*), CCI (r = -0,244**), and death (r = -0,288**) too. Age was weakly correlated with myocardial infarction (r = 0,207*), renal failure (r = 0,205*), dementia (r = 0,192*), CCI (r = 0,360**), number of visits to primary care (r = 0,176*), and death (0.273**). We found no significant associations for muscle strength.

The rest of the correlations of comorbidities outcomes with baseline characteristics are shown in Table 4.8. Full details of the correlation analysis of comorbidities at baseline (2015) and at the two-year follow-up (2017) can be found in Annex 9.

Table 4.8 Correlations of Comorbidities Outcomes with Baseline Characteristics (n = 101)										
Variables	***Age (years)***	***Weight (kg)***	***Height (m)***	***BMI (kg/m²)***	***Gait Speed (s)***	***Frailty Phenotype***	***SFT (cm)***	***MT (cm)***	***MS (kg)***	***OPQoL (A.U.)***
Associated Diseases										
Hypertension	0,101	-0,079	-0,055	-0,061	0,08	0,116	-0,04	-0,062	0,056	-0,097
Hyperlipidemia	0,097	-0,015	-0,02	0,015	-0,045	0,037	-0,033	-0,044	-0,048	0,001
DM	0,13	0,052	0,003	0,063	0,086	-0,042	-0,121	0,012	-0,104	0,029
COPD	0,022	0,006	0,063	-0,025	0,102	0,123	-0,1	-0,065	-0,048	-,178*
Hearing Impairment	0,05	-0,084	-0,016	-0,082	0,031	0,112	-0,072	-0,116	0,074	-0,066
Visual Impairment	0,119	0,132	0,048	,170*	-0,014	0,104	0,041	-0,13	0,071	0,119
Parkinson Disease	0,128	-0,055	0,059	-0,09	0,133	0,123	-0,115	-0,079	-0,113	-0,127
Previous Stroke	0,151	-,164*	-,169*	-0,016	,167*	,250**	-0,069	-,202*	-0,084	-,243**
Congestive Heart Failure	0,08	0,036	-0,062	0,05	,166*	0,175	0,078	-0,054	0,073	-0,067
Heart Disease	0,139	0,049	-0,064	0,072	0,138	,184*	-0,018	-0,001	-0,055	-0,053
Myocardial Infarction	,207*	-0,005	0,104	-0,065	,263**	,267**	-,165*	-,188*	-0,008	-0,155
Renal Disease	,205*	0,111	-0,07	0,157	0,074	0,077	0,034	-0,052	0,127	0,002
Previous Cancer	0,124	-0,091	-0,147	0,028	0,157	0,167	-0,036	-,183*	0,015	-,176*
Arthritis / Osteoarthritis	0,056	0,098	0,065	0,074	-0,046	0,021	0,031	0,072	0,004	0,015
Anxiety / Depression	0,12	0,037	-0,05	0,103	-0,009	0,019	0,066	-0,064	0,026	0,108
Previous fractures / Osteoporosis	-0,017	0,059	-0,028	0,11	-0,003	0	,241**	-0,071	0,14	0,012
Liver Disease / Hepatopathy	-0,039	0,045	-0,061	0,065	-0,008	0,034	0,13	0,104	-0,025	0,112
Dementia / Memory Loss	,192*	-0,098	-0,107	-0,078	0,097	0,179	-0,11	-,163*	-0,032	-0,085
Connective Tissue Disease	-0,141	-0,074	0,111	-0,133	-0,115	-0,131	-0,076	0,084	0,02	0,15
Hemiplegia	0,128	-0,107	-0,136	0	0,13	0,123	0,017	-0,135	-0,068	-0,134
Neoplasm	0,03	-0,033	-0,007	-0,021	0,085	0,093	-0,099	-0,139	-0,01	0,015
Leukemia/Malignant Lymphoma	0,058	-,196*	-0,105	-,198*	0,123	0,112	-0,076	-,182*	-0,13	0,017
Solid Metastasis	-0,073	0,073	-0,013	0,084	0,011	-0,05	-0,034	0,068	-0,082	0,099
Peripheral Vascular Disease	0,036	0,066	-0,114	0,136	-0,048	0,023	0,1	0,005	-0,036	0,069
Risk Factors										
Smoker	-0,02	0	0,043	-0,023	-0,034	-0,034	0,059	-0,017	-0,01	-0,014
Alcohol										
Falls	0,162	0,024	-0,029	0,069	0,047	0,159	0,038	-0,021	-0,051	-0,063
Obesity	-0,024	0,115	0,002	0,124	0,002	0,015	-0,013	0,122	-0,077	0,03
Associated with Frailty										
CCI	,360**	0,035	-,165*	,147*	,269**	,306**	-0,05	-,224**	0,013	-0,117
Estimated 10-year survival	-,191**	-0,068	,148*	-,171*	-,158*	-,191*	0,023	0,127	-0,047	0,079
# of visits to PC	,176*	0,066	0,022	0,052	0,112	,177*	-0,059	-,139*	-0,011	-0,027
# of visits to ED	0,116	0,066	0,076	0,023	-0,003	0,08	-0,056	-0,048	-0,046	-0,142
# of Hospitalizations	0,137	-0,009	0,031	-0,03	0,141	0,165	-0,042	-0,116	-0,135	0,04
Death	,273**	-0,135	-0,073	-0,089	,349**	,370**	-0,101	-,288**	-0,013	-0,112

Abbreviations: BMI: body mass index; MS: muscle strength; MT: muscle thickness; SFT: subcutaneous fat thickness; OPQoL: Older´s People Quality of Life; AU: arbitrary units; DM: diabetes mellitus; COPD: chronic bbstructive pulmonary disease; CCI: Charlson comorbidity index; #: number; PC: primary care; ED: emergency department.

Tau B of Kendal used for the statistical analysis. Comorbidities of 2015 were subtracted to 2017, and the results were used for the statistical analysis.

* The correlation is significant at the 0.05 level (bilateral).

** The correlation is significant at the 0.05 level (bilateral).

4.4.3 Correlations of Texture Features with Baseline Characteristics

Table 4.9 is a summary of the correlations with baseline characteristics in both muscles (*Rectus Femoris* and *Vastus Intermedius*) and planes (axial and sagittal). The information presented is the range of correlations of the four analyses done, with the minimum and maximum correlation shown in each box. Texture features had statistically significant correlations with frailty phenotype, age, gait speed and muscle thickness. Frailty phenotype had 21 out of 43 features statistically significant with weak to moderate association. Age had 12 out of 43 features and gait speed 11 out of 43. Muscle thickness had 17 out of 43 features and the association range from weak to strong depending on the muscle and plane evaluated.

Weight, BMI and subcutaneous fat tissue had weak to moderate association but only significant in some of the muscles or planes, with no clear pattern discern. Muscle strength and quality of life had no significant correlation with texture features. Full details of the analysis for texture features and baseline characteristics for both muscles and planes can be found in Annex 10.

Table 4.9 Summary of Textures Features Correlations with Baseline Characteristics (n = 101)											
	Texture Features	***Age (years)***	***Weight (kg)***	***Height (m)***	***BMI (kg/m²)***	***Gait Speed (s)***	***Frailty Phenotype***	***SFT (cm)***	***MT (cm)***	***MS (kg)***	***OPQoL (A.U.)***
IHF	Variance	0,109 - 0,197*	-0,152 – -0,252	-0,012 - - 0,067	-0,126 – -0,306**	0,006 – 0,221*	0,066 – 0,183	-0,053 – -0,241*	-0,115 - 0,347**	-0,012 – -0,189	-0,012 – -0,139
	Skewness	-0,176 - 0,536**	0,054 – -0,158	0,064 - 0,205*	0,033 - 0,123	-0,088 – -0,458**	0,149 – -0,499*	0,003 - 0,095	0,078 - 0,673**	0,008 - 0,056	0,065 - 0,171
	Kurtosis	-0,231* - 0,473**	0,011 - 0,206*	0,034 - 0,153	0,033 – 0,132	-0,100 – -0,407**	0,190 – -0,457**	0 - 0,144	0,170 - 0,640**	0,013 - 0,067	0,056 - 0,193
GLCM	Energy	-0,258 - 0,495**	0,083 - 0,247*	0,096 - 0,169*	0,019 - 0,146	-0,229* - -0,518**	-0,260** - -0,457**	0,043 - 0,263**	0,259** - 0,781**	0,012 - 0,096	0,002 - 0,179
	Contrast	0,011 - 0,175*	-0,075 – -0,277**	0,021 - 0,063	-0,041 – -0,309**	0,051 – 0,242*	0,036 – 0,156*	-0,069 – -0,279**	-0,052 – -0,467**	-0,070 – -0,129	0,005 - 0,026
	Entropy	0,195 0,443**	-0,121 – -0,274**	-0,090 – -0,108	0,070 – -0,212*	0,165 - 0,459**	0,209* - 0,455**	-0,098 – -0,315**	-0,219* - -0,736**	0,070 – -0,113	-0,020 – -0,123
	Homogeneity	-0,185 - 0,437**	0,087 - 0,275**	0,096 - 0,155	0,021 - 0,207*	-0,182 – -0,453	-0,204* - -0,443**	0,005 - 0,154	0,205* - 0,747**	0,040 - 0,061	0,031 - 0,097
	Correlation	-0,023 - 0,249*	0,013 – -0,283**	-0,001 – -0,114	0,010 - 0,164*	0,007 – 0,189	0,045 – 0,210*	-0,060 – -0,273**	-0,070 – -0,333**	-0,064 – -0,099	-0,037 – -0,084
	Sum Average	0,204 - 0,497*	-0,070 – -0,283**	-0,049 – -0,150	0,002 - 0,301*	0,192 - 0,522**	0,231* - 0,509**	-0,126 – -0,353**	-0,199* - -0,766**	-0,063 – -0,136	-0,032 – -0,152
	Variance	0,072 0,264**	-0,130 – -0,257**	0,038 - 0,059	-0,138 – -0,301**	0,040 - 0,310**	0,060 - 0,265**	-0,168 - 0,402**	-0,102 – -0,501**	-0,075 – -0,168	-0,019 – -0,067
	Dissimilarity	0,053 0,276**	-0,097 – -0,293**	-0,010 – -0,069	-0,070 – -0,219*	0,083 - 0,322**	0,081 - 0,295**	-0,063 – -0,249*	-0,112 – -0,598**	-0,007 – -0,126	-0,002 – -0,049
	Auto-Correlation	0,178 0,456**	-0,082 – -0,292**	-0,044 – -0,113	-0,041 - 0,231*	0,164 - 0,486**	0,240* - 0,469**	-0,140 – -0,370**	-0,194 – -0,732**	-0,070 – -0,133	-0,029 – -0,147
GLRLM	Short Run Emphasis	0,253* 0,439*	-0,088 – -0,283**	-0,096 – -0,181	-0,014 – -0,219*	0,244* - 0,486**	0,264** - 0,442**	-0,010 – -0,179	-0,283** - -0,742**	-0,054 – -0,079	0,024 – -0,095
	Long Run Emphasis	-0,299** - 0,477**	0,003 - 0,235*	0,140 - 0,178**	-0,010 – -0,141	-0,264** - -0,522**	-0,325** - -0,509**	-0,003 – -0,095	0,242* - 0,760**	0,025 - 0,107	0,045 - 0,158
	Gray-Level Nonuniformity	-0,212** - 0,449*	0,085 - 0,261**	0,004 - 0,100	0,028 - 0,215*	-0,149 – -0,456**	-0,192 – -0,435**	0,119 - 0,353**	0,185 - 0,691**	0,062 - 0,153	0,045 - 0,116
	Run Length Nonuniformity	0,253* - 0,429**	-0,045 – -0,286**	-0,092 – -0,183	-0,022 – -0,224*	0,246* - 0,452**	0,264** - 0,433**	-0,010 – -0,185	-0,287** - -0,738**	-0,053 – -0,079	-0,023 – -0,093

	Run Percentage	0,291** - 0,470**	-0,045 – -0,251*	-0,130 – -0,168*	0 - 0,163	0,266** - 0,493**	0,305** - 0,488**	-0,131 - 0	-0,277** - -0,738**	-0,014 – -0,087	0,036 - 0,137
	Low Gray-Level Run Emphasis	0,290** - 0,510**	0,057 - 0,201*	0,014 - 0,152	0,014 - 0,169	-0,233* - -0,543**	0,300** - -0,552**	0,040 - 0,274**	0,253* - 0,752**	0,023 - 0,063	0,002 - 0,113
	High Gray-Level Run Emphasis	0,177 - 0,423**	-0,088 – -0,286**	0,020 - 0,079	-0,048 – -0,246*	0,156 - 0,468**	0,204* - 0,441**	-0,15 – -0,368**	-0,187 – -0,698**	-0,067 – -0,126	-0,027 – -0,119
	Short Run Low Gray-Level	-0,295** - 0,502**	0,049 - 0,194	0 - 0,143	-0,005 – -0,175	-0,223* - -0,536**	-0,279** - -0,543**	0,037 – -0,366**	0,245* - 0,748**	0,026 - 0,087	0,025 - 0,162
	Short Run High Gray-Level	0,181 - 0,419**	-0,093 – -0,288**	-0,010 – -0,075	0,051 – -0,241*	0,157 - 0,464**	0,209* - 0,436**	-0,147 – -0,366**	-0,189 - 0,693**	-0,066 – -0,125	-0,028 – -0,135
	Long Run Low Gray-Level	-0,131 - 0,486**	0,010 - 0,182	0,110 - 0,176*	-0,018 – -0,1,39	-0,153 – -0,512**	-0,221* - -0,506**	0,018 – -0,046	0,152 - 0,698**	-0,028 - 0,063	0,033 - 0,146
	Long Run High Gray-Level	0,145 - 0,437**	-0,084 – -0,296**	-0,019 – -0,103	-0,078 – -0,241*	0,132 - 0,473**	0,161 - 0,447**	-0,154 – -0,381**	-0,184 - 0,712**	-0,070 – -0,134	-0,030 – -0,141
	Gray-Level Variance	0,127 - 0,516**	-0,030 – -0,124	-0,120 – -0,166*	0,019 – -0,203*	0,214* - 0,529**	0,200* - 0,543**	-0,001 – -0,094	-0,075 – -0,727**	-0,026 - 0,093	0,085 – -0,306**
	Run-Length Variance	0,190 - 0,227*	0,003 - 0,158	-0,027 – -0,176*	0,093 - 0,191	0,060 – 0,192	0,017 - 0,265**	0,157 - 0,277**	0,043 – -0,221*	0,010 - 0,164	-0,005 – -0,128
GLSZM	Small Zone Emphasis	0,168 - 0,214*	-0,079 – -0,154	0,108 - 0,156	-0,014 – -0,283**	0,079 – 0,238*	0,012 - 0,241*	-0,043 – -0,370**	-0,098 – -0,332**	-0,047 – -0,092	-0,012 – -0,045
	Large Zone Emphasis	0,285** - 0,464**	0,007 - 0,243*	0,125 - 0,191	-0,013 – -0,139	-0,248* - -0,530**	-0,321** - -0,510**	0,003 - 0,089	0,238* - 0,757**	0,024 - 0,096	0,032 - 0,177
	Gray-Level Nonuniformity	-0,150 - 0,415**	0,092 - 0,273**	0,015 - 0,068	0,090 - 0,254*	-0,089 – -0,429**	-0,180 – -0,422**	0,157 - 0,369**	0,150 - 0,655**	0,072 - 0,134	0,037 - 0,097
	Zone-Size Nonuniformity	0,070 - 0,211*	-0,080 – -0,156	0,086 - 0,158	-0,016 - - 0,285**	0,078 – 0,235*	0,012 - 0,240*	-0,046 – -0,370**	-0,098 – -0,331**	-0,043 – -0,094	-0,012 – -0,045
	Zone Percentage	0,245* - 0,442**	-0,056 – -0,277**	-0,120 – -0,156	0,014 - 0,221*	0,229* - 0,457**	0,254* - 0,441**	-0,023 – -0,200*	-0,220* - -0,724**	-0,065 – -0,087	-0,028 – -0,092
	Low Gray-Level Zone Emphasis	-0,496** - 0,512**	-0,052 - 0,228*	0,050 - 0,143	0,024 - 0,129	-0,269** - -0,540**	-0,340** - -0,545**	0,086 - 0,320**	0,288** - 0,767**	0,009 - 0,097	0,035 - 0,158
	High Gray-Level Zone Emphasis	0,164 - 0,418**	-0,094 - 0,289**	-0,03 - -0,077	-0,062 – -0,248*	0,149 - 0,466**	0,192 - 0,434**	-0,160 – -0,380**	-0,169 – -0,688**	-0,072 – -0,128	-0,024 – -0,134
	Small Zone Low Gray-Level Zone Emphasis	-0,252* - 0,515**	0,118 - 0,228*	0,040 - 0,133	0,027 - 0,121	-0,244* - -0,534**	-0,305** - -0,543**	0,016 - 0,355**	0,255** - 0,771**	0,006 - 0,120	0,027 - 0,165

	Small Zone High Gray-Level Zone Emphasis	0,169 - 0,400**	-0,093 – -0,288**	-0,002 – -0,059	-0,055 – -0,285**	0,156 - 0,448**	-0,200* - 0,415**	-0,158 – -0,374**	-0,167 - 0,674**	-0,076 – -0,129	-0,094 – -0,121
	Large Zone Low Gray-Level Zone Emphasis	-0,092 - 0,463**	0,016 - 0,180	0,104 - 0,180**	-0,012 – -0,198*	-0,162 – -0,492**	-0,200* - -0,501**	-0,123 - 0	0,113 - 0,684**	0,028 - 0,059	0,035 - 0,164
	Large Zone High Gray-Level Zone Emphasis	0,045 - 0,225*	-0,054 - 0,122	0,045 - 0,102	-0,052 – -0,148	0,006 – 0,100	0,009 – 0,146	-0,165 – -0,389**	-0,160 – -0,201*	0,021 - 0,137	-0,092 – -0,174*
	Grey-Level Variance	0,151 - 0,492**	0,026 – -0236*	-0,089 – -0,161	0,006 - 0,126	0,190 - 0,553**	0,290** - 0,543**	0,023 - 0,084	-0,211* - -0,759**	0,026 - 0,112	0,049 - 0,181
	Zone-Size Variance	0,021 - 0,184	0,033 - 0,152	-0,046 – -0,131	0,039 - 0,214*	0,022 - 0,196*	0,102 – 0,193	0,080 - 0,183	0,050 – -0,220*	0,021 - 0,242*	-0,034 – -0,145
NGTDM	Coarseness	0,170 - 0,332**	0,004 - 0,128	-0,011 – -0,113	0,048 - 0,157	0,053 - 0,340**	0,108 - 0,360**	0,017 - 0,131	-0,141 – -0,469**	-0,014 – -0,053	-0,085 – -0,146*
	Contrast	0,021 - 0,200**	-0,081 – -0,240*	-0,060 – -0,059	-0,090 – -0,290**	0,013 - 0,212*	0,074 – 0,119	-0,001 – -0,268**	-0,004 – -0,409**	-0,007 – -0,207*	0,009 - 0,041
	Busyness	-0,168 - 0,490**	-0,033 - 0,228*	0,027 - 0,157	0,023 - 0,130	-0,180 – -0,518**	-0,176 – -0,532**	0,043 - 0,167	0,201* - 0,730**	0,020 - 0,111	0,095 - 0,178
	Complexity	0,074 - 0,290**	-0,114 – -0,294**	-0,007 – -0,041	-0,081 – -0,296**	0,076 - 0,354**	0,103 - 0,305**	-0,093 - 0,323**	-0,113 – -0,576**	-0,060 – -0,136	-0,016 – -0,073
	Strength	0,078 0,203*	-0,02 – -0,206*	0,014 - 0,085	-0,018 – -0,269**	0,028 - 0,243*	0,067 - 0,220*	-0,029 – -0,367**	-0,121 – -0,325**	-0,029 – -0,147	-0,029 – -0,075

Abbreviations: BMI: body mass index; MS: muscle strength; MT: muscle thickness; SFT: subcutaneous fat thickness; OPQoL: Older´s People Quality of Life; AU: arbitrary units; IHF: Intensity Histogram Features; GLCM: Gray-Level Co-occurrence Matrix; GLRLM: Gray-Level run-Length Matrix; GLSZM: Gray-Level Size Zone Matrix; NGTDM: Neighborhood Gray-Tone Difference Matrix.

Rho of Spearman used for the statistical analysis

* The correlation is significant at the 0.05 level (bilateral).

** The correlation is significant at the 0.01 level (bilateral).

4.4.4 Correlations of Texture Features with Outcomes

Table 4.10 is a summary of the correlations with outcomes in both muscles (*Rectus Femoris* and *Vastus Intermedius*) and planes (axial and sagittal). The information presented is the range of correlations of the four analyses done, with the minimum and maximum correlation shown in each box. Full details of the analysis for texture features and comorbidities outcomes for both muscles and planes can be found in Annex 11.

Statistically significant associations between texture features and comorbidities outcomes were found. This includes the development of hearing impairment (for 35 out of 43 features), stroke (37 out of 43 features), myocardial infarction (37 out of 43 features), dementia/memory loss (30 out of 43 features), increased CCI (30 out of 43 features), falls (29 out of 43 features), increased visits to primary care (25 out of 43 features), and death (40 out of 43 features). All of these associations were weak.

The data for hypertension, hyperlipidemia, diabetes mellitus, chronic obstructive pulmonary disease, visual impairment, Parkinson disease, congestive heart failure, renal disease, previous cancer, arthritis/osteoarthritis, anxiety/depression, previous fracture, liver disease, connective tissue disease, hemiplegia, neoplasm, leukemia, solid metastasis, peripheral vascular disease, smoker, obesity, number of visits to emergency department and number of hospitalization are not shown in table 3.10, due to the lack of statistically significant associations. See Annex 11 for full results.

Table 4.10 Summary of Texture Features Correlations with Outcomes (n = 101)									
	Texture Feature	*Hearing Impairment*	*Previous Stroke*	*Myocardial Infarction*	*Dementia/ Memory Loss*	*CCI*	*Falls*	*# of Visits to PC*	*Death*
IHF	Variance	0,034 - 0,188*	0,024 – 0,151	0,010 - 0,195*	0,039 – 0,121	0,014 – 0,115	0,001 – 0,149	0,064 - 0,144*	0,107 - 0,297**
	Skewness	-0,062 – -0,146	-0,104 – -0,179*	-0,089 – -0,197*	-0,023 – -0,214**	-0,072 – -0,245**	-0,012 – -0,127	-0,002 – -0,185**	-0,140 – -0,356**
	Kurtosis	-0,058 – -0,190*	-0,129 – -0,189*	-0,079 – -0,230**	-0,029 – -0,223**	-0,061 – -0,222**	-0,035 – -0,175*	-0,027 – -0,190**	-0,158 - 0,366**
GLCM	Energy	-0,180* - -0,198*	-0,177 – -0,244**	-0,082 - 0,213**	-0,104 – 0,223**	-0,061 – -0,206**	-0,081 – -0,217**	-0,052 – -0,164*	-0,117 – -0,326**
	Contrast	0,148 - 0,194*	0,067 - 0,186*	0,008 – 0,159	0,032 – 0,159	0,002 – 0,061	0,042 – 0,080	-0,001 – -0,092	0,022 - 0,258**
	Entropy	0,170* - 0,196*	0,156 - 0,233**	0,054 - 0,219**	0,140 – 0,184*	0,018 - 0,188*	0,080 - 0,199*	0,022 - 0,162*	0,071 - 0,309**
	Homogeneity	-0,180* - -0,198*	-0,103 – -0,230**	-0,067 – -0,215**	-0,124 – -0,164*	-0,004 - 0,183*	-0,058 – -0,162*	-0,017 – -0,148*	-0,073 – -0,288**
	Correlation	-0,002 – -0,146	0,073 – 0,134	-0,010 – -0,118	0 - 0,116	0,071 - 0,157*	0,019 – 0,118	0,006 - 0,147*	0,015 – 0,109
	Sum Average	0,166* - 0,198*	0,140 - 0,226**	0,083 - 0,216**	0,110 – 0,232**	0,051 - 0,198**	0,066 - 0,222**	0,033 - 0,163*	0,127 - 0,349**
	Variance	0,136 - 0,196*	0,107 - 0,199*	0,004 - 0,192*	0,119 – 0,169*	0,011 – 0,119	0,067 - 0,194*	0,005 – 0,127	0,008 - 0,287**
	Dissimilarity	0,164* - 0,196*	0,087 - 0,199*	0,029 - 0,189*	0,072 – 0,150	0,031 – 0,120	0,041 – 0,100	0,012 – 0,102	0,011 - 0,282**
	Auto-Correlation	0,160 - 0,198*	0,133 - 0,223**	0,071 - 0,215**	0,116 – 0,222**	0,036 - 0,180*	0,073 - 0,220**	0,023 - 0,155*	0,113 - 0,340**
GLRLM	Short Run Emphasis	0,174* - 0,198*	0,114 - 0,234**	0,080 - 0,221**	0,123 – 0,156	0,054 - 0,180*	0,066 – 0,63*	0,030 - 0,148*	0,121 – 0,309*
	Long Run Emphasis	-0,170* - -0,196*	-0,090 – -0,226**	-0,080 - 0,221**	-0,114 – -0,198*	-0,072 – -0,164*	-0,099 – -0,180*	-0,059 – -0,126	-0,115 – -0,290**

	Gray-Level Nonuniformity	-0,156 – -0,194*	-0,159 – -0,227**	-0,064 – -0,222**	-0,131 – -0,203*	-0,059 – -0,187*	-0,087 – -0,230**	-0,014 - 0,145*	-0,088 – -0,338*
	Run Length Nonuniformity	0,174* - 0,198*	-0,159 – -0,227**	0,081 - 0,219**	0,118 – 0,153	0,057 - 0,179*	0,063 - 0,164*	0,047 - 0,145*	0,123 - 0,313**
	Run Percentage	0,172* - 0,198*	0,103 - 0,237**	-0,079 – -0,214**	0,121 – 0,192*	0,063 - 0,188*	0,059 - 0,171*	0,047 - 0,145*	0,124 - 0,297**
	Low Gray-Level Run Emphasis	-0,092 – -0,178*	-0,111 – -0,223**	-0,039 – -0,232**	0,079 – -0,233**	-0,127 – -0,227**	-0,006 – -0,188*	-0,069 – -0,145*	-0,146 – -0,285**
	High Gray-Level Run Emphasis	0,158 - 0,198*	-0,111 - 0,226**	0,065 - 0,213**	0,125 – 0,209*	0,033 - 0,165*	0,076 - 0,221**	0,035 - 0,145*	0,109 - 0,348**
	Short Run Low Gray-Level	-0,108 – -0,180*	-0,093 – -0,224**	-0,002 – -0,250**	-0,081 – -0,239**	-0,119 – -0,219**	-0,014 – -0,182*	-0,067 – -0,162*	-0,130 – -0,264**
	Short Run High Gray-Level	0,158 - 0,198*	0,136 - 0,227**	0,067 - 0,219**	0,127 – 0,206*	0,032 - 0,163*	0,076 - 0,220**	0,032 - 0,147*	0,108 - 0,349**
	Long Run Low Gray-Level	-0,074 – -0,122	0,061 – -0,176*	-0,097 – -0,194**	-0,086 – 0,204*	-0,015 – -0,217**	-0,004 – -0,175*	-0,018 – -0,138*	-0,013 – -0,239**
	Long Run High Gray-Level	0,160 - 0,196*	0,117 - 0,227**	0,061 - 0,230**	0,119 – 0,224**	0,031 - 0,172*	0,092 - 0,215**	0,029 - 0,152*	0,111 - 0,348**
	Gray-Level Variance	0,038 - 0,184*	0,066 – 0,144	0,055 - 0,177*	0,038 – 0,219**	0,057 - 0,194**	0,006 - 0,209*	0,067 - 0,150*	0,036 - 0,294**
	Run-Length Variance	-0,026 – -0,146	0,023 – -0,187*	-0,001 – -0,025	-0,035 – -0,081	0,039 – 0,122	-0,051 – -0,164*	-0,038 – -0,130	-0,012 – -0,084
GLSZM	Small Zone Emphasis	0,142 - 0,198*	0,056 - 0,190*	0,056 - 0,169*	0,009 – 0,148	0,011 – 0,020	0,003 – 0,159	0 - 0,107	0,078 - 0,233**
	Large Zone Emphasis	-0,166* - -0,198*	0,084 – -0,223**	-0,081 – -0,194*	-0,119 – -0,182*	-0,091 – -0,165*	-0,053 – -0,166*	-0,056 – -0,119	-0,122 – -0,283**
	Gray-Level Nonuniformity	-0,146 – -0,194*	-0,143 – -0,226**	-0,034 – -0,221*	-0,135 – -0,186*	-0,032 – -0,173*	-0,053 – -0,166*	-0,007 – -0,159*	-0,059 – -0,331**
	Zone-Size Nonuniformity	0,142 - 0,198*	0,057 - 0,189*	0,054 - 0,168*	0,010 – 0,157	0,010 – 0,020	0,046 – 0,158	0,001 – -0,108	0,077 - 0,231**
	Zone Percentage	0,174* - 0,198*	0,091 - 0,229**	0,064 - 0,218**	0,127 - 0,166*	0,036 - 0,178*	0,060 - 0,175*	0,018 - 0,136	0,107 - 0,299**
	Low Gray-Level Zone Emphasis	-0,110 – -0,190*	-0,134 – -0,226**	-0,067 – -0,232**	-0,099 – -0,257**	-0,099 - 0,221**	-0,028 – -0,194*	-0,035 – -0,157*	-0,174* - 0,306**

	High Gray-Level Zone Emphasis	0,154 - 0,198*	0,127 - 0,226**	0,056 - 0,218**	0,129 – 0,205*	0,026 - 0,164*	0,077 - 0,218**	0,035 - 0,145*	0,092 - 0,345**
	Small Zone Low Gray-Level Zone Emphasis	-0,110 – -0,190*	-0,137 – -0,236**	-0,082 - 0,236**	-0,098 – -0,258**	-0,093 – -0,221**	0,036 – -0,185*	-0,040 – -0,151*	-0,154 – -0,307**
	Small Zone High Gray-Level Zone Emphasis	0,152 - 0,198*	0,127 - 0,227**	0,059 - 0,215**	0,128 – 0,96*	0,018 - 0,153*	0,076 - 0,221**	0,038 - 0,141*	0,090 - 0,339**
	Large Zone Low Gray-Level Zone Emphasis	-0,030 – -0,140	-0,013 - 0,170*	-0,067 – -0,173*	-0,034 – 0,178*	-0,022 – -0,192**	0,001 – 0,073	0,010 – 0,093	0,042 – 0,213*
	Large Zone High Gray-Level Zone Emphasis	0,034 - 0,176*	0,061 - 0,217**	0,025 - 0,181*	0,013 – 0,124	0,003 – 0,113	0,014 - 0,167*	0,056 – 0,093	0,091 – 0,173*
	Grey-Level Variance	0,056 – 0,144	0,087 - 0,200*	0,022 - 0,184*	0,081 – 0,180*	0,007 - 0,147*	0,018 – 0,107	0,056 – 0,131	0,015 - 0,288**
	Zone-Size Variance	-0,014 – -0,154	-0,003 – -0,120	-0,035 – 0,129	0,009 – 0,082	0,007 – 0,053	-0,033 – -0,122	-0,012 – -0,073	0,021 – 0,124
NGTDM	Coarseness	0,026 – 0,058	0,010 – 0,033	0,098 – 0,136	0,055 – 0,163*	0,005 – 0,141	-0,009 – -0,125	0,005 – 0,033	0,089 – 0,202*
	Contrast	0,134 – 0,192*	0,064 – 0,160	0,005 – 0,188*	0,050 – 0,131	0,032 – 0,115	0,015 – 0,132	0,058 – 0,113	0,029 – 0,271**
	Busyness	0,114 – -0,170*	-0,133 – -0,171*	0,058 – -0,216**	0,076 – -0,236**	0,011 - 0,196**	-0,022 – -0,140	-0,019 – -0,132	-0,122 - 0,347**
	Complexity	0,154 – 0,196*	0,106 – 0,214**	0,015 – 0,197*	0,089 – 0,164*	0,005 – 0,118	0,063 - 0,177*	0,020 – 0,110	0,013 - 0,288**
	Strength	0,068 – 0,162*	0,004 – 0,107	0,009 – 0,157	0,054 – 0,148	0,002 – 0,085	0,064 – 0,091	0,015 – 0,033	0,035 – 0,212**

Abbreviations: CCI: Charlson Comorbidity Index; PC: Primary Care; #: Number; IHF: Intensity Histogram Features; GLCM: Gray-Level Co-occurrence Matrix; GLRLM: Gray-Level Run-Length Matrix; GLSZM: Gray-Level Size Zone Matrix; NGTDM: Neighborhood Gray-Tone Difference Matrix.

Tau B of Kendal used for the statistical analysis.

* The correlation is significant at the 0.05 level (bilateral).

** The correlation is significant at the 0.01 level (bilateral).

The data for hypertension, hyperlipidemia, diabetes mellitus, chronic obstructive pulmonary disease, visual impairment, Parkinson disease, congestive heart failure, renal disease, previous cancer, arthritis/osteoarthritis, anxiety/depression, previous fracture, liver disease, connective tissue disease, hemiplegia, neoplasm, leukemia, solid metastasis, peripheral vascular disease, smoker, obesity, number of visits to emergency department and number of hospitalization are not shown.

4.5 Texture Analysis

4.5.1 ROC of Texture Features

To determine the accuracy or discriminative power of each texture feature from both muscles (*Rectus Femoris* and *Vastus Intermedius*) and plane (axial and sagittal) area under receiver operator characteristic curve (AUC) were calculated. Frailty phenotype was dichotomized into non-frail (controls and robust group) and at risk of frailty or frail (pre-frail and frail groups) for the analysis. Only one feature out of 43 in *Rectus Femoris* axial plane and *Rectus Femoris* sagittal plane had a good AUC. In *Vastus Intermedius* axial plane, 8 out of 43 features had good AUC and 4 out of 43 features in the *Vastus Intermedius* sagittal plane. The rest of the features performed either moderately or poorly. The complete results are shown in Table 4.11.

Table 4.11 AUC of Texture Features by Muscle and Plane

Muscle and Plane		*Rectus Femoris*		*Vastus Intermedius*	
		Axial	*Sagittal*	*Axial*	*Sagittal*
Texture Features		***AUC ± 95%CI***	***AUC ± 95%CI***	***AUC ± 95%CI***	***AUC ± 95%CI***
IHF	Variance	0,577 ± 0,112	0,519 ± 0,114	0,502 ± 0,113	0,571 ± 0,112
	Skewness	0,345 ± 0,109	0,420 ± 0,106	0,316 ± 0,112	0,264 ± 0,100
	Kurtosis	0,326 ± 0,106	0,406 ± 0,110	0,353 ± 0,111	0,288 ± 0,103
GLCM	Energy	0,338 ± 0,105	0,361 ± 0,092	0,226 ± 0,108	0,284 ± 0,103
	Contrast	0,528 ± 0,114	0,590 ± 0,114	0,551± 0,112	0,555 ± 0,115
	Entropy	0,610 ± 0,110	0,620 ± 0,101	0,711 ± 0,110	0,687 ± 0,107
	Homogeneity	0,385 ± 0,110	0,347 ± 0,099	0,281 ± 0,108	0,313 ± 0,106
	Correlation	0,515 ± 0,113	0,366 ± 0,112	0,589 ± 0,109	0,564 ± 0,114
	Sum Average	0,631 ± 0,110	0,627 ± 0,095	0,747 ± 0,110	0,715 ± 0,103
	Variance	0,532 ± 0,114	0,530 ± 0,113	0,582 ± 0,114	0,586 ± 0,113
	Dissimilarity	0,549 ± 0,113	0,601 ± 0,110	0,622 ± 0,111	0,617 ± 0,112
	Auto-Correlation	0,613 ± 0,110	0,601 ± 0,099	0,720 ± 0,111	0,695 ± 0,105
GLRLM	Short Run Emphasis	0,643 ± 0,107	0,679 ± 0,104	0,693 ± 0,104	0,691 ± 0,106
	Long Run Emphasis	0,326 ± 0,104	0,285 ± 0,096	0,240 ± 0,100	0,276 ± 0,102
	Gray-Level Nonuniformity	0,386 ± 0,110	0,408 ± 0,105	0,322 ± 0,112	0,323 ± 0,107
	Run Length Nonuniformity	0,643 ± 0,107	0,678 ± 0,104	0,691 ± 0,104	0,685 ± 0,106
	Run Percentage	0,661 ± 0,105	0,700 ± 0,097	0,750 ± 0,102	0,711 ± 0,103
	Low Gray-Level Run Emphasis	0,326 ± 0,110	0,343 ± 0,091	0,208 ± 0,109	0,250 ± 0,099
	High Gray-Level Run Emphasis	0,608 ± 0,111	0,609 ± 0,102	0,695 ± 0,112	0,682 ± 0,106
	Short Run Low Gray-Level	0,325 ± 0,110	0,353 ± 0,093	0,212 ± 0,109	0,254 ± 0,099
	Short Run High Gray-Level	0,606 ± 0,111	0,613 ± 0,102	0,695 ± 0,111	0,679 ± 0,106
	Long Run Low Gray-Level	0,334 ± 0,111	0,368 ± 0,097	0,226 ± 0,109	0,267 ± 0,101
	Long Run High Gray-Level	0,599 ± 0,111	0,586 ± 0,100	0,714 ± 0,113	0,687 ± 0,106
	Gray-Level Variance	0,720 ± 0,102	0,619 ± 0,098	0,763 ± 0,110	0,749 ± 0,098

	Run-Length Variance	0,638 ± 0,108	0,525 ± 0,113	0,638 ± 0,114	0,635 ± 0,110
GLSZM	Small Zone Emphasis	0,600 ± 0,110	0,641 ± 0,116	0,478 ± 0,108	0,534 ± 0,117
	Large Zone Emphasis	0,334 ± 0,105	0,268 ± 0,096	0,242 ± 0,097	0,274 ± 0,100
	Gray-Level Nonuniformity	0,410 ± 0,111	0,442 ± 0,107	0,340 ± 0,113	0,343 ± 0,108
	Zone-Size Nonuniformity	0,599 ± 0,110	0,639 ± 0,116	0,478 ± 0,108	0,533 ± 0,117
	Zone Percentage	0,643 ± 0,107	0,681 ± 0,102	0,702 ± 0,104	0,689 ± 0,106
	Low Gray-Level Zone Emphasis	0,325 ± 0,108	0,314 ± 0,092	0,216 ± 0,107	0,254 ± 0,100
	High Gray-Level Zone Emphasis	0,603 ± 0,111	0,605 ± 0,103	0,690 ± 0,112	0,679 ± 0,107
	Small Zone Low Gray-Level Zone Emphasis	0,319 ± 0,106	0,322 ± 0,090	0,209 ± 0,109	0,257 ± 0,101
	Small Zone High Gray-Level Zone Emphasis	0,604 ± 0,111	0,609 ± 0,104	0,680 ± 0,112	0,666 ± 0,107
	Large Zone Low Gray-Level Zone Emphasis	0,375 ± 0,111	0,377 ± 0,098	0,239 ± 0,109	0,268 ± 0,099
	Large Zone High Gray-Level Zone Emphasis	0,573 ± 0,114	0,495 ± 0,119	0,567 ± 0,115	0,530 ± 0,117
	Grey-Level Variance	0,629 ± 0,110	0,689 ± 0,100	0,744 ± 0,103	0,748 ± 0,095
	Zone-Size Variance	0,555 ± 0,115	0,628 ± 0,116	0,556 ± 0,108	0,634 ± 0,113
NGTDM	Coarseness	0,572 ± 0,113	0,521 ± 0,107	0,653 ± 0,114	0,627 ± 0,109
	Contrast	0,510 ± 0,113	0,563 ± 0,116	0,534 ± 0,112	0,559 ± 0,114
	Busyness	0,369 ± 0,110	0,422 ± 0,097	0,253 ± 0,113	0,277 ± 0,099
	Complexity	0,562 ± 0,113	0,594 ± 0,110	0,622 ± 0,113	0,611 ± 0,111
	Strength	0,564 ± 0,114	0,513 ± 0,116	0,515 ± 0,115	0,549 ± 0,113

AUC: Area Under the Curve; CI: Confidence Interval; IHF: Intensity Histogram Features; GLCM: Gray-Level Co-occurrence Matrix; GLRLM: Gray-Level run-Length Matrix; GLSZM: Gray-Level Size Zone Matrix; NGTDM: Neighbourhood Gray-Tone Difference Matrix, NA: Not Applicable.

All data presented as AUC ± 95%CI. The AUC values were classified poor for values ≤0.60, fair for 0.61-0.70, moderate for 0.71-0.80, good for 0.81-0.90 and very good for 0.91-1.00.

4.5.2 Classification and Selection of Texture Features

We used the machine learning approach, described in the materials and methods section, for the selection and classification of the texture features. The predictive performance of different feature selection and classification methods was assessed using the area under receiver operator characteristic curve (AUC). Table 4.12 summarizes the AUC ± 95%CI of the process by both ranking methods (P-value and RFE-SVM), by the six predictive models used (NB, k-NN, RF, MLP, SVM_L, and SVM_R), by both muscles (*Rectus Femoris* and *Vastus Intermedius*), by both planes (axial and sagittal), and by four different numbers of gray levels (256, 128, 64 and 32). Table 4.12 also depicts the performance of feature selection (in columns) and classification (in rows), using the 43 texture features of the study. The best predictive models after the combination of feature selection and classification for every muscle and plane are marked in orange; and all the predictive models that achieve an AUC above 0,700 are marked in yellow.

able 4.12 ROC Curves of Predictive Models by Texture Feature Selection and Classification Method by Muscle, Plane and Gray Levels (n = 101)									
Selection Method	***P-value***				***Clasification Method***	***RFE-SVM***			
Muscle and Plane	***Rectus Femoris***		***Vastus Intermedius***			***Rectus Femoris***		***Vastus Intermedius***	
	Axial	***Sagittal***	***Axial***	***Sagittal***		***Axial***	***Sagittal***	***Axial***	***Sagittal***
256 Ng	0,662 ± 0,186	0,682 ± 0,188	0,772 ± 0,184	0,735 ± 0,196	*NB*	0,639 ± 0,202	0,644 ± 0194	0,661 ± 0,182	0,728 ± 0,204*
	0,645 ± 0,196	0,655 ± 0,159	0,760 ± 0,178	0,723 ± 0,198	*k-NN*	0,600 ± 0,206	0,654 ± 0,188	0,730 ± 0,198	0,708 ± 0,194
	0,678 ± 0,218	0,624 ± 0,167	0,737 ± 0,159	0,700 ± 0,192	*RF*	0,665 ± 0,194*	0,627 ± 0,174	0,723 ± 0,171	0,697 ± 0,192
	0,687 ± 0,204*	0,706 ± 0,167	0,785 ± 0.174*	0,730 ± 0,192	*MLP*	0,654 ± 0,206	0,657 ± 0,180	0,739 ± 0,200	0,726 ± 0,235
	0,684 ± 0,204	0,720 ± 0,180*	0,782 ± 0,174	0,742 ± 0.200*	*SVM_L*	0,657 ± 0,198	0,675 ± 0,174*	0,743 ± 0,214	0,726 ± 0,235
	0,645 ± 0,261	0,595 ± 0,245	0,750 ± 0,174	0,722 ± 0,202	*SVM_R*	0,643 ± 0,200	0,577 ± 0,253	0,749 ± 0,180*	0,705 ± 0,210
128 Ng	0,642 ± 0,218	0,682 ± 0,188	0,783 ± 0,172	0,740 ± 0,206	*NB*	0,619 ± 0,204	0,634 ± 0,167	0,767 ± 0180*	0,730 ± 0,204*
	0,606 ± 0,188	0,646 ± 0,218	0,778 ± 0,172	0,734 ± 0,214	*k-NN*	0.612 ± 0.100	0,622 ± 0,202	0,727 ± 0,192	0,700 ± 0,221
	0,663 ± 0,206*	0,670 ± 0,198	0,757 ± 0,178	0,715 ± 0,192	*RF*	0,670 ± 0.204*	0,624 ± 0,182	0,734 ± 0,171	0,712 ± 0,198
	0,642 ± 0,220	0,680 ± 0,194*	0,800 ± 0,174*	0,729 ± 0,018	*MLP*	0,638 ± 0,184	0,677 ± 0,196*	0,742 ± 0,216	0,726 ± 0,204
	0,641 ± 0,188	0,675 ± 0,231	0,795 ± 0,165	0,745 ± 0,190*	*SVM_L*	0,635 ± 0,172	0,664 ± 0,196	0,748 ± 0,174	0,719 ± 0,227
	0,589 ± 0,265	0,648 ± 0,231	0,761 ± 0,182	0,712 ± 0,206	*SVM_R*	0,609 ± 0,243	0,579 ± 0,249	0,739 ± 0,188	0,698 ± 0,204
64 Ng	0,651 ± 0,097	0,627 ± 0,188	0,778 ± 0,180	0,743 ± 0,202*	*NB*	0,622 ± 0,182	0,597 ± 0,194	0,756 ± 0.183*	0,724 ± 0,208
	0,622 ± 0,098	0,618 ± 0,220	0,772 ± 0,178	0,730 ± 0,206	*k-NN*	0,613 ± 0,227	0,593 ± 0,192	0,710 ± 0,194	0,715 ± 0,204
	0,653 ± 0,202	0,608 ± 0,188	0,755 ± 0,169	0,728 ± 0,190	*RF*	0,653 ± 0,210	0,612 ± 0,188	0,732 ± 0,161	0,726 ± 0,196
	0,703 ± 0,188*	0,660 ± 0,206*	0,801 ± 0,169*	0,717 ± 0,200	*MLP*	0,660 ± 0,243*	0,647 ± 0,210	0,745 ± 0,212	0,727 ± 0,198
	0,642 ± 0,097	0,657 ± 0,196	0,798 ± 0,186	0,733 ± 0,208	*SVM_L*	0,608 ± 0,190	0,658 ± 0,204*	0,751 ± 0,196	0,728 ± 0.198*
	0,637 ± 0,124	0,583 ± 0,233	0,754 ± 0,190	0,729 ± 0,198	*SVM_R*	0,614 ± 0,210	0,575 ± 0,241	0,743 ± 0,182	0,692 ± 0,216
32 Ng	0,647 ± 0,194	0,626 ± 0,200	0,762 ± 0,180	0,732 ± 0,208*	*NB*	0,641 ± 0,200	0,593 ± 0,206	0,755 ± 0,174*	0,720 ± 0,216
	0,627 ± 0,229	0,616 ± 0,204	0,758 ± 0,178	0,706 ± 0,198	*k-NN*	0,590 ± 0,212	0,590 ± 0,218	0,700 ± 0,206	0,702 ± 0,214
	0,647 ± 0,188	0,620 ± 0,208	0,720 ± 0,172	0,695 ± 0,198	*RF*	0,618 ± 0,192	0,616 ± 0,206	0,712 ± 0,180	0,699 ± 0,196
	0,643 ± 0,192	0,678 ± 0,204*	0,780 ± 0,180*	0,710 ± 0,208	*MLP*	0,599 ± 0,210	0,655 ± 0,184	0,732 ± 0,190	0,712 ± 0,206
	0,609 ± 0,196	0,694 ± 0,202	0,775 ± 0,180	0,721 ± 0,204	*SVM_L*	0,587 ± 0,208	0,684 ± 0,182*	0,733 ± 0,188	0,712 ± 0,206
	0,659 ± 0,216*	0,578 ± 0,241	0,767 ± 0,174	0,717 ± 0,208	*SVM_R*	0,608 ± 0,247	0,576 ± 0.249	0,714 ± 0,204	0,722 ± 0,190*

Abbreviations: RFE-SVM: recursive feature elimination-support vector machine; RF: Rectus Femoris, VI: Vastus Intermedius; Ng: Number of gray levels; NB: naïve Bayes; k-NN: k-nearest neighbours classifier, RF: random forests; MLP: multilayer perceptron; SVM_L: support vector machine with linear kernel; SVM_R: support vector machine with radial kernel; AUC: area under the curve; CI: confidence interval.

All data presented as AUC ± 95%CI. The AUC values were classified poor for values ≤0.60, fair for 0.61-0.70, moderate for 0.71-0.80, good for 0.81-0.90 and very good for 0.91-1.00. Moderate or greater mark in yellow.

* Represents the best model for each ranking, muscle, plane and number of gray levels

Higher AUCs were achieved with P-value than with recursive feature elimination-support vector machine (RFE-SVM) for the feature selection process. For classification methods, multilayer perceptron (MLP) and support vector machine with linear kernel (SVM_L) had the highest predictive performance.

When we compare the AUC of the different gray levels, we can see that there is little or no improvement in the AUC when diminishing the number of gray levels. For this reason, we used the best model (marked in orange) in each muscle, plane and ranking method for further analysis from the 256 gray level (see next section).

4.5.3 Description of Best Frailty Models with Stepwise Multiple Logistic Regression

In the next section, we describe each predictive model, the selection and classification method applied, the optimal number of texture features that comprised each model, and the AUC with its corresponding sensitivity and specificity. To quantify the effects of each model on the likelihood of having frailty phenotype, after adjusting for ultrasound characteristic (subcutaneous fat thickness and muscle thickness) and physical characteristics (age, sex, BMI, gait speed, and muscle strength) a stepwise multiple logistic regression analysis was applied.

4.5.3.1 Frailty Model 1

The frailty model 1 corresponds to the *Rectus Femoris* muscle in the axial plane, from the P-value feature selection method and MLP classification method. The optimal texture features selected were 22 for this model. The AUC ± SD was 0,687 ± 0,104 with a sensitivity of 55% and specificity of 73% (See Graph 4.1).

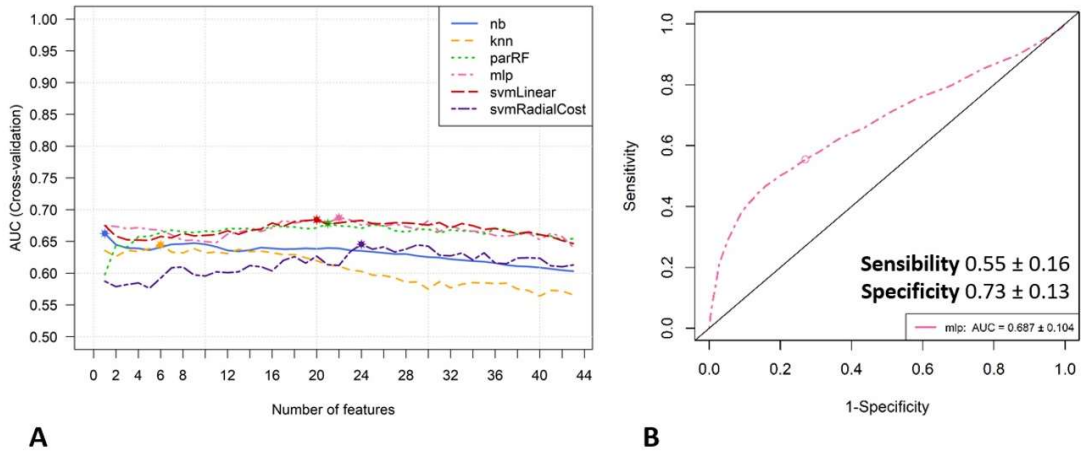

Graph 4.1 (A) Graphical representation depicting the predictive performance (AUC) of the classifier to discriminate between at risk of frailty vs. non-frail for frailty model 1 (B) ROC curve for frailty model 1

Table 4.13 Stepwise Multiple Logistic Regression Analysis of Texture Analysis Frailty Model 1 (Ranking P value, ROI: RF and Axial Plane, Ng = 256, Predictive Model = MLP)									
	Texture Analysis Frailty Model			**Adjustment with Ultrasound Characteristics**			**Adjustment with Physical Characteristics**		
Variable	**Coefficient**	**Wald Statistic***	**OR**	**Coefficient**	**Wald Statistic***	**OR**	**Coefficient**	**Wald Statistic***	**OR**
Frailty Phenotype (Constant)	-2709,9	0,218	0,00	-2874,0	0,258	0,00	-7475,9	0,109	0,00
Subcutaneous Fat Thickness (cm)				0,7	0,356	2,10	-1,0	0,786	0,38
Muscle Thickness (cm)				-1,9	0,004	0,15	-0,4	0,788	0,66
Age (years)							0,1	0,258	1,12
Sex (Female = 0/Male = 1)							1,8	0,577	5,93
BMI (kg/m2)							0,3	0,404	1,29
Gait Speed (s)							3,9	0,076	48
Muscle Strenght (kg)							-0,1	0,301	0,92
Block Chi-Square [df]				11,18 [2], p = 0,003			43,59 [5], p = <0,001		
Model Chi-Square [df]	51,57 [22], p = 0,<0,001			62,75 [24], p = <0,001			106,34 [29], p = <0,001		
Nagelkerke-R^2	0,535			0,619			0,870		
Hosmer y Lemeshow Test	0,959			0,065			0,242		
Correct Predictions (%)	80,2			85,1			96,0		

Abbreviations: ROI: Region of Interest; RF: Rectus Femoris, Ng: Number of gray levels; MLP: multilayer perceptron; OR: Odd Ratio; IHF: Intensity Histogram Features; GLCM: Gray-Level Co-occurrence Matrix; GLRLM: Gray-Level run-Length Matrix; GLSZM: Gray-Level Size Zone Matrix; NGTDM: Neighbourhood Gray-Tone Difference Matrix.

*The Wald statistics are distributed chi-square with 1 degree of freedom.

The stepwise multiple logistic regression analysis for frailty model 1 (see Table 4.13) was statistically significant in the first step, $\chi2(22) = 51.57$, $p < 0.001$. The model explained 53,5% (Nagelkerke R^2) of the variance in the frailty phenotype and correctly classified 80,2% of cases. When adjusted for ultrasound characteristics the second block and model was statistically significant, $\chi2(24) = 62,75$, $p < 0.001$. The model explained 61,9% (Nagelkerke R^2) of the variance in the frailty phenotype and correctly classified 85,2% of cases. When adjusted for physical characteristics the third block and model was statistically significant, $\chi2(29) = 106,34$, $p < 0.001$. The model explained 87,0% (Nagelkerke R^2) of the variance in the frailty phenotype and correctly classified 96,0% of cases. The model was independent of age, sex, BMI, subcutaneous fat thickness and muscle strength. Increased muscle thickness decreased the likelihood of exhibiting frailty by 75%, but decreased gait speed was associated with being 48 times more likely to exhibit frailty phenotype.

4.5.3.2 Frailty Model 2

The frailty model 2 corresponds to the *Rectus Femoris* muscle in the sagittal plane from the P-value feature selection method and SVM_L classification method. The optimal texture features selected were 14. The AUC ± SD was 0,720 ± 0.092 with a sensitivity of 64% and specificity of 65% (See Graph 4.2).

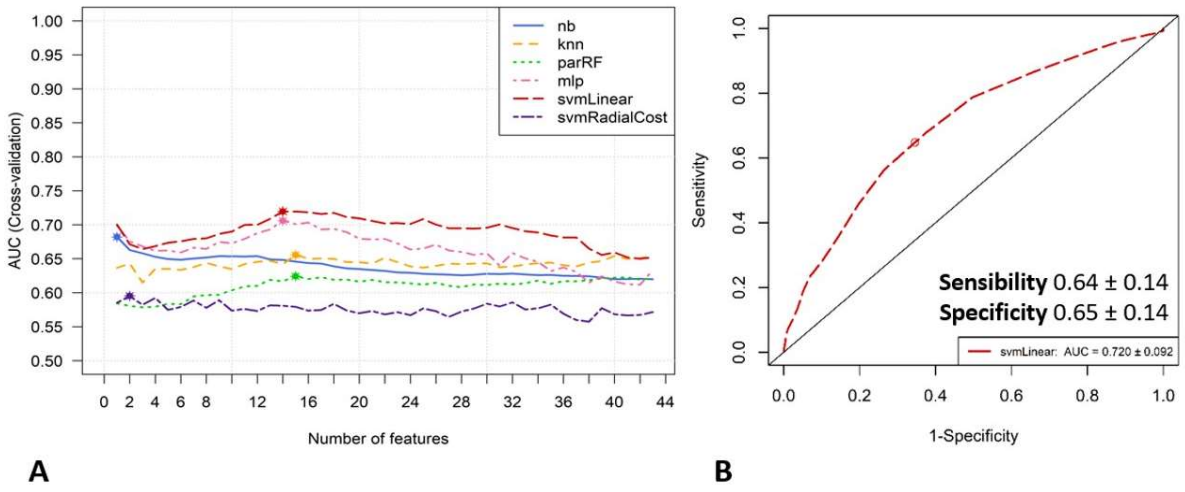

Graph 4.2 (A) Graphical representation depicting the predictive performance (AUC) of the classifier to discriminate between at risk of frailty vs. non-frail for frailty model 2 (B) ROC curve for frailty model 2

Table 4.14 Stepwise Multiple Logistic Regression Analysis of Texture Analysis Frailty Model 2 (Ranking P value, ROI: RF and Sagittal Plane, Ng = 256, Predictive Model = SVM_L)									
	Texture Analysis Frailty Model			**Adjustment with Ultrasound Characteristics**			**Adjustment with Physical Characteristics**		
Variable	**Coefficient**	**Wald Statistic***	**OR**	**Coefficient**	**Wald Statistic***	**OR**	**Coefficient**	**Wald Statistic***	**OR**
Frailty Phenotype (Constant)	-494	0,428	0,00	-1349	0,271	0,000	133978	0,998	
Subcutaneous Fat Thickness (cm)				-0,3	0,667	0,713	-265	0,984	0,00
Muscle Thickness (cm)				0,0	0,042	0,007	1,0	0,000	0,00
Age (years)							20,6	0,992	8,80e+8
Sex (Female = 0/Male = 1)							512	0,973	2,27e+222
BMI (kg/m2)							4,3	0,985	74
Gait Speed (s)							115	0,995	6,07e+49
Muscle Strenght (kg)							-7,4	0,992	0,00
Block Chi-Square [df]				21,07 [2], p = <0,001			70,34 [5], p = <0,001		
Model Chi-Square [df]	47,17 [14], p = 0,<0,001			68,88 [16], p = <0,001			139,21 [21], p = <0,001		
Nagelkerke-R^2	0,499			0,661			1,000		
Hosmer y Lemeshow Test	0,092			0,220			1,000		
Correct Predictions (%)	80,2			84,2			100		

Abbreviations: ROI: Region of Interest; RF: Rectus Femoris, Ng: Number of gray levels; SVM L: support vector machine with linear kernel; OR: Odd Ratio; GLCM: Gray-Level Co-occurrence Matrix; GLRLM: Gray-Level run-Length Matrix; GLSZM: Gray-Level Size Zone Matrix.

*The Wald statistics are distributed chi-square with 1 degree of freedom.

The stepwise multiple logistic regression analysis for frailty model 2 (see Table 4.14) was statistically significant in the first step, $\chi2(14) = 47,17$, $p < 0.001$. The model explained 49,9% (Nagelkerke R^2) of the variance in the frailty phenotype and correctly classified 80,2% of cases. When adjusted for ultrasound characteristics the second block and model was statistically significant, $\chi2(16) = 68,88$, $p < 0.001$. The model explained 66,1% (Nagelkerke R^2) of the variance in the frailty phenotype and correctly classified 84,2% of cases. When adjusted for physical characteristics the third block and model was statistically significant, $\chi2(21) = 139,21$, $p < 0.001$. The model explained 100,0% (Nagelkerke R^2) of the variance in the frailty phenotype and correctly classified 100,0% of cases. The model was independent of age, sex, BMI, subcutaneous fat thickness, gait speed, and muscle strength. Increased muscle thickness decreased the likelihood of exhibiting frailty by 93%.

4.5.3.3 Frailty Model 3

The frailty model 3 corresponds to the *Vastus Intermedius* muscle in the axial plane, from the P-value feature selection method and MLP classification method. The optimal texture features selected were two. The AUC ± SD was of 0,785 ± 0.089 with a sensitivity of 72% and specificity of 77% (See Graph 4.3).

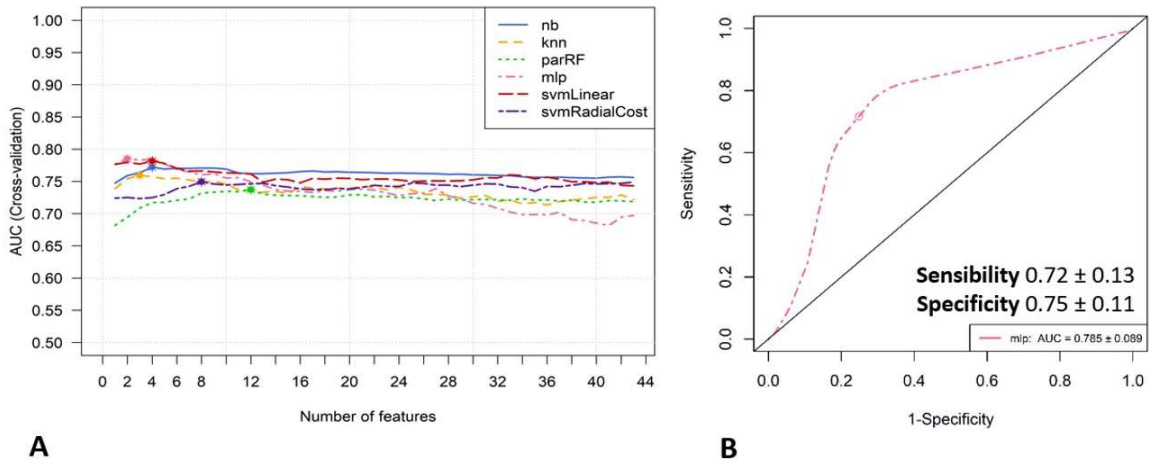

Graph 4.3 (A) Graphical representation depicting the predictive performance (AUC) of the classifier to discriminate between at risk of frailty vs. non-frail for frailty model 3 (B) ROC curve for frailty model 3

Table 4.15 Stepwise Multiple Logistic Regression Analysis of Texture Analysis Frailty Model 3 Ranking P value, ROI: VI and Axial Palne, Ng = 256, Predictive Model = MLP									
	Texture Analysis Frailty Model			**Adjustment with Ultrasound Characteristics**			**Adjustment with Physical Characteristics**		
Variable	**Coefficient**	**Wald Statistic***	**OR**	**Coefficient**	**Wald Statistic***	**OR**	**Coefficient**	**Wald Statistic***	**OR**
Frailty Phenotype (Constant)	1,0	0,005	2,72	2,8	0,013	17	-16	0,003	0,00
Subcutaneous Fat Thickness (cm)				0,1	0,900	1,06	-0,5	0,682	0,61
Muscle Thickness (cm)				-0,9	0,042	0,40	-0,4	0,644	0,66
Age (years)							0,1	0,048	1,11
Sex (Female = 0/Male = 1)							1,0	0,438	2,78
BMI (kg/m2)							0,2	0,128	1,20
Gait Speed (s)							1,9	0,001	6,89
Muscle Strenght (kg)							0,0	0,378	0,97
Block Chi-Square [df]				4,56 [2], p = 0,102			57,77 [5], p = <0,001		
Model Chi-Square [df]	19,07 [2], p = 0,<0,001			23,62 [4], p = <0,001			81,39 [9], p = <0,001		
Nagelkerke-R^2	0,230			0,279			0,740		
Hosmer y Lemeshow Test	0,025			0,622			0,334		
Correct Predictions (%)	70,3			71,3			87,1		

Abbreviations: ROI: Region of Interest; VI: Vastus Intermedius; Ng: Number of gray levels; MLP: multilayer perceptron; OR: Odd Ratio; GLRLM: Gray-Level run-Length Matrix; GLSZM: Gray-Level Size Zone Matrix.

*The Wald statistics are distributed chi-square with 1 degree of freedom.

The stepwise multiple logistic regression analysis for frailty model 3 (see Table 4.15) was statistically significant in the first step, $\chi2(2) = 19,07$, $p < 0.001$. The model explained 23,0% (Nagelkerke R^2) of the variance in the frailty phenotype and correctly classified 70,3% of cases. When adjusted for ultrasound characteristics the second block was not statically significant but the model was, $\chi2(4) = 23,62$, $p < 0.001$. The model explained 27,9% (Nagelkerke R^2) of the variance in the frailty phenotype and correctly classified 71,3% of cases. When adjusted for physical characteristics the third block and model was statistically significant, $\chi2(9) = 81,39$, $p < 0.001$. The model explained 74,0% (Nagelkerke R^2) of the variance in the frailty phenotype and correctly classified 87,1% of cases. The model was independent of sex, BMI, subcutaneous fat thickness, and muscle strength. Increased muscle thickness decreased the likelihood of exhibiting frailty by 60%. Increased age increased the likelihood of exhibiting frailty by 11%, but decreased gait speed was associated with being 7 times more likely to exhibit frailty phenotype.

4.5.3.4 Frailty Model 4

The frailty model 4 corresponds to the *Vastus Intermedius* muscle in the sagittal plane from the P-value feature selection method and SVM_L classification method. The optimal texture features selected were 11. The AUC ± SD was of 0,742 ± 0.101 with a sensitivity of 64% and specificity of 71% (See Graph 4.4).

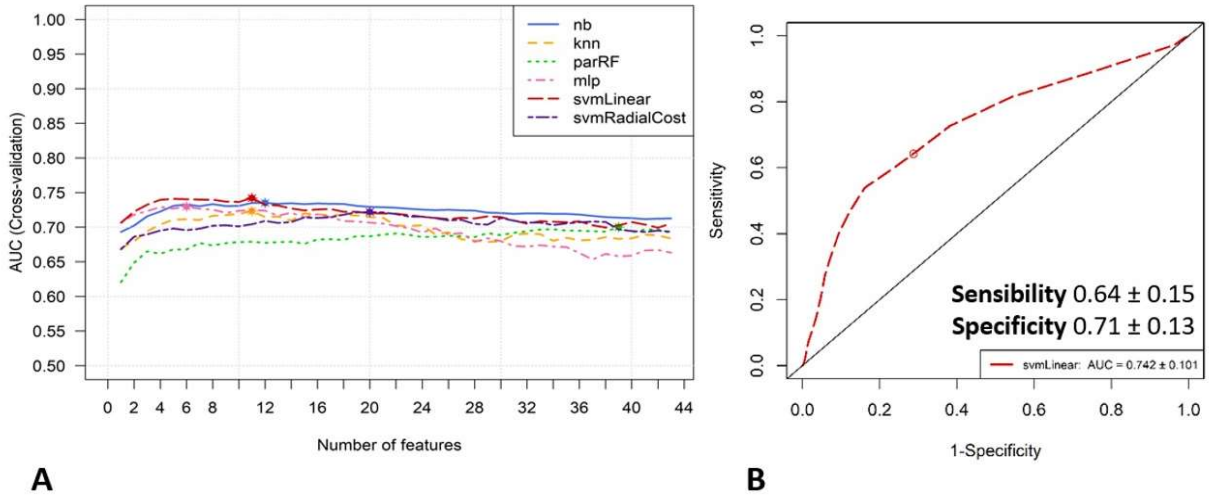

Graph 4.4 (A) Graphical representation depicting the predictive performance (AUC) of the classifier to discriminate between at risk of frailty vs. non-frail for frailty model 4 (B) ROC curve for frailty model 4

Table 4.16 Stepwise Multiple Logistic Regression Analysis of Texture Analysis Frailty Model 4 (Ranking P value, ROI: VI and Sagittal Plane, Ng = 256, Predictive Model = SVM_L)									
	Texture Analysis Frailty Model			**Adjustment with Ultrasound Characteristics**			**Adjustment with Physical Characteristics**		
Variable	**Coefficient**	**Wald Statistic***	**OR**	**Coefficient**	**Wald Statistic***	**OR**	**Coefficient**	**Wald Statistic***	**OR**
Frailty Phenotype (Constant)	1,6	0,225	5,17	1,9	0,319	6,73	-15,0	0,020	0,00
Subcutaneous Fat Thickness (cm)				0,6	0,309	1,85	0,5	0,781	1,66
Muscle Thickness (cm)				-0,5	0,508	0,63	-0,4	0,771	0,68
Age (years)							0,0	0,425	1,05
Sex (Female = 0/Male = 1)							0,7	0,645	2,04
Gait Speed (s)							2,4	0,003	10,80
Muscle Strenght (kg)							-0,1	0,096	0,92
Block Chi-Square [df]				2,10 [2], p = 0,351			53,22 [5], p = <0,001		
Model Chi-Square [df]	39,21 [11], p = 0,<0,001			41,30 [13], p = <0,001			94,52 [18], p = <0,001		
Nagelkerke-R^2	0,430			0,449			0,812		
Hosmer y Lemeshow Test	0,244			0,411			0,275		
Correct Predictions (%)	74,3			77,2			93,1		

Abbreviations: ROI: Region of Interest; VI: Vastus Intermidius; Ng: Number of gray levels; SVM L: support vector machine with linear kernel; OR: Odd Ratio; IHF: Intensity Histogram Features; GLRLM: Gray-Level run-Length Matrix; GLSZM: Gray-Level Size Zone Matrix; NGTDM: Neighborhood Gray-Tone Difference Matrix.

*The Wald statistics are distributed chi-square with 1 degree of freedom.

The stepwise multiple logistic regression analysis for frailty model 4 (see Table 4.16) was statistically significant in the first step, $\chi2(2) = 39,21$, $p < 0.001$. The model explained 43,0% (Nagelkerke R^2) of the variance in the frailty phenotype and correctly classified 74,3% of cases. When adjusted for ultrasound characteristics the second block was not statically significant but the model was, $\chi2(4) = 41,30$, $p < 0.001$. The model explained 44,9% (Nagelkerke R^2) of the variance in the frailty phenotype and correctly classified 77,2% of cases. When adjusted for physical characteristics the third block and model was statistically significant, $\chi2(9) = 94,52$, $p < 0.001$. The model explained 81,2% (Nagelkerke R^2) of the variance in the frailty phenotype and correctly classified 93,1% of cases. The model was independent of age, sex, BMI, subcutaneous fat thickness, muscle thickness, and muscle strength. Decreased gait speed was associated with being 10 times more likely to exhibit frailty phenotype.

4.5.3.5 Frailty Model 5

The frailty model 5 corresponds to the *Rectus Femoris* muscle in the axial plane from the SVM-RFE feature selection method and RF classification method. The optimal texture features selected were 29 for this model. The AUC ± SD was of 0,665 ± 0.099 with a sensitivity of 55% and specificity of 64% (See Graph 4.5).

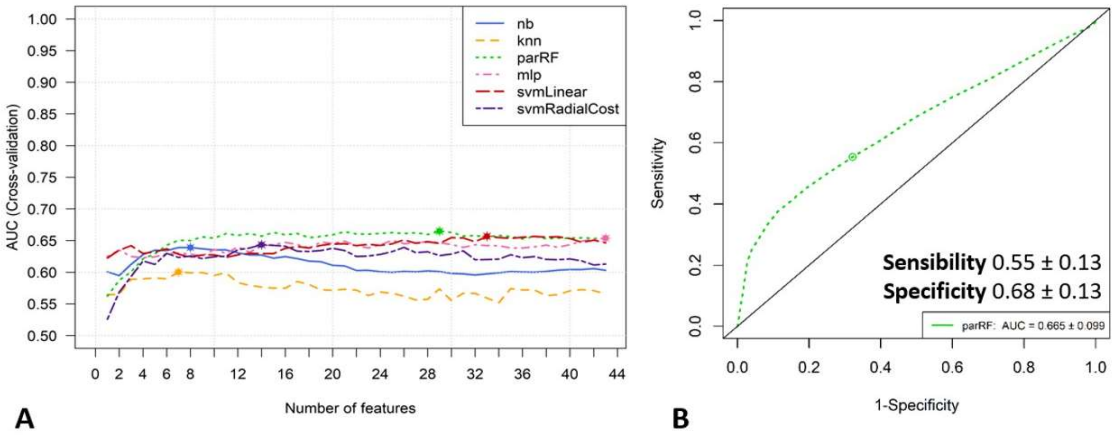

Graph 4.5 (A) Graphical representation depicting the predictive performance (AUC) of the classifier to discriminate between at risk of frailty vs. non-frail for frailty model 5 (B) ROC curve for frailty model 5

Table 4.17 Stepwise Multiple Logistic Regression Analysis of Texture Analysis Frailty Model 5 (Ranking SVM-RFE, ROI: RF and Axial Plane, Ng = 256, Predictive Model = RF)									
	Texture Analysis Frailty Model			**Adjustment with Ultrasound Characteristics**			**Adjustment with Physical Characteristics**		
Variable	**Coefficient**	**Wald Statistic***	**OR**	**Coefficient**	**Wald Statistic***	**OR**	**Coefficient**	**Wald Statistic***	**OR**
Frailty Phenotype (Constant)	-2149	0,012	0,00	-2996	0,020	0,00	-65565,8	0,994	0,00
Subcutaneous Fat Thickness (cm)				4,5	0,042	86	40,4	0,997	3,45e+17
Muscle Thickness (cm)				-5,4	0,006	0,00	-134	0,991	0,00
Age (years)							3,6	0,996	34,90
Sex (Female = 0/Male = 1)							-119	0,991	0,00
BMI (kg/m2)							15,3	0,987	4203771
Gait Speed (s)							83	0,992	1,71e+36
Muscle Strenght (kg)							-1,1	0,998	0,33
Block Chi-Square [df]				19,51 [2], p = <0,001			46,63 [5], p = <0,001		
Model Chi-Square [df]	73,07 [29], p = <0,001			92,58 [31], p = <0,001			139,21 [36], p = <0,002		
Nagelkerke-R^2	0,688			0,802			1,000		
Hosmer y Lemeshow Test	0,315			0,434			1,000		
Correct Predictions (%)	87,1			91,1			100,0		

Abbreviations: RFE-SVM: recursive feature elimination-support vector machine; ROI: Region of Interest; RF: Rectus Femoris, Ng: Number of gray levels; RF: random forests; OR: Odd Ratio; IHF: Intensity Histogram Features; GLCM: Gray-Level Co-occurrence Matrix; GLRLM: Gray-Level run-Length Matrix; GLSZM: Gray-Level Size Zone Matrix; NGTDM: Neighborhood Gray-Tone Difference Matrix.

*The Wald statistics are distributed chi-square with 1 degree of freedom.

The stepwise multiple logistic regression analysis for frailty model 5 (see Table 4.17) was statistically significant in the first step, $\chi2(29) = 73,07$, $p < 0.001$. The model explained 68,8% (Nagelkerke R^2) of the variance in the frailty phenotype and correctly classified 87,1% of cases. When adjusted for ultrasound characteristics the second block and model was statistically significant, $\chi2(31) = 92,58$, $p < 0.001$. The model explained 80.2% (Nagelkerke R^2) of the variance in the frailty phenotype and correctly classified 91,1% of cases. When adjusted for physical characteristics the third block and model was statistically significant, $\chi2(36) = 139,21$, $p < 0.001$. The model explained 100,0% (Nagelkerke R^2) of the variance in the frailty phenotype and correctly classified 100,0% of cases. The model was independent of age, sex, BMI, subcutaneous fat thickness, gait speed, and muscle strength. Increased muscle thickness decreased the likelihood of exhibiting frailty by less than 1%.

4.5.3.6 Frailty Model 6

The frailty model 6 corresponds to the *Rectus Femoris* muscle in the sagittal plane, from the SVM-RFE feature selection method and SVM_R classification method. The optimal texture features selected were 11. The AUC ± SD was of 0,675 ± 0.089 with a sensitivity of 60% and specificity of 64% (See Graph 4.6).

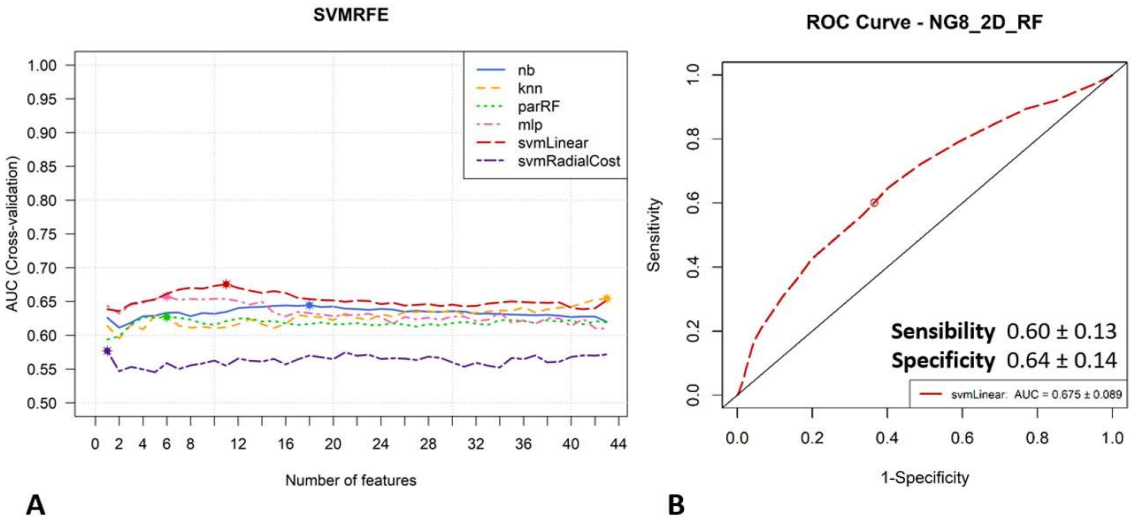

Graph 4.6 (A) Graphical representation depicting the predictive performance (AUC) of the classifier to discriminate between at risk of frailty vs. non-frail for frailty model 6 (B) ROC curve for frailty model 6

Table 4.18 Stepwise Multiple Logistic Regression Analysis of Texture Analysis Frailty Model 6 (Ranking SVM-RFE, ROI: RF and sagittal plane, Ng = 256, Predictive Model = SVM_R)									
	Texture Analysis Frailty Model			**Adjustment with Ultrasound Characteristics**			**Adjustment with Physical Characteristics**		
Variable	**Coefficient**	**Wald Statistic***	**OR**	**Coefficient**	**Wald Statistic***	**OR**	**Coefficient**	**Wald Statistic***	**OR**
Frailty Phenotype (Constant)	-289	0,108	0,00	-278	0,180	0,00	671,7	0,294	5,33e+291
Subcutaneous Fat Thickness (cm)				0,5	0,453	1,69	-2,9	0,293	0,05
Muscle Thickness (cm)				-1,8	0,001	0,17	-6,1	0,047	0,00
Age (years)							0,3	0,074	1,30
Sex (Female = 0/Male = 1)							2,6	0,327	13,90
Gait Speed (s)							5,7	0,031	299,45
Muscle Strenght (kg)							-0,2	0,048	0,80
Block Chi-Square [df]				14,92 [2], p = 0,001			56,32 [5], p = <0,001		
Model Chi-Square [df]	38,44 [11], p = <0,001			53,37 [13], p = <0,001			109,60 [18], p = <0,001		
Nagelkerke-R^2	0,423			0,549			0,885		
Hosmer y Lemeshow Test	0,392			0,185			1,000		
Correct Predictions (%)	73,3			75,2			95,0		

Abbreviations: RFE-SVM: recursive feature elimination-support vector machine; RF: Rectus Femoris; Ng: Number of gray levels; MLP: multilayer perceptron; OR: Odd Ratio; GLCM: Gray-Level Co-occurrence Matrix; GLRLM: Gray-Level run-Length Matrix; GLSZM: Gray-Level Size Zone Matrix; NGTDM: Neighborhood Gray-Tone Difference Matrix.

*The Wald statistics are distributed chi-square with 1 degree of freedom.

The stepwise multiple logistic regression analysis for frailty model 6 (see Table 4.18) was statistically significant in the first step, $\chi2(11) = 38,44$, $p < 0.001$. The model explained 42,3% (Nagelkerke R^2) of the variance in the frailty phenotype and correctly classified 73,3% of cases. When adjusted for ultrasound characteristics the second block and model was statistically significant, $\chi2(13) = 53,37$, $p < 0.001$. The model explained 54,9% (Nagelkerke R^2) of the variance in the frailty phenotype and correctly classified 75,2% of cases. When adjusted for physical characteristics the third block and model was statistically significant, $\chi2(18) = 109,60$, $p < 0.001$. The model explained 88,5% (Nagelkerke R^2) of the variance in the frailty phenotype and correctly classified 95,0% of cases. The model was independent of age, sex, BMI, and subcutaneous fat thickness. Increased muscle thickness decreased the likelihood of exhibiting frailty by less than 83%. Increased muscle strength decreased the likelihood of exhibiting frailty by 20%, but decreased gait speed was associated with being 300 times more likely to exhibit frailty phenotype.

4.5.3.7 Frailty Model 7

The frailty model 7 corresponds to the *Vastus Intermedius* muscle in the axial plane from the SVM-RFE feature selection method and SVM_R classification method. The optimal texture features selected were 43. The AUC ± SD was of 0,749 ± 0.093 with a sensitivity of 66% and specificity of 72% (See Graph 4.7).

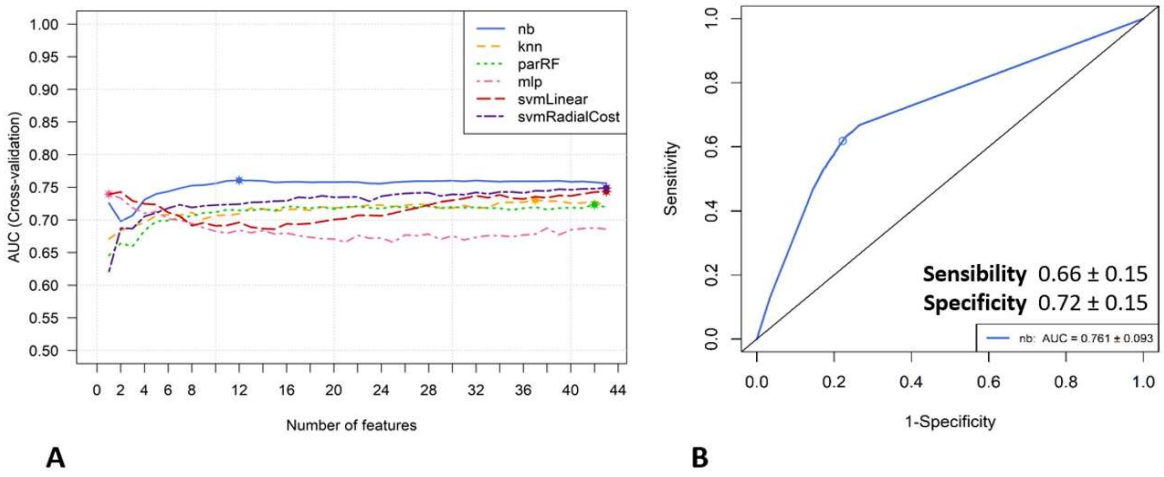

Graph 4.7 (A) Graphical representation depicting the predictive performance (AUC) of the classifier to discriminate between at risk of frailty vs. non-frail for frailty model 7 (B) ROC curve for frailty model 7

Table 4.19 Stepwise Multiple Logistic Regression Analysis of Texture Analysis Frailty Model 7 (Ranking SVM-RFE, ROI: VI and Axial Plane, Ng = 256, Predictive Model = SVM R)									
	Texture Analysis Frailty Model			Adjustment with Ultrasound Characteristics			Adjustment with Physical Characteristics		
Variable	**Coefficient**	**Wald Statistic***	**OR**	**Coefficient**	**Wald Statistic***	**OR**	**Coefficient**	**Wald Statistic***	**OR**
Frailty Phenotype (Constant)	6417	0,050		NA	NA	NA	NA	NA	NA
Subcutaneous Fat Thickness (cm)				NA	NA	NA	NA	NA	NA
Muscle Thickness (cm)				NA	NA	NA	NA	NA	NA
Age (years)							NA	NA	NA
Sex (Female = 0/Male = 1)							NA	NA	NA
BMI (kg/m2)							NA	NA	NA
Gait Speed (s)							NA	NA	NA
Muscle Strenght (kg)							NA	NA	NA
Block Chi-Square [df]				NA			NA		
Model Chi-Square [df]	93,27 [43], p = <0,001			NA			NA		
Nagelkerke-R^2	0,806			NA			NA		
Hosmer y Lemeshow Test	0,981			NA			NA		
Correct Predictions (%)	87,1			NA			NA		

Abbreviations: RFE-SVM: recursive feature elimination-support vector machine; ROI: Region of Interest, VI: Vastus Intermidius; Ng: Number of gray levels; SVM_R: support vector machine with radial kernel; OR: Odd Ratio; IHF: Intensity Histogram Features; GLCM: Gray-Level Co-occurrence Matrix; GLRLM: Gray-Level run-Length Matrix; GLSZM: Gray-Level Size Zone Matrix; NGTDM: Neighborhood Gray-Tone Difference Matrix, NA: Not Applicable.

*The Wald statistics are distributed chi-square with 1 degree of freedom.

The stepwise multiple logistic regression analysis for frailty model 7 (see Table 4.19) was statistically significant in the first step, $\chi 2(43) = 93,27$, $p < 0.001$. The model explained 80,6% (Nagelkerke R^2) of the variance in the frailty phenotype and correctly classified 87,1% of cases. The step 2 and step 3 of the stepwise multivariate logistic analysis were not able to run in the SPSS program due to high number of variables for this model (43 texture features), for a relative small number of subjects (n = 101).

4.5.3.8 Frailty Model 8

The frailty model 8 corresponds to the *Vastus Intermedius* muscle in the sagittal plane from the SVM-RFE feature selection method and SVM_R classification method. The optimal texture features selected were 15. The AUC ± SD was of 0,728 ± 0.104 with a sensitivity of 55% and specificity of 78% (See Graph 4.8).

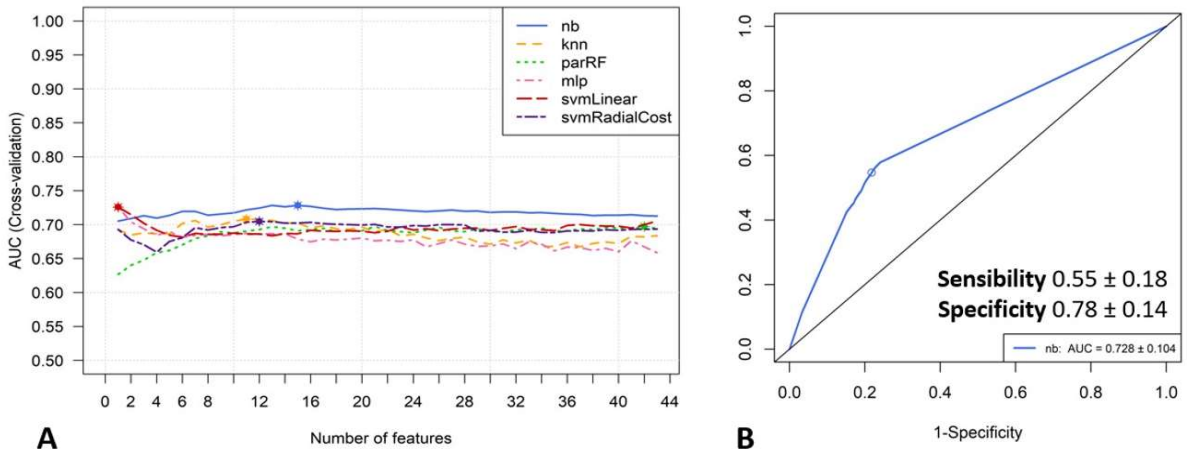

Graph 4.8 (A) Graphical representation depicting the predictive performance (AUC) of the classifier to discriminate between at risk of frailty vs. non-frail for frailty model 8 (B) ROC curve for frailty model 8

Table 4.20 Stepwise Multiple Logistic Regression Analysis of Texture Analysis Frailty Model 8 (Ranking: SVM-RFE, ROI: VI and Sagittal Plane, Ng = 256, Model = SVM_R)									
	Texture Analysis Frailty Model			**Adjustment with Ultrasound Characteristics**			**Adjustment with Physical Characteristics**		
Variable	**Coefficient**	**Wald Statistic***	**OR**	**Coefficient**	**Wald Statistic***	**OR**	**Coefficient**	**Wald Statistic***	**OR**
Frailty Phenotype (Constant)	26,5	0,077	32e+11	31,9	0,044	6,82e13	-1,2	0,974	0,30
Subcutaneous Fat Thickness (cm)				0,9	0,191	2,36	0,2	0,911	1,24
Muscle Thickness (cm)				-1,0	0,198	0,36	-0,4	0,806	0,70
Age (years)							0,1	0,166	1,09
Sex (Female = 0/Male = 1)							0,6	0,750	1,84
BMI (kg/m2)							0,2	0,260	1,25
Gait Speed (s)							3,8	0,006	43,11
Muscle Strenght (kg)							-0,1	0,087	0,90
Block Chi-Square [df]				4,69 [2], p = 0,096			49,10 [5], p = <0,001		
Model Chi-Square [df]	47,81 [15], p = <0,001			52,51 [17], p = <0,001			101,61 [22], p = <0,001		
Nagelkerke-R^2	0,504			0,542			0,848		
Hosmer y Lemeshow Test	0,071			0,462			0,951		
Correct Predictions (%)	77,2			82,2			91,1		

Abbreviations: RFE-SVM: recursive feature elimination-support vector machine; ROI: Region of Interest; VI: Vastus Intermidius; Ng: Number of gray levels; SVM_R: support vector machine with radial kernel; OR: Odd Ratio; IHF: Intensity Histogram Features; GLCM: Gray-Level Co-occurrence Matrix; GLRLM: Gray-Level run-Length Matrix; GLSZM: Gray-Level Size Zone Matrix; NGTDM: Neighborhood Gray-Tone Difference Matrix.

*The Wald statistics are distributed chi-square with 1 degree of freedom.

The stepwise multiple logistic regression analysis for frailty model 8 (see Table 3.20) was statistically significant in the first step, $\chi2(15) = 47,81$, $p < 0.001$. The model explained 50,2% (Nagelkerke R^2) of the variance in the frailty phenotype and correctly classified 77% of cases. When adjusted for ultrasound characteristics the second block and model was statistically significant, $\chi2(17) = 52,51$, $p < 0.001$. The model explained 54,2% (Nagelkerke R2) of the variance in the frailty phenotype and correctly classified 82,2% of cases. When adjusted for physical characteristics the third block and model was statistically significant, $\chi2(22) = 101,61$, $p < 0.001$. The model explained 84,8% (Nagelkerke R^2) of the variance in the frailty phenotype and correctly classified 91,1% of cases. The model was independent of age, sex, BMI, subcutaneous fat thickness, muscle thickness, gait speed, and muscle strength. Decreased gait speed was associated with being 43 times more likely to exhibit frailty phenotype.

In summary, the eight-tested predictive models for frailty with stepwise multiple logistic regression analysis were statistically significant ($p < 0.001$) for the determination of people at risk of frailty or frail. The models explained 50,2% to 100% (Nagelkerke R^2) of the variance in the frailty phenotype and correctly classified from 70.3% to a 100% of cases. The models were independent of age, sex, BMI, subcutaneous fat thickness, and muscle strength, with two exceptions for age and one for muscle strength. Decreased gait speed was associated with a very high likelihood of exhibiting frailty phenotype, while increased muscle thickness decreased that likelihood.

4.6 Regression Analysis of Outcomes with Frailty Models

To quantify the effects of each frailty predictive models on the likelihood of having adverse outcomes, a multiple logistic regression analysis was applied to the texture analysis models. The outcomes evaluated were hearing impairment, stroke, myocardial infarction, dementia/memory loss, increased CCI, falls, increased number of visits to primary care and death. Due to the small number of patients that develop hearing impairment, stroke, myocardial infarction, dementia/memory loss, falls, and increased number of visits to primary care, the regression analyses of some of the models were not able to run in the SPSS program due to a relative small number of subjects with the outcome in question ($n < 5$). We present the results for CCI and death only.

The logistic regression analysis for all eight predictive models (see Table 4.21) on the CCI as an outcome were statistically significant in 6 out of 8 models ($p = 0.180$ to < 0.001). The models explained 12.0% to a 64.2% (Nagelkerke R^2) of the variance in the outcome of CCI. Although the data

showed correct prediction of the CCI outcome from 66.3% to 82.2% of the cases, the regression analysis plots revealed these were actual associations, and not predictions.

Table 4.21 Multiple Logit Regression Analysis of Frailty Texture Analysis Models for CCI Outcome						
Ranking	***Frailty Textures Analysis Models***	***Model Chi-Square [df]***	***% Correct Predictions***	***Hosmer y Lemeshow Test***	***Nagelkerke-R^2***	***Plot***
P-Value	Frailty Model 1	27,87 [22], p = 0,180	78,2	0,223	0,325	Association
	Frailty Model 2	27,99 [14], p =0,014	69,3	0,683	0,327	Association
	Frailty Model 3	9,44 [2], p = 0,009	66,3	0,701	0,120	Association
	Frailty Model 4	25,25 [11], p = 0,008	73,3	0,373	0,299	Association
SVM-RFE	Frailty Model 5	39,40 [29], p=0,094	73,3	0,535	0,436	Association
	Frailty Model 6	25,07 [11], p = 0,009	71,3	0,388	0,297	Association
	Frailty Model 7	66,24 [43], p =0,016	83,2	0,904	0,642	Predictive
	Frailty Model 8	46,68 [15], p = <0.001	82,2	0,076	0,500	Association

Abbreviations: CCI: charlson comorbidity index; RFE-SVM: recursive feature elimination-support vector machine.

The logistic regression analysis for all eight predictive models (see Table 4.22) on death as an outcome were statistically significant (p = 0.019 to < 0.001). The models explained 38.5% to a 100% (Nagelkerke R^2) of the variance in the outcome of death and correctly predicted 89.1% to 100% of cases.

Table 4.22 Multiple Logit Regression Analysis of Frailty Texture Analysis Models for Death Outcome						
Ranking	***Frailty Textures Analysis Models***	***Model Chi-Square [df]***	***% Correct Predictions***	***Hosmer y Lemeshow Test***	***Nagelkerke-R^2***	***Plot***
P-Value	Frailty Model 1	38,58 [22], p = 0,016	91,1	0,903	0,613	Predictive
	Frailty Model 2	31,57 [14], p = 0,005	91,1	0,731	0,519	Predictive
	Frailty Model 3	22,44 [2], p = <0,001	89,1	0,833	0,385	Predictive
	Frailty Model 4	44,11 [11], p = <0,001	93,1	1,000	0,684	Predictive
SVM-RFE	Frailty Model 5	73,64 [29], p = <0,001	100	1,000	1,000	Predictive
	Frailty Model 6	23,82 [11], p = 0,014	90,1	0,940	0,406	Predictive
	Frailty Model 7	73,64 [43], p = 0,002	100	1,000	1,000	Predictive
	Frailty Model 8	58,45 [15], p = <0,001	97,0	1,000	0,849	Predictive

Abbreviations: RFE-SVM: recursive feature elimination-support vector machine.

4.7 Reliability and Repeatability of Texture Features

We believe that reproducibility (repeatability) and consistency (reliability) are as important as accuracy, for that reason we performed ICC and Bland-Altman Limits of Agreement to compare the performance of the texture features achieved by each muscle (*Rectus Femoris* and *Vastus Intermedius*) in both planes (axial and sagittal).

Table 4.23 ICC of Texture Features					
Muscle and Plane		***RF Axial vs Sagittal***	***VI Axial vs Sagittal***	***Axial RF vs VI***	***Sagittal RF vs VI***
Texture Feature		***ICC (95%CI)***	***ICC (95%CI)***	***ICC (95%CI)***	***ICC (95%CI)***
IHF	Variance	0,43 (0,16-0,61)	0,67 (0,51-0,78)	0,20 (-0,12-0,44)	0,47 (0,23-0,64)
	Skewness	0,72 (0,58-0,82)	0,82 (0,72-0,88)	0,32 (-0,10-0,59)	0,22 (-0,10-0,45)
	Kurtosis	0,55 (0,34-0,70)	0,67 (0,51-0,78)	0,32 (-0,10-0,59)	0,25 (-0,06-0,48)
GLCM	Energy	0,76 (0,64-0,84)	0,86 (0,79-0,90)	0,01 (-0,37-0,30)	0,00 (-0,39-0,30)
	Contrast	0,80 (0,70-0,87)	0,57 (0,31-0,72)	0,17 (-0,14-0,45)	0,44 (-0,18-0,72)
	Entropy	0,75 (0,62-0,83)	0,88 (0,80-0,93)	0,17 (-0,14-0,43)	0,18 (-0,13-0,42)
	Homogeneity	0,81 (0,72-0,87)	0,87 (0,79-0,92)	0,16 (-0,14-0,41)	0,18 (-0,13-0,42)
	Correlation	0,65 (0,34-0,80)	0,67 (0,44-0,80)	0,32 (0,01-0,54)	0,30 (-0,02-0,52)
	Sum Average	0,65 (0,40-0,78)	0,88 (0,80-0,92)	0,24 (-0,14-0,58)	0,24 (-0,16-0,52)
	Variance	0,617 (0,38-0,76)	0,82 (0,70-0,87)	0,28 (-0,18-0,60)	0,41 (-0,04-0,65)
	Dissimilarity	0,80 (0,70-0,86)	0,70 (0,44-0,83)	0,17 (-0,12-0,45)	0,33 (-0,19-0,64)
	Auto-Correlation	0,62 (0,35-0,77)	0,82 (0,72-0,88)	0,23 (-0,12-0,55)	0,32 (-0,18-0,61)
GLRLM	Short Run Emphasis	0,83 (0,75-0,88)	0,85 (0,75-0,91)	0,19 (-0,15-0,47)	0,22 (-0,14-0,48)
	Long Run Emphasis	0,84 (0,76-0,90)	0,85 (0,78-0,90)	0,01 (-0,42-0,31)	0,01 (-0,42-0,31)
	Gray-Level Nonuniformity	0,15 (-0,12-0,38)	0,88 (0,82-0,92)	0,15 (-0,12-0,38)	0,11 (-0,15-0,34)
	Run Length Nonuniformity	0,83 (0,75-0,87)	0,85 (0,73-0,91)	0,20 (-0,15-0,50)	0,25 (-0,16-0,53)
	Run Percentage	0,84 (0,76-0,89)	0,90 (0,82-0,93)	0,14 (-0,13-0,36)	0,12 (-0,15-0,34)
	Low Gray-Level Run Emphasis	0,78 (0,68-0,85)	0,91 (0,86-0,94)	0,12 (-0,15-0,34)	0,10 (-0,18-0,33)
	High Gray-Level Run Emphasis	0,82 (0,35-0,77)	0,81 (0,71-0,88)	0,23 (-0,15-0,55)	0,32 (0,18-0,62)
	Short Run Low Gray-Level	0,79 (0,69-0,86)	0,90 (0,85-0,93)	0,16 (-0,12-0,39)	0,17 (-0,12-0,40)
	Short Run High Gray-Level	0,63 (0,36-0,77)	0,81 (0,69-0,88)	0,23 (-0,15-0,55)	0,33 (-0,18-0,62)
	Long Run Low Gray-Level	0,78 (0,68-0,86)	0,85 (0,78-0,90)	0,00 (-0,43-0,31)	0,00 (-0,42-0,31)
	Long Run High Gray-Level	0,60 (0,35-0,75)	0,83 (0,74-0,89)	0,25 (-0,16-0,57)	0,33 (-0,17-0,62)
	Gray-Level Variance	0,18 (-0,14-0,43)	0,78 (0,68-0,85)	0,32 (-0,19-0,62)	0,07 (-0,18-0,29)
	Run-Length Variance*	0,11 (-0,03-0,30)	0,06 (-0,05-0,20)	0,45 (0,18-0,63)	0,19 (-0,10-0,52)
GLSZM	Small Zone Emphasis	0,79 (0,66-0,86)	0,80 (0,59-0,89)	0,18 (-0,15-0,46)	0,30 (-0,12-0,57)
	Large Zone Emphasis	0,54 (0,32-0,69)	0,72 (0,59-0,81)	0,00 (-0,44-0,31)	0,00 (-0,44-0,31)
	Gray-Level Nonuniformity	0,56 (0,31-0,71)	0,87 (0,80-0,91)	0,15 (-0,13-0,38)	0,11 (-0,16-0,34)
	Zone-Size Nonuniformity	0,79 (0,66-0,86)	0,78 (0,55-0,88)	0,19 (-0,15-0,49)	0,32 (-0,13-0,59)
	Zone Percentage	0,83 (0,74-0,88)	0,86 (0,75-0,92)	0,20 (-0,15-0,50)	0,23 (-0,16-0,51)
	Low Gray-Level Zone Emphasis	0,81 (0,72-0,86)	0,90 (0,84-0,93)	0,14 (-0,13-0,37)	0,13 (-0,14-0,36)
	High Gray-Level Zone Emphasis	0,60 (0,32-0,76)	0,82 (0,72-0,88)	0,23 (-0,15-0,55)	0,32 (-0,17-0,61)
	Small Zone Low Gray-Level Zone Emphasis	0,80 (0,70-0,86)	0,90 (0,85-0,93)	0,14 (-0,13-0,36)	0,12 (-0,15-0,34)
	Small Zone High Gray-Level Zone Emphasis	0,62 (0,33-0,77)	0,80 (0,68-0,87)	0,23 (0,15-0,55)	0,34 (-0,17-0,63)
	Large Zone Low Gray-Level Zone Emphasis	0,51 (0,28-0,67)	0,72 (0,59-0,82)	0,00 (-0,47-0,32)	0,00 (-0,44-0,31)
	Large Zone High Gray-Level Zone Emphasis	0,57 (0,35-0,71)	0,70 (0,56-0,80)	0,00 (-0,44-0,31)	0,04 (-0,41-0,34)
	Grey-Level Variance	0,47 (0,22-0,64)	0,65 (0,48-0,76)	0,24 (-0,15-0,51)	0,18 (-0,13-0,43)
	Zone-Size Variance*	0,16 (-0,22-0,42)	0,14 (-0,20-0,39)	0,05 (-0,07-0,22)	0,19 (-0,10-0,52)
NGTDM	Coarseness	0,70 (0,52-0,81)	0,78 (0,60-0,87)	0,63 (0,45-0,75)	0,65 (0,48-0,77)
	Contrast	0,75 (0,63-0,83)	0,67 (0,45-0,80)	0,17 (-0,14-0,45)	0,36 (-0,09-0,63)
	Busyness	0,71 (0,52-0,82)	0,83 (0,74-0,88)	0,05 (-0,27-0,31)	0,01 (0,35-0,30)
	Complexity	0,77 (0,66-0,85)	0,64 (0,45-0,76)	0,22 (-0,16-0,52)	0,50 (-0,15-0,76)
	Strength	0,52 (0,24-0,70)	0,79 (0,70-0,86)	0,52 (0,13-0,72)	0,51 (0,25-0,68)

Abbreviations: CI: Confidence Interval; IHF: Intensity Histogram Features; GLCM: Gray-Level Co-occurrence Matrix; GLRLM: Gray-Level run-Length Matrix; GLSZM: Gray-Level Size Zone Matrix; NGTDM: Neighborhood Gray-Tone Difference Matrix.

The ICC values were classified poor for values ≤0,20, fair for 0,21-0,40, moderate for 0,41-0,60, good for 0,61-0,80 and very good for 0,81-1,00.

* Run-Length Variance and Zone-Size Variance are small with a restricted range of scales, so logarithms were used to transform the data.

We found very good ICCs when we compared the same muscle but in different planes, however, when we compared the same plane but in different muscles, the ICC of the texture features were very poor (see Table 4.23). We can interpret that as long as the image comes from the same muscle, the image plane does not significantly influence the texture features, and that there is a slightly better ICC with *Vastus Intermedius* muscle than with *Rectus Femoris*.

Since only the comparison of same muscles in different planes was reliable, we used this data for the Bland-Altman Limits of Agreement. From both muscles, only 13 out of 43 features had high reproducibility (or low error of measurement) when different planes of the same muscle were used (See Table 4.24).

Table 4.24 Blant-Altman Limits of Agreement of Textures Features							
Muscle and Plane		***RF Axial vs Sagittal***			***VI Axial vs Sagittal***		
Texture Feature		***Bias (± 95%LoA)***	***T-Test****	***Regression Analysis*****	***Bias ± 95%LoA***	***T-Test****	***Regression Analysis*****
IHF	Variance	15,05 (-97,14-127,24)	0,010	NA	-6,24 (-131,31-9,87)	0,328	0,328
	Skewness	-0,11 (-0,80-0,57)	0,002	NA	0,16 (-0,94-1,26)	0,005	NA
	Kurtosis	-0,37 (-3,22-2,48)	0,012	NA	0,87 (-6,77-8,51)	0,027	NA
GLCM	Energy	0,0001(-0,0014-0,0012)	0,132	0,001	0,01 (-0,13-0,14)	0,199	0,002
	Contrast	0,90 (-63,92-65,71)	0,786	0,492	-13,61 (-72,20-44,97)	<0,001	NA
	Entropy	0,14 (-0,84-1,11)	0,007	NA	-0,41(-2,47-1,66)	<0,001	NA
	Homogeneity	-0,002(-0,04-0,05)	0,364	0,193	0,03 (-0,11-0,17)	<0,001	NA
	Correlation	0,02 (-0,04-0,07)	<0,001	NA	0,02 (-0,04-0,07)	<0,001	NA
	Sum Average	0,0001 (-0,0001-0,0002)	<0,001	NA	-0,00003 (-0,00020-0,00014)	<0,001	NA
	Variance	-193,75 (-285,09 -102,42)	<0,001	NA	-0,0005 (-0,0037-0,0027)	0,004	NA
	Dissimilarity	0,05 (-2,07-2,17)	0,640	0,350	-0,64 (-2,84-1,56)	<0,001	NA
	Auto-Correlation	324,06 (-864,54-1512,66)	<0,001	NA	-130,11 (-877,81-617,59)	0,001	NA
GLRLM	Short Run Emphasis	0,001 (-0,02-0,02)	0,446	0,147	-0,01 (-0,07-0,05)	<0,001	NA
	Long Run Emphasis	0,01 (-0,22-0,23)	0,644	<0,001	1,95 (-25,99-29,89)	0,172	<0,001
	Gray-Level Nonuniformity	-0,002 (-0,01-0,01	<0,001	NA	0,003 (-0,023-0,028)	0,036	NA
	Run Length Nonuniformity	0,002 (-0,04-0,04)	0,447	0,169	-0,02 (-0,12-0,08)	<0,001	NA
	Run Percentage	0,001 (-0,03-0,03)	0,575	0,014	0,02 (-0,19-0,14)	0,004	NA
	Low Gray-Level Run Emphasis	0,00004 (-0,01-0,1)	0,942	0,005	0,01 (-0,06-0,08)	0,075	0,027
	High Gray-Level Run Emphasis	334,02 (-887,43-1555,46)	<0,001	NA	-134,53 (-899,94-630,88)	0,001	NA
	Short Run Low Gray-Level	0,0003 (-0,01-0,01)	0,347	0,347	0,003 (-0,026-0,031)	0,079	0,011
	Short Run High Gray-Level	318,82 (-846,76-1484,41)	<0,001	NA	-131,94 (-863,99-600,10)	0,001	NA
	Long Run Low Gray-Level	0,02 (-0,17-0,21)	0,048	NA	1,90 (-26,11-29,91)	0,184	<0,001
	Long Run High Gray-Level	399,25 (-1157,40-1955,89)	<0,001	NA	-145,88 (-1137,23-845,47)	0,005	NA
	Gray-Level Variance	0,01 (0,0001-0,0099)	<0,001	NA	0,002 (-0,002-0,005)	<0,001	NA
	Run-Length Variance	0,1e-6 (-3,43e-6-3,65e-6)	0,536	<0,001	0,1e-6 (-0,4e-5-0,4e-5)	0,692	0,105

GLSZM	Small Zone Emphasis	0,01 (-0,04-0,05)	<0,001	NA	-0,02 (-0,09-0,05)	<0,001	NA
	Large Zone Emphasis	2,59 (-26,99-32,16)	0,088	<0,001	17,03 (-32358,32-32,392,38)	0,992	0,103
	Gray-Level Nonuniformity	-0,002 (-0,01-0,01)	<0,001	NA	0,002(-0,019-0,023)	0,046	NA
	Zone-Size Nonuniformity	0,01 (-0,05-0,08)	<0,001	NA	-0,03 (-0,12-0,06)	<0,001	NA
	Zone Percentage	0,01 (-0,07-0,08)	0,018	NA	-0,04 (-0,19-0,12)	<0,001	NA
	Low Gray-Level Zone Emphasis	-0,0003 (-0,0040-0,0034)	0,177	0,017	0,002 (-0,021-0,025)	0,045	NA
	High Gray-Level Zone Emphasis	360,78 (-909,39-1630,96)	<0,001	NA	-137,88 (-0,011-0,014)	0,001	NA
	Small Zone Low Gray-Level Zone Emphasis	-0,0002 (-0,0022-0,0018)	0,076	0,013	126,64 (-799,66-546,38)	0,055	0,010
	Small Zone High Gray-Level Zone Emphasis	311,47 (-761,73-1384,67)	<0,001	NA	126,64 (-799,66-546,38)	<0,001	NA
	Large Zone Low Gray-Level Zone Emphasis	2,73 (-26,88-32,35)	0,072	NA	15,52 (-32359,67-32390,71)	0,992	0,103
	Large Zone High Gray-Level Zone Emphasis	708,89 (-3535,02-4952,80)	0,001	NA	11,20 (-32049,08-32071,48)	0,995	0,087
	Grey-Level Variance	0,0002 (-0,0016-0,0019)	0,068	NA	-0,0001(0,0008-0,0007)	0,045	NA
	Zone-Size Variance	-0,01e-6 (-1,15e-6-0,92e-6)	0,035	NA	0,2e-6 (-1,8e-6-0,21e-6)	0,128	<0,001
NGTDM	Coarseness	0,0001 (-0,0003-0,0005)	<0,001	NA	0,0001 (-0,0003-0,0005)	<0,001	NA
	Contrast	0,01 (-0,14-0,16)	0,416	NA	-0,03 (-0,17-0,11)	<0,001	NA
	Busyness	-0,15 (-0,82-0,52)	<0,001	NA	-0,42 (13,90-13,07)	0,544	0,155
	Complexity	960,75 (-5578,98-7500,48)	0,005	NA	-1045,45 (-7465,94-5375,04)	0,002	NA
	Strength	0,60 (-1,61-2,82)	<0,001	NA	0,22 (-1,55-1,98)	0,017	NA

Abbreviations: LoA: Limits of Agreement; IHF: Intensity Histogram Features; GLCM: Gray-Level Co-occurrence Matrix; GLRLM: Gray-Level run-Length Matrix; GLSZM: Gray-Level Size Zone Matrix; NGTDM: Neighborhood Gray-Tone Difference Matrix; NA: Not Applicable.

* T-test was used to determine the presence of systemic bias. P value <0,05 indicates the presence of systemic bias.

**Regression Analysis was used determine the presence of heteroscedasticity in the data. P value <0,05 indicates presence of heteroscedaticity.

4.8 False Discovery Rate for Multiple Comparisons

In this study, we tested the significance of thousands of variables, which creates serious concerns over the accumulated Type 1 error. Many of the significant developments within the field of so-called "large-p, small-n" data analysis problems are robust methods for accommodation of multiple testing issues (Kumar et al., 2012). For this reason, false discovery rates (FDR) have been assessed to provide more reasonable error estimates. We applied FDR method by Benjamini & Hochberg to give reasonable guidance on the validity of our results (Benjamini & Hochberg, 1995). The q-value in this study is of 10.8%, which means that 11% of significant results are false positives (see Table 3.25).

Table 4.25 False Discovery Rate

	Frequency	***Porcentage***
Not Significant	9792	89,2
Significant	1184	10,8
Total	10976	100,0

Benjamini & Hochberg method used.

5. DISCUSSION

Our results indicate that it is possible to identify subjects at risk of frailty (pre-frail) or of being frail with the aid of machine learning texture analysis models as an accurate QIB obtained from muscle ultrasound imaging.

The identification of an accurate QIB for frailty has been demonstrated in three ways. First, the development of multiple predictive models with good AUC for the identification of subjects at risk of frailty or of being frail (Table 4.12). Second, the stepwise multiple logistic regression analysis of the best models demonstrated that the developed QIBs correctly classified 70 to 87% of the cases, and explained between 23% to 80% of the variance in the identification of frailty phenotype with the predictive models alone. These models could be improved if muscle thickness or gait speed were inputted into the predictive models and correctly classified 87% to 100% of the cases. After adjustment, the predicted models were independent of age, sex, BMI, SFT and MS (Table 4.13 to table 4.20). Third, the QIBs were also associated with increased morbidity (Table 4.21) and were highly predictive of death at the 2 year follow-up (Table 4.22).

These results thus lend further credence to our earlier work that ultrasonic measurement of echo intensity is a promising, potentially effective non-invasive biomarker for the identification frailty (Mirón Mombiela et al., 2017). Muscle dysfunction is involved at the core of the frailty phenotype that Fried and colleagues described (Fried et al., 2001) which is most likely why we found a correlation between the texture analysis of the quadriceps muscle and the frailty phenotype. Aging greatly affects muscle quality, including the decline in mitochondrial function for protein synthesis, increase in oxidative stress, altered neuromuscular activation, slower contraction speed, greater fatty infiltration, and fibrotic transformation (Bartley & Studenski, 2017; Baumann, Kwak, Liu, & Thompson, 2016; Marzetti et al., 2013; Y. Watanabe et al., 2013). This is particularly important when considering that the skeletal muscle is the second largest store of energy in the body (Ticinesi et al., 2017). These alterations in the muscle cell and cell environment translate into an abnormal muscle architecture, explaining in part why the echo intensity texture features have higher heterogeneity of the muscle in frail and at risk of frailty subjects. We demonstrated that texture analysis from ultrasound images gives the information about the quality of muscle and further demonstrates that the texture analysis models can be an accurate QIB for frailty phenotype. However, to be proven, a study with animals or human biopsy samples would help to clarify the histologic or pathophysiologic correlation with changes in the textures parameters (Sogawa et al., 2017).

To our knowledge, this study and the previously published study (Mirón Mombiela et al., 2017) are the first to link muscle quality (increased echo intensity or heterogeneity of texture features) to

frailty. There are some studies published linking sarcopenia by ultrasound and frailty (Mueller et al., 2016b), sarcopenia on CT and frailty assessment for the prediction of post-surgical complications in older adults (Sur et al., 2015), and on muscle size or quality by CT to predict frailty and survival (Boutin et al., 2017; Paknikar et al., 2016). What these studies have in common is the link between musculoskeletal dysfunction and outcome, implying an important link between the two and the possible use of muscle quality in radiological images prompt further studies. Skeletal muscle is the most abundant tissue in the body (≈40% of body mass) and secretes hundreds of myokine peptides that influence insulin sensitivity, inflammation, immune function and regulates anabolism and catabolism. Muscle depletion in the frail elderly is not just about mechanical function loss, it is a major cause of whole-body metabolic impairment, in turn responsible for negative outcomes (Argilés, Campos, Lopez-Pedrosa, Rueda, & Rodriguez-Mañas, 2016; Vanitallie, 2003). As frailty denotes a syndrome with poor ability to respond to stressors and maintain homeostasis, rendering the person vulnerable to a variety of adverse outcomes (falls, fractures, disability, death), the ability to identify who is at risk of these adverse events is invaluable (Bartley & Studenski, 2017).

No other studies have been published to support our data, but the fact that the correlation between muscle texture features and age is weaker (12 out of 43 features) than the correlation between the texture features and frail phenotype (21 out of 43 features) supports our findings (Table 4.9) that chronological age by itself does not define frailty, nor is it the only determining factor in prognosis. Other known variables like gait speed and muscle thickness, increased morbidity, hearing impairment (Kamil, Li, & Lin, 2014; Kamil et al., 2016; Liljas et al., 2017), stroke (Lichtman, Krumholz, Wang, Radford, & Brass, 2002; Longstreth et al., 2001; White et al., 2016; Winovich et al., 2017), myocardial infarction (Alonso Salinas et al., 2016; Alonso Salinas et al., 2017; Ekerstad et al., 2011; Graham et al., 2013; Kang et al., 2015; Sanchis et al., 2014; White et al., 2016), dementia/memory loss (Avila-Funes et al., 2009; Boyle, Buchman, Wilson, Leurgans, & Bennett, 2010; Jacobs, Cohen, Ein-Mor, Maaravi, & Stessman, 2011), falls (Cheng & Chang, 2017; Ensrud et al., 2007; Kojima, 2015), increased CCI (Fried, Ferrucci, Darer, Williamson, & Anderson, 2004; Klein, Klein, Knudtson, & Lee, 2005; Llibre et al., 2014; Vetrano et al., 2018), increased visits to primary care (Zylberglait Lisigurski et al., 2017)], and death (Chang & Lin, 2015; Shamliyan, Talley, Ramakrishnan, & Kane, 2013)(Table 4.10), whose relationships have been previously established with frailty support the association between the texture features and the frailty phenotype (Table 4.6, 4.8, and 4.10). Furthermore, our integrated analysis shows that the develop predictive models, were also informative models, which indicates the power of integrating clinical data with texture analysis for frailty predictive model building (Aerts, Hugo J W L et al., 2014). These predictive models not only capture muscle quality based on its heterogeneity, but these changes were also strongly prognostic of death (Table 4.22).

We propose the use of QIB for frailty for several reasons and advantages. As increased heterogeneity of the echo intensity texture features reflects frailty-related muscle dysfunction, these anatomical and physiological characteristics are what makes it a quality imaging biomarker (Sullivan et al., 2015). A biomarker, as mentioned earlier, is defined as "a characteristic that is objectively measured and evaluated as an indicator of normal biological processes, pathogenic processes or response to a therapeutic interventions" (Calvani et al., 2015; Prescott, 2013; Sullivan et al., 2015). Hence, an ideal biomarker should support the diagnosis, facilitate the tracking of the condition of interest over time, and assist healthcare professionals in clinical and therapeutic decision-making. Although a wide range of functional, anthropometric and biochemical biomarkers have become available, there is an absence of reliable biomarker of frailty that could be utilized the clinical settings. Examples include deregulation of myocyte apoptosis, derangement in mitochondrial functions, oxidative/nitrosative stress, iron dyshomeostasis, alteration in protein synthesis, hormones, growth factors, cytokines, telomere length, antioxidants, and inflammatory markers; all have shown limited clinical applicability (Calvani et al., 2015; Mitnitski et al., 2015; Pilleron et al., 2018).

We believe that QIB's in frailty can succeed were other biomarkers have failed. Medical imaging for clinical decision-making has been steadily increasing over the last four decades (Prescott, 2013). There are very well established examples of successful use of medical imaging for preclinical decision-making, like mammography use for cancer screening or ultrasound for the detection of free fluid in the abdomen in the trauma setting. Medical imaging provides the ability to detect and localize many changes that are important to determine whether a disease is present, whether there has been progression of the disease or whether therapy is effective, by depicting alterations in anatomic, physiologic, biochemical or molecular processes (Smith, Sorensen, & Thrall, 2003). QIB's are sensitive, specific, accurate, and reproducible imaging measures of these changes (Prescott, 2013), and as the results of this study suggest, can be used in frailty screening or diagnosis. Known circulating biomarker candidates have weak associations with relevant clinical outcomes, this highlights the idea that there might not be one single biological marker that can reliably track frailty and that there is a room for improvement with the use of new tools (Li et al., 2015; Rodríguez-Mañas, 2015). ROC analysis of 40 biomarkers of cellular ageing, inflammation, hematology and immunosenescence showed moderate discriminative ability for mortality, with no individual biomarker´s AUC exceeded 0.61 (Mitnitski et al., 2015), while all the predictive models developed here achieved AUC above 0.70. The developed QIB of this study had strong associations and predictive value with clinical outcomes of the study. This is important, as the use of biomarkers in any study must also be "fit for purpose" and clinically meaningful; we believe we have achieved that.

Our predictive models for ultrasound imaging provide a non-invasive, fast and low cost, as well as repeatable, QIB. Ultrasound imaging is widely available and accessible in the European region and its use is increasing worldwide. Ultrasound imaging is also more simple and cheaper than other imaging modalities. There is no radiation, it is easily applied in clinical practice or large population surveys, and it can be used for bed-ridden and mobility impaired individuals. Muscle architecture and dysfunction can be appraised by ultrasound (Akima et al., 2017; Cadore et al., 2012; Fukumoto et al., 2012; Pillen et al., 2009; Pillen & van Alfen, 2011; Rech et al., 2014; Strasser et al., 2013; Y. Watanabe et al., 2013; Wilhelm et al., 2014), but the added utilization of texture analysis allows for a precise quantitative and simple method for detecting muscle changes. Ultrasound imaging has many advantages over other techniques for determining muscle quality as mentioned previously, but it is still operator-dependent, and it is affected by the thickness of tissues and by the ultrasound scanner settings (T. Watanabe et al., 2017). Contrary to conventional first-order statistical feature like echo intensity (histogram analysis or grey texture analysis) used in our previous study (Mirón Mombiela et al., 2017), second order or higher order texture analysis, like the texture features applied in this study, have little effect on change by gain or frequency and are intensity invariant (Molinari et al., 2015; T. Watanabe et al., 2017). This was proven not only with the achieved accuracy of the models (AUC´s above 0,700) and the higher reliability found with the *Vastus Intermidius* muscle (Table 4.23), which is the deep head of quadriceps muscle, but also by the not significant effect subcutaneous fat tissue had over the frailty predictive models after adjustment. The application of texture features can overcome effectively some limitations of ultrasound imaging, like tissue thickness, ultrasound parameters or intrinsic characteristics that come from the use of different ultrasound devices.

This may have a clinical impact as imaging is routinely used in clinical practice, providing an unprecedented opportunity to improve decision-support in frailty treatment and prevention. Radiologists play an important role in the evaluation of geriatric patients as clinical evaluation of these patients becomes increasingly difficult because of overall frailty, comorbidities, and medication effects (Sadro, Sandstrom, Verma, & Gunn, 2015). As these patients have an increased number of illnesses and use the health care system more frequently, like increased primary care visits, emergency visits, and hospitalizations (Cesari et al., 2016; Prince et al., 2015), it is inevitable that their own doctors will ask for more imaging studies, and this trend is also on the rise. In our institution, 4,400 ultrasound exams were performed on patients over 60 years-old in the year 2007. In the year 2017, that has almost quadrupled as 12,536 patients over 60 years-old had 26,654 ultrasounds performed (Data from CHGUV Radiology Department). This includes patients referred from emergency department as well as outpatient clinics.

The use of computer assisted image processing and analysis could be extremely important for not only the discovery, characterization and validation of QIB´s, as done in this study, but also for the wider application of these frailty predictive models. In particular, the application of advanced image processing and analysis procedures (e.g. semi-automated or automated segmentation and registration) provide for a more robust and efficient incorporation of QIB's into clinical and preclinical decision making (Aerts, Hugo J W L et al., 2014; Gillies et al., 2016; Kumar et al., 2012; Lambin et al., 2012). This includes the development of apps, artificial intelligence (AI) software and/or automatization of QIBs that can be added directly to the pipeline and workflow of radiological studies already performed in a Radiological Department. For example, the automatic inclusion of our QIB for muscle quality in radiology reports for patients over 60 years-old that get an ultrasound in our emergency department, or at the ultrasound outpatient clinic, could be considered. This will help determine if the patients have increased risk of frailty and adverse outcome, which in turn could be useful for patient prognosis, and influence any medical or surgical decision making. This approach may promote the early detection of otherwise subclinical or unsuspected frailty; diagnostic assessment of clinically manifest frailty, and risk stratification of subjects with a suspected or confirmed diagnosis. In the long term, it might be possible to track frailty over time with ultrasound imaging, select an appropriate therapeutic intervention, and monitor response to treatment, including exercise and/or physical therapy (Narici et al., 2011; Reeves, Narici, & Maganaris, 2004; Scanlon et al., 2014).

The knowledge presented here could also be used to improve clinical trials involving frailty. These tools have mostly been used in the research setting, meaning there is still a long road for the incorporation of frailty QIB's into any clinical algorithm. We believe this QIB for frailty can be used for the optimization of clinical trials, which in turn will have to produce evidence-based practice implementation for the use of QIB´s. It will be particularly useful to recognize persons at high risk of developing functional impairment and loss of activities of daily living (Morley, 2016). It would be an accomplishment for QIB's to be included as a part of the clinical algorithms clinicians and geriatricians use to select and direct management of the frail individuals, through developing guidelines and establishing best practice diagnostic pathways. Although the long-term impact of the treatment and/or prevention of frailty is still unknown, an early, simple and objective diagnosis is necessary to evaluate prevention programs and develop appropriate therapy.

We still need better understanding of the clinical implication of the use of the QIB frailty models. The impact of these results will be important not only for understanding the potential connections

between clinical and radiological realm of decline in strength, endurance and muscle mass within the musculoskeletal system, but also the physiology and biology that underlies these clinical and radiological changes in the frail elderly population. Although we are applying these techniques to the study of frailty, the knowledge obtained can be used to study a diverse group of diseases with muscle degeneration and muscle dysfunction as a common characteristic, including dermatomyositis, polymyositis, amyotrophic lateral sclerosis, sarcopenia, post-polio syndrome, cancer related muscle weakness, among others. Recently, similar quantitative assessment of muscle texture has enabled differentiation between normal and pathologic muscles, suggesting that muscle texture analysis may be a promising diagnostic tool for differentiation various muscle diseases (Gdynia, Müller, Ludolph, Köninger, & Huber, 2009; Martínez-Payá et al., 2017; Molinari et al., 2015; Sogawa et al., 2017). The application of created QIB and their further optimization for wider use is possible.

A result that requires further explanation or discussion is why decreased gait speed was associated with very high likelihood of exhibiting frailty phenotype, while increased MT decreased that likelihood within the context of the developed QIBs. In the stepwise multiple analysis regression, we included muscle thickness in the second step and gait speed in the third step, so we could evaluate the degree of effect each variable had over the overall predictive models. What was found is that muscle thickness, although it was significant variable, its overall effect was smaller in comparison with gait speed. Although both variables add important information to the predictive models and improve their discriminative capacity, gait speed plays a much greater role than muscle thickness (Table 4.13 to 4.20).

We believe this is because gait speed represents the physical performance of the subjects, which refers to their capacity to function and the muscle quality it poses to perform those functions. Muscle characteristics beyond size are known to affect muscle function, strength, and contribute to mobility limitations (Pillen & van Alfen, 2011). Muscle quality has been described in myriad ways by clinicians and investigators. Correa-de Araujo and colleagues aptly convey the broad concept of muscle quality with a description that includes glucose metabolism, oxidative damage, protein metabolism, intramuscular adipose tissue, capillary density, structural composition, contractility, and fatigability (Correa-de-Araujo et al., 2017). The general definition of quality incorporates an object's "essential character" and its "distinguishing attributes," and may include a comparative "degree of excellence" (Merriam-Webster, 2004). Thus, the inherent meaning of muscle quality is inextricably linked to the primary functions of skeletal muscle, and this conclusion may be further expanded to consider normal physiology vs. pathophysiology. It is critical to note the complexity of skeletal muscle tissue and its physiologic roles that include not only movement via force production, but also metabolism

through its maintenance of glucose/insulin homeostasis and amino acid storage (Correa-de-Araujo et al., 2017). Considering this expansive view of muscle quality is essential to improve our understanding of frailty and its relation to muscle dysfunction.

Within the context of aging, loss of muscle quantity (i.e., atrophy) is referred to as sarcopenia, while loss of muscle strength is termed dynapenia. Although sarcopenia contributes to dynapenia, several reports have demonstrated strength deficits with aging are more rapid than the concomitant loss of muscle size, which has led some to suggest muscle quantity plays a relatively minor role in dynapenia compared with muscle quality. Since increased muscle mass may not always translate into an improved level of physical function (Cooper et al., 2013), for this reason, we wanted to test the predictive models not only with muscle thickness, but with gait speed and muscle strength as well. Even if there is evidence that muscle mass and muscle strength predict longer-term outcomes of clinical importance such as disability, likelihood of frailty, and in some studies even mortality. In our circumstances, it seems more prudent to reserve muscle strength and gait speed as co-variable measures of the predictive models in addition to muscle thickness (Cesari et al., 2012; Cruz-Jentoft et al., 2010).

We must also underline that another explanation for this result is that of the Fried items, gait speed appears to be the strongest predictor over the other four items (unintentional weight loss, self-reported exhaustion, weakness and low physical activity) (Afilalo et al., 2010; Jung et al., 2018; Silva, Silvia Lanziotti Azevedo da, Neri, Ferrioli, Lourenço, & Dias, 2016). Gait speed can predict life expectancy, functional dependency, and institutionalization in older adults, and it has been used as a marker for physical fitness (Jung et al., 2018; Sanchis et al., 2014). A study performed among elderly Brazilians evaluated the contribution of each item to determine the frailty phenotype. They concluded that when gait speed was positive, subjects were more likely to develop frailty (OR = 10.50, $p < 0.001$); as the same for muscle strength (OR = 7.31, $p < 0.001$), but to a lesser degree (Silva, Silvia Lanziotti Azevedo da et al., 2016).

Muscle strength in our study was not significantly associated with the predictive models, a discrepancy when compared to other studies. Not only because muscle weakness is another Fried item, but also because previously published ultrasound studies on muscle echogenicity have found increased echo intensity to be inversely related with grip strength and general measures of muscle performance (Akima et al., 2017; Cadore et al., 2012; Fukumoto et al., 2012; Nishihara et al., 2014; Rech et al., 2014; Y. Watanabe et al., 2013), including our previous work (Mirón Mombiela et al., 2017).

In our previous study, the correlation between frailty and muscle strength was weak, but significant. We believe the reason for this was that muscle strength measured by hand dynamometer indicated the strength of the arm, and not the femoral quadriceps that was measured by ultrasound. This may also explain why in this study gait speed had such a high correlation with the predictive models, one that was lacking with muscle strength. Lower limbs are more relevant for physical function that upper limbs, even when handgrip strength has been widely used and is well correlated with most relevant outcomes (Chan, van Houwelingen, Gussekloo, Blom, & den Elzen, Wendy P. J., 2014). There is also factors unrelated to muscle that can alter the measurement, like motivation, disease, or cognition, hampering a correct measurement. Even if low handgrip strength has consistently been linked with poor health outcomes, there is widespread variation in the clinical setting on how it is measured. A 70 year-old man may have the same handgrip strength of a 20 year-old (Cooper et al., 2013). While grip dynamometry is the recommended mean of strength testing according to the leading sarcopenia consensus organizations (Bohannon, 2008; Cruz-Jentoft et al., 2010; Massy-Westropp et al., 2011; Mijnarends et al., 2015), the study findings may have been enhanced by obtaining estimates of lower extremity muscle strength.

Although the previous explanation may apply to this study as well, we should contemplate another explanation. Compared to the previous studies (Akima et al., 2017; Cadore et al., 2012; Fukumoto et al., 2012; Mirón Mombiela et al., 2017; Nishihara et al., 2014; Rech et al., 2014; Y. Watanabe et al., 2013), our selection process of control subjects was more rigorous in the current study. None of the previous studies shared this selection process. Thus, the main difference in our current results to previous studies is that our selection process eliminated these individuals with early sings of muscle dysfunction or altered muscle architecture, but who are still not “elderly” by definition.

Conventionally, “elderly” has been defined as a chronological age of 65 years old or older, but the evidence on which this definition is based is unknown (Orimo, 2006). In this study, we have set arbitrarily that definition at 60 years old or older because there were several patients between 60 and 65 years-old that clinically or by imaging were frail or at risk of frailty. Although the increase in longevity is a worldwide trend, there is little evidence that older people living today are accompanied by an extended period of good health too (Beard et al., 2016). Federal agencies have identified the age range of 55–65 as a benchmark period to observe the emergence of age-related health problems within U.S. populations (Ismail et al., 2015). There are reports that in high-income countries at age 50-65 years there is a prevalence of frail of 4%, which raises to 17% for people older than 65 years (Beard et al., 2016). Perhaps we should consider lowering the threshold so we can identify those at

risk of frailty when preventing treatments can be administrated and have a true long-term effect in their health and quality of life.

It has been stated that for those tested for frailty there is a sound reliability and specificity with respect to mortality risk, with high negative predictive value, but disappointing low sensitivity and positive predictive value (Rodriguez-Mañas & Fried, 2015). With our proposed QIB we have replicated very similar results. We have already considered our QIB could be improved when muscle thickness or gait speed were input into the models, in such a way that the sensitivity and specificity of the predictive models is improved, but mostly improved to identify the frail and those at high risk of morbidity and mortality. Another way diagnostic tests can be influenced is by the prevalence of the disease, if we lower the thresholds to include people 55 years-old or older, the positive predictive value of the test could improve. This in turn will lower the rate of false positives and identify more people at risk for frailty, instead of frail.

An interesting, but unexpected finding was that developed predictive models identified a general prognostic phenotype existing in the frail and pre-frail subjects of the study. This phenotype of altered muscle function and architecture determined by the heterogeneity of texture features is associated with a distinct group of diseases. Muscle dysfunction in the context of frailty in this study had an increased incidence of hearing impairment, stroke, myocardial infarction, dementia/memory loss, and falls in the following two years (Table 4.10).

The conversion of digital medical images into mineable data, a process known as radiomics, is motivated by the concept that biomedical images contain information that reflects underlying pathophysiology and that these relationships can be revealed by quantitative image analyses (Gillies et al., 2016). These patterns can be expressed in terms of macroscopic image-based texture features. This allow us to infer phenotypes or gene-protein signatures, possibly containing prognostic information from quantitative analysis of medical image data. This hypothesis could be supported by image-guided biopsies, which demonstrated that image muscle shows spatial differences in protein expression, gene expression, etc. More specifically, it has been demonstrated that major differences in protein expression patterns within tumors can be correlated to radiographic findings (or radiophenotypes) such as contrast-enhanced and non-enhanced region based on CT data. Some authors suggest that image-guided proteomics holds promise for characterizing tissues prior to treatment decisions (Lambin et al., 2012). It should be emphasized that radiomic analyses can be used to identify correlations or associations, not causes; thus, they are not expected to enable definitive assessment of contents of tissue through imaging alone (Gillies et al., 2016).

We believe this group of diseases that we identified (hearing impairment, stroke, myocardial infarction, dementia/memory loss, and falls) share a mitochondrial link. It is hypothesized that phenotype similarities of different disorders may indicate biological relationships of the underlying genes (Scharfe et al., 2009). Mitochondrial dysfunction has been identified in cancer, infertility, diabetes, heart diseases, blindness, deafness, kidney disease, liver disease, stroke, migraine, dwarfism, and resulting from numerous medication toxicities. Mitochondrial dysfunction is also involved in normal aging and age-related neurodegenerative diseases, such as Parkinson and Alzheimer diseases (Goldstein & Wolfe, 2013). The pathogenesis of muscle dysfunction in the aging individual is multifaceted and encompasses lifestyle habits, systemic factors local environment perturbations and intramuscular specific processes. In this scenario, derangements in skeletal myocyte mitochondrial function are also recognized as major factors contributing to the age-dependent muscle dysfunction (Marzetti et al., 2013).

Mitochondrial diseases are caused by an abnormal function of mitochondria. They may be the result of spontaneous or inherited mutations in the mitochondrial genome (mtDNA) or in nuclear genes that code for mitochondrial components, but may also be acquired secondary to adverse effects of drugs, infections, or other environmental causes. The mtDNA encodes only 13 proteins of the respiratory chain, while most of the estimated 1,500 mitochondrial proteins are nuclear-encoded. Mitochondrial deficiencies often affect multiple tissues leading to multi-system diseases that present with many phenotypic features. These dysfunctions appear to be more prevalent in hereditary diseases than previously anticipated and have also been attributed to the pathogenesis of common conditions associated with aging including neurodegenerative diseases, cardiovascular disorders, diabetes mellitus, and several cancer types (Scharfe et al., 2009). Mitochondrial disorders should be considered any time a progressive multisystem disorder is suspected and sometimes for isolated symptoms, such as optic atrophy, sensorineural deafness, cardiomyopathy, diabetes, pseudo-obstruction, neuropathy, myopathy, liver disease, early strokes, or seizures. The phenotype we described shares four diseases from this list.

Mitochondria are intracellular organelles found in every human cell that are responsible for generating energy in the form of adenosine triphosphate (ATP). Other than the generation of energy, mitochondria also function in fatty acid and amino acid oxidation, heme and pyrimidine synthesis, calcium homeostasis, and apoptosis (Goldstein & Wolfe, 2013). It is now known that disease can occur across the lifespan, secondary to the developmental regulation of many mitochondrial proteins. Environmental toxins or medication toxicities may also affect secondary mitochondrial

dysfunction. Carrier proteins acting as chaperonins and mitochondrial fusion/fission abnormalities have reported to cause mitochondrial diseases (Goldstein & Wolfe, 2013). Decades of biochemical and ultrastructural studies have shown that mitochondrial function and structure varies across cell types. Large-scale proteomic surveys have provided valuable molecular insights into this tissue diversity. The heart, for example, contains over twice the mitochondria than any other tissue. There are qualitative differences in these mitochondria, too (Calvo & Mootha, 2010). When the mitochondria do not function properly, they cause symptoms usually presenting in the organs with the highest energy needs, such as brain, cranial and/or peripheral nerves, skeletal muscle, heart muscle, endocrine glands, and/or the kidneys (Goldstein & Wolfe, 2013).

Although mitochondrial defects affect many cellular processes, the phenotype patterns predominantly represent deficiencies in energy metabolism with the nervous system being most susceptible. The distribution of phenotypes within clinical categories is largely consistent with the tissue distribution of energy expenditure in the resting state. Mitochondria provide most of the body's energy and measurements of mitochondrial respiration have shown that brain tissue contains more active respiratory chain complexes than liver, heart, or muscle (Scharfe et al., 2009). Thus, our results showing a higher proportion of neurological (e.g. stroke and hearing impairment), cardiological (e.g. myocardial infarction) and musculoskeletal features positively correlate to basal metabolic rate and respiratory-chain activities.

Traditionally, mitochondrial disease has been referred primarily to disorders of oxidative ATP production. However, the breadth of the mitochondrial proteome now implicates a large number of additional phenotypes (Calvo & Mootha, 2010). Many late-onset mitochondrial diseases are related to mtDNA point mutations or deletions that must meet a tissue-specific threshold before disease symptoms manifest (Goldstein & Wolfe, 2013).

How can we begin to systematically further understand or study these findings? A useful approach may lie in connecting disease genes, clinical features, and biological pathways. Data sets could be used as an initial framework for linking genes and pathways to clinical phenotypes (Calvo & Mootha, 2010). It would be interesting to investigate genotype-radiological-phenotype associations in frailty and the application of muscle ultrasound for frailty phenotype can be used to investigate evolving physiology in this field.

Finally, we must point out that for the evaluation of biomarkers from medical images, accuracy and precision are two of the most important factors. The term accuracy is synonymous with the area

under the receiver operating characteristic curve, and this will be dependent on the "ground truth" or "gold standard" utilized for identifying frailty phenotype. In the majority of studies, the phenotype described by Fried et al. is utilized, but more recent frailty scales have emerged or variations on the original, making the process of identifying frail or at risk of frailty highly variable (Davies et al., 2018; Rizzoli et al., 2013). Hence, precision takes a prominent role in the validation of QIB for frailty. Precision refers to variability of the measurement process regarding the expected value for different measurements (Sullivan et al., 2015). We tested the variation of the measurement when it came from two different muscles (*Rectus Femoris* and *Vastus Intermidius*), and if the plane (axial vs. sagittal) of the image had any effect. We concluded that when images were taken from the same muscle, either axial or sagittal, their variability or bias was low, but when the same plane was taken from different muscles, the variability was extremely high, suggesting that each muscle has intrinsic characteristics not shared by other muscles (Table 4.23 and 4.24). Therefore, for diagnostic purposes, the predictive models will perform better when used for the same muscle it was developed, even when the plane of the image is modified.

Throughout the study, we also identified a trend where data from *Vastus Intermidius* outperformed the data from the *Rectus Femoris* muscle. In the final analysis, we compared if this was true and confirmed that there is a better ICC of the texture features with *Vastus Intermidius* muscle than with *Rectus Femoris*. This could be explained due to the unique anatomy of the RF muscle as it has two tendinous origins. One of the tendons contributes to the anterior fascia, while the other contributes to the deep, central intramuscular tendon (Kerr, 2014). This internal fascia increases the echo intensity of the ROI measurements where the surface of the *Rectus Femoris* was included, even if we tried to avoid it. There is one study that has performed echo intensity analysis of the whole quadriceps. This study found that the relation between echo intensity and muscle power has stronger correlation with *vastus lateralis*, *vastus medialis* and *vastus intermedius*, than *Rectus Femoris* muscle (Wilhelm et al., 2014). Most studies on echo intensity and muscle strength (Cadore et al., 2012; Fukumoto et al., 2012; Rech et al., 2014; Y. Watanabe et al., 2013), echo intensity and sarcopenia (Yamada et al., 2017) or echo intensity and frailty (Mirón Mombiela et al., 2017) have been performed in the *Rectus Femoris* muscle, but some consideration should be given to the use of *vastus intermedius* or *vastus lateralis* in future studies as better choice for region of study than *Rectus Femoris*.

These findings must be interpreted in light of several limitations. First, this remains a small cross sectional study with an ethnicity bias, as only Spaniards were taken into account. Although the baseline demographics and clinical characteristics of the participants, like the distribution of

comorbidities and the prevalence of pre-frail and frail individuals is similar to that of other published cohorts (Boyle et al., 2010; Kang et al., 2015; Lichtman et al., 2002). Still, larger longitudinal studies in diverse populations are needed to determine whether changes over time in echo intensity are meaningful and whether interventions that improve muscle dysfunction can be followed-up by ultrasound. While a cross-sectional study may be the only type of study feasible given time, due to patient or monetary constraints, it is nonetheless important to develop a plan or method to expand any analysis to include longitudinal data (Prescott, 2013). Second, it was a single sonographer and same ultrasound machine used throughout the study. Therefore, the actual capability of using echo intensity texture features from ultrasound images, including the influence of a plurality of devices remains unknown. Third, standardization of the technique requires further research and the best region for measurement must be determined. Unrecognized confounding variables in the databases used are a concern even when we performed a robust statistical validation to avoid bias and over-fitting of the predictive models. Hence, our study must be validated against a completely independent data set, preferably from another institution (Gillies et al., 2016). Further on, the study did not investigate the exercise habits of the participants, which is important because there are reports that resistance exercise can decrease intermuscular adipose tissue in older individuals (Jenkins, 2016), or because muscle edema induced by intense exercise could increase echo intensity values (Thiago Torres da Matta et al., 2017), this being a possible source of false positives or false negatives.

In summary, the clinical impact of our results is illustrated by the fact that it advances knowledge in the analysis and characterization of frailty in medical images, previously not done; and provides knowledge currently not used in the clinic. We showed the complementary performance of machine learning texture features with comorbidities and mortality for prediction of outcome, which illustrates the clinical importance of our findings. In future clinical trials, this method could be used for risk stratification (frail and non-frail). We also demonstrated that the method improves when muscle thickness and gait speed information is input to the predictive models.

The developed method provides a non-invasive, fast, low cost, accurate and precise way of investigating phenotypic information. Analyzing medical images is a natural fit for “machine learning”, a form of artificial intelligence. A variety of stakeholders in the medical field hope that bringing artificial intelligence into the clinic will make diagnosis faster and cheaper (Blease, 2018). The developed predictive models will be able to detect nuances that humans cannot, assessing the risk of frailty in patients simply by looking at an image, opening up entire new applications for medical

imaging. Even in the rich world, radiology is expensive. If machine learning can make it more efficient, then the price should come down, allowing its benefits to be spread more widely (Blease, 2018).

There is a need to develop innovative tools to evaluate muscle dysfunction in the frail elderly; we believe that the developed QIB could become an accurate evaluation of skeletal muscle quality. This QIB can transform how doctors deal with patients. The development of tools and software (e.g. machine learning, artificial intelligence software, App's, hand-held devices), will not only help the development and use of imaging techniques and technologies, but also its dissemination and implementation. Radiomic texture feature-metrics are platform independent, thus the predictive model developed here can potentially be applied to other modalities such as CT or MRI. In the future, Ultrasound, CT, and MRI manufacturers will be able to add frailty QIB's to their portfolio as a respond to increasing clinical request.

6. CONCLUSIONS

In light of the results obtained, we can draw the following conclusions:

1. The developed quantitative imaging biomarkers from muscle ultrasound can identify subjects at risk of frailty (pre-frail) or frail with good accuracy, with the aid of machine learning texture analysis.

2. The heterogeneity of the muscle texture features captures the muscle quality and/or muscle dysfunction of the subjects. These characteristics make ultrasound imaging, with the aid of machine learning texture analysis, a good quantitative imaging biomarker.

3. The predictive models developed for ultrasound imaging provide a non-invasive, fast, and low cost as well as repeatable quantitative imaging biomarkers.

4. The diagnostic accuracy of the developed quantitative imaging biomarkers can be improved if muscle thickness and gait speed are input into the models.

5. The quantitative imaging biomarkers models perform better when used for *Vastus Intermedius* muscle than *Rectus Femoris* muscle, in either axial or sagittal plane.

6. The developed quantitative imaging biomarkers were strongly prognostic of death and were associated with higher morbidity.

7. The developed quantitative imaging biomarkers identify a general prognostic phenotype existing in the frail and pre-frail subjects of the study, characterized by an increased incidence of hearing impairment, stroke, myocardial infarction, dementia/memory loss, and falls in the following two years in the context of identified muscle dysfunction.

7. REFERENCES

Aerts, Hugo J W L, Velazquez, E. R., Leijenaar, R. T. H., Parmar, C., Grossmann, P., Carvalho, S., . . . Lambin, P. (2014). Decoding tumour phenotype by noninvasive imaging using a quantitative radiomics approach. *Nature Communications, 5*, 4006. doi:10.1038/ncomms5006

Afilalo, J. (2011). Frailty in patients with cardiovascular disease: Why, when, and how to measure. *Current Cardiovascular Risk Reports, 5*(5), 467-472. doi:10.1007/s12170-011-0186-0

Afilalo, J., Eisenberg, M. J., Morin, J., Bergman, H., Monette, J., Noiseux, N., . . . Boivin, J. (2010). Gait speed as an incremental predictor of mortality and major morbidity in elderly patients undergoing cardiac surgery. *Journal of the American College of Cardiology, 56*(20), 1668-1676. doi:10.1016/j.jacc.2010.06.039

Akazawa, N., Okawa, N., Tamura, K., & Moriyama, H. (2017). Relationships between intramuscular fat, muscle strength and gait independence in older women: A cross-sectional study. *Geriatrics & Gerontology International, 17*(10), 1683-1688. doi:10.1111/ggi.12869

Akima, H., Hioki, M., Yoshiko, A., Koike, T., Sakakibara, H., Takahashi, H., & Oshida, Y. (2016). Intramuscular adipose tissue determined by T1-weighted MRI at 3T primarily reflects extramyocellular lipids. *Magnetic Resonance Imaging, 34*(4), 397-403. doi:10.1016/j.mri.2015.12.038

Akima, H., Yoshiko, A., Tomita, A., Ando, R., Saito, A., Ogawa, M., . . . Tanaka, N. I. (2017). Relationship between quadriceps echo intensity and functional and morphological characteristics in older men and women. *Archives of Gerontology and Geriatrics, 70*, 105-111. doi:10.1016/j.archger.2017.01.014

Alonso Salinas, G. L., Sanmartín Fernández, M., Pascual Izco, M., Martín Asenjo, R., Recio-Mayoral, A., Salvador Ramos, L., . . . Zamorano Gómez, J. L. (2016). Frailty is a short-term prognostic marker in acute coronary syndrome of elderly patients. *European Heart Journal. Acute Cardiovascular Care, 5*(5), 434-440. doi:10.1177/2048872616644909

Alonso Salinas, G. L., Sanmartin, M., Pascual Izco, M., Rincon, L. M., Pastor Pueyo, P., Marco Del Castillo, A., . . . Zamorano, J. L. (2017). Frailty is an independent prognostic marker in elderly patients with myocardial infarction. *Clinical Cardiology, 40*(10), 925-931. doi:10.1002/clc.22749

Alvarado, B. E., Zunzunegui, M., Béland, F., & Bamvita, J. (2008). Life course social and health conditions linked to frailty in latin american older men and women. *The Journals of Gerontology. Series A, Biological Sciences and Medical Sciences, 63*(12), 1399-1406.

Amadasun, M., & King, R. (1989). Textural features corresponding to textural properties. *IEEE Transactions on Systems, Man, and Cybernetics, 19*(5), 1264-1274. doi:10.1109/21.44046

Argilés, J. M., Campos, N., Lopez-Pedrosa, J. M., Rueda, R., & Rodriguez-Mañas, L. (2016). Skeletal muscle regulates metabolism via interorgan crosstalk: Roles in health and disease. *Journal of the American Medical Directors Association, 17*(9), 789-796. doi:10.1016/j.jamda.2016.04.019

Arts, I. M., Pillen, S., Overeem, S., Schelhaas, H. J., & Zwarts, M. J. (2007). Rise and fall of skeletal muscle size over the entire life span. *Journal of the American Geriatrics Society, 55*(7), 1150-1152. doi:JGS1228 [pii]

Arts, I. M. P., Pillen, S., Schelhaas, H. J., Overeem, S., & Zwarts, M. J. (2010). Normal values for quantitative muscle ultrasonography in adults. *Muscle & Nerve, 41*(1), 32-41. doi:10.1002/mus.21458

Avila-Funes, J. A., Amieva, H., Barberger-Gateau, P., Le Goff, M., Raoux, N., Ritchie, K., . . . Dartigues, J. (2009). Cognitive impairment improves the predictive validity of the phenotype of frailty for adverse health outcomes: The three-city study. *Journal of the American Geriatrics Society, 57*(3), 453-461. doi:10.1111/j.1532-5415.2008.02136.x

Bartley, J. M., & Studenski, S. A. (2017). Muscle ultrasound as a link to muscle quality and frailty in the clinic. *Journal of the American Geriatrics Society,* doi:10.1111/jgs.15075

Barzilay, J. I., Blaum, C., Moore, T., Xue, Q. L., Hirsch, C. H., Walston, J. D., & Fried, L. P. (2007). Insulin resistance and inflammation as precursors of frailty: The cardiovascular health study. *Archives of Internal Medicine, 167*(7), 635-641. doi:10.1001/archinte.167.7.635

Baumann, C. W., Kwak, D., Liu, H. M., & Thompson, L. V. (2016). Age-induced oxidative stress: How does it influence skeletal muscle quantity and quality? *Journal of Applied Physiology (Bethesda, Md.: 1985), 121*(5), 1047-1052. doi:10.1152/japplphysiol.00321.2016

Baylis, D., Bartlett, D. B., Syddall, H. E., Ntani, G., Gale, C. R., Cooper, C., . . . Sayer, A. A. (2013). Immune-endocrine biomarkers as predictors of frailty and mortality: A 10-year longitudinal study in community-dwelling older people. *Age (Dordrecht, Netherlands), 35*(3), 963-971. doi:10.1007/s11357-012-9396-8

Beard, J. R., Officer, A., de Carvalho, I. A., Sadana, R., Pot, A. M., Michel, J., . . . Chatterji, S. (2016). The world report on ageing and health: A policy framework for healthy ageing. *Lancet (London, England), 387*(10033), 2145-2154. doi:10.1016/S0140-6736(15)00516-4

Benjamini, Y., & Hochberg, Y. (1995). Controlling the false discovery rate: A practical and powerful approach to multiple testing. *Journal of the Royal Statistical Society. Series B (Methodological), 57*(1), 289-300. Retrieved from http://www.jstor.org/stable/2346101

Blease, G. (2018). AI, radiology and the future of work. *The Economist,* Retrieved from https://www.economist.com/leaders/2018/06/07/ai-radiology-and-the-future-of-work?frsc=dg%7Ce

Blume, S. W., & Curtis, J. R. (2011). Medical costs of osteoporosis in the elderly medicare population. *Osteoporosis International: A Journal Established as Result of Cooperation between the European Foundation for Osteoporosis and the National Osteoporosis Foundation of the USA, 22*(6), 1835-1844. doi:10.1007/s00198-010-1419-7

Bohannon, R. W. (2008). Hand-grip dynamometry predicts future outcomes in aging adults. *Journal of Geriatric Physical Therapy (2001), 31*(1), 3-10.

Bouillon, K., Kivimaki, M., Hamer, M., Sabia, S., Fransson, E. I., Singh-Manoux, A., . . . Batty, G. D. (2013). Measures of frailty in population-based studies: An overview. *BMC Geriatrics, 13*, 64. doi:10.1186/1471-2318-13-64 [doi]

Boutin, R. D., Bamrungchart, S., Bateni, C. P., Beavers, D. P., Beavers, K. M., Meehan, J. P., & Lenchik, L. (2017). CT of patients with hip fracture: Muscle size and attenuation help predict mortality. *AJR. American Journal of Roentgenology, 208*(6), W215. doi:10.2214/AJR.16.17226

Bowling, A. (2009). The psychometric properties of the older people's quality of life questionnaire, compared with the CASP-19 and the WHOQOL-OLD. *Current Gerontology and Geriatrics Research, 2009*, 298950. doi:10.1155/2009/298950 [doi]

Boyle, P. A., Buchman, A. S., Wilson, R. S., Leurgans, S. E., & Bennett, D. A. (2010). Physical frailty is associated with incident mild cognitive impairment in community-based older persons. *Journal of the American Geriatrics Society, 58*(2), 248-255. doi:10.1111/j.1532-5415.2009.02671.x

Cadore, E. L., Izquierdo, M., Conceicao, M., Radaelli, R., Pinto, R. S., Baroni, B. M., . . . Kruel, L. F. (2012). Echo intensity is associated with skeletal muscle power and cardiovascular performance in elderly men. *Experimental Gerontology, 47*(6), 473-478. doi:10.1016/j.exger.2012.04.002 [doi]

Calvani, R., Marini, F., Cesari, M., Tosato, M., Anker, S. D., von Haehling, S., . . . SPRINTT consortium. (2015). Biomarkers for physical frailty and sarcopenia: State of the science and future developments. *Journal of Cachexia, Sarcopenia and Muscle, 6*(4), 278-286. doi:10.1002/jcsm.12051 [doi]

Calvo, S. E., & Mootha, V. K. (2010). The mitochondrial proteome and human disease. *Annual Review of Genomics and Human Genetics, 11*, 25-44. doi:10.1146/annurev-genom-082509-141720

Cesari, M., Fielding, R. A., Pahor, M., Goodpaster, B., Hellerstein, M., van Kan, G. A., . . . International Working Group on Sarcopenia. (2012). Biomarkers of sarcopenia in clinical trials-recommendations from the international working group on sarcopenia. *Journal of Cachexia, Sarcopenia and Muscle, 3*(3), 181-190. doi:10.1007/s13539-012-0078-2 [doi]

Cesari, M., Prince, M., Thiyagarajan, J. A., De Carvalho, I. A., Bernabei, R., Chan, P., . . . Vellas, B. (2016). Frailty: An emerging public health priority. *Journal of the American Medical Directors Association, 17*(3), 188-192. doi:10.1016/j.jamda.2015.12.016

Chan, O. Y. A., van Houwelingen, A. H., Gussekloo, J., Blom, J. W., & den Elzen, Wendy P. J. (2014). Comparison of quadriceps strength and handgrip strength in their association with health outcomes in older adults in primary care. *Age (Dordrecht, Netherlands), 36*(5), 9714. doi:10.1007/s11357-014-9714-4

Chang, S., & Lin, P. (2015). Frail phenotype and mortality prediction: A systematic review and meta-analysis of prospective cohort studies. *International Journal of Nursing Studies, 52*(8), 1362-1374. doi:10.1016/j.ijnurstu.2015.04.005

Charlson, M. E., Pompei, P., Ales, K. L., & MacKenzie, C. R. (1987). A new method of classifying prognostic comorbidity in longitudinal studies: Development and validation. *Journal of Chronic Diseases, 40*(5), 373-383.

Chen, L., Liu, L., Woo, J., Assantachai, P., Auyeung, T., Bahyah, K. S., . . . Arai, H. (2014). Sarcopenia in asia: Consensus report of the asian working group for sarcopenia. *Journal of the American Medical Directors Association, 15*(2), 95-101. doi:10.1016/j.jamda.2013.11.025

Cheng, M., & Chang, S. (2017). Frailty as a risk factor for falls among community dwelling people: Evidence from a meta-analysis. *Journal of Nursing Scholarship: An Official Publication of Sigma Theta Tau International Honor Society of Nursing, 49*(5), 529-536. doi:10.1111/jnu.12322

Chu, A., Sehgal, C. M., & Greenleaf, J. F. (1990a). Use of gray value distribution of run lengths for texture analysis. *Pattern Recognition Letters, 11*(6), 415-419. doi:10.1016/0167-8655(90)90112-F

Chu, A., Sehgal, C. M., & Greenleaf, J. F. (1990b). Use of gray value distribution of run lengths for texture analysis. *Pattern Recognition Letters, 11*(6), 415-419. doi:10.1016/0167-8655(90)90112-F

Chumlea, W. C., Cesari, M., Evans, W. J., Ferrucci, L., Fielding, R. A., Pahor, M., . . . International Working Group on Sarcopenia Task Force Members. (2011). Sarcopenia: Designing phase IIB trials. *The Journal of Nutrition, Health & Aging, 15*(6), 450-455.

Cooper, C., Fielding, R., Visser, M., van Loon, L. J., Rolland, Y., Orwoll, E., . . . Kanis, J. A. (2013). Tools in the assessment of sarcopenia. *Calcified Tissue International, 93*(3), 201-210. doi:10.1007/s00223-013-9757-z [doi]

Correa-de-Araujo, R., Harris-Love, M. O., Miljkovic, I., Fragala, M. S., Anthony, B. W., & Manini, T. M. (2017). The need for standardized assessment of muscle quality in skeletal muscle function deficit and other aging-related muscle dysfunctions: A symposium report. *Frontiers in Physiology, 8*, 87. doi:10.3389/fphys.2017.00087

Cruz-Jentoft, A. J., Baeyens, J. P., Bauer, J. M., Boirie, Y., Cederholm, T., Landi, F., . . . European Working Group on Sarcopenia in Older People. (2010). Sarcopenia: European consensus on definition and diagnosis: Report of the european working group on sarcopenia in older people. *Age and Ageing, 39*(4), 412-423. doi:10.1093/ageing/afq034 [doi]

Dasarathy, B. V., & Holder, E. B. (1991). Image characterizations based on joint gray level—run length distributions. *Pattern Recognition Letters, 12*(8), 497-502. doi:10.1016/0167-8655(91)80014-2

Davies, B., García, F., Ara, I., Artalejo, F. R., Rodriguez-Mañas, L., & Walter, S. (2018). Relationship between sarcopenia and frailty in the toledo study of healthy aging: A population based cross-sectional study. *Journal of the American Medical Directors Association, 19*(4), 282-286. doi:10.1016/j.jamda.2017.09.014

Ekerstad, N., Swahn, E., Janzon, M., Alfredsson, J., Löfmark, R., Lindenberger, M., & Carlsson, P. (2011). Frailty is independently associated with short-term outcomes for elderly patients with non-ST-segment elevation myocardial infarction. *Circulation, 124*(22), 2397-2404. doi:10.1161/CIRCULATIONAHA.111.025452

Ensrud, K. E., Kats, A. M., Schousboe, J. T., Taylor, B. C., Cawthon, P. M., Hillier, T. A., . . . Langsetmo, L. (2018). Frailty phenotype and healthcare costs and utilization in older women. *Journal of the American Geriatrics Society, 66*(7), 1276-1283. doi:10.1111/jgs.15381

Ensrud, K. E., Ewing, S. K., Taylor, B. C., Fink, H. A., Stone, K. L., Cauley, J. A., . . . Cawthon, P. M. (2007). Frailty and risk of falls, fracture, and mortality in older women: The study of osteoporotic fractures. *The Journals of Gerontology. Series A, Biological Sciences and Medical Sciences, 62*(7), 744-751.

Erickson, B. J., Korfiatis, P., Akkus, Z., & Kline, T. L. (2017). Machine learning for medical imaging. *Radiographics: A Review Publication of the Radiological Society of North America, Inc, 37*(2), 505-515. doi:10.1148/rg.2017160130

Erickson, B. J., Korfiatis, P., Kline, T. L., Akkus, Z., Philbrick, K., & Weston, A. D. (2018). Deep learning in radiology: Does one Size Fit all? *Journal of the American College of Radiology: JACR, 15*(3 Pt B), 521-526. doi:10.1016/j.jacr.2017.12.027

Ferrucci, L., Penninx, Brenda W J H, Volpato, S., Harris, T. B., Bandeen-Roche, K., Balfour, J., . . . Md, J. M. G. (2002). Change in muscle strength explains accelerated decline of physical function in older women with high interleukin-6 serum levels. *Journal of the American Geriatrics Society, 50*(12), 1947-1954.

Fried, L. P., Tangen, C. M., Walston, J., Newman, A. B., Hirsch, C., Gottdiener, J., . . . McBurnie, M. A. (2001). Frailty in older adults: Evidence for a phenotype. *The Journals of Gerontology. Series A, Biological Sciences and Medical Sciences, 56*(3), 146.

Fried, L. P., Ferrucci, L., Darer, J., Williamson, J. D., & Anderson, G. (2004). Untangling the concepts of disability, frailty, and comorbidity: Implications for improved targeting and care. *The Journals of Gerontology. Series A, Biological Sciences and Medical Sciences, 59*(3), 255-263.

Fukumoto, Y., Ikezoe, T., Yamada, Y., Tsukagoshi, R., Nakamura, M., Mori, N., . . . Ichihashi, N. (2012). Skeletal muscle quality assessed from echo intensity is associated with muscle strength of middle-aged and elderly persons. *European Journal of Applied Physiology, 112*(4), 1519-1525. doi:10.1007/s00421-011-2099-5 [doi]

Galloway, M. M. (1975). Texture analysis using gray level run lengths. *Computer Graphics and Image Processing, 4*(2), 172-179. doi:10.1016/S0146-664X(75)80008-6

Gdynia, H. -., Müller, H. -., Ludolph, A. C., Köninger, H., & Huber, R. (2009). Quantitative muscle ultrasound in neuromuscular disorders using the parameters 'intensity', 'entropy', and 'fractal dimension'. *European Journal of Neurology, 16*(10), 1151-1158. doi:10.1111/j.1468-1331.2009.02663.x

Gibbs, P., & Turnbull, L. W. (2003). Textural analysis of contrast-enhanced MR images of the breast. *Magnetic Resonance in Medicine, 50*(1), 92-98. doi:10.1002/mrm.10496

Gillies, R. J., Kinahan, P. E., & Hricak, H. (2016). Radiomics: Images are more than pictures, they are data. *Radiology, 278*(2), 563-577. doi:10.1148/radiol.2015151169 [doi]

Goldstein, A., & Wolfe, L. A. (2013). The elusive magic pill: Finding effective therapies for mitochondrial disorders. *Neurotherapeutics: The Journal of the American Society for Experimental NeuroTherapeutics, 10*(2), 320-328. doi:10.1007/s13311-012-0175-0

Graham, M. M., Galbraith, P. D., O'Neill, D., Rolfson, D. B., Dando, C., & Norris, C. M. (2013). Frailty and outcome in elderly patients with acute coronary syndrome. *The Canadian Journal of Cardiology, 29*(12), 1610-1615. doi:10.1016/j.cjca.2013.08.016

Gruther, W., Benesch, T., Zorn, C., Paternostro-Sluga, T., Quittan, M., Fialka-Moser, V., . . . Crevenna, R. (2008). Muscle wasting in intensive care patients: Ultrasound observation of the M. quadriceps femoris muscle layer. *Journal of Rehabilitation Medicine, 40*(3), 185-189. doi:10.2340/16501977-0139

Guralnik, J. M., Seeman, T. E., Tinetti, M. E., Nevitt, M. C., & Berkman, L. F. (1994). Validation and use of performance measures of functioning in a non-disabled older population: MacArthur studies of successful aging. *Aging (Milan, Italy), 6*(6), 410-419.

Hajek, A., Bock, J., Saum, K., Matschinger, H., Brenner, H., Holleczek, B., . . . König, H. (2018). Frailty and healthcare costs-longitudinal results of a prospective cohort study. *Age and Ageing, 47*(2), 233-241. doi:10.1093/ageing/afx157

Haralick, R. M., Shanmugam, K., & Dinstein, I. (1973). Textural features for image classification. *IEEE Transactions on Systems, Man, and Cybernetics, 3*(6), 610-621. doi:10.1109/TSMC.1973.4309314

Holanda, Cristina Marques de Almeida, Guerra, R. O., Nóbrega, Patrícia Vidal de Negreiros, Costa, H. F., Piuvezam, M. R., & Maciel, Á C. C. (2012). Salivary cortisol and frailty syndrome in elderly residents of long-stay institutions: A cross-sectional study. *Archives of Gerontology and Geriatrics, 54*(2), 146. doi:10.1016/j.archger.2011.11.006

Hubbard, R. E., Lang, I. A., Llewellyn, D. J., & Rockwood, K. (2010). Frailty, body mass index, and abdominal obesity in older people. *The Journals of Gerontology. Series A, Biological Sciences and Medical Sciences, 65*(4), 377-381. doi:10.1093/gerona/glp186

Hyde, Z., Flicker, L., Almeida, O. P., Hankey, G. J., McCaul, K. A., Chubb, S. A. P., & Yeap, B. B. (2010). Low free testosterone predicts frailty in older men: The health in men study. *The Journal of Clinical Endocrinology and Metabolism, 95*(7), 3165-3172. doi:10.1210/jc.2009-2754

Inglés, M., Gambini, J., Carnicero, J. A., García-García, F. J., Rodríguez-Mañas, L., Olaso-González, G., . . . Viña, J. (2014). Oxidative stress is related to frailty, not to age or sex, in a geriatric population: Lipid and protein oxidation as biomarkers of frailty. *Journal of the American Geriatrics Society, 62*(7), 1324-1328. doi:10.1111/jgs.12876

Inglés, M., Gambini, J., Mas-Bargues, C., García-García, F. J., Viña, J., & Borrás, C. (2017). Brain-derived neurotrophic factor as a marker of cognitive frailty. *The Journals of Gerontology. Series A, Biological Sciences and Medical Sciences, 72*(3), 450-451. doi:10.1093/gerona/glw145

Ismail, C., Zabal, J., Hernandez, H. J., Woletz, P., Manning, H., Teixeira, C., . . . Harris-Love, M. O. (2015). Diagnostic ultrasound estimates of muscle mass and muscle quality discriminate between women with and without sarcopenia. *Frontiers in Physiology, 6*, 302. doi:10.3389/fphys.2015.00302

Jacobs, J. M., Cohen, A., Ein-Mor, E., Maaravi, Y., & Stessman, J. (2011). Frailty, cognitive impairment and mortality among the oldest old. *The Journal of Nutrition, Health & Aging, 15*(8), 678-682.

Jenkins, N. D. M. (2016). Are resistance training-mediated decreases in ultrasound echo intensity caused by changes in muscle composition, or is there an alternative explanation? *Ultrasound in Medicine & Biology, 42*(12), 3050-3051. doi:10.1016/j.ultrasmedbio.2016.07.011

Jirák, D., Dezortová, M., & Hájek, M. (2004). Phantoms for texture analysis of MR images. long-term and multi-center study. *Medical Physics, 31*(3), 616-622. doi:10.1118/1.1646231

Jung, H., Kang, M., Choi, J., Yoon, S., Kim, S., Kim, K., & Kim, C. (2018). Simple method of screening for frailty in older adults using a chronometer and tape measure in clinic. *Journal of the American Geriatrics Society, 66*(1), 157-160. doi:10.1111/jgs.15204

Kamil, R. J., Betz, J., Powers, B. B., Pratt, S., Kritchevsky, S., Ayonayon, H. N., . . . Lin, F. R. (2016). Association of hearing impairment with incident frailty and falls in older adults. *Journal of Aging and Health, 28*(4), 644-660. doi:10.1177/0898264315608730

Kamil, R. J., Li, L., & Lin, F. R. (2014). Association between hearing impairment and frailty in older adults. *Journal of the American Geriatrics Society, 62*(6), 1186-1188. doi:10.1111/jgs.12860

Kang, L., Zhang, S., Zhu, W., Pang, H., Zhang, L., Zhu, M., . . . Liu, Y. (2015). Is frailty associated with short-term outcomes for elderly patients with acute coronary syndrome? *Journal of Geriatric Cardiology: JGC, 12*(6), 662-667. doi:10.11909/j.issn.1671-5411.2015.06.010

Kawai, H., Kera, T., Hirayama, R., Hirano, H., Fujiwara, Y., Ihara, K., . . . Obuchi, S. (2018). Morphological and qualitative characteristics of the quadriceps muscle of community-dwelling older adults based on ultrasound imaging: Classification using latent class analysis. *Aging Clinical and Experimental Research, 30*(4), 283-291. doi:10.1007/s40520-017-0781-0

Kerr, R. M. (2014). MRI of rectus femoris / quadriceps injury. Retrieved from http://radsource.us/rectus-femoris-quadriceps-injury/

Klein, B. E. K., Klein, R., Knudtson, M. D., & Lee, K. E. (2005). Frailty, morbidity and survival. *Archives of Gerontology and Geriatrics, 41*(2), 141-149. doi:10.1016/j.archger.2005.01.002

Kojima, G. (2015). Frailty as a predictor of future falls among community-dwelling older people: A systematic review and meta-analysis. *Journal of the American Medical Directors Association, 16*(12), 1027-1033. doi:10.1016/j.jamda.2015.06.018

Kuhn Max. (2008). Building predictive models in R using the caret package. *Journal of Statistical Software, 28*(5), 1-26. doi:10.18637/jss.v028.i05

Kuhn, M., & Johnson, K. (2013). *Applied predictive modeling*. New York, NY [u.a.]: Springer.

Kumar, V., Gu, Y., Basu, S., Berglund, A., Eschrich, S. A., Schabath, M. B., . . . Gillies, R. J. (2012). Radiomics: The process and the challenges. *Magnetic Resonance Imaging, 30*(9), 1234-1248. doi:10.1016/j.mri.2012.06.010

Lambert, C. P., & Evans, W. J. (2002). Effects of aging and resistance exercise on determinants of muscle strength. *Journal of the American Aging Association, 25*(2), 73-78. doi:10.1007/s11357-002-0005-0 [doi]

Lambin, P., Rios-Velazquez, E., Leijenaar, R., Carvalho, S., van Stiphout, Ruud G P M, Granton, P., . . . Aerts, Hugo J W L. (2012). Radiomics: Extracting more information from medical images using advanced feature analysis. *European Journal of Cancer, 48*(4), 441-446. doi:10.1016/j.ejca.2011.11.036

Lang, T., Streeper, T., Cawthon, P., Baldwin, K., Taaffe, D. R., & Harris, T. B. (2010). Sarcopenia: Etiology, clinical consequences, intervention, and assessment. *Osteoporosis International: A Journal Established as Result of Cooperation between the European Foundation for Osteoporosis and the National Osteoporosis Foundation of the USA, 21*(4), 543-559. doi:10.1007/s00198-009-1059-y

Larroza, A., Bodí, V., & Moratal, D. (2016). Texture analysis in magnetic resonance imaging: Review and considerations for future applications. *Assessment of Cellular and Organ Function and Dysfunction using Direct and Derived MRI Methodologies,* doi:10.5772/64641

Leng, S. X., Cappola, A. R., Andersen, R. E., Blackman, M. R., Koenig, K., Blair, M., & Walston, J. D. (2004). Serum levels of insulin-like growth factor-I (IGF-I) and dehydroepiandrosterone sulfate (DHEA-S), and their relationships with serum interleukin-6, in the geriatric syndrome of frailty. *Aging Clinical and Experimental Research, 16*(2), 153-157.

Li, Q., Wang, S., Milot, E., Bergeron, P., Ferrucci, L., Fried, L. P., & Cohen, A. A. (2015). Homeostatic dysregulation proceeds in parallel in multiple physiological systems. *Aging Cell, 14*(6), 1103-1112. doi:10.1111/acel.12402

Lichtman, J. H., Krumholz, H. M., Wang, Y., Radford, M. J., & Brass, L. M. (2002). Risk and predictors of stroke after myocardial infarction among the elderly: Results from the cooperative cardiovascular project. *Circulation, 105*(9), 1082-1087.

Liljas, A. E. M., Carvalho, L. A., Papachristou, E., Oliveira, C. D., Wannamethee, S. G., Ramsay, S. E., & Walters, K. (2017). Self-reported hearing impairment and incident frailty in english community-dwelling older adults: A 4-year follow-up study. *Journal of the American Geriatrics Society, 65*(5), 958-965. doi:10.1111/jgs.14687

Lipsitz, L. A. (2004). Physiological complexity, aging, and the path to frailty. *Science of Aging Knowledge Environment : SAGE KE, 2004*(16), pe16. doi:10.1126/sageke.2004.16.pe16 [doi]

Lipsitz, L. A. (2008). Dynamic models for the study of frailty. *Mechanisms of Ageing and Development, 129*(11), 675-676. doi:10.1016/j.mad.2008.09.012 [doi]

Llibre, J. d. J., López, A. M., Valhuerdi, A., Guerra, M., Llibre-Guerra, J. J., Sánchez, Y. Y., . . . Moreno, C. (2014). Frailty, dependency and mortality predictors in a cohort of cuban older adults, 2003-2011. *MEDICC Review, 16*(1), 24-30.

Longstreth, W. T., Bernick, C., Fitzpatrick, A., Cushman, M., Knepper, L., Lima, J., & Furberg, C. D. (2001). Frequency and predictors of stroke death in 5,888 participants in the cardiovascular health study. *Neurology, 56*(3), 368-375.

Lubner, M. G., Smith, A. D., Sandrasegaran, K., Sahani, D. V., & Pickhardt, P. J. (2017). CT texture analysis: Definitions, applications, biologic correlates, and challenges. *Radiographics: A Review Publication of the Radiological Society of North America, Inc, 37*(5), 1483-1503. doi:10.1148/rg.2017170056

Lutz, H., & Elisabetta Buscarini. (2011). *Manual of diagnostic ultrasound* (2nd edition ed.) Retrieved from http://search.credoreference.com/content/entry/heliconhe/manual/0

Martínez-Payá, J. J., Ríos-Díaz, J., Del Baño-Aledo, M. E., Tembl-Ferrairó, J. I., Vazquez-Costa, J. F., & Medina-Mirapeix, F. (2017). Quantitative muscle ultrasonography using textural analysis in amyotrophic lateral sclerosis. *Ultrasonic Imaging, 39*(6), 357-368. doi:10.1177/0161734617711370

Marzetti, E., Calvani, R., Cesari, M., Buford, T. W., Lorenzi, M., Behnke, B. J., & Leeuwenburgh, C. (2013). Mitochondrial dysfunction and sarcopenia of aging: From signaling pathways to clinical trials. *The International Journal of Biochemistry & Cell Biology, 45*(10), 2288-2301. doi:10.1016/j.biocel.2013.06.024

Massy-Westropp, N. M., Gill, T. K., Taylor, A. W., Bohannon, R. W., & Hill, C. L. (2011). Hand grip strength: Age and gender stratified normative data in a population-based study. *BMC Research Notes, 4*, 127. doi:10.1186/1756-0500-4-127 [doi]

Mayerhoefer, M. E., Szomolanyi, P., Jirak, D., Materka, A., & Trattnig, S. (2009). Effects of MRI acquisition parameter variations and protocol heterogeneity on the results of texture analysis and pattern discrimination: An application-oriented study. *Medical Physics, 36*(4), 1236-1243. doi:10.1118/1.3081408

McKee, P. A., Castelli, W. P., McNamara, P. M., & Kannel, W. B. (1971). The natural history of congestive heart failure: The framingham study. *The New England Journal of Medicine, 285*(26), 1441-1446. doi:10.1056/NEJM197112232852601

Mijnarends, D. M., Schols, Jos M G A, Meijers, J. M. M., Tan, F. E. S., Verlaan, S., Luiking, Y. C., . . . Halfens, R. J. G. (2015). Instruments to assess sarcopenia and physical frailty in older people living in a community (care) setting: Similarities and discrepancies. *Journal of the American Medical Directors Association, 16*(4), 301. doi:10.1016/j.jamda.2014.11.011

Mirón Mombiela, R., Facal de Castro, F., Moreno, P., & Borras, C. (2017). Ultrasonic echo intensity as a new noninvasive in vivo biomarker of frailty. *Journal of the American Geriatrics Society, 65*(12), 2685-2690. doi:10.1111/jgs.15002

Mitnitski, A., Collerton, J., Martin-Ruiz, C., Jagger, C., von Zglinicki, T., Rockwood, K., & Kirkwood, T. B. L. (2015). Age-related frailty and its association with biological markers of ageing. *BMC Medicine, 13*, 161. doi:10.1186/s12916-015-0400-x

Molinari, F., Caresio, C., Acharya, U. R., Mookiah, M. R. K., & Minetto, M. A. (2015). Advances in quantitative muscle ultrasonography using texture analysis of ultrasound images. *Ultrasound in Medicine & Biology, 41*(9), 2520-2532. doi:10.1016/j.ultrasmedbio.2015.04.021

Morley, J. E. (2016). Frailty and sarcopenia: The new geriatric giants. *Revista De Investigacion Clinica; Organo Del Hospital De Enfermedades De La Nutricion, 68*(2), 59-67.

Mueller, N., Murthy, S., Tainter, C., Lee, J., Riddell, K., Fintelmann, F., . . . Eikermann, M. (2016a). Can sarcopenia quantified by ultrasound of the rectus femoris muscle predict adverse outcome of surgical intensive care unit patients as well as frailty? A prospective, observational cohort study. *Annals of Surgery, 264*(6), 1116-1124. doi:10.1097/SLA.0000000000001546

Mueller, N., Murthy, S., Tainter, C., Lee, J., Riddell, K., Fintelmann, F., . . . Eikermann, M. (2016b). Can sarcopenia quantified by ultrasound of the rectus femoris muscle predict adverse outcome of surgical intensive care unit patients as well as frailty? A prospective, observational cohort study. *Annals of Surgery, 264*(6), 1116-1124. doi:10.1097/SLA.0000000000001546

Narici, M. V., Flueck, M., Koesters, A., Gimpl, M., Reifberger, A., Seynnes, O. R., . . . Mueller, E. (2011). Skeletal muscle remodeling in response to alpine skiing training in older individuals. *Scandinavian Journal of Medicine & Science in Sports, 21*(s1), 23-28. doi:10.1111/j.1600-0838.2011.01338.x

Nishihara, K., Kawai, H., Hayashi, H., Naruse, H., Kimura, A., Gomi, T., & Hoshi, F. (2014). Frequency analysis of ultrasonic echo intensities of the skeletal muscle in elderly and young individuals. *Clinical Interventions in Aging, 9*, 1471-1478. doi:10.2147/CIA.S67820 [doi]

Orimo, H. (2006). [Reviewing the definition of elderly]. *Nihon Ronen Igakkai Zasshi. Japanese Journal of Geriatrics, 43*(1), 27-34.

Ortiz-Ramon, R., Larroza, A., Arana, E., & Moratal, D. (2017). A radiomics evaluation of 2D and 3D MRI texture features to classify brain metastases from lung cancer and melanoma. *Conference Proceedings: ... Annual International Conference of the IEEE Engineering in Medicine and Biology Society. IEEE Engineering in Medicine and Biology Society. Annual Conference, 2017*, 493-496. doi:10.1109/EMBC.2017.8036869

Paknikar, R., Friedman, J., Cron, D., Deeb, G. M., Chetcuti, S., Grossman, P. M., . . . Patel, H. J. (2016). Psoas muscle size as a frailty measure for open and transcatheter aortic valve replacement. *The Journal of Thoracic and Cardiovascular Surgery, 151*(3), 745-751. doi:10.1016/j.jtcvs.2015.11.022

Pillen, S., Tak, R. O., Zwarts, M. J., Lammens, M. M., Verrijp, K. N., Arts, I. M., . . . Verrips, A. (2009). Skeletal muscle ultrasound: Correlation between fibrous tissue and echo intensity. *Ultrasound in Medicine & Biology, 35*(3), 443-446. doi:10.1016/j.ultrasmedbio.2008.09.016 [doi]

Pillen, S., & van Alfen, N. (2011). Skeletal muscle ultrasound. *Neurological Research, 33*(10), 1016-1024. doi:10.1179/1743132811Y.0000000010

Pilleron, S., Weber, D., Pérès, K., Colpo, M., Gomez-Cabrero, D., Stuetz, W., . . . Féart, C. (2018). Patterns of circulating fat-soluble vitamins and carotenoids and risk of frailty in four european cohorts of older adults. *European Journal of Nutrition,* doi:10.1007/s00394-017-1602-0

Prescott, J. (2013). Quantitative imaging biomarkers: The application of advanced image processing and analysis to clinical and preclinical decision making. *Journal of Digital Imaging, 26*(1), 97-108. doi:10.1007/s10278-012-9465-7

Prince, M. J., Wu, F., Guo, Y., Gutierrez Robledo, L. M., O'Donnell, M., Sullivan, R., & Yusuf, S. (2015). The burden of disease in older people and implications for health policy and practice. *Lancet (London, England), 385*(9967), 549-562. doi:10.1016/S0140-6736(14)61347-7

Puts, M. T. E., Visser, M., Twisk, J. W. R., Deeg, D. J. H., & Lips, P. (2005). Endocrine and inflammatory markers as predictors of frailty. *Clinical Endocrinology, 63*(4), 403-411. doi:10.1111/j.1365-2265.2005.02355.x

Quan, H., Li, B., Couris, C. M., Fushimi, K., Graham, P., Hider, P., . . . Sundararajan, V. (2011). Updating and validating the charlson comorbidity index and score for risk adjustment in hospital discharge abstracts using data from 6 countries. *American Journal of Epidemiology, 173*(6), 676-682. doi:10.1093/aje/kwq433

Radovanovic, D., Seifert, B., Urban, P., Eberli, F. R., Rickli, H., Bertel, O., . . . Erne, P. (2014). Validity of charlson comorbidity index in patients hospitalised with acute coronary syndrome. insights from the nationwide AMIS plus registry 2002-2012. *Heart (British Cardiac Society), 100*(4), 288-294. doi:10.1136/heartjnl-2013-304588

Ranieri, P., Rozzini, R., Franzoni, S., Barbisoni, P., & Trabucchi, M. (1998). Serum cholesterol levels as a measure of frailty in elderly patients. *Experimental Aging Research, 24*(2), 169-179. doi:10.1080/036107398244300

Rech, A., Radaelli, R., Goltz, F. R., da Rosa, L. H., Schneider, C. D., & Pinto, R. S. (2014). Echo intensity is negatively associated with functional capacity in older women. *Age (Dordrecht, Netherlands), 36*(5), 2. Epub 2014 Aug 29. doi:10.1007/s11357-014-9708-2 [doi]

Reeves, N. D., Narici, M. V., & Maganaris, C. N. (2004). Effect of resistance training on skeletal muscle-specific force in elderly humans. *Journal of Applied Physiology (Bethesda, Md.: 1985), 96*(3), 885-892. doi:10.1152/japplphysiol.00688.2003

Reuben, D. B., Ferrucci, L., Wallace, R., Tracy, R. P., Corti, M. C., Heimovitz, H., & Harris, T. B. (2000). The prognostic value of serum albumin in healthy older persons with low and high serum interleukin-6 (IL-6) levels. *Journal of the American Geriatrics Society, 48*(11), 1404-1407.

Rizzoli, R., Reginster, J. Y., Arnal, J. F., Bautmans, I., Beaudart, C., Bischoff-Ferrari, H., . . . Bruyere, O. (2013). Quality of life in sarcopenia and frailty. *Calcified Tissue International, 93*(2), 101-120. doi:10.1007/s00223-013-9758-y [doi]

Rodríguez-Mañas, L. (2015). Use of biomarkers. *The Journal of Frailty & Aging, 4*(3), 125-128. doi:10.14283/jfa.2015.46

Rodríguez-Mañas, L., Féart, C., Mann, G., Viña, J., Chatterji, S., Chodzko-Zajko, W., . . . Vega, E. (2013). Searching for an operational definition of frailty: A delphi method based consensus statement: The frailty operative definition-consensus conference project. *The Journals of Gerontology. Series A, Biological Sciences and Medical Sciences, 68*(1), 62-67. doi:10.1093/gerona/gls119

Rodriguez-Mañas, L., & Fried, L. P. (2015). Frailty in the clinical scenario. *Lancet (London, England), 385*(9968), e9. doi:10.1016/S0140-6736(14)61595-6

Roubenoff, R. (2000). Sarcopenia: A major modifiable cause of frailty in the elderly. *The Journal of Nutrition, Health & Aging, 4*(3), 140-142.

Sadro, C. T., Sandstrom, C. K., Verma, N., & Gunn, M. L. (2015). Geriatric trauma: A radiologist's guide to imaging trauma patients aged 65 years and older. *Radiographics: A Review Publication of the Radiological Society of North America, Inc, 35*(4), 1263-1285. doi:10.1148/rg.2015140130

Sanchis, J., Bonanad, C., Ruiz, V., Fernández, J., García-Blas, S., Mainar, L., . . . Núñez, J. (2014). Frailty and other geriatric conditions for risk stratification of older patients with acute coronary syndrome. *American Heart Journal, 168*(5), 784-791. doi:10.1016/j.ahj.2014.07.022

Scanlon, T. C., Fragala, M. S., Stout, J. R., Emerson, N. S., Beyer, K. S., Oliveira, L. P., & Hoffman, J. R. (2014). Muscle architecture and strength: Adaptations to short-term resistance training in older adults. *Muscle & Nerve, 49*(4), 584-592. doi:10.1002/mus.23969

Schalk, B. W. M., Visser, M., Deeg, D. J. H., & Bouter, L. M. (2004). Lower levels of serum albumin and total cholesterol and future decline in functional performance in older persons: The longitudinal aging study amsterdam. *Age and Ageing, 33*(3), 266-272. doi:10.1093/ageing/afh073

Scharfe, C., Lu, H. H., Neuenburg, J. K., Allen, E. A., Li, G., Klopstock, T., . . . Davis, R. W. (2009). Mapping gene associations in human mitochondria using clinical disease phenotypes. *PLoS Computational Biology, 5*(4), e1000374. doi:10.1371/journal.pcbi.1000374

Shamliyan, T., Talley, K. M. C., Ramakrishnan, R., & Kane, R. L. (2013). Association of frailty with survival: A systematic literature review. *Ageing Research Reviews, 12*(2), 719-736. doi:10.1016/j.arr.2012.03.001

Shardell, M., D'Adamo, C., Alley, D. E., Miller, R. R., Hicks, G. E., Milaneschi, Y., . . . Ferrucci, L. (2012). Serum 25-hydroxyvitamin D, transitions between frailty states, and mortality in older adults: The invecchiare in chianti study. *Journal of the American Geriatrics Society, 60*(2), 256-264. doi:10.1111/j.1532-5415.2011.03830.x

Silva, Silvia Lanziotti Azevedo da, Neri, A. L., Ferrioli, E., Lourenço, R. A., & Dias, R. C. (2016). [Phenotype of frailty: The influence of each item in determining frailty in community-dwelling elderly - the fibra study]. *Ciencia & Saude Coletiva, 21*(11), 3483-3492. doi:10.1590/1413-812320152111.23292015

Sipila, S., & Suominen, H. (1991). Ultrasound imaging of the quadriceps muscle in elderly athletes and untrained men. *Muscle & Nerve, 14*(6), 527-533. doi:10.1002/mus.880140607 [doi]

Sipila, S., & Suominen, H. (1994). Knee extension strength and walking speed in relation to quadriceps muscle composition and training in elderly women. *Clinical Physiology (Oxford, England), 14*(4), 433-442.

Smith, J. J., Sorensen, A. G., & Thrall, J. H. (2003). Biomarkers in imaging: Realizing radiology's future. *Radiology, 227*(3), 633-638. doi:10.1148/radiol.2273020518

Sogawa, K., Nodera, H., Takamatsu, N., Mori, A., Yamazaki, H., Shimatani, Y., . . . Kaji, R. (2017). Neurogenic and myogenic diseases: Quantitative texture analysis of muscle US data for differentiation. *Radiology, 283*(2), 492-498. doi:10.1148/radiol.2016160826

Strasser, E., Draskovits, T., Praschak, M., Quittan, M., & Graf, A. (2013). Association between ultrasound measurements of muscle thickness, pennation angle, echogenicity and skeletal muscle strength in the elderly. *Age, 35*(6), 2377-2388. doi:10.1007/s11357-013-9517-z

Sullivan, D. C., Obuchowski, N. A., Kessler, L. G., Raunig, D. L., Gatsonis, C., Huang, E. P., . . . Wahl, R. L. (2015). Metrology standards for quantitative imaging biomarkers. *Radiology, 277*(3), 813-825. doi:10.1148/radiol.2015142202

Sur, M. D., Namm, J. P., Hemmerich, J. A., Buschmann, M. M., Roggin, K. K., & Dale, W. (2015). Radiographic sarcopenia and self-reported exhaustion independently predict NSQIP serious

complications after pancreaticoduodenectomy in older adults. *Annals of Surgical Oncology, 22*(12), 3897-3904. doi:10.1245/s10434-015-4763-1

Thiago Torres da Matta, Wagner Coelho de Albuquerque Pereira, Regis Radaelli, Ronei Silveira Pinto, Liliam Fernandes de Oliveira, 1U F R J P E B, . . . Brasil. (2017). *Texture analysis of ultrasound images is a sensitive method to follow-up muscle damage induced by eccentric exercise* doi:10.1111/cpf.12441

THIBAULT, G., FERTIL, B., NAVARRO, C., PEREIRA, S., CAU, P., LEVY, N., . . . MARI, J. (2013). Shape and texture indexes application to cell nuclei classification. *International Journal of Pattern Recognition and Artificial Intelligence, 27*(1) doi:10.1142/S0218001413570024

Ticinesi, A., Meschi, T., Narici, M. V., Lauretani, F., & Maggio, M. (2017). Muscle ultrasound and sarcopenia in older individuals: A clinical perspective. *Journal of the American Medical Directors Association, 18*(4), 290-300. doi:10.1016/j.jamda.2016.11.013

Vallières, M., Freeman, C. R., Skamene, S. R., & El Naqa, I. (2015). A radiomics model from joint FDG-PET and MRI texture features for the prediction of lung metastases in soft-tissue sarcomas of the extremities. *Physics in Medicine and Biology, 60*(14), 5471-5496. doi:10.1088/0031-9155/60/14/5471

Vanitallie, T. B. (2003). Frailty in the elderly: Contributions of sarcopenia and visceral protein depletion. *Metabolism: Clinical and Experimental, 52*(10 Suppl 2), 22-26.

Vetrano, D. L., Palmer, K., Marengoni, A., Marzetti, E., Lattanzio, F., Roller-Wirnsberger, R., . . . Onder, G. (2018). Frailty and multimorbidity: A systematic review and meta-analysis. *The Journals of Gerontology. Series A, Biological Sciences and Medical Sciences,* doi:10.1093/gerona/gly110

Walston, J., McBurnie, M. A., Newman, A., Tracy, R. P., Kop, W. J., Hirsch, C. H., . . . Fried, L. P. (2002). Frailty and activation of the inflammation and coagulation systems with and without clinical comorbidities: Results from the cardiovascular health study. *Archives of Internal Medicine, 162*(20), 2333-2341.

Watanabe, T., Murakami, H., Fukuoka, D., Terabayashi, N., Shin, S., Yabumoto, T., . . . Seishima, M. (2017). Quantitative sonographic assessment of the quadriceps femoris muscle in healthy japanese adults. *Journal of Ultrasound in Medicine: Official Journal of the American Institute of Ultrasound in Medicine, 36*(7), 1383-1395. doi:10.7863/ultra.16.07054

Watanabe, Y., Yamada, Y., Fukumoto, Y., Ishihara, T., Yokoyama, K., Yoshida, T., . . . Kimura, M. (2013). Echo intensity obtained from ultrasonography images reflecting muscle strength in elderly men. *Clinical Interventions in Aging, 8*, 993-998. doi:10.2147/CIA.S47263

White, H. D., Westerhout, C. M., Alexander, K. P., Roe, M. T., Winters, K. J., Cyr, D. D., . . . Ohman, E. M. (2016). Frailty is associated with worse outcomes in non-ST-segment elevation acute coronary syndromes: Insights from the TaRgeted platelet inhibition to cLarify the optimal strateGy to medicallY manage acute coronary syndromes (TRILOGY ACS) trial. *European Heart Journal. Acute Cardiovascular Care, 5*(3), 231-242. doi:10.1177/2048872615581502

Wilhelm, E. N., Rech, A., Minozzo, F., Radaelli, R., Botton, C. E., & Pinto, R. S. (2014). Relationship between quadriceps femoris echo intensity, muscle power, and functional capacity of older men. *Age (Dordrecht, Netherlands), 36*(3), 9625. doi:10.1007/s11357-014-9625-4

Wilhelm-Leen, E. R., Hall, Y. N., Deboer, I. H., & Chertow, G. M. (2010). Vitamin D deficiency and frailty in older americans. *Journal of Internal Medicine, 268*(2), 171-180. doi:10.1111/j.1365-2796.2010.02248.x

Winovich, D. T., Longstreth, W. T., Arnold, A. M., Varadhan, R., Zeki Al Hazzouri, A., Cushman, M., . . . Odden, M. C. (2017). Factors associated with ischemic stroke survival and recovery in older adults. *Stroke, 48*(7), 1818-1826. doi:10.1161/STROKEAHA.117.016726

Woods, N. F., LaCroix, A. Z., Gray, S. L., Aragaki, A., Cochrane, B. B., Brunner, R. L., . . . Newman, A. B. (2005). Frailty: Emergence and consequences in women aged 65 and older in the women's health initiative observational study. *Journal of the American Geriatrics Society, 53*(8), 1321-1330. doi:10.1111/j.1532-5415.2005.53405.x

Yamada, M., Kimura, Y., Ishiyama, D., Nishio, N., Abe, Y., Kakehi, T., . . . Arai, H. (2017). Differential characteristics of skeletal muscle in community-dwelling older adults. *Journal of the American Medical Directors Association, 18*(9), 807.e16. doi:S1525-8610(17)30278-5 [pii]

Zylberglait Lisigurski, M., Bueno, Y. A., Karanam, C., Andrade, A. D., Akkineni, S., Cevallos, V., & Ruiz, J. G. (2017). Healthcare utilization by frail, community-dwelling older veterans: A 1-year follow-up study. *Southern Medical Journal, 110*(11), 699-704. doi:10.14423/SMJ.0000000000000722

8. ANNEXES AND SUPPLEMENTAL MATERIALS

8.1 ANNEX 1: INFORM CONSENT (in Spanish)

IMPRESO DE INFORMACIÓN Y CONSENTIMIENTO INFORMADO DE LOS SUJETOS A INCLUIR EN EL PROYECTO DE INVESTIGACIÓN

TÍTULO: "Correlación de la ecointensidad muscular y la fuerza muscular en el diagnóstico del síndrome de fragilidad en el adulto mayor".

INVESTIGADOR PRINCIPAL: Dra. Rebeca Mirón Mombiela

OBJETIVO:

1. El objetivo de este estudio es investigar si una ecografía muscular puede ser útil para valorar la calidad y cantidad de grasa, además de la pérdida de fuerza muscular para predecir la fragilidad física del adulto mayor.

DESCRIPCIÓN DEL ESTUDIO

Se realizará una ecografía muscular del muslo donde se tomaran medidas del grosor muscular y una estimación numérica de la cantidad de grasa del músculo por ecografía. Al concluir la ecografía se les realizará una medición de fuerza muscular con un dinamómetro, se les medirá la altura y el peso corporal. Luego los pacientes rellenarán un cuestionario con preguntas personales y generales del paciente (Ejemplo: edad, género, etc), seguido de preguntas en relación a la calidad de vida del paciente en el momento actual. Por último se le solicitará al paciente que camine 4 metros lo más rápido que pueda para evaluar la velocidad con la que camina.

Si Ud. está de acuerdo, libremente firme el consentimiento de participación en este estudio que para este fin se ha añadido al final de este impreso.

RIESGOS Y BENEFICIOS

No existen riesgos asociados al uso de ecografía.
Con su participación en este estudio, usted va a ayudar a realizar el diagnóstico de síndrome de fragilidad del adulto mayor.
Según su condición clínica esta información podrá o no ser aprovechada en su propia salud.

PARTICIPACIÓN EN EL ESTUDIO

Su participación en este estudio es totalmente voluntaria y no recibirá remuneración alguna.

Como paciente, el rechazo a participar no supondrá ninguna penalización o ni afectará en modo alguno a la calidad de la asistencia sanitaria que reciba.

CONFIDENCIALIDAD

Toda la información obtenida será confidencial, los datos recogidos se introducirán, por el Equipo investigador, en una base de datos para realizar el análisis estadístico pero su nombre no aparecerá en ningún documento del estudio, sólo se le asignará un número. En concreto, las muestras se identificarán con un número y se agruparan por patologías afines. En ningún caso se le identificará en las publicaciones que puedan realizarse con los resultados del estudio. Sin embargo, esta información podrá ser revisada por el Comité Ético de Investigación Clínica de este Hospital así como por organismos gubernamentales competentes.

El procedimiento de destrucción de las muestras será el mismo que se utiliza habitualmente con el resto de las muestras del Consorcio Hospital General Universitario de Valencia. Puede ejercer su derecho de acceso y rectificación de sus datos. También, si así lo desea, puede ser informado de los resultados del estudio.

El estudio se realizará asegurando el cumplimiento de normas éticas y legales vigentes (Declaración de Helsinki).

Si tiene alguna duda o no entiende este texto consulte antes de firmar el documento con El Dr. Rebeca Mirón Mombiela con nº de teléfono 601 209 362, que es el médico responsable de esta investigación y le puede preguntar cualquier duda o problema que tenga relacionado con este estudio o consulte con sus familiares y, finalmente, si está de acuerdo firme este consentimiento. Se le entregará una copia.

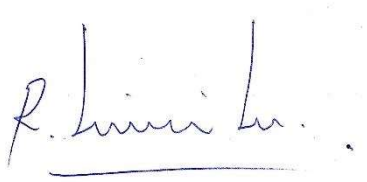

Fdo.:

Rebeca Mirón Mombiela
Investigador Principal del Proyecto
Servicio de Diagnóstico por la Imagen

CONSENTIMIENTO DEL PACIENTE SUJETO DE ESTUDIO

Título del proyecto de investigación: "Correlación de la ecointensidad muscular y la fuerza muscular en el diagnóstico del síndrome de fragilidad en el adulto mayor".

Yo, ……..……

He leído la hoja de información anterior.
He podido hacer preguntas sobre el estudio.
He recibido suficiente información sobre el estudio.

He hablado con Dra. Rebeca Mirón Mombiela.

Comprendo que mi participación es voluntaria.
Comprendo que puedo retirarme del estudio:

- **Cuando quiera.**
- **Sin tener que dar explicaciones.**
- **Sin que esto repercuta en mis cuidados médicos.**

Doy mi consentimiento para que este material aparezca en informes y artículos de revista de publicaciones médicas.
Entiendo que:

- **Mi nombre no será publicado.**
- **El material no será utilizado para publicidad o embalaje.**
- **El material no será utilizado fuera de contexto.**

Firmado…….. **Fecha……..**

8.2 ANNEX 2: FRAILTY CRITERIA (in Spanish)

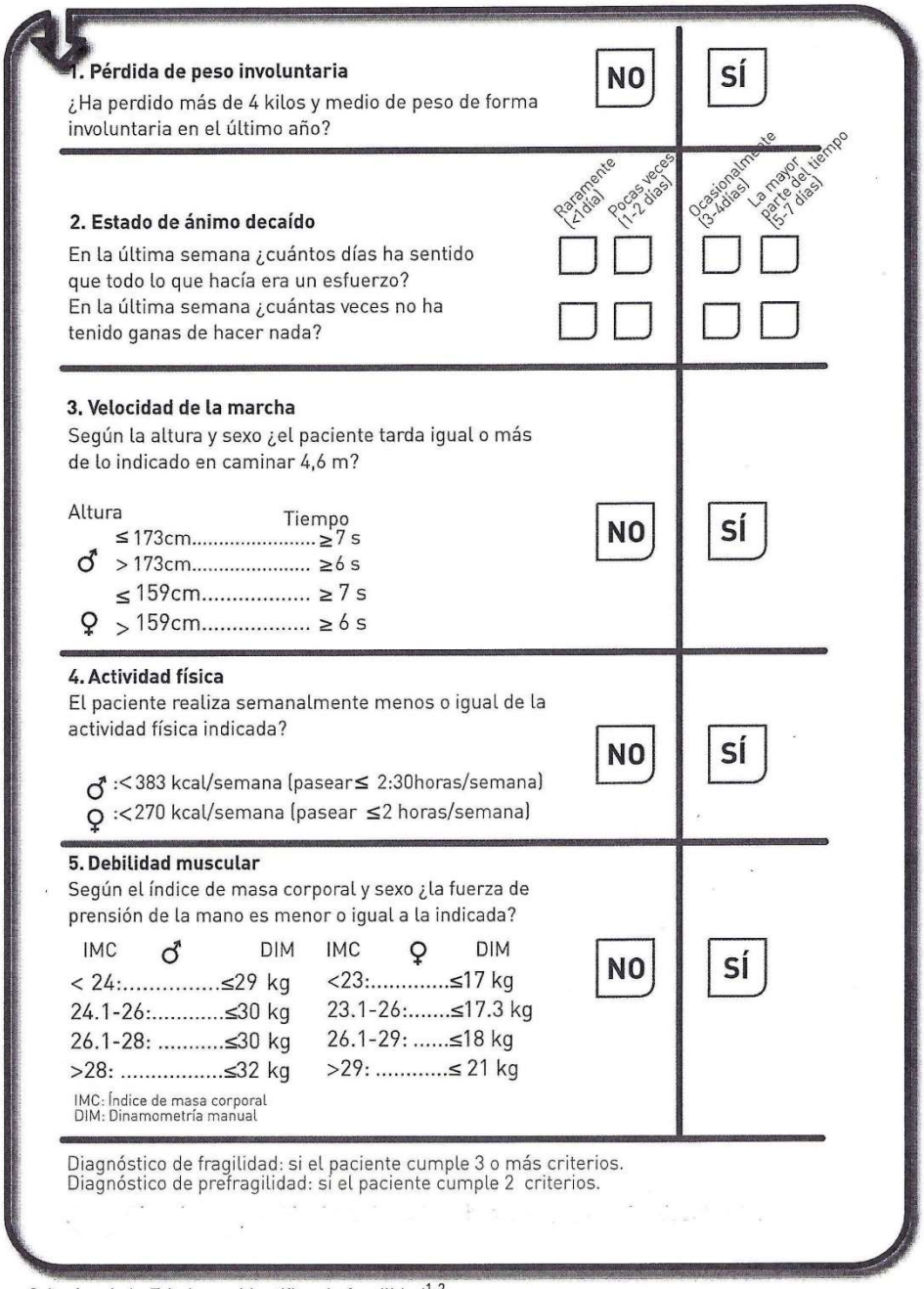

1. Pérdida de peso involuntaria

¿Ha perdido más de 4 kilos y medio de peso de forma involuntaria en el último año?

NO / SÍ

2. Estado de ánimo decaído

	Raramente (<1 día)	Pocas veces (1-2 días)	Ocasionalmente (3-4 días)	La mayor parte del tiempo (5-7 días)
En la última semana ¿cuántos días ha sentido que todo lo que hacía era un esfuerzo?	☐	☐	☐	☐
En la última semana ¿cuántas veces no ha tenido ganas de hacer nada?	☐	☐	☐	☐

3. Velocidad de la marcha

Según la altura y sexo ¿el paciente tarda igual o más de lo indicado en caminar 4,6 m?

	Altura	Tiempo
♂	≤ 173cm	≥ 7 s
	> 173cm	≥ 6 s
♀	≤ 159cm	≥ 7 s
	> 159cm	≥ 6 s

NO / SÍ

4. Actividad física

El paciente realiza semanalmente menos o igual de la actividad física indicada?

♂ :< 383 kcal/semana (pasear ≤ 2:30horas/semana)
♀ :< 270 kcal/semana (pasear ≤2 horas/semana)

NO / SÍ

5. Debilidad muscular

Según el índice de masa corporal y sexo ¿la fuerza de prensión de la mano es menor o igual a la indicada?

IMC	♂ DIM	IMC	♀ DIM
< 24:	≤29 kg	<23:	≤17 kg
24.1-26:	≤30 kg	23.1-26:	≤17.3 kg
26.1-28:	≤30 kg	26.1-29:	≤18 kg
>28:	≤32 kg	>29:	≤ 21 kg

IMC: Índice de masa corporal
DIM: Dinamometría manual

NO / SÍ

Diagnóstico de fragilidad: si el paciente cumple 3 o más criterios.
Diagnóstico de prefragilidad: si el paciente cumple 2 criterios.

Criterios de L. Fried para identificar la fragilidad[1-2].

1- Fried L et al. "Frailty in Older Adults: Evidence for a Phenotype". J Gerontol A Biol Sci Med Sci 2001:56(3): M146–M156. **2-** Fried LP, Ferrucci L, Darer J, Williamson JD, Anderson G. "Untangling the concepts of disability, frailty, and comorbidity: implications for improved targeting and care". J Gerontol A Biol Sci Med Sci. 2004;59:255-63.

8.3 ANNEX 3: QUALITY OF LIFE FOR OLDER PEOPLE QUESTIONAIRE

CONFIDENTIAL **SERIAL NO.** ☐☐☐☐

Older People's Quality of Life Questionnaire (OPQOL-35)

We would like to ask you about your quality of life:
Please tick one box in each row. There are no right or wrong answers. Please select the response that best describes you/your views.

1. Thinking about both the good and bad things that make up your quality of life, how would you rate the quality of your life as a whole?

Your quality of life as a whole is:	Very good	Good	Alright	Bad	Very bad
	(1)	(2)	(3)	(4)	(5)
	☐	☐	☐	☐	☐

2. Please indicates the extent to which you agree or disagree with each of the following statements.

Tick one box in each row

Life overall

	Strongly agree	Agree	Neither agree or disagree	Disagree	Strongly disagree
(1) **I enjoy my life overall**	(1) ☐	(2) ☐	(3) ☐	(4) ☐	(5) ☐
(2) **I am happy much of the time**	(1) ☐	(2) ☐	(3) ☐	(4) ☐	(5) ☐
(3) **I look forward to things**	(1) ☐	(2) ☐	(3) ☐	(4) ☐	(5) ☐

(4)	**Life gets me down**	Strongly agree (1) ☐	Agree (2) ☐	Neither agree or disagree (3) ☐	Disagree (4) ☐	Strongly disagree (5) ☐

Health (wt 4)

(5)	**I have a lot of physical energy**	Strongly agree (1) ☐	Agree (2) ☐	Neither agree or disagree (3) ☐	Disagree (4) ☐	Strongly disagree (5) ☐
(6)	**Pain affects my well-being**	Strongly agree (1) ☐	Agree (2) ☐	Neither agree or disagree (3) ☐	Disagree (4) ☐	Strongly disagree (5) ☐
(7)	**My health restricts me looking after myself or my home**	Strongly agree (1) ☐	Agree (2) ☐	Neither agree or disagree (3) ☐	Disagree (4) ☐	Strongly disagree (5) ☐
(8)	**I am healthy enough to get out and about**	Strongly agree (1) ☐	Agree (2) ☐	Neither agree or disagree (3) ☐	Disagree (4) ☐	Strongly disagree (5) ☐

Social relationships (wt 8)

(9)	**My family, friends or neighbours would help me if needed**	Strongly agree (1) ☐	Agree (2) ☐	Neither agree or disagree (3) ☐	Disagree (4) ☐	Strongly disagree (5) ☐
(10)	**I would like more companionship or contact with other people**	Strongly agree (1) ☐	Agree (2) ☐	Neither agree or disagree (3) ☐	Disagree (4) ☐	Strongly disagree (5) ☐
(11)	**I have someone who gives me love and affection**	Strongly agree ☐	Agree (1) ☐	Neither agree or disagree (2) ☐	Disagree (3) ☐	Strongly disagree (4) (5) ☐

	Strongly agree (1)	Agree (2)	Neither agree or disagree (3)	Disagree (4)	Strongly disagree (5)
(12) **I'd like more people to enjoy life with**	☐	☐	☐	☐	☐
(13) I have my children around which is important	☐	☐	☐	☐	☐

Independence, control over life, freedom (wt 3)

	Strongly agree (1)	Agree (2)	Neither agree or disagree (3)	Disagree (4)	Strongly disagree (5)
(14) **I am healthy enough to have my independence**	☐	☐	☐	☐	☐
(15) **I can please myself what I do**	☐	☐	☐	☐	☐
(16) **The cost of things compared to my pension/ income restricts my life**	☐	☐	☐	☐	☐
(17) **I have a lot of control** over the important things in my life	☐	☐	☐	☐	☐

Home and neighbourhood (wt 4)

	Strongly agree (1)	Agree (2)	Neither agree or disagree (3)	Disagree (4)	Strongly disagree (5)
(18) **I feel safe where I live**	☐	☐	☐	☐	☐

	Strongly agree (1)	Agree (2)	Neither agree or disagree (3)	Disagree (4)	Strongly disagree (5)
(19) **The local shops, services and facilities are good overall**	☐	☐	☐	☐	☐
(20) **I get pleasure from my home**	☐	☐	☐	☐	☐
(21) **I find my neighbourhood friendly**	☐	☐	☐	☐	☐

Psychological and emotional well-being (wt 4)

	Strongly agree (1)	Agree (2)	Neither agree or disagree (3)	Disagree (4)	Strongly disagree (5)
(22) **I take life as it comes and make the best of things**	☐	☐	☐	☐	☐
(23) **I feel lucky compared to most people**	☐	☐	☐	☐	☐
(24) **I tend to look on the bright side**	☐	☐	☐	☐	☐
(25) **If my health limits social/ leisure activities, then I will compensate and find something else I can do**	☐	☐	☐	☐	☐

Financial circumstances (wt 3)

		Strongly agree (1)	Agree (2)	Neither agree or disagree (3)	Disagree (4)	Strongly disagree (5)
(26)	**I have enough money to pay for household bills**	☐	☐	☐	☐	☐
(27)	**I have enough money to pay for household repairs or help needed in the house**	☐	☐	☐	☐	☐
(28)	**I can afford to buy what I want to**	☐	☐	☐	☐	☐
(29)	**I cannot afford to do things I would enjoy**	☐	☐	☐	☐	☐

Leisure and activities (wt 6)

		Strongly agree (1)	Agree (2)	Neither agree or disagree (3)	Disagree (4)	Strongly disagree (5)
(30)	**I have social or leisure activities/hobbies that I enjoy doing**	☐	☐	☐	☐	☐
(31)	**I try to stay involved with things**	☐	☐	☐	☐	☐
(32)	**I do paid or unpaid work or activities that give me a role in life**	☐	☐	☐	☐	☐
(33)	**I have responsibilities to others that restrict my social or leisure activities**	☐	☐	☐	☐	☐

(34) **Religion, belief or philosophy is important to my quality of life**	Strongly agree (1) ☐	Agree (2) ☐	Neither agree or disagree (3) ☐	Disagree (4) ☐	Strongly disagree (5) ☐
(35) **Cultural/religious events/festivals are important to my quality of life**	Strongly agree (1) ☐	Agree (2) ☐	Neither agree or disagree (3) ☐	Disagree (4) ☐	Strongly disagree (5) ☐

Thank you for your help.

8.4 ANNEX 4: ETHICS AND RESEARCH COMMITTEE STUDY PROTOCOL APPROVAL (in Spanish)

Consorcio Hospital General Universitario de Valencia

Comité Ético de Investigación Clínica

APROBACIÓN PROYECTOS DE INVESTIGACIÓN

- ANEXO 11 -

Este CEIC tras evaluar en su reunión de 27 de Noviembre de 2014 el Proyecto de Investigación:

Título:	Correlación de la ecointensidad muscular y la fuerza muscular en el diagnóstico del síndrome de fragilidad en el adulto mayor		
I.P.:	Rebeca Miron Mombiela	Servicio/Unidad	Diagnóstico y Imagen

Acuerda respecto a esta documentación:

Que la Hoja de Información al Paciente y Consentimiento Informado presentado reúnen las condiciones exigidas por este CEIC, por tanto se decide su APROBACIÓN.

Los miembros que evaluaron esta documentación:

		Presente	Ausente	Disculpa
Presidente	Dr. Severiano Marín Bertolín			x
	D. Ernesto Ballaller Alonso	x		
	D. Alejandro Monar González			x
	Dña. Mª Teresa Jareño Roglar		x	
Miembros Lego	Dña. Encarna Domingo Cebrián	X		
	D. Jaime Alapont Pérez	X		
	Dña. Carmen Sarmiento Cabañes	X		
	D. Antonio Baltasar Olivas Novado		x	
	Dr. D. José Manuel Iranzo Miguélez		X	
	Dr. D. Miguel Armengot Carceller	X		
	Dr. D. Julio Cortijo Gimeno	x		
Vocales	Dra. Dña. Elena Rubio Gomis	X		
	Dr. D. Gustavo Juan Samper	X		
	Dra. Pilar Blasco Segura	X		
	Dra. Mª José Safont Aguilera	x		
	Dra. Ana Blasco Cordellat	X		

Consorcio Hospital General Universitario de Valencia

Comité Ético de Investigación Clínica

		Presente	Ausente	Disculpa
	Dr. Antonio Martorell Aragonés	X		
	Dr. Aurelio Quesada Dorador	X		
	Dr. Pedro Polo Martín	x		
	Dra. Inmaculada Sáez Ferrer	x		
	Dr. Alberto Berenguer Jofresa	x		
	Dra. Goitzane Marcaida Benito			x
	Dr. Javier Milara Payá			x
Secretario	Dra. Ana Mínguez Martí	X		

En dicha reunión se cumplieron los requisitos establecidos en la legislación vigente- Real Decreto 223/2004- para que la decisión del citado CEIC sea válida. El CEIC en su composición, como en los PNT cumple con las normas de BPC (CPMP/ICH/135/95).

Lo que comunico a efectos oportunos:

Valencia a 04 de diciembre de 2014

Fdo. Dra Elena Rubio Gomis
(Presidenta en funciones CEIC CHGUV)

Consorcio Hospital General Universitario de Valencia

Comisión de Investigación

APROBACIÓN PROYECTO DE INVESTIGACIÓN

Esta Comisión tras evaluar en su reunión de 30 de Septiembre de 2014 el Proyecto de Investigación:

Título:	Correlación de la ecointensidad muscular y la fuerza muscular en el diagnóstico del síndrome de fragilidad en el adulto mayor		
I.P.:	Rebeca Mirón Mombiela	Servicio/Unidad	Diagnostico y Imagen

Acuerda respecto a esta documentación:

- Que cumple con los requisitos exigidos por esta Comisión para su realización por tanto se decide su APROBACION.

Los miembros que evaluaron esta documentación:

		Presente	Ausente	Disculpa
Presidente	Dr. Ricardo Guijarro Jorge	X		
Vocales	Dr. Julio Conejo Gimeno	x		
	Dra. Gozare Marcaida Benito	x		
	Dr. Carlos Sánchez Juan	X		
	D. Federico Palomar Llatas		x	
	Dr. Emilio Lopez Alcina	x		
	Dr. Alfonso Benosa Jaime	x		
	Dr. Julio Álvarez Pitti	x		
	Dr. Miguel Arregui Carceller		x	
	Dra. Angela Garrido Bartolomé	x		
	Dr. Miguel Sanfeliu Giner		x	
	Dr. Manuel Navarro Villena			x
	Dra. Amparo Esteban Rebolli	x		
Secretario	D. Carlos Gil Santiago	x		

Lo que comunico a efectos oportunos a miércoles, 08 de octubre de 2014

FUNDACIÓ D'INVESTIGACIÓ HOSPITAL GENERAL UNIVERSITARI VALÈNCIA

Fdo. Dr. Ricardo Guijarro Jorge
Presidente de la Comisión de Investigación

8.5 ANNEX 5: ULTRASOUND RADIOLOGICAL REPORT (in Spanish)

ECOGRAFÍA MUSCULAR EXPERIMENTAL:

El paciente antes de iniciar exploración ha revisado y firmado el consentimiento informado para participar en el estudio: "Correlación de la ecointensidad muscular y la fuerza muscular en el diagnóstico del síndrome de fragilidad en el adulto mayor"

Se procede en modo B con transductor lineal de 6-15MHz a identificar en planos transversales dos de los vientres musculares del cuádriceps (recto femoral y vasto interno) derecho. Se procede a realizar tres mediciones del grosor muscular (GM) y del grosor del tejido graso subcutáneo (GG).

GM1:		GG1:	
GM2:		GG2:	
GM3:		GG3:	
GM media		GG media	

Se concluye exploración sin incidencias.

Firma Radiólogo: Dra. Rebeca Mirón Mombiela.

8.6 ANNEX 6: PATIENT'S ELECTRONIC QUESTIONAIRE (in Spanish)

CONFIDENCIAL SIP: _____.

CUESTIONARIO ELECTRÓNICO SOBRE CALIDAD DE VIDA Y GENERALIDADES DEL PARTICIPANTE DEL PROYECTO SOBRE ECOINTENSIDAD Y FRAGILIDAD

TÍTULO DEL PROYECTO: "Correlación de la ecointensidad muscular y la fuerza muscular en el diagnóstico del síndrome de fragilidad en el adulto mayor"

SECCIÓN A: Datos generales sobre el paciente. A rellenar por el investigador.

Fecha de nacimiento		Edad actual en años:	
Género:		Peso (Kgs):	
		Altura (Mts):	
		BMI	

SECCIÓN B: Cuestionario sobre estado de fragilidad del paciente. Por favor dé la respuesta que mejor describa sus opiniones al investigador. Recuerde que no existen respuestas correctas ni incorrectas.

1. ¿He perdido más de 4.5 kg de peso en el último año? Sí ☐ No ☐
2. Siento que todo lo que hago es un esfuerzo. Sí ☐ No ☐
3. Tengo muy poca energía para realizar cosas que yo quiero hacer. Sí ☐ No ☐
4. No hago actividad física. Sí ☐ No ☐
5. No hago camino más de una o dos veces por semana. Sí ☐ No ☐
6. Tiempo para caminar 4.6m (segundos) : _____
7. Fuerza muscular de mano:

8. Total de puntos: _____ = Robusto ☐ Pre-Frágil ☐ Frágil ☐

SECCIÓN C: Cuestionario sobre calidad de vida en el adulto mayor (OPQOL-35). Nos gustaría preguntarle sobre su calidad de vida. Por favor dé la respuesta que mejor describe sus opiniones al investigador. Recuerde que no existen respuestas correctas ni incorrectas.

1. Piense en las cosas buenas y malas que son parte de su vida. En base a ello, ¿qué valoración le da a la calidad de vida que ahora tiene?

Muy bien	Bien	Regular	Mal	Muy mal

Por favor indique si está de acuerdo o no con las siguientes frases.

2. Yo disfruto de mi vida.

Totalmente de acuerdo	De acuerdo	Ni de acuerdo ni en desacuerdo	En desacuerdo	Totalmente en desacuerdo

3. Yo soy feliz la mayor parte del tiempo.

Totalmente de acuerdo	De acuerdo	Ni de acuerdo ni en desacuerdo	En desacuerdo	Totalmente en desacuerdo

4. Tengo ganas de seguir adelante con mis cosas.

Totalmente de acuerdo	De acuerdo	Ni de acuerdo ni en desacuerdo	En desacuerdo	Totalmente en desacuerdo

5. La vida me baja el ánimo.

Totalmente de acuerdo	De acuerdo	Ni de acuerdo ni en desacuerdo	En desacuerdo	Totalmente en desacuerdo

6. Tengo mucha energía física.

Totalmente de acuerdo	De acuerdo	Ni de acuerdo ni en desacuerdo	En desacuerdo	Totalmente en desacuerdo

7. El dolor que tengo afecta a mi bienestar.

Totalmente de acuerdo	De acuerdo	Ni de acuerdo ni en desacuerdo	En desacuerdo	Totalmente en desacuerdo

8. Mi estado de salud actual impide que pueda cuidar de mí mismo o de mi casa.

Totalmente de acuerdo	De acuerdo	Ni de acuerdo ni en desacuerdo	En desacuerdo	Totalmente en desacuerdo

9. Me encuentro lo suficientemente saludable como para salir y pasear.

Totalmente de acuerdo	De acuerdo	Ni de acuerdo ni en desacuerdo	En desacuerdo	Totalmente en desacuerdo

10. Mi familia, amigos o vecinos me ayudarían si lo necesito.

Totalmente de acuerdo	De acuerdo	Ni de acuerdo ni en desacuerdo	En desacuerdo	Totalmente en desacuerdo

11. Me gustaría tener más compañía o contacto con otras personas.

Totalmente de acuerdo	De acuerdo	Ni de acuerdo ni en desacuerdo	En desacuerdo	Totalmente en desacuerdo

12. Tengo a alguien en mi vida que me da amor y cariño.

Totalmente de acuerdo	De acuerdo	Ni de acuerdo ni en desacuerdo	En desacuerdo	Totalmente en desacuerdo

13. Me gustaría tener más personas con quien disfrutar de la vida.

Totalmente de acuerdo	De acuerdo	Ni de acuerdo ni en desacuerdo	En desacuerdo	Totalmente en desacuerdo

14. Tener niños cerca es importante.

Totalmente de acuerdo	De acuerdo	Ni de acuerdo ni en desacuerdo	En desacuerdo	Totalmente en desacuerdo

15. Estoy lo suficientemente saludable como para mantener mi independencia.

Totalmente de acuerdo	De acuerdo	Ni de acuerdo ni en desacuerdo	En desacuerdo	Totalmente en desacuerdo

16. Me puedo dar placeres si lo deseo.

Totalmente de acuerdo	De acuerdo	Ni de acuerdo ni en desacuerdo	En desacuerdo	Totalmente en desacuerdo

17. El coste de las cosas comparado con mis ingresos/pensión restringe mi vida.

Totalmente de acuerdo	De acuerdo	Ni de acuerdo ni en desacuerdo	En desacuerdo	Totalmente en desacuerdo

18. Yo tengo control sobre las cosas importantes.

Totalmente de acuerdo	De acuerdo	Ni de acuerdo ni en desacuerdo	En desacuerdo	Totalmente en desacuerdo

19. Me siento seguro donde vivo.

Totalmente de acuerdo	De acuerdo	Ni de acuerdo ni en desacuerdo	En desacuerdo	Totalmente en desacuerdo

20. Las tiendas y servicios locales son buenos.

Totalmente de acuerdo	De acuerdo	Ni de acuerdo ni en desacuerdo	En desacuerdo	Totalmente en desacuerdo

21. Mi casa me da placer.

Totalmente de acuerdo	De acuerdo	Ni de acuerdo ni en desacuerdo	En desacuerdo	Totalmente en desacuerdo

22. Pienso que mi vecindario es muy amigable.

Totalmente de acuerdo	De acuerdo	Ni de acuerdo ni en desacuerdo	En desacuerdo	Totalmente en desacuerdo

23. Tomo la vida como viene y hago lo mejor de ello.

Totalmente de acuerdo	De acuerdo	Ni de acuerdo ni en desacuerdo	En desacuerdo	Totalmente en desacuerdo

24. Me siento afortunado en comparación con otras personas.

Totalmente de acuerdo	De acuerdo	Ni de acuerdo ni en desacuerdo	En desacuerdo	Totalmente en desacuerdo

25. Tiendo a ver el lado positivo de las cosas.

Totalmente de acuerdo	De acuerdo	Ni de acuerdo ni en desacuerdo	En desacuerdo	Totalmente en desacuerdo

26. Mi salud limita mis actividades sociales.

Totalmente de acuerdo	De acuerdo	Ni de acuerdo ni en desacuerdo	En desacuerdo	Totalmente en desacuerdo

27. Tengo suficiente dinero para pagar las facturas de la casa.

Totalmente de acuerdo	De acuerdo	Ni de acuerdo ni en desacuerdo	En desacuerdo	Totalmente en desacuerdo

28. Tengo suficiente dinero para realizar reparaciones en la casa.

Totalmente de acuerdo	De acuerdo	Ni de acuerdo ni en desacuerdo	En desacuerdo	Totalmente en desacuerdo

29. Puedo comprarme las cosas que quiero.

Totalmente de acuerdo	De acuerdo	Ni de acuerdo ni en desacuerdo	En desacuerdo	Totalmente en desacuerdo

30. Tengo el poder adquisitivo para practicar actividades que me gustan.

Totalmente de acuerdo	De acuerdo	Ni de acuerdo ni en desacuerdo	En desacuerdo	Totalmente en desacuerdo

31. Tengo actividades sociales o hobbies.

Totalmente de acuerdo	De acuerdo	Ni de acuerdo ni en desacuerdo	En desacuerdo	Totalmente en desacuerdo

32. Me gusta involucrarme en las cosas.

Totalmente de acuerdo	De acuerdo	Ni de acuerdo ni en desacuerdo	En desacuerdo	Totalmente en desacuerdo

33. Puedo realizar trabajos, ya sean pagados o no.

Totalmente de acuerdo	De acuerdo	Ni de acuerdo ni en desacuerdo	En desacuerdo	Totalmente en desacuerdo

34. Tengo responsabilidades hacia otras personas que restringen mis actividades de sociales o de ocio.

Totalmente de acuerdo	De acuerdo	Ni de acuerdo ni en desacuerdo	En desacuerdo	Totalmente en desacuerdo

35. Participar en eventos culturales o religiosos es importante para la calidad de vida.

Totalmente de acuerdo	De acuerdo	Ni de acuerdo ni en desacuerdo	En desacuerdo	Totalmente en desacuerdo

8.7 ANNEX 7: DEFINITION OF TEXTURE FEATURES (Adapted from Vallières, et al. 2015) (Vallières et al., 2015)

The texture of an image region is determined by the way the gray levels are distributed over the pixels in the region. The features described and quantify properties of an image region by exploiting space relations underlying the gray-level distribution of a given image. In first-order statistical texture analysis, information on texture is extracted from the histogram of image intensity. This approach measures the frequency of a particular grey-level at a random image position and does not take into account correlation, or co-occurrences, between pixels. In second-order statistical texture analysis, information on texture is based on the probability of finding a pair of grey-levels at random distances and orientations over an entire image. We now describe the texture features applied in this study.

First-order gray-level statistics

Let P define the first-order histogram of an area A *(x,y)*. *P(i)* represents the number of pixels with gray-level i, and N_g represents the number of gray-level bins set for P. The i^{th} entry of the normalized histogram is then defined as:

$$p(i) = \frac{P(i)}{\sum_{i=1}^{Ng} P\ (i)}$$

The first-order textures are then define as:

- Variance

$$\sigma^2 = \sum_{i=1}^{N_g} (i-\mu)^2\ p(i)$$

- Skewness

$$s = \sigma^{-3} \sum_{i=1}^{N_g} (i-\mu)^3\ p(i)$$

- Kurtosis

$$k = \sigma^{-4} \sum_{i=1}^{N_g} [(i-\mu)^4\ p(i)] - 3$$

Gray-Level Co-occurence Matrix (GLCM) texture features

Let P define the GLCM of a quantized area $A(x,y)$. $P(i,j)$ represents the number of times pixels of gray-level i were neighbours with pixels of gray-level j in A, and N_g represents the predefined number of quantized gray-levels set in A. Only one GLCM of size $N_g \times N_g$ is computed per area A by simultaneously adding up the frequency of co-occurences of all pixels with their 8-connected neighbours in 2D space, with all pixels (including the peripheral region) considered once as a center pixel (according to (Haralick, Shanmugam, & Dinstein, 1973) thus always using $d = 1$). GLCMs are computed in four directions (0º, 45º, 90º and 135º). The neighboring properties of pixels in the four

directions are averaged equally to obtain rotation invariant features. The entry (i, j) of the of the normalized GLCM is then defined as:

$$p(i,j) = \frac{P\ (i,j)}{\sum_{j=1}^{N_g}\sum_{i=1}^{N_g} P(i,j)}$$

The following quantities are also defined:

$$\mu_i = \sum_{i=1}^{N_g} i \sum_{j=1}^{N_g} p(i,j), \quad \mu_j = \sum_{j=1}^{N_g} j \sum_{i=1}^{N_g} p(i,j),$$

$$\sigma_i = \sum_{i=1}^{N_g}(i - \mu_i)^2 \sum_{j=1}^{N_g} p\ (i,j), \quad \sigma_j = \sum_{j=1}^{N_g}(j - j)^2 \sum_{i=1}^{N_g} p\ (i,j),$$

The GLCM texture features are then define as:

- Energy (Haralick et al., 1973):

$$energy = \sum_{i=1}^{N_g}\sum_{j=1}^{N_g}[p(i,j)]^2$$

- Contrast (Haralick et al., 1973):

$$contrast = \sum_{i=1}^{N_g}\sum_{j=1}^{N_g}(i-j)^2\, p(i,j)$$

- Correlation (adapted from Haralick, et al 1973) (Haralick et al., 1973):

$$correlation = \sum_{i=1}^{N_g}\sum_{j=1}^{N_g}\frac{(i-\mu_i)(j-\mu_j)p(i,j)}{\sigma_i\sigma_j}$$

- Homogeneity (adapted from Haralick, et al 1973) (Haralick et al., 1973):

$$homogeneity = \sum_{i=1}^{N_g}\sum_{j=1}^{N_g}\frac{p(i,j)}{1+\ |i-j|}$$

- Variance (sum of squares) (adapted from Haralick, et al 1973) (Haralick et al., 1973):

$$variance = \frac{1}{N_g \times N_g}\sum_{i=1}^{N_g}\sum_{j=1}^{N_g}\left[(i-\mu_i)^2 p(i,j) + (j-\mu_j)^2 p(i,j)\right]$$

- Sum Average (adapted from Haralick, et al 1973) (Haralick et al., 1973):

$$sum\ average = \frac{1}{N_g \times N_g} \sum_{i=1}^{N_g} \sum_{j=1}^{N_g} [i\ p(i,j) + j\ p(i,j)]$$

- Dissimilarity (Galloway, 1975; THIBAULT et al., 2013):

$$dissimilarity = \sum_{i=1}^{N_g} \sum_{j=1}^{N_g} |i-j| p(i,j)$$

- Entropy (Haralick et al., 1973):

$$entropy = -\sum_{i=1}^{N_g} \sum_{j=1}^{N_g} p(i,j) log_2(p\ (i,j))$$

Gray-Level Run-Length Matrix (GLRLM) texture features.

Let P define the GLRLM of a quantized area *A (x,y)*. *P (i,j)* represents the number of runs of gray-level *i* and of length *j* in *A* , N_g represents the pre-defined number of quantized gray-levels set in *A*, and L_r represents the length of the longest run (of any gray-level) in A. As previously mentioned for the GLCM method, averaging over all directions is necessary to obtain rotation invariant features. The entry *(i,j)* of the of the normalized GLRLM is then defined as:

$$p(i,j) = \frac{P(i,j)}{\sum_{i=1}^{N_g} \sum_{j=1}^{L_r} P(i,j)}$$

The following quantities are also defined:

$$\mu_i = \sum_{i=1}^{N_g} i \sum_{j=1}^{L_r} p\ (i,j), \qquad \mu_j = \sum_{j=1}^{L_r} j \sum_{i=1}^{N_g} p(i,j)$$

The GLRLM texture features are then defined as:

- Short Run Emphasis (SRE) (Galloway, 1975):

$$SRE = \sum_{i=1}^{N_g} \sum_{j=1}^{L_r} \frac{p(i,j)}{j^2}$$

- Long Run Emphasis (LRE) (Galloway, 1975):

$$LRE = \sum_{i=1}^{N_g} \sum_{j=1}^{L_r} j^2\ p(i,j)$$

- Gray-Level Nonuniformity (GLN) (adapted from Galloway, 1975) (Galloway, 1975):

$$GLN = \sum_{i=1}^{N_g} \left(\sum_{j=1}^{L_r} p(i,j) \right)^2$$

- Run-Length Nonuniformity (RLN) (adapted from Galloway, 1975) (Galloway, 1975):

$$RLN = \sum_{j=1}^{L_r} \left(\sum_{i=1}^{N_g} p(i,j) \right)^2$$

- Run percentage (RP) (adapted from Galloway, 1975) (Galloway, 1975):

$$RP = \frac{\sum_{i=1}^{N_g} \sum_{j=1}^{L_r} p(i,j)}{\sum_{j=1}^{L_r} j \sum_{i=1}^{N_g} p(i,j)}$$

- Low Gray-Level Run Emphasis (LGRE) (Chu, Sehgal, & Greenleaf, 1990a):

$$LGRE = \sum_{i=1}^{N_g} \sum_{j=1}^{L_r} \frac{p(i,j)}{i^2}$$

- High Gray-Level Run Emphasis (HGRE) (Chu et al., 1990a):

$$HGRE = \sum_{i=1}^{N_g} \sum_{j=1}^{L_r} i^2 \, p(i,j)$$

- Short Run Low Gray-Level Emphasis (SRLGE) (Dasarathy & Holder, 1991):

$$SRLE = \sum_{i=1}^{N_g} \sum_{j=1}^{L_r} \frac{p(i,j)}{i^2 j^2}$$

- Short Run High Gray-Level Emphasis (SRHGE) (Dasarathy & Holder, 1991):

$$SRHGE = \sum_{i=1}^{N_g} \sum_{j=1}^{L_r} \frac{i^2 \, p(i,j)}{j^2}$$

- Long Run Low Gray-Level Emphasis (LRLGE) (Dasarathy & Holder, 1991):

$$LRLGE = \sum_{i=1}^{N_g} \sum_{j=1}^{L_r} \frac{j^2 p(i,j)}{i^2}$$

- Long Run High Gray-Level emphasis (LRHGE) (Dasarathy & Holder, 1991):

$$LRHGE = \sum_{i=1}^{N_g} \sum_{j=1}^{L_r} i^2 \, j^2 \, p(i,j)$$

- Gray-Level Variance (GLV)(Adapted from Thibault, et al 2009) (THIBAULT et al., 2013):

$$LRHGE = \frac{1}{N_g \times L_r} \sum_{i=1}^{N_g} \sum_{j=1}^{L_r} (i\, p(i,j) - \mu_i)^2$$

- Run-Length Variance (RLV) (Adapted from Thibault, et al 2009) (THIBAULT et al., 2013):

$$RLV = \frac{1}{N_g \times L_r} \sum_{i=1}^{N_g} \sum_{j=1}^{L_r} \left(j\, p(i,j) - \mu_j\right)^2$$

Gray-Level Size Zone Matrix (GLSZM) texture features

Let P define the GLSZM of a quantized area A (x,y). $\mathrm{P}(i,j)$ represents the number of 2D zones of gray-levels i and of size j in A, $\mathrm{N_g}$ represents the pre-defined number of quantized gray-levels set in A, and $\mathrm{L_z}$ represents the size of the largest zone (of any gray-level) in A. One GLSZM of size $\mathrm{N_g} \times \mathrm{L_z}$ is computed per area *A* by adding up all possible largest zone-sizes, with zones constructed from 8-connected neighbours of the same gray-level in 2D space (one pixel can be part of only one zone). The entry (i,j) of the normalized GLSZM is then defined as:

$$p(i,j) = \frac{P(i,j)}{\sum_{i=1}^{N_g} \sum_{j=1}^{L_z} P(i,j)}$$

The following quantities are also defined:

$$\mu_i = \sum_{i=1}^{N_g} i \sum_{j=1}^{L_z} p(i,j), \qquad \mu_j = \sum_{j=1}^{L_z} j \sum_{i=1}^{N_g} p(i,j)$$

The GLSZN texture features are then define as:

- Small Zone Emphasis (SZE) (Galloway, 1975; THIBAULT et al., 2013):

$$SZE = \sum_{i=1}^{N_g} \sum_{j=1}^{L_z} \frac{p(i,j)}{j^2}$$

- Large Zone Emphasis (LZE) (Galloway, 1975; THIBAULT et al., 2013):

$$LZE = \sum_{i=1}^{N_g} \sum_{j=1}^{L_z} j^2 p(i,j)$$

- Gray-Level Nonuniformity (GLN) (Galloway, 1975; THIBAULT et al., 2013):

$$GLN = \sum_{i=1}^{N_g} \left(\sum_{j=1}^{L_z} p(i,j) \right)^2$$

- Zone-Size Nonuniformity (ZSN) (Galloway, 1975; THIBAULT et al., 2013):

$$ZSN = \sum_{j=1}^{L_z} \left(\sum_{i=1}^{N_g} p(i,j) \right)^2$$

- Zone Percentage (ZP) (Galloway, 1975; THIBAULT et al., 2013):

$$ZP = \frac{\sum_{i=1}^{N_g} \sum_{j=1}^{L_z} p(i,j)}{\sum_{j=1}^{L_z} j \sum_{i=1}^{N_g} p(i,j)}$$

- Low Gray-Level Zone Emphasis (LGZE) (Chu, Sehgal, & Greenleaf, 1990b; THIBAULT et al., 2013):

$$LGZE = \sum_{i=1}^{N_g} \sum_{j=1}^{L_z} \frac{p(i,j)}{i^2}$$

- High Gray-Level Zone Emphasis (HGZE) (Chu et al., 1990b; THIBAULT et al., 2013):

$$HGZE = \sum_{i=1}^{N_g} \sum_{j=1}^{L_z} i^2 \, p(i,j)$$

- Small Zone Low Gray-Level Emphasis (SLGE) (Chu et al., 1990b; THIBAULT et al., 2013):

$$SZLGE = \sum_{i=1}^{N_g} \sum_{j=1}^{L_z} \frac{p(i,j)}{i^2 j^2}$$

- Small Zone High Gray-Level Emphasis (SZHGE) (Chu et al., 1990b; THIBAULT et al., 2013):

$$SZHGE = \sum_{i=1}^{N_g} \sum_{j=1}^{L_z} \frac{i^2 p(i,j)}{j^2}$$

- Large Zone Low Gray-Level Emphasis (LZLGE) (Chu et al., 1990b; THIBAULT et al., 2013):

$$LZLGE = \sum_{i=1}^{N_g} \sum_{j=1}^{L_z} \frac{j^2 p(i,j)}{i^2}$$

- Large Zone High Gray-Level Emphasis (LZHGE) (Chu et al., 1990b; THIBAULT et al., 2013):

$$LZHGE = \sum_{i=1}^{N_g} \sum_{j=1}^{L_z} i^2 \, j^2 \, p(i,j)$$

- Gray-Level Variance (GLV) (Chu et al., 1990b; THIBAULT et al., 2013):

$$GLV = \frac{1}{N_g \times L_z} \sum_{i=1}^{N_g} \sum_{j=1}^{L_z} (i\, p(i,j) - \mu_i)^2$$

- Zone-Size Variance (ZSV) (Chu et al., 1990b; THIBAULT et al., 2013):

$$ZSV = \frac{1}{L_z \times N_g} \sum_{i=1}^{N_g} \sum_{j=1}^{L_z} \left(j\, p(i,j) - \mu_j\right)^2$$

Neighbourhood Gray-Tone Difference Matrix (NGTDM) texture features

The NGTDM was introduced by Amadasun and King (Amadasun & King, 1989) aiming to describe the visual properties of textures. To compute a NGTDM from an image, let $P(i)$ represent the summation of gray-level differences among all pixels with gray-level i. N_g represents the highest gray-level value present in the image and $(N_g)_{eff}$ is the total number of different gray levels in the image. The i^{th} entry of the NGTDM is defines as:

$$P(i) = \sum_{0} |i - \mu_i| \quad for\ i \in N_i\ if\ N_i \neq 0,\ \ otherwise$$

Where N_i is the set of all pixels with gray-level i in the image excluding the peripheral region of width d, and μ_i is the average gray-level of the neighbors around a center pixel with gray-level i located at position (k, l) so:

$$\mu_i = \mu(k,l) = \frac{1}{W-1} \left[\sum_{m=-d}^{d} \sum_{n=-d}^{d} f\ (k+m, l+n)\right], (m,n) \neq (0,0)$$

Where d specifies the neighbourhood size and $W = (2d+1)^2$.

For an N x N images the probability of occurrence of the gray-level value i is defined as:

$$n_i = \frac{N_i}{N}$$

Where N is the total number of pixels in the 2D image. The NGTDM texture features are then define as:

- Coarseness (Amadasun & King, 1989):

$$coarseness = \left[\epsilon + \sum_{i=1}^{N_g} n_i P(i)\right]^{-1}$$

- Contrast (Amadasun & King, 1989):

$$contrast = \left[\frac{1}{(N_g)_{eff}\left[(N_g)_{eff} - 1\right]} \sum_{i=1}^{N_g} \sum_{j=1}^{N_g} n_i n_j (i-j)^2\right] \left[\frac{1}{N} \sum_{i=1}^{N_g} P(i)\right]$$

- Busyness (Amadasun & King, 1989):

$$busyness = \frac{\sum_{i=1}^{N_g} n_i P(i)}{\sum_{i=1}^{N_g} \sum_{j=1}^{N_g} (i n_i - j\, n_j)}, \qquad n_i \neq 0, n_j \neq 0$$

- Complexity (Amadasun & King, 1989):

$$complexity = \sum_{i=1}^{N_g} \sum_{j=1}^{N_g} \frac{|i-j|\left[n_i P(i) + n_j P(j)\right]}{N(n_i + n_j)}, \qquad n_i \neq 0, n_j \neq 0$$

- Strength (Amadasun & King, 1989):

$$strength = \frac{\sum_{i=1}^{N_g} \sum_{j=1}^{N_g} (n_i + n_j)(i-j)^2}{\left[\epsilon + \sum_{i=1}^{N_g} P(i)\right]}, \qquad n_i \neq 0, n_j \neq 0$$

Where ϵ is a small number to prevent strength becoming infinite.

References:

1. Vallières M, Freeman CR, Skamene SR, El Naqa I. A radiomics model from joint FDG-PET and MRI texture features for the prediction of lung metastases in soft-tissue sarcomas of the extremities. Phys Med Biol. 2015 Jul 21,;60(14):5471-96.
2. Haralick RM, Shanmugam K, Dinstein I. Textural Features for Image Classification. T-SMC. 1973;3(6):610-21.
3. Galloway MM. Texture analysis using gray level run lengths. Computer Graphics and Image Processing. 1975;4(2):172-9.
4. Chu A, Sehgal CM, Greenleaf JF. Use of gray value distribution of run lengths for texture analysis. Pattern Recognition Letters. 1990 June 1,;11(6):415-9.
5. Dasarathy BV, Holder EB. Image characterizations based on joint gray level—run length distributions. Pattern Recognition Letters. 1991 August 1,;12(8):497-502.
6. Thubault G, Fertil B, Navarro C, Pereira S, CAU P, Levy N, et al. Shapre and Textures Indexes Appñication to Cell Nuclei Classification. International Journal of Pattern Recognition and Artificial Intelligence. 2013 Feb;27(1).
7. Chu A, Sehgal CM, Greenleaf JF. Use of gray value distribution of run lengths for texture analysis. Pattern Recognition Letters. 1990;11(6):415-9.
8. Amadasun M, King R. Textural features corresponding to textural properties. T-SMC. 1989;19(5):1264-74.

8.8 ANNEX 8: TEXTURE FEATURES CHARACTERISTICS AND POST HOC ANALYSIS

Table Annex 8.8.1 Texture Features of Axial Rectus Femoris According to Sex and Frailty Phenotype

	Group	*Female (n=46)*	*Male (n=55)*	*Total (n=101)*	*Statistical Test*	*Controls (n = 24)*	*Robust (n = 22)*	*Pre-frail (n = 30)*	*Frail (n =25)*	*Total (n=101)*	*Statistical Test*
	Texture Feature	*Mean ± SD*	*Mean ± SD*	*Mean ± SD*	*P value*	*Mean ± SD*	*Mean ± SD*	*Mean ± SD*	*Mean ± SD*	*Mean ± SD*	*P value*
IHF	Variance	203 ± 47	213 ± 50	209 ± 49	0,324	198 ± 48	206 ± 45	212 ± 56	218 ± 46	209 ± 49	0,550
	Skewness	0,94 ± 0,38	0,92 ± 0,40	0,93 ± 0,39	0,877	1,23 ± 0,40	0,84 ± 0,35	0,84 ± 0,32	0,82 ± 0,37	0,93 ± 0,39	<0,001
	Kurtosis	1,40 ± 1,20	1,29 ± 1,33	1,34 ± 1,27	0,526*	2,37 ± 1,64	1,10 ± 0,81	1,01 ± 0,96	0,96 ± 1,00	1,34 ± 1,27	<0,001*
GLCM	Energy	0,0015 ± 0,001	0,0013 ± 0,0006	0,0014 ± 0,0008	0,429*	0,0019 ± 0,0012	0,0013 ± 0,0006	0,0013 ± 0,0006	0,0011 ± 0,0005	0,0014 ± 0,0008	0,008*
	Contrast	87,4 ± 35,0	92,3 ± 42,3	90,1 ± 39,0	0,733*	90,9 ± 40,0	85,1 ± 39,7	90,7 ± 38,1	92,9 ± 40,7	90,1 ± 39,0	0,933*
	Entropy	10,67 ± 0,60	10,80 ± 0,53	10,74 ± 0,56	0,251	10,54 ± 0,54	10,71 ± 0,58	10,81 ± 0,59	10,87 ± 0,52	10,74 ± 0,56	0,180
	Homogeneity	0,31 ± 0,03	0,31 ± 0,03	0,31 ± 0,03	0,717	0,32 ± 0,03	0,31 ± 0,03	0,31 ± 0,04	0,30 ± 0,03	0,31 ± 0,03	0,190
	Correlation	0,88 ± 0,03	0,90 ± 0,03	0,89 ± 0,03	0,037	0,88 ± 0,03	0,90 ± 0,02	0,89 ± 0,03	0,89 ± 0,04	0,89 ± 0,03	0,584
	Sum Average	0,0006 ± 0,0001	0,0006 ± 0,0001	0,0006 ± 0,0001	0,082	0,0005 ± 0,0001	0,0006 ± 0,0001	0,0006 ± 0,0001	0,0006 ± 0,0001	0,0006 ± 0,0001	0,004
	Variance	0,0059 ± 0,0024	0,0068 ± 0,0022	0,0064 ± 0,0023	0,055	0,006 ± 0,002	0,006 ± 0,002	0,006 ± 0,002	0,007 ± 0,003	0,0064 ± 0,0023	0,840
	Dissimilarity	6,06 ± 1,21	6,12 ± 1,34	6,09 ± 1,28	0,792	6,03 ± 1,25	5,91 ± 1,28	6,15 ± 1,33	6,24 ± 1,28	6,09 ± 1,28	0,834
	Auto-Correlation	1708 ± 754	1939 ± 626	1834 ± 694	0,096	1479 ± 624	1872 ± 597	1943 ± 693	2009 ± 752	1834 ± 694	0,031
GLRLM	Short Run Emphasis	0,93 ± 0,01	0,93 ± 0,01	0,93 ± 0,01	0,865*	0,92 ± 0,01	0,93 ± 0,01	0,93 ± 0,01	0,93 ± 0,01	0,93 ± 0,01	0,054*
	Long Run Emphasis	1,46 ± 0,21	1,46 ± 0,14	1,46 ± 0,18	0,648*	1,59 ± 0,28	1,44 ± 0,09	1,42 ± 0,11	1,40 ± 0,08	1,46 ± 0,18	0,008*
	Gray-Level Nonuniformity	0,019 ± 0,005	0,017 ± 0,004	0,018 ± 0,004	0,036*	0,020 ± 0,004	0,018 ± 0,005	0,018 ± 0,004	0,017 ± 0,004	0,018 ± 0,004	0,088*
	Run Length Nonuniformity	0,83 ± 0,03	0,83 ± 0,03	0,83 ± 0,03	0,870*	0,82 ± 0,03	0,83 ± 0,02	0,83 ± 0,03	0,84 ± 0,02	0,83 ± 0,03	0,054*
	Run Percentage	0,89 ± 0,02	0,89 ± 0,02	0,89 ± 0,02	0,754*	0,88 ± 0,02	0,89 ± 0,02	0,90 ± 0,02	0,90 ± 0,02	0,89 ± 0,02	0,016*
	Low Gray-Level Run Emphasis	0,009 ± 0,008	0,007 ± 0,005	0,008 ± 0,006	0,070*	0,0139 ± 0,0100	0,0063 ± 0,0025	0,0061 ± 0,0015	0,0057 ± 0,0013	0,008 ± 0,006	<0,001*
	High Gray-Level Run Emphasis	1785 ± 768	2025 ± 644	1916 ± 709	0,091	1568 ± 641	1952 ± 617	2021 ± 713	2091 ± 767	1916 ± 709	0,043
	Short Run Low Gray-Level	0,006 ± 0,005	0,005 ± 0,003	0,006 ± 0,004	0,045*	0,0094 ± 0,0059	0,0047 ± 0,0017	0,0046 ± 0,0011	0,0043 ± 0,0010	0,006 ± 0,004	<0,001*
	Short Run High Gray-Level	1684 ± 735	1909 ± 619	1806 ± 680	0,098	1475 ± 610	1838 ± 592	1908 ± 689	1975 ± 734	1806 ± 680	0,044
	Long Run Low Gray-Level	0,07 ± 0,18	0,05 ± 0,1	0,06 ± 0,14	0,210*	0,16 ± 0,26	0,03 ± 0,04	0,02 ± 0,02	0,02 ± 0,02	0,06 ± 0,14	0,008*
	Long Run High Gray-Level	2384 ± 964	2716 ± 787	2565 ± 883	0,059	2140 ± 836	2638 ± 775	2684 ± 837	2765 ± 982	2565 ± 884	0,054
	Gray-Level Variance	0,005 ± 0,003	0,005 ± 0,002	0,005 ± 0,002	0,908*	0,0031 ± 0,0017	0,0051 ± 0,0020	0,0058 ± 0,0025	0,0059 ± 0,0025	0,005 ± 0,002	<0,001*
	Run-Length Variance**	-5,44 - 0,21	-5,50 ± 0,17	-5,47 ± 0,19	0,150*	-5,57 ± 0,19	-5,47 ± 0,17	-5,43 ± 0,13	-5,44 ± 0,24	-5,47 ± 0,19	0,050*
GLSZM	Small Zone Emphasis	0,78 ± 0,03	0,78 ± 0,03	0,78 ± 0,03	0,995*	0,78 ± 0,03	0,78 ± 0,03	0,79 ± 0,03	0,79 ± 0,03	0,78 ± 0,03	0,387*
	Large Zone Emphasis	9,33 ± 23,43	7,63 ± 12,60	8,40 ± 18,26	0,687*	19,89 ± 35,44	5,36 ± 2,62	4,79 ± 1,85	4,40 ± 1,17	8,40 ± 18,26	0,009*
	Gray-Level Nonuniformity	0,017 ± 0,004	0,016 ± 0,003	0,016 ± 0,003	0,020*	0,020 ± 0,004	0,018 ± 0,005	0,017 ± 0,003	0,017 ± 0,003	0,016 ± 0,003	0,263*
	Zone-Size Nonuniformity	0,57 ± 0,04	0,57 ± 0,04	0,57 ± 0,04	0,968	0,56 ± 0,04	0,57 ± 0,04	0,58 ± 0,05	0,58 ± 0,04	0,57 ± 0,04	0,410
	Zone Percentage	0,65 ± 0,05	0,65 ± 0,05	0,65 ± 0,05	0,697	0,63 ± 0,05	0,64 ± 0,04	0,66 ± 0,06	0,66 ± 0,04	0,65 ± 0,05	0,049
	Low Gray-Level Zone Emphasis	0,0047 ± 0,0031	0,0039 ± 0,0018	0,0043 ± 0,0025	0,052*	0,0067 ± 0,0038	0,0036 ± 0,0014	0,0036 ± 0,0010	0,0033 ± 0,0010	0,0043 ± 0,0025	<0,001*
	High Gray-Level Zone Emphasis	1875 ± 786	2135 ± 661	2016 ± 729	0,074	1670 ± 655	2057 ± 646	2119 ± 728	2190 ± 793	2016 ± 729	0,055
	Small Zone Low Gray-Level Zone Emphasis	0,0027 ± 0,0016	0,0022 ± 0,0010	0,0024 ± 0,0013	0,029*	0,0037 ± 0,0019	0,0021 ± 0,0007	0,0021 ± 0,0005	0,0019 ± 0,0006	0,0024 ± 0,0013	<0,001*
	Small Zone High Gray-Level Zone Emphasis	1533 ± 674	1743 ± 570	1648 ± 625	0,052	1361 ± 550	1672 ± 556	1737 ± 639	1794 ± 677	1648 ± 625	0,067
	Large Zone Low Gray-Level Zone Emphasis	4,88 ± 23,13	2,94 ± 12,46	3,82 ± 18,04	0,035*	14,77 ± 35,31	0,72 ± 2,07	0,29 ± 0,45	0,29 ± 0,47	3,82 ± 18,04	0,079*
	Large Zone High Gray-Level Zone Emphasis	6579 ± 2425	7624 ± 1944	7148 ± 2227	0,001*	6414 ± 2421	7504 ± 2166	7367 ± 1810	7276 ± 2501	7148 ± 2227	0,093*
	Grey-Level Variance	0,0013 ± 0,001	0,0011 ± 0,0007	0,0012 ± 0,0009	0,609*	0,0007 ± 0,0007	0,0013 ± 0,0009	0,0014 ± 0,0010	0,0014 ± 0,0008	0,0012 ± 0,0009	0,005*
	Zone-Size Variance**	-6,11 ± 0,37	-6,18 ± 0,31	-6,15 ± 0,34	0,061*	-6,35 ± 0,48	-6,08 ± 0,31	-6,08 ± 0,23	-6,08 ± 0,23	-6,15 ± 0,34	0,168*
NGTDM	Coarseness	0,0008 ± 0,0003	0,0008 ± 0,0003	0,0008 ± 0,0003	0,859*	0,0007 ± 0,0002	0,0008 ± 0,0003	0,0008 ± 0,0003	0,0009 ± 0,0003	0,0008 ± 0,0003	0,142*
	Contrast	0,30 ± 0,07	0,30 ± 0,08	0,30 ± 0,08	0,924*	0,32 ± 0,07	0,28 ± 0,08	0,30 ± 0,09	0,31 ± 0,08	0,30 ± 0,08	0,678
	Busyness	0,68 ± 0,36	0,63 ± 0,37	0,65 ± 0,36	0,333*	0,92 ± 0,51	0,58 ± 0,24	0,60 ± 0,28	0,52 ± 0,24	0,65 ± 0,36	0,007*
	Complexity	8719 ± 3814	9633 ± 4127	9217 ± 3994	0,254	8647 ± 3794	8859 ± 4012	9507 ± 4205	9732 ± 4051	9217 ± 3994	0,749*
	Strength	2,47 ± 1,02	2,88 ± 1,40	2,69 ± 1,25	0,186*	2,43 ± 1,20	2,68 ± 1,25	2,64 ± 1,19	3,02 ± 1,38	2,69 ± 1,25	0,384*

Abbreviations: SD: standard deviation; IHF: Intensity Histogram Features; GLCM: Gray-Level Co-occurrence Matrix; GLRLM: Gray-Level run-Length Matrix; GLSZM: Gray-Level Size Zone Matrix; NGTDM: Neighborhood Gray-Tone Difference Matrix.

* Variables without normal distribution, nonparametric tests used for the analysis.

** Run-Length Variance and Zone-Size Variance are small with a restricted range of scales, so logarithms were used to transform the data.

Table Annex 8.8.2 Texture Features of Axial Vastus Intermedius According to Sex and Frailty Phenotype

	Group	Female (n=46)	Male (n=55)	Total (n=101)	Statistical Test	Controls (n = 24)	Robust (n = 22)	Pre-frail (n = 30)	Frail (n =25)	Total (n=101)	Statistical Test
	Texture Feature	Mean ± SD	Mean ± SD	Mean ± SD	P value	Mean ± SD	Mean ± SD	Mean ± SD	Mean ± SD	Mean ± SD	P value
IHF	Variance	174 ± 62	172 ± 63	173 ± 62	0,967*	148 ± 50	195 ± 53	171 ± 64	181 ± 71	173 ± 62	0,025*
	Skewness	1,47 ± 0,69	1,70 ± 0,78	1,60 ± 0,74	0,144*	2,19 ± 0,58	1,39 ± 0,56	1,54 ± 0,78	1,28 ± 0,67	1,60 ± 0,74	<0,001*
	Kurtosis	3,70 ± 3,04	4,88 ± 4,88	4,34 ± 4,16	0,350*	6,82 ± 3,23	2,90 ± 2,40	4,47 ± 5,64	3,07 ± 3,01	4,34 ± 4,16	<0,001
GLCM	Energy	0,03 ± 0,08	0,06 ± 0,12	0,05 ± 0,10	0,179*	0,12 ± 0,15	0,02 ± 0,04	0,04 ± 0,11	0,01 ± 0,02	0,05 ± 0,10	<0,001*
	Contrast	26,1 ± 14,9	29,5 ± 16,1	27,9 ± 15,6	0,303*	21,5 ± 15,6	30,8 ± 10,3	27,4 ± 16,3	32,1 ± 17,3	27,9 ± 15,6	0,006*
	Entropy	8,48 ± 1,63	8,37 ± 1,76	8,42 ± 1,69	0,738*	6,72 ± 1,80	8,96 ± 0,92	8,66 ± 1,60	9,31 ± 0,99	8,42 ± 1,69	<0,001*
	Homogeneity	0,44 ± 0,11	0,47 ± 0,12	0,46 ± 0,11	0,222*	0,57 ± 0,13	0,43 ± 0,07	0,44 ± 0,11	0,40 ± 0,06	0,46 ± 0,11	<0,001*
	Correlation	0,90 ± 0,04	0,92 ± 0,03	0,91 ± 0,03	0,008*	0,89 ± 0,03	0,92 ± 0,03	0,92 ± 0,03	0,92 ± 0,03	0,91 ± 0,03	0,004*
	Sum Average	0,0003 ± 0,0001	0,0003 ± 0,0001	0,0003 ± 0,0001	0,934	0,0001 ± 0,0001	0,0003 ± 0,0001	0,0003 ± 0,0001	0,0004 ± 0,0001	0,0003 ± 0,0001	<0,001
	Variance	0,0024 ± 0,0016	0,0031 ± 0,0018	0,0028 ± 0,0017	0,595*	0,0017 ± 0,0013	0,0033 ± 0,0012	0,0027 ± 0,0014	0,0034 ± 0,0022	0,0028 ± 0,0017	<0,001*
	Dissimilarity	3,20 ± 1,04	3,26 ± 0,99	3,23 ± 1,01	0,777	2,48 ± 1,04	3,53 ± 0,62	3,26 ± 0,99	3,66 ± 0,91	3,23 ± 1,01	<0,001
	Auto-Correlation	578 ± 439	609 ± 401	595 ± 417	0,709	219 ± 185	643 ± 278	611 ± 348	892 ± 492	595 ± 417	<0,001
GLRLM	Short Run Emphasis	0,87 ± 0,05	0,87 ± 0,04	0,87 ± 0,04	0,398*	0,83 ± 0,04	0,88 ± 0,02	0,87 ± 0,04	0,89 ± 0,03	0,87 ± 0,04	<0,001*
	Long Run Emphasis	5,50 ± 13,68	11,15 ± 28,76	8,58 ± 23,21	0,044*	18,49 ± 26,66	3,79 ± 4,65	9,57 ± 33,77	2,10 ± 1,79	8,58 ± 23,21	<0,001*
	Gray-Level Nonuniformity	0,04 ± 0,03	0,04 ± 0,01	0,04 ± 0,02	0,249*	0,06 ± 0,03	0,03 ± 0,01	0,04 ± 0,02	0,03 ± 0,01	0,04 ± 0,02	<0,001*
	Run Length Nonuniformity	0,72 ± 0,08	0,71 ± 0,06	0,72 ± 0,07	0,429*	0,64 ± 0,07	0,74 ± 0,04	0,72 ± 0,07	0,75 ± 0,05	0,72 ± 0,07	<0,001*
	Run Percentage	0,78 ± 0,13	0,74 ± 0,16	0,76 ± 0,15	0,084*	0,62 ± 0,17	0,79 ± 0,09	0,78 ± 0,14	0,83 ± 0,06	0,76 ± 0,15	<0,001*
	Low Gray-Level Run Emphasis	0,05 ± 0,07	0,06 ± 0,06	0,06 ± 0,06	0,202*	0,13 ± 0,07	0,04 ± 0,04	0,04 ± 0,06	0,02 ± 0,03	0,06 ± 0,06	<0,001*
	High Gray-Level Run Emphasis	620 ± 445	685 ± 391	655 ± 416	0,343*	300 ± 204	715 ± 272	661 ± 348	937 ± 507	655 ± 416	<0,001*
	Short Run Low Gray-Level	0,03 ± 0,03	0,03 ± 0,02	0,03 ± 0,03	0,425*	0,06 ± 0,02	0,02 ± 0,01	0,02 ± 0,02	0,01 ± 0,01	0,03 ± 0,03	<0,001*
	Short Run High Gray-Level	567 ± 415	628 ± 365	600 ± 388	0,340*	273 ± 192	655 ± 252	603 ± 325	860 ± 478	600 ± 388	<0,001*
	Long Run Low Gray-Level	3,84 ± 13,75	9,57 ± 28,85	6,96 ± 23,30	0,046*	16,91 ± 26,83	2,20 ± 4,73	7,90 ± 33,84	0,46 ± 1,76	6,96 ± 23,30	<0,001*
	Long Run High Gray-Level	970,60 ± 626,09	1069,23 ± 543,82	1024,31 ± 581,83	0,310*	500,17 ± 286,32	1102,41 ± 398,70	1054,48 ± 485,17	1422,55 ± 679,57	1024,31 ± 581,83	<0,001*
	Gray-Level Variance	0,0020 ± 0,0018	0,0014 ± 0,0015	0,0017 ± 0,0016	0,108*	0,0003 ± 0,0004	0,0016 ± 0,0016	0,0018 ± 0,0014	0,0029 ± 0,0017	0,0017 ± 0,0016	<0,001*
	Run-Length Variance**	-5,35 ± 0,28	-5,56 ± 0,29	-5,46 ± 0,30	0,001*	-5,53 ± 0,29	-5,56 ± 0,36	5,44 ± 0,28	-5,34 ± 0,23	-5,46 ± 0,30	0,089
GLSZM	Small Zone Emphasis	0,70 ± 0,05	0,72 ± 0,04	0,71 ± 0,04	0,043*	0,69 ± 0,07	0,72 ± 0,03	0,70 ± 0,04	0,71 ± 0,04	0,71 ± 0,04	0,514
	Large Zone Emphasis	2659 ± 9102	6693 ± 22364	4856 ± 17647	0,024*	12742 ± 22285	704 ± 1777	5468 ± 24362	204 ± 884	4856 ± 17647	<0,001*
	Gray-Level Nonuniformity	0,03 ± 0,02	0,03 ± 0,01	0,03 ± 0,02	0,134*	0,045 ± 0,023	0,024 ± 0,005	0,029 ± 0,015	0,025 ± 0,010	0,03 ± 0,02	<0,001*
	Zone-Size Nonuniformity	0,45 ± 0,06	0,48 ± 0,05	0,47 ± 0,06	0,045*	0,45 ± 0,08	0,48 ±0,03	0,46 ± 0,05	0,47 ± 0,05	0,47 ± 0,06	0,517
	Zone Percentage	0,46 ± 0,12	0,45 ± 0,12	0,46 ± 0,12	0,405*	0,34 ± 0,11	0,49 ± 0,07	0,47 ± 0,11	0,52 ± 0,08	0,46 ± 0,12	<0,001*
	Low Gray-Level Zone Emphasis	0,02 ± 0,03	0,02 ± 0,02	0,02 ± 0,02	0,558*	0,04 ± 0,02	0,02 ± 0,01	0,02 ± 0,02	0,01 ± 0,01	0,02 ± 0,02	<0,001*
	High Gray-Level Zone Emphasis	673,08 ± 470,48	761 ± 415	721 ± 441	0,238*	350 ± 226	788 ± 283	726 ± 372	1011 ± 543	721 ± 441	<0,001*
	Small Zone Low Gray-Level Zone Emphasis	0,012 ± 0,013	0,012 ± 0,009	0,012 ± 0,011	0,517*	0,024 ± 0,012	0,009 ± 0,005	0,010 ± 0,011	0,005 ± 0,006	0,012 ± 0,011	<0,001*
	Small Zone High Gray-Level Zone Emphasis	506 ± 374	580 ± 334	546 ± 353	0,190*	264 ± 185	598 ± 219	547 ± 301	771 ± 447	546 ± 353	<0,001*
	Large Zone Low Gray-Level Zone Emphasis	2645 ± 9101	6682 ± 22365	4843 ± 17648	0,035*	12725 ± 22290	695 ± 1777	5455 ± 24363	193 ± 882	4843 ± 17648	<0,001*
	Large Zone High Gray-Level Zone Emphasis	7274 ± 8552	11752 ± 21561	9713 ± 16999	0,019*	15577 ± 21797	5674 ± 1976	10764 ± 23706	6374 ± 1972	9712 ± 16999	0,640*
	Grey-Level Variance	0,0003 ± 0,0003	0,0002 ± 0,0003	0,0002 ± 0,0003	0,095*	0,00002 ± 0,00003	0,00025 ± 0,00034	0,00022 ± 0,00022	0,00047 ± 0,00042	0,0002 ± 0,0003	<0,001*
	Zone-Size Variance	-6,18 ± 0,41	-6,39 ± 0,54	-6,29 ± 0,49	0,036*	-6,27 ± 0,54	-6,44 ± 0,58	-6,31 ± 0,45	-6,16 ± 0,37	-6,29 ± 0,49	0,247
NGTDM	Coarseness	0,0008 ± 0,0003	0,0007 ± 0,0003	0,0007 ± 0,0003	0,390*	0,00053 ± 0,00016	0,00079 ± 0,00031	0,00069 ± 0,00024	0,00093 ± 0,00031	0,0007 ± 0,0003	<0,001*
	Contrast	0,16 ± (0,06	0,17 ± 0,06	0,17 ± 0,06	0,051	0,13 ± 0,07	0,19 ± 0,03	0,17 ± 0,06	0,18 ± 0,05	0,17 ± 0,06	0,005
	Busyness	5,17 ± 9,18	4,66 ± 6,94	4,89 ± 8,00	0,817*	11,64 ± 11,29	2,18 ± 1,92	4,45 ± 7,77	1,32 ± 1,56	4,89 ± 8,00	<0,001*
	Complexity	2567 ± 1867	2961 ± 1977	2782 ± 1928	0,266*	1574 ± 1407	3107 ± 1211	2748 ± 1746	3695 ± 2490	2782 ± 1928	<0,001*
	Strength	1,57 ± 1,14	2,01 ± 1,08	1,81 ± 1,12	0,007*	1,42 ± 0,86	2,12 ± 1,12	1,53 ± 0,76	2,26 ± 1,48	1,81 ± 1,12	0,032*

Abbreviations: SD: standard deviation; IHF: Intensity Histogram Features; GLCM: Gray-Level Co-occurrence Matrix; GLRLM: Gray-Level run-Length Matrix; GLSZM: Gray-Level Size Zone Matrix; NGTDM: Neighborhood Gray-Tone Difference Matrix.

* Variables without normal distribution, nonparametric tests used for the analysis.

** Run-Length Variance and Zone-Size Variance are small with a restricted range of scales, so logarithms were used to transform the data.

Table Annex 8.8.3 Texture Features of Sagittal Rectus Femoris According to Sex and Frailty Phenotype											
Group		Female (n=46)	Male (n=55)	Total (n=101)	Statistical Test	Controls (n = 24)	Robust (n = 22)	Pre-frail (n = 30)	Frail (n =25)	Total (n=101)	Statistical Test
Texture Feature		Mean ± SD	Mean ± SD	Mean ± SD	P value	Mean ± SD	Mean ± SD	Mean ± SD	Mean ± SD	Mean ± SD	P value
IHF	Variance	194 ± 40	194 ± 52	194 ± 47	0,998	182 ± 32	203 ± 38	194 ± 58	196 ± 49	198 ± 47	0,499
	Skewness	1,05 ± 0,41	1,04 ± 0,36	1,04 ± 0,38	0,894	1,18 ± 0,41	1,01 ± 0,32	0,97 ± 0,36	1,03 ± 0,42	1,04 ± 0,38	0,235
	Kurtosis	1,80 ± 1,56	1,64 ± 1,20	1,71 ± 1,37	0,956*	2,27 ± 1,34	1,42 ± 0,92	1,50 ± 1,33	1,69 ± 1,68	1,71 ± 1,37	0,090*
GLCM	Energy	0,0015 ± 0,0008	0,0015 ± 0,0006	0,0015 ± 0,0007	0,682*	0,0019 ± 0,0008	0,0015 ± 0,0005	0,0014 ± 0,0007	0,0013 ± 0,0007	0,0015 ± 0,0007	0,043*
	Contrast	89,7 ± 35,7	88,8 ± 46,1	89,2 ± 41,5	0,713*	81,7 ± 34,1	82,5 ± 34,6	96,3 ± 47,8	93,6 ± 45,5	89,2 ± 41,5	0,469*
	Entropy	10,62 ± 0,57	10,59 ± 0,58	10,61 ± 0,57	0,764	10,40 ± 0,50	10,60 ± 0,49	10,71 ± 0,65	10,70 ± 0,58	10,61 ± 0,57	0,189
	Homogeneity	0,31 ± 0,03	0,32 ± 0,03	0,31 ± 0,03	0,281	0,32 ± 0,03	0,32 ± 0,03	0,31 ± 0,04	0,30 ± 0,03	0,31 ± 0,03	0,087
	Correlation	0,87 ± 0,03	0,88 ± 0,03	0,87 ± 0,03	0,151	0,88 ± 0,03	0,89 ± 0,02	0,87 ± 0,03	0,87 ± 0,03	0,87 ± 0,03	0,049
	Sum Average	0,0005 ± 0,0001	0,0005 ± 0,0001	0,0005 ± 0,0001	0,786	0,0005 ± 0,0001	0,0005 ± 0,0001	0,0005 ± 0,0001	0,0005 ± 0,0001	0,0005 ± 0,0001	0,032
	Variance	0,0052 ± 0,0019	0,0054 ± 0,0021	0,0053 ± 0,002	0,728*	0,0049 ± 0,0018	0,0055 ± 0,0018	0,0056 ± 0,0025	0,0052 ± 0,0017	0,0053 ± 0,002	0,513*
	Dissimilarity	6,12 ± 1,21	5,98 ± 1,44	6,04 ± 1,33	0,615	5,75 ± 1,11	5,83 ± 1,14	6,26 ± 1,51	6,25 ± 1,45	6,04 ± 1,33	0,379
	Auto-Correlation	1497 ± 547	1521 ± 507	1510 ± 523	0,658*	1289 ± 498	1535 ± 455	1649 ± 582	1531 ± 486	1510 ± 523	0,050*
GLRLM	Short Run Emphasis	0,93 ± 0,01	0,93 ± 0,01	0,93 ± 0,01	0,319	0,92 ± 0,01	0,92 ± 0,01	0,93 ± 0,01	0,93 ± 0,01	0,93 ± 0,01	0,016
	Long Run Emphasis	1,45 ± 0,16	1,46 ± 0,10	1,45 ± 0,13	0,421*	1,53 ± 0,18	1,46 ± 0,07	1,42 ± 0,10	1,41 ± 0,10	1,45 ± 0,13	0,001*
	Gray-Level Nonuniformity	0,020 ± 0,004	0,020 ± 0,004	0,020 ± 0,004	0,965	0,022 ± 0,004	0,020 ± 0,004	0,020 ± 0,005	0,020 ± 0,004	0,020 ± 0,004	0,275
	Run Length Nonuniformity	0,83 ± 0,03	0,82 ± 0,03	0,83 ± 0,03	0,322	0,81 ± 0,02	0,82 ± 0,02	0,83 ± 0,03	0,84 ± 0,03	0,83 ± 0,03	0,016
	Run Percentage	0,89 ± 0,02	0,89 ± 0,02	0,89 ± 0,02	0,377	0,88 ± 0,02	0,89 ± 0,01	0,90 ± 0,02	0,90 ± 0,02	0,89 ± 0,02	0,004
	Low Gray-Level Run Emphasis	0,009 ± 0,007	0,007 ± 0,003	0,008 ± 0,005	0,946*	0,012 ± 0,010	0,007 ± 0,002	0,006 ± 0,001	0,007 ± 0,003	0,008 ± 0,005	0,008*
	High Gray-Level Run Emphasis	1565 ± 560	1595 ± 529	1581 ± 540	0,614*	1360 ± 508	1606 ± 474	1725 ± 605	1601 ± 504	1582 ± 540	0,056*
	Short Run Low Gray-Level	0,006 ± 0,004	0,006 ± 0,002	0,006 ± 0,004	0,929*	0,0089 ± 0,0061	0,0051 ± 0,0013	0,0049 ± 0,0007	0,0053 ± 0,0019	0,006 ± 0,004	0,010*
	Short Run High Gray-Level	1473 ± 538	1499 ± 510	1488 ± 520	0,648*	1274 ± 486	1506 ± 452	1627 ± 586	1509 ± 488	1488 ± 520	0,054*
	Long Run Low Gray-Level	0,05 ± 0,13	0,03 ± 0,03	0,04 ± 0,09	0,354*	0,09 ± 0,17	0,02 ± 0,02	0,02 ± 0,004	0,02 ± 0,02	0,04 ± 0,09	0,067*
	Long Run High Gray-Level	2137 ± 697	2190 ± 653	2166 ± 670	0,553*	18945 ± 639	2235 ± 618	2340 ± 743	2156 ± 604	2166 ± 670	0,082*
	Gray-Level Variance	0,0038 ± 0,0015	0,0038 ± 0,0014	0,0038 ± 0,0014	0,553*	0,0034 ± 0,0018	0,0036 ± 0,0010	0,0041 ± 0,0015	0,0040 ± 0,0013	0,0038 ± 0,0014	0,217*
	Run-Length Variance**	-5,48 ± 0,18	-5,48 ± 0,14	-5,46 ± 0,30	0,647	-5,47 ± 0,19	-5,50 ± 0,11	-5,49 ± 0,18	5,46 ± 0,14	-5,46 ± 0,30	0,693
GLSZM	Small Zone Emphasis	0,78 ± 0,03	0,77 ± 0,03	0,78 ± 0,03	0,414	0,77 ± 0,02	0,77 ± 0,02	0,78 ± 0,03	0,78 ± 0,03	0,78 ± 0,03	0,142
	Large Zone Emphasis	6,40 ± 7,82	5,33 ± 1,84	5,82 ± 5,44	0,394*	8,97 ± 10,33	5,28 ± 1,31	4,67 ± 1,52	4,64 ±1,86	5,82 ± 5,44	<0,001*
	Gray-Level Nonuniformity	0,018 ± 0,003	0,018 ± 0,004	0,018 ± 0,003	0,796*	0,019 ± 0,003	0,018 ± 0,003	0,018 ± 0,004	0,018 ± 0,003	0,018 ± 0,003	0,171*
	Zone-Size Nonuniformity	0,56 ± 0,04	0,56 ± 0,04	0,56 ± 0,04	0,428	0,55 ± 0,04	0,55 ± 0,04	0,57 ± 0,05	0,57 ± 0,04	0,56 ± 0,04	0,130
	Zone Percentage	0,65 ± 0,05	0,63 ± 0,05	0,64 ± 0,05	0,299	0,62 ± 0,04	0,63 ± 0,04	0,65 ± 0,05	0,66 ± 0,05	0,64 ± 0,05	0,015
	Low Gray-Level Zone Emphasis	0,0048 ± 0,0029	0,0043 ± 0,0017	0,0045 ± 0,0023	0,535*	0,0065 ± 0,0037	0,0041 ± 0,0011	0,0037 ± 0,0007	0,0040 ± 0,0014	0,0045 ± 0,0023	0,001*
	High Gray-Level Zone Emphasis	1630 ± 569	1677 ± 544	1656 ± 553	0,576*	1436 ± 524	1690 ± 495	1800 ± 617	1663 ± 511	1656 ± 553	0,070*
	Small Zone Low Gray-Level Zone Emphasis	0,0028 ± 0,0015	0,0025 ± 0,0009	0,0026 ± 0,0012	0,336*	0,0036 ± 0,0019	0,0024 ± 0,0006	0,0022 ± 0,0004	0,0024 ± 0,0008	0,0026 ± 0,0012	0,003*
	Small Zone High Gray-Level Zone Emphasis	1316 ± 490	1352 ± 475	1336 ± 480	0,623*	1147 ± 449	1355 ± 422	1462 ± 541	1350 ± 448	1336 ± 480	0,064*
	Large Zone Low Gray-Level Zone Emphasis	1,86 ± 7,53	0,45 ± 0,99	1,09 ± 5,15	0,350*	3,71 ± 10,22	0,29 ± 0,53	0,17 ± 0,10	0,39 ± 1,07	1,09 ± 5,15	0,102*
	Large Zone High Gray-Level Zone Emphasis	6265 ± 1793	6584 ± 1739	6439 ± 1762	0,367	5980 ± 1827	6977 ± 1627	6736 ± 1918	6050 ± 1495	6439 ± 1762	0,123
	Grey-Level Variance	0,0011 ± 0,0007	0,0010 ± 0,0005	0,0010 ± 0,0006	0,302	0,0008 ± 0,0006	0,0009 ± 0,0004	0,0013 ± 0,0006	0,0012 ± 0,0006	0,0010 ± 0,0006	0,008
	Zone-Size Variance**	-5,48 ± 0,18	-5,48 ± 0,14	-6,29 ± 0,49	0,406	6,17 ± 0,19	-5,50 ± 0,11	-5,49 ± 0,18	-5,46 ± 0,14	-6,29 ± 0,49	0,065
NGTDM	Coarseness	0,0007 ± 0,0002	0,0007 ± 0,0002	0,0007 ± 0,0002	0,157	0,0006 ± 0,0002	0,0007 ± 0,0002	0,0007 ± 0,0002	0,0008 ± 0,0002	0,0007 ± 0,0002	0,188
	Contrast	0,30 ± 0,08	0,29 ± 0,10	0,30 ± 0,09	0,343*	0,29 ± 0,08	0,28 ± 0,06	0,31 ± 0,11	0,30 ± 0,09	0,30 ± 0,09	0,665*
	Busyness	0,78 ± 0,40	0,81 ± 0,39	0,80 ± 0,39	0,609*	0,99 ± 0,53	0,72 ± 0,27	0,78 ± 0,42	0,71 ± 0,22	0,80 ± 0,39	0,110*
	Complexity	8228 ± 3477	8280 ± 4304	8256 ± 3930	0,849*	7326 ± 3101	7868 ± 3238	9157 ± 4913	8411 ± 3843	8256 ± 3930	0,353*
	Strength	2,09 ± 0,68	2,09 ± 0,85	2,09 ± 0,78	0,822*	1,92 ± 0,69	2,26 ± 0,85	2,07 ± 0,83	2,13 ± 0,72	2,09 ± 0,78	0,519*

Abbreviations: SD: standard deviation; IHS: Intensity Histogram Statistics; GLCM: Gray-Level Co-occurrence Matrix; GLRLM: Gray-Level run-Length Matrix; GLSZM: Gray-Level Size Zone Matrix; NGTDM: Neighborhood Gray-Tone Difference Matrix.

* Variables without normal distribution, nonparametric tests used for the analysis.

** Run-Length Variance and Zone-Size Variance are small with a restricted range of scales, so logarithms were used to transform the data.

Table Annex 8.8.4 Texture Features of Sagittal Vastus Intermedius According to Sex and Frailty Phenotype											
	Group	*Female (n=46)*	*Male (n=55)*	*Total (n=101)*	*Statistical Test*	*Controls (n = 24)*	*Robust (n = 22)*	*Pre-frail (n = 30)*	*Frail (n =25)*	*Total (n=101)*	*Statistical Test*
	Texture Feature	*Mean ± SD*	*Mean ± SD*	*Mean ± SD*	*P value*	*Mean ± SD*	*Mean ± SD*	*Mean ± SD*	*Mean ± SD*	*Mean ± SD*	*P value*
IHF	Variance	174 ± 68	184 ± 65	179 ± 66	0,261*	155 ± 48	182 ± 56	187 ± 82	190 ± 65	179 ± 66	0,216*
	Skewness	1,35 ± 0,63	1,52 ± 0,77	1,44 ± 0,71	0,390*	2,03 ± 0,55	1,32 ± 0,65	1,32 ± 0,76	1,12 ± 0,52	1,44 ± 0,71	<0,001*
	Kurtosis	3,22 ± 3,35	3,68 ± 4,06	3,47 ± 3,74	0,723*	5,82 ± 3,14	2,78 ± 2,84	3,05 ± 4,30	2,33 ± 3,45	3,47 ± 3,74	<0,001*
GLCM	Energy	0,02 ± 0,06	0,05 ± 0,11	0,04 ± 0,09	0,801*	0,09 ± 0,11	0,03 ± 0,08	0,03 ± 0,10	0,01 ± 0,01	0,04 ± 0,09	<0,001*
	Contrast	34,3 ± 19,5	47,6 ± 45,8	41,5 ± 36,7	0,120*	31,3 ± 21,8	41,0 ± 19,7	45,7 ± 56,7	46,9 ± 27,8	41,5 ± 36,7	0,119*
	Entropy	8,79 ± 1,57	8,87 ± 1,85	8,83 ± 1,72	0,522*	7,38 ± 1,75	9,16 ± 1,53	9,07 ± 1,63	9,65 ± 1,08	8,83 ± 1,72	<0,001*
	Homogeneity	0,42 ± 0,10	0,43 ± 0,13	0,43 ± 0,11	0,838*	0,52 ± 0,12	0,41 ± 0,10	0,41 ± 0,11	0,37 ± 0,06	0,43 ± 0,11	<0,001*
	Correlation	0,89 ± 0,03	0,90 ± 0,03	0,90 ± 0,03	0,064	0,88 ± 0,03	0,91 ± 0,03	0,90 ± 0,03	0,90 ± 0,03	0,90 ± 0,03	0,021
	Sum Average	0,0003 ± 0,0001	0,0003 ± 0,0002	0,0003 ± 0,0002	0,553	0,0002 ± 0,0001	0,0003 ± 0,0001	0,0003 ± 0,0001	0,0004 ± 0,0001	0,0003 ± 0,0002	<0,001
	Variance	0,0028 ± 0,0020	0,0036 ± 0,0026	0,0032 ± 0,0023	0,024*	0,0021 ± 0,0013	0,0036 ± 0,0018	0,0033 ± 0,0030	0,0040 ± 0,0024	0,0032 ± 0,0023	0,004*
	Dissimilarity	3,64 ± 1,22	4,07 ± 1,67	3,87 ± 1,49	0,153	3,06 ± 1,27	4,01 ± 1,23	4,04 ± 1,78	4,34 ± 1,28	3,87 ± 1,49	0,015
	Auto-Correlation	665 ± 514	775 ± 632	725 ± 581	0,357*	303 ± 282	789 ± 478	754 ± 657	1040 ± 569	724 ± 581	<0,001*
GLRLM	Short Run Emphasis	0,88 ± 0,05	0,88 ± 0,04	0,88 ± 0,04	0,658*	0,84 ± 0,05	0,89 ± 0,04	0,89 ± 0,04	0,90 ± 0,03	0,88 ± 0,04	<0,001*
	Long Run Emphasis	4,37 ± 10,35	8,52 ± 19,21	6,63 ± 15,86	0,619*	12,06 ± 17,82	4,83 ± 12,30	7,61 ± 21,41	1,83 ± 0,73	6,63 ± 15,86	<0,001*
	Gray-Level Nonuniformity	0,04 ± 0,02	0,03 ± 0,02	0,04 ± 0,02	0,222*	0,05 ± 0,02	0,03 ± 0,02	0,03 ± 0,01	0,03 ± 0,01	0,04 ± 0,02	<0,001*
	Run Length Nonuniformity	0,73 ± 0,08	0,74 ± 0,07	0,74 ± 0,08	0,614*	0,67 ± 0,08	0,75 ± 0,07	0,75 ± 0,06	0,77 ± 0,05	0,74 ± 0,08	<0,001*
	Run Percentage	0,80 ± 0,11	0,77 ± 0,16	0,78 ± 0,14	0,849*	0,67 ± 0,16	0,81 ± 0,12	0,80 ± 0,14	0,85 ± 0,05	0,78 ± 0,14	<0,001*
	Low Gray-Level Run Emphasis	0,05 ± 0,06	0,05 ± 0,06	0,05 ± 0,06	0,718*	0,11 ± 0,07	0,04 ± 0,05	0,04 ± 0,05	0,02 ± 0,03	0,05 ± 0,06	<0,001*
	High Gray-Level Run Emphasis	714 ± 527	854 ± 634	790 ± 589	0,207*	386 ± 292	850 ± 481	814 ± 675	1096 ± 589	790 ± 589	<0,001*
	Short Run Low Gray-Level	0,02 ± 0,03	0,02 ± 0,02	0,02 ± 0,02	0,854*	0,051 ± 0,025	0,019 ± 0,016	0,019 ± 0,017	0,012 ± 0,015	0,02 ± 0,02	<0,001*
	Short Run High Gray-Level	659 ± 495	793 ± 606	732 ± 559	0,190*	355 ± 275	787 ± 452	754 ± 649	1018 ± 560	732 ± 559	<0,001*
	Long Run Low Gray-Level	2,73 ± 10,37	7,00 ± 19,28	5,05 ± 15,93	0,263*	10,49 ± 17,91	3,25 ± 12,35	6,04 ± 21,48	0,24 ± 0,72	5,05 ± 15,93	<0,001*
	Long Run High Gray-Level	1078 ± 725	1247 ± 808	1170 ± 772	0,266*	610 ± 400	1265 ± 680	1206 ± 833	1581 ± 766	1170 ± 772	<0,001*
	Gray-Level Variance	0,0020 ± 0,0016	0,0020 ± 0,0018	0,0020 ± 0,0017	0,790*	0,0005 ± 0,0011	0,0020 ± 0,0016	0,0022 ± 0,0017	0,0031 ± 0,0016	0,0020 ± 0,0017	<0,001*
	Run-Length Variance**	-6,04 ± 0,27	-6,06 ± 0,23	-6,05 ± 0,25	0,019*	-6,17 ± 0,35	-6,07 ± 0,21	-5,98 ± 0,18	-6,01 ± 0,21	-6,05 ± 0,25	0,062*
GLSZM	Small Zone Emphasis	0,71 ± 0,05	0,74 ± 0,04	0,73 ± 0,05	0,003	0,71 ± 0,06	0,73 ± 0,05	0,73 ± 0,04	0,74 ± 0,05	0,73 ± 0,05	0,248
	Large Zone Emphasis	2146 ± 9583	7091 ± 22334	4839 ± 17799	0,495*	10121 ± 22598	4898 ± 21487	4570 ± 17607	39 ± 95	4839 ± 17799	<0,001*
	Gray-Level Nonuniformity	0,03 ± 0,02	0,03 ± 0,01	0,03 ± 0,01	0,134*	0,040 ± 0,019	0,026 ± 0,012	0,026 ± 0,009	0,024 ± 0,011	0,03 ± 0,01	<0,001*
	Zone-Size Nonuniformity	0,47 ± 0,07	0,51 ± 0,06	0,49 ± 0,07	0,003	0,47 ± 0,08	0,50 ± 0,06	0,50 ± 0,06	0,50 ± 0,06	0,49 ± 0,07	0,285
	Zone Percentage	0,49 ± 0,12	0,50 ± 0,13	0,49 ± 0,13	0,562	0,38 ± 0,12	0,51 ± 0,11	0,51 ± 0,11	0,55 ± 0,09	0,49 ± 0,13	<0,001*
	Low Gray-Level Zone Emphasis	0,02 ± 0,02	0,02 ± 0,02	0,02 ± 0,02	0,908*	0,038 ± 0,021	0,015 ± 0,013	0,014 ± 0,013	0,010 ± 0,010	0,02 ± 0,02	<0,001*
	High Gray-Level Zone Emphasis	773 ± 554	930 ± 651	859 ± 611	0,173*	443 ± 307	923 ± 496	880 ± 691	1177 ± 623	859 ± 611	<0,001*
	Small Zone Low Gray-Level Zone Emphasis	0,011 ± 0,011	0,010 ± 0,010	0,011 ± 0,010	0,967*	0,021 ± 0,012	0,008 ± 0,008	0,008 ± 0,008	0,005 ± 0,005	0,011 ± 0,010	<0,001*
	Small Zone High Gray-Level Zone Emphasis	597 ± 448	736 ± 559	673 ± 514	0,135*	342 ± 250	722 ± 400	689 ± 609	927 ± 523	673 ± 514	<0,001*
	Large Zone Low Gray-Level Zone Emphasis	2131 ± 9582	7083 ± 22334	4828 ± 17799	0,212*	10105 ± 22600	4888 ± 21488	4561 ± 17607	28 ± 94	4828 ± 17799	<0,001*
	Large Zone High Gray-Level Zone Emphasis	7016 ± 9098	11947 ± 21503	9701 ± 17118	0,235*	13128 ± 22191	10228 ± 20763	9437 ± 16827	6264 ± 2295	9701 ± 17118	0,440*
	Grey-Level Variance	0,0003 ± 0,0003	0,0003 ± 0,0005	0,0003 ± 0,0004	0,567*	0,0001 ± 0,0002	0,0002 ± 0,0002	0,0004 ± 0,0004	0,0006 ± 0,0005	0,0003 ± 0,0004	<0,001*
	Zone-Size Variance**	-6,04 ± 0,27	-6,06 ± 0,23	-6,05 ± 0,25	0,207*	-6,17 ± 0,35	-6,07 ± 0,21	-5,98 ± 0,18	-6,01 ± 0,21	-6,05 ± 0,25	0,115*
NGTDM	Coarseness	0,0007 ± 0,0003	0,0006 ± 0,0002	0,0006 ± 0,0002	0,310*	0,0005 ± 0,0002	0,0007 ± 0,0002	0,0006 ± 0,0002	0,0008 ± 0,0003	0,0006 ± 0,0002	<0,001*
	Contrast	0,18 ± 0,07	0,22 ± 0,10	0,20 ± 0,09	0,062	0,17 ± 0,08	0,21 ± 0,07	0,21 ± 0,12	0,21 ± 0,08	0,20 ± 0,09	0,256
	Busyness	5,04 ± 9,15	5,54 ± 10,34	5,31 ± 9,77	0,956*	12,09 ± 13,85	3,70 ± 8,47	4,09 ± 8,30	1,68 ± 1,97	5,31 ± 9,77	<0,001*
	Complexity	3144 ± 2310	4399 ± 5187	3827 ± 4162	0,122*	2230 ± 1815	3920 ± 2244	4210 ± 6495	4820 ± 3142	3827 ± 4162	0,003*
	Strength	1,44 ± 1,21	1,72 ± 0,96	1,60 ± 1,09	0,054*	1,25 ± 0,80	1,65 ± 0,69	1,44 ± 0,97	2,06 ± 1,54	1,60 ± 1,09	0,012*

Abbreviations: SD: standard deviation; IHS: Intensity Histogram Statistics; GLCM: Gray-Level Co-occurrence Matrix; GLRLM: Gray-Level run-Length Matrix; GLSZM: Gray-Level Size Zone Matrix; NGTDM: Neighborhood Gray-Tone Difference Matrix.

* Variables without normal distribution, nonparametric tests used for the analysis.

** Run-Length Variance and Zone-Size Variance are small with a restricted range of scales, so logarithms were used to transform the data.

Table Annex 8.8.5 Post-hoc Analysis of Muscles Textures Features by Frailty Phenotype (N = 101)

Axial Rectus Femoris

Testure Features	*Group*	*Control (n = 24)*	*Robust (n = 22)*	*Pre-frail (n = 30)*	*Frail (n = 25)*
Skewness of IHF	Control	-	0,002	0,001	0,001
	Robust	0,002	-	1,000	1,000
	Pre-frail	0,001	1,000	-	1,000
	Frail	0,001	1,000	1,000	-
Sum Average of GLCM	Control	-	0,066	0,012	0,006
	Robust	0,066	-	1,000	1,000
	Pre-frail	0,012	1,000	-	1,000
	Frail	0,006	1,000	1,000	-
Auto-Correlation of GLCM	Control	-	0,305	0,082	0,042
	Robust	0,305	-	1,000	1,000
	Pre-frail	0,082	1,000	-	1,000
	Frail	0,042	1,000	1,000	-
High Gray-Level Run Emphasis of GLRLM	Control	-	0,378	0,111	0,057
	Robust	0,378	-	1,000	1,000
	Pre-frail	0,111	1,000	-	1,000
	Frail	0,057	1,000	1,000	-
Short Run High Gray-Level of GLRLM	Control	-	0,4	0,114	0,058
	Robust	0,4	-	1,000	1,000
	Pre-frail	0,114	1,000	-	1,000
	Frail	0,058	1,000	1,000	-
Zone Percentage of GLSZM	Control	-	1,000	0,188	0,059
	Robust	1,000	-	1,000	0,891
	Pre-frail	0,188	1,000	-	1,000
	Frail	0,059	0,891	1,000	-
High Gray-Level Zone Emphasis of GLSZM	Control	-	0,41	0,139	0,072
	Robust	0,41	-	1,000	1,000
	Pre-frail	0,139	1,000	-	1,000
	Frail	0,072	1,000	1,000	-

Sagittal Rectus Femoris

Texture Features	*Group*	*Control (n = 24)*	*Robust (n = 22)*	*Pre-frail (n = 30)*	*Frail (n = 25)*
Correlation of GLCM	Control	-	0,704	1,000	1,000
	Robust	0,704	-	0,203	0,042
	Pre-frail	1,000	0,203	-	1,000
	Frail	1,000	0,042	1,000	-
Sum Average of GLCM	Control	-	0,363	0,025	0,219
	Robust	0,363	-	1,000	1,000
	Pre-frail	0,025	1,000	-	1,000
	Frail	0,219	1,000	1,000	-
Short Run Emphasis of GLRLM	Control	-	1,000	0,070	0,024
	Robust	1,000	-	1,000	0,529
	Pre-frail	0,070	1,000	-	1,000
	Frail	0,024	0,529	1,000	-
Run length Nonuniformity of GLRLM	Control	-	1,000	0,070	0,024
	Robust	1,000	-	1,000	0,516
	Pre-frail	0,070	1,000	-	1,000
	Frail	0,024	0,516	1,000	-
Run Percentage of GLRLM	Control	-	0,964	0,022	0,006
	Robust	0,964	-	0,948	0,388
	Pre-frail	0,022	0,948	-	1,000
	Frail	0,006	0,388	1,000	-
Zone Percentage of GLSZM	Control	-	1,000	0,084	0,024
	Robust	1,000	-	0,858	0,321
	Pre-frail	0,084	0,858	-	1,000
	Frail	0,024	0,321	1,000	-
Grey-Level Variance of GLSZM	Control	-	1,000	0,011	0,081
	Robust	1,000	-	0,197	0,767
	Pre-frail	0,011	0,197	-	1,000
	Frail	0,081	0,767	1,000	-

Axial Vastus Intermedius

Sum Average of GLCM	Control	-	<0,001	<0,001	<0,001
	Robust	<0,001	-	1,000	0,095
	Pre-frail	<0,001	1,000	-	0,03
	Frail	<0,001	0,095	0,03	-
Dissimilarity of GLCM	Control	-	0,001	0,014	<0,001
	Robust	0,001	-	1,000	1,000
	Pre-frail	0,014	1,000	-	0,671
	Frail	<0,001	1,000	0,671	-
Auto-Correlation of GLCM	Control	-	<0,001	<0,001	<0,001
	Robust	<0,001	-	1	0,095
	Pre-frail	<0,001	1	-	0,021
	Frail	<0,001	0,095	0,021	-
Contrast of NGTDM	Control	-	0,004	0,171	0,035
	Robust	0,004	-	0,787	1,000
	Pre-frail	0,171	0,787	-	1,000
	Frail	0,035	1,000	1,000	-

Sagittal Vastus Intermedius

Texture Features	*Group*	*Control (n = 24)*	*Robust (n = 22)*	*Pre-frail (n = 30)*	*Frail (n = 25)*
Correlation of GLCM	Control	-	0,03	0,141	0,082
	Robust	0,03	-	1,000	1,000
	Pre-frail	0,141	1,000	-	1,000
	Frail	0,082	1,000	1,000	-
Sum Average of GLCM	Control	-	<0,001	<0,001	<0,001
	Robust	<0,001	-	1,000	0,393
	Pre-frail	<0,001	1,000	-	0,186
	Frail	<0,001	0,393	0,186	-
Dissimilarity of GLCM	Control	-	0,164	0,086	0,014
	Robust	0,164	-	1,000	1,000
	Pre-frail	0,086	1,000	-	1,000
	Frail	0,014	1,000	1,000	-
-					

Abbreviations: IHF: Intensity Histogram Features; GLCM: Gray-Level Co-occurrence Matrix; GLRLM: Gray-Level run-Length Matrix; GLSZM: Gray-Level Size Zone Matrix; NGTDM: Neighborhood Gray-Tone Difference Matrix.

* <0,05 represent significant diferrences between the groups

8.9 ANNEX 9: CORRELATIONS OF COMORBIDITIES WITH PHYSICAL CHARACTERISTICS, ULTRASOUND CHARACTERISTICS, FRAILTY CRITERIA, AND QUALITY OF LIFE AT BASELINE AND FOLLOW-UP

Table 8.9.1 Correlations of 2015 Comorbidities with Baseline Characteristics (n = 101)

Variables	*Age (years)*	*Weight (kg)*	*Height (m)*	*BMI (kg/m²)*	*Gait Speed (s)*	*Frailty Phenotype*	*SFT (cm)*	*MT (cm)*	*MS (kg)*	*OPQoL (A.U.)*
Associated Diseases										
Hypertension	,231**	,193*	-0,142	,310**	,185*	,281**	,176*	-0,141	-0,066	0,022
Hyperlipidemia	,179*	0,116	-0,104	,167*	0,108	,218*	-0,018	-0,134	,206*	-0,033
DM	,224**	0,075	-0,13	,184*	0,126	,288**	0,045	-,252**	0,106	-0,058
COPD	0,003	0,025	-0,011	0,023	0,029	,210*	0,024	-0,023	-0,037	-0,045
Hearing Impairment	0,066	-0,052	-0,037	0,008	0,037	0,1	0,015	-0,056	0,019	-0,038
Visual Impairment	,323**	-0,04	-0,062	-0,033	,185*	,229*	-0,015	-,202*	-0,066	-0,04
Parkinson Disease	0,089	-0,11	0,021	-0,158	0,115	0,048	-0,102	-,162*	0,044	0,045
Previous Stroke	-0,058	0,054	-0,033	0,053	0,062	,200*	0,035	-0,001	0,026	,180*
Congestive Heart Failure	0,01	0,041	-0,022	0,058	0,034	0,089	0,024	0,037	-,198*	-0,095
Heart Disease	,284**	-0,087	-0,031	-0,084	0,092	0,131	-0,078	-,162*	-0,062	-0,084
Myocardial Infarction	0,017	0,032	0,112	-0,036	-0,105	-0,124	-0,098	0,015	-0,104	0,004
Renal Disease	,380**	-0,051	-0,079	-0,014	,295**	,279**	-0,022	-,235**	-0,153	-0,068
Previous Cancer	,207*	0,065	-0,052	0,089	0,118	0,16	0,005	-0,049	0,076	-0,04
Arthritis / Osteoarthritis	,307**	0,11	-,178*	,255**	,274**	,363**	0,057	-,342**	0,02	0,08
Anxiety / Depression	0,08	0,037	-0,128	0,098	,205*	,304**	0,011	-0,048	-0,009	0,003
Previous fractures / Osteoporosis	,246**	-,275**	-,326**	-0,106	,196*	,240**	0,028	-,266**	-0,1	-0,149
Liver Disease / Hepatopathy	-0,044	0,036	-0,098	0,111	0,105	,205*	-0,032	-0,055	-0,036	-0,081
Dementia / Memory Loss	0,097	0,107	0,112	0,048	0,117	0,123	-0,008	-0,011	-0,124	0,014
Connective Tissue Disease	NA	NA	NA	NA	NA	NA	NA	NA	NA	NA
Hemiplegia	NA	NA	NA	NA	NA	NA	NA	NA	NA	NA
Neoplasm	NA	NA	NA	NA	NA	NA	NA	NA	NA	NA
Leukemia / Malignant Lymphoma	NA	NA	NA	NA	NA	NA	NA	NA	NA	NA
Solid Metastasis	NA	NA	NA	NA	NA	NA	NA	NA	NA	NA
AIDS	NA	NA	NA	NA	NA	NA	NA	NA	NA	NA
Peripheral Vascular Disease	0,058	0,15	,174*	0,042	0,108	0,112	-0,044	-0,002	-0,102	-0,02
Risk Factors										
Smoker	-,208*	0,047	0,116	-0,029	-0,075	0,027	0,005	,181*	-0,005	0,006
Alcohol	-,186*	0,103	0,078	0,075	0,043	-0,024	-0,157	0,096	-0,05	-0,138
Falls	,244**	-0,044	-,229**	0,086	,199*	,198*	0,13	-0,143	-0,026	-0,082
Obesity	0,091	,258**	0,001	,263**	0,14	,234*	,167*	-0,103	0,011	-0,124
Associated with Frailty										
CCI	,671**	0,037	-,146*	0,126	,426**	,626**	-0,052	-,407**	-0,132	-0,009
Estimated 10-year survival	-,673**	-0,032	,149*	-0,122	-,426**	-,627**	0,053	,408**	0,133	0,004
# of visits to PC	0,091	0,047	-0,106	0,118	,229**	,201**	-0,024	-0,095	0,033	-,188**
# of visits to ED	0,05	-0,049	-0,13	0,027	,161*	0,146	0,054	-,169*	0,001	0,07
# of Hospitalizations	-0,001	0,017	0,006	0,008	0,073	0,024	-0,06	-0,002	-0,039	-0,16
Death	,273**	-0,135	-0,073	-0,089	,349**	,370**	-0,101	-,288**	-0,013	-0,112

Abbreviations: BMI: body mass index; MS: muscle strength; MT: muscle thickness; SFT: subcutaneous fat thickness; OPQoL: Older´s People Quality of Life; AU: arbitrary units; DM: diabetes mellitus; COPD: chronic obstructive pulmonary disease; AIDS: auto immune disease syndrome; CCI: Charlson comorbidity index; #: number; PC: primary care; ED: emergency department; NA: Not Applicable.

Tau B of Kendal used for the statistical analysis.

* The correlation is significant at the 0.05 level (bilateral).

** The correlation is significant at the 0.01 level (bilateral).

Table 8.9.2 Correlations of 2017 Comorbidities with Baseline Characteristics (n = 101)										
Variables	***Age (years)***	***Weight (kg)***	***Height (m)***	***BMI (kg/m²)***	***Gait Speed (s)***	***Frailty Phenotype***	***SFT (cm)***	***MT (cm)***	***MS (kg)***	***OPQoL (A.U.)***
Associated Diseases										
Hypertension	,302**	0,132	-,181*	,260**	,241**	,362**	0,144	-,184*	-0,023	-0,05
Hyperlipidemia	,256**	0,109	-0,126	,185*	0,081	,254**	-0,042	-,172*	,184*	-0,033
DM	,283**	0,1	-0,122	,209*	,166*	,252**	-0,021	-,234**	0,046	-0,039
COPD	0,015	0,026	0,027	0,007	0,086	,267**	-0,035	-0,059	-0,063	-0,145
Hearing Impairment	0,08	-0,078	-0,041	-0,02	0,046	0,134	-0,01	-0,093	0,043	-0,058
Visual Impairment	,394**	0,04	-0,032	0,068	,176*	,291**	0,01	-,279**	-0,025	0,03
Parkinson Disease	0,148	-0,122	0,052	-,182*	,172*	0,112	-0,151	-,179*	-0,03	-0,037
Previous Stroke	0,059	-0,071	-0,141	0,029	0,161	,323**	-0,021	-0,139	-0,038	-0,03
Congestive Heart Failure	0,053	0,055	-0,053	0,077	0,12	0,172	0,064	0,002	-0,129	-0,117
Heart Disease	,342**	-0,039	-0,074	-0,02	,179*	,249**	-0,08	-0,137	-0,096	-0,114
Myocardial Infarction	,193*	0,011	0,148	-0,075	,183*	0,177	-,195*	-0,16	-0,058	-0,136
Renal Disease	,472**	0,045	-0,121	0,113	,298**	,286**	0,011	-,231**	-0,026	-0,052
Previous Cancer	,262**	0,015	-0,124	0,1	,193*	,238**	-0,014	-0,139	0,08	-0,127
Arthritis / Osteoarthritis	,336**	0,158	-0,149	,293**	,255**	,376**	0,073	-,310**	0,022	0,088
Anxiety / Depression	0,156	0,06	-0,159	,164*	,195*	,311**	0,056	-0,09	0,008	0,074
Previous fractures / Osteoporosis	,211*	-,211*	-,308**	-0,031	,173*	,215*	,165*	-,280**	-0,007	-0,126
Liver Disease / Hepatopathy	-0,056	0,051	-0,114	0,128	0,096	,205*	0,018	-0,013	-0,043	-0,035
Dementia / Memory Loss	,215**	-0,061	-0,069	-0,06	0,129	,210*	-0,109	-0,161	-0,068	-0,078
Connective Tissue Disease	-0,141	-0,074	0,111	-0,133	-0,115	-0,131	-0,076	0,084	0,02	0,15
Hemiplegia	0,128	-0,107	-0,136	0	0,13	0,123	0,017	-0,135	-0,068	-0,134
Neoplasm	0,03	-0,033	-0,007	-0,021	0,085	0,093	-0,099	-0,139	-0,01	0,015
Leukemia/Malignant Lymphoma	0,058	-,196*	-0,105	-,198*	0,123	0,112	-0,076	-,182*	-0,13	0,017
Solid Metastasis	-0,073	0,073	-0,013	0,084	0,011	-0,05	-0,034	0,068	-0,082	0,099
AIDS	NA	NA	NA	NA	NA	NA	NA	NA	NA	NA
Peripheral Vascular Disease	0,083	,189*	0,027	,172*	0,04	0,114	0,066	0,003	-0,12	0,052
Risk Factors										
Smoker	-,215**	0,047	0,127	-0,034	-0,083	0,02	0,018	,179*	-0,007	0,003
Alcohol	-,186*	0,103	0,078	0,075	0,043	-0,024	-0,157	0,096	-0,05	-0,138
Falls	,298**	-0,016	-,194*	0,114	,183*	,261**	0,125	-0,123	-0,055	-0,106
Obesity	0,062	,303**	0	,313**	0,124	,216*	0,139	-0,007	-0,044	-0,089
Associated with Frailty										
CCI	,642**	0,057	-,184*	,168*	,430**	,574**	-0,041	-,389**	-0,082	-0,065
Estimated 10-year survival	-,643**	-0,059	,195**	-,181*	-,434**	-,595**	0,044	,382**	0,078	0,067
# of visits to PC	,227**	0,114	-0,082	,175*	,275**	,338**	-0,067	-,180**	0,034	-,170*
# of visits to ED	,241**	0,037	-0,047	0,068	,204**	,308**	0,02	-,226**	-0,083	-,156*
# of Hospitalizations	,187*	-0,004	-0,001	-0,002	,203*	,206*	-0,041	-0,135	-,179*	-0,08
Death	,273**	-0,135	-0,073	-0,089	,349**	,370**	-0,101	-,288**	-0,013	-0,112

Abbreviations: BMI: body mass index; MS: muscle strength; MT: muscle thickness; SFT: subcutaneous fat thickness; OPQoL: Older´s People Quality of Life; AU: arbitrary units; DM: diabetes mellitus; COPD: chronic obstructive pulmonary disease; AIDS: acquired immune deficiency syndrome; CCI: Charlson comorbidity index; #: number; PC: primary care; ED: emergency department.

Tau B of Kendal used for the statistical analysis.

* The correlation is significant at the 0.05 level (bilateral).

** The correlation is significant at the 0.05 level (bilateral).

8.10 ANNEX 10: TEXTURE FEATURES CORRELATIONS WITH BASELINE CHARACTERISTICS

Table 8.10.1 Axial Rectus Femoris Textures Features Correlations with Baseline Characteristics (n = 101)

	Texture Features	Age (years)	Weight (kg)	Height (m)	BMI (kg/m²)	Gait Speed (s)	Frailty Criteria	Frailty Phenotype	SFT (cm)	MT (cm)	MS (kg)	OPQoL (A.U.)
IHF	Variance	,197*	-0,157	-0,012	-0,126	0,144	0,105	0,163	-,241*	-0,115	-0,189	-0,085
	Skewness	-,433**	-0,019	0,095	-0,114	-,258**	-0,15	-,340**	0,095	,343**	0,047	0,079
	Kurtosis	-,408**	0,025	0,083	-0,065	-,293**	-,199*	-,357**	0,144	,339**	0,067	0,115
GLCM	Energy	-,365**	0,086	0,096	-0,015	-,251*	-,217*	-,317**	,263**	,322**	0,096	-0,002
	Contrast	0,011	-0,157	-0,021	-0,122	0,051	0,067	0,036	-,230*	-0,052	-0,051	0,026
	Entropy	,230*	-0,139	-0,054	-0,07	0,165	0,136	,209*	-,315**	-,229*	-0,113	-0,02
	Homogeneity	-0,185	0,129	0,123	0,021	-0,182	-0,184	-,204*	0,154	,205*	0,048	-0,025
	Correlation	0,131	0,013	0,016	0,01	0,007	-0,044	0,045	-0,099	-0,070	-0,068	-0,084
	Sum Average	,362**	-0,070	0,010	-0,044	,196*	0,128	,276**	-,353**	-,300**	-0,136	-0,032
	Variance	0,114	-0,132	0,059	-0,138	0,032	0,014	0,071	-,369**	-0,102	-0,107	-0,037
	Dissimilarity	0,053	-0,166	-0,054	-0,108	0,083	0,099	0,081	-,210*	-0,112	-0,044	0,033
	Auto-Correlation	,327**	-0,087	0,016	-0,067	0,164	0,103	,240*	-,370**	-,273**	-0,133	-0,029
GLRLM	Short Run Emphasis	,253*	-0,129	-0,133	-0,014	,244*	,216*	,264**	-0,17	-,283**	-0,054	0,024
	Long Run Emphasis	-,299**	0,024	0,140	-0,100	-,264**	-,247*	-,325**	0,095	,242*	0,066	-0,045
	Gray-Level Nonuniformity	-,303**	0,085	0,004	0,048	-0,159	-0,117	-,228*	,353**	,209*	0,153	0,045
	Run Length Nonuniformity	,253*	-0,136	-0,133	-0,022	,246*	,218*	,264**	-0,173	-,287**	-0,056	0,023
	Run Percentage	,291**	-0,078	-0,144	0,044	,266**	,238*	,305**	-0,131	-,277**	-0,056	0,036
	Low Gray-Level Run Emphasis	-,477**	0,057	0,014	0,014	-,322**	-,239*	-,397**	,274**	,466**	0,063	0,002
	High Gray-Level Run Emphasis	,315**	-0,093	0,02	-0,074	0,156	0,095	,229*	-,368**	-,262**	-0,126	-0,027
	Short Run Low Gray-Level	-,501**	0,049	0	0,021	-,324**	-,238*	-,400**	,307**	,479**	0,087	0,025
	Short Run High Gray-Level	,309**	-0,099	0,01	-0,075	0,157	0,095	,227*	-,366**	-,267**	-0,125	-0,028
	Long Run Low Gray-Level	-,201*	-0,031	0,129	-0,139	-,250*	-0,185	-,301**	-0,039	,208*	0,062	-0,066
	Long Run High Gray-Level	,317**	-0,084	0,05	-0,087	0,142	0,074	,216*	-,381**	-,267**	-0,134	-0,03
	Gray-Level Variance	,429**	0,030	-0,12	0,118	,263**	,255*	,426**	-0,037	-,339**	-0,093	0,085
	Run-Length Variance	0,190	0,158	-0,056	0,191	0,174	0,168	,242*	,227*	-0,139	0,136	0,129
GLSZM	Small Zone Emphasis	0,168	-0,154	-0,087	-0,068	0,171	0,155	0,162	-,207*	-0,174	-0,075	0,03
	Large Zone Emphasis	-,285**	0,007	0,125	-0,108	-,248*	-,231*	-,321**	0,089	,238*	0,070	-0,032
	Gray-Level Nonuniformity	-,238*	0,092	-0,032	0,081	-0,116	-0,084	-0,18	,369**	0,154	0,134	0,037
	Zone-Size Nonuniformity	0,167	-0,156	-0,086	-0,071	0,171	0,153	0,161	-,209*	-0,175	-0,075	0,031
	Zone Percentage	,245*	-0,096	-0,12	0,014	,229*	,215*	,254*	-0,153	-,220*	-0,078	0,028
	Low Gray-Level Zone Emphasis	-,496**	0,107	0,041	0,063	-,355**	-,236*	-,404**	,320**	,503**	0,097	0,035
	High Gray-Level Zone Emphasis	,306**	-0,094	0,030	-0,085	0,149	0,086	,222*	-,380**	-,258**	-0,128	-0,024
	Small Zone Low Gray-Level Zone Emphasis	-,495**	0,118	0,040	0,073	-,362**	-,228*	-,413**	,355**	,495**	0,12	0,027
	Small Zone High Gray-Level Zone Emphasis	,299**	-0,103	0,022	-0,089	0,156	0,096	,222*	-,374**	-,255**	-0,129	-0,028
	Large Zone Low Gray-Level Zone Emphasis	-0,092	-0,062	0,163	-,198*	-0,162	-0,141	-,242*	-0,123	0,113	0,028	-0,104
	Large Zone High Gray-Level Zone Emphasis	,225*	-0,059	0,102	-0,106	0,056	0,011	0,146	-,389**	-,201*	-0,107	-0,098
	Grey-Level Variance	,246*	0,026	-0,089	0,121	0,190	0,147	,290**	-0,063	-,243*	-0,055	0,049
	Zone-Size Variance	0,052	0,152	-0,046	,214*	0,038	0,053	0,141	0,183	-0,075	0,085	0,111
NGTDM	Coarseness	,250*	0,128	-0,011	0,157	0,088	0,13	,197*	0,106	-0,141	-0,041	-0,085
	Contrast	-0,052	-0,162	-0,047	-0,109	0,013	0,049	-0,01	-0,166	0,043	-0,062	0,009
	Busyness	-,377**	-0,033	0,027	-0,074	-0,18	-0,182	-,303**	0,125	,264**	0,111	0,095
	Complexity	0,101	-0,167	-0,020	-0,126	0,076	0,072	0,103	-,286**	-0,124	-0,102	-0,016
	Strength	,203*	-0,020	0,022	-0,018	0,092	0,114	0,159	-0,152	-0,121	-0,108	-0,064

Abbreviations: BMI: body mass index; MS: muscle strength; MT: muscle thickness; SFT: subcutaneous fat thickness; OPQoL: Older´s People Quality of Life; AU: arbitrary anits; IHF: Intensity Histogram Features; GLCM: Gray-Level Co-occurrence Matrix; GLRLM: Gray-Level run-Length Matrix; GLSZM: Gray-Level Size Zone Matrix; NGTDM: Neighborhood Gray-Tone Difference Matrix.

Rho of Spearman used for the statistical analysis

* The correlation is significant at the 0.05 level (bilateral).

** The correlation is significant at the 0.01 level (bilateral).

Table 8.10.2 Sagittal Rectus Femoris Texture Features Correlations with Baseline Characteristics (n = 101)												
	Texture Feature	*Age (years)*	*Weight (kg)*	*Height (m)*	*BMI (kg/m²)*	*Gait Speed (s)*	*Frailty Criteria*	*Frailty Phenotype*	*SFT (cm)*	*MT (cm)*	*MS (kg)*	*OPQoL (A.U.)*
IHF	Variance	0,109	-0,194	0,005	-,199*	0,006	0,057	0,087	-0,053	-,223*	-0,021	-0,015
	Skewness	-0,176	-0,054	0,064	-0,123	-0,088	-0,1	-0,149	-0,05	0,078	0,056	0,165
	Kurtosis	-,231*	0,011	0,034	-0,033	-0,100	-0,133	-0,19	0	0,170	0,058	0,178
GLCM	Energy	-,258**	0,083	0,144	-0,038	-,229*	-,222*	-,260**	0,085	,259**	0,074	0,086
	Contrast	0,045	-0,073	-0,036	-0,041	0,103	0,134	0,127	-0,069	-0,071	-0,014	0,010
	Entropy	0,195	-0,121	-0,108	-0,038	0,193	0,184	,217*	-0,098	-,219*	-0,085	-0,076
	Homogeneity	-,206*	0,087	0,155	-0,029	-,235*	-,260**	-,251*	-0,005	,223*	0,040	0,0310
	Correlation	0,023	-0,056	0,094	-0,122	-0,152	-,277**	-0,193	-0,06	-0,001	-0,077	-0,064
	Sum Average	,204*	-0,048	-0,049	0,002	0,192	0,149	,231*	-0,126	-,199*	-0,109	-0,157
	Variance	0,072	-0,166	-0,01	-0,157	0,04	0,015	0,06	-0,168	-0,104	-0,075	-0,019
	Dissimilarity	0,075	-0,097	-0,069	-0,046	0,132	0,166	0,155	-0,063	-0,120	-0,007	-0,002
	Auto-Correlation	0,178	-0,082	-0,044	-0,041	0,172	0,131	,206*	-0,14	-0,194	-0,108	-0,147
GLRLM	Short Run Emphasis	,291**	-0,088	-0,181	0,051	,305**	,301**	,317**	-0,01	-,319**	-0,059	-0,043
	Long Run Emphasis	-,334**	0,003	0,174	-0,135	-,332**	-,341**	-,376**	-0,003	,257**	0,107	0,058
	Gray-Level Nonuniformity	-,212*	0,102	0,100	0,028	-0,149	-0,120	-0,192	0,119	0,185	0,109	0,108
	Run Length Nonuniformity	,289**	-0,094	-0,183	0,047	,305**	,301**	,316**	-0,010	-,320**	-0,058	-0,044
	Run Percentage	,319**	-0,045	-0,17	0,092	,319**	,322**	,351**	-0,018	-,297**	-0,087	-0,052
	Low Gray-Level Run Emphasis	-,290**	-0,061	0,100	-0,169	-,243*	-0,184	-,300**	0,04	,253*	0,023	0,113
	High Gray-Level Run Emphasis	0,177	-0,088	-0,042	-0,048	0,170	0,128	,204*	-0,15	-0,187	-0,106	-0,141
	Short Run Low Gray-Level	-,295**	-0,075	0,094	-0,175	-,223*	-0,151	-,279**	0,037	,245*	0,043	0,105
	Short Run High Gray-Level	0,181	-0,093	-0,045	-0,051	0,175	0,135	,209*	-0,147	-0,189	-0,109	-0,135
	Long Run Low Gray-Level	-0,131	0,010	0,110	-0,075	-0,153	-0,161	-,221*	-0,046	0,152	-0,009	0,033
	Long Run High Gray-Level	0,145	-0,098	-0,019	-0,078	0,132	0,078	0,161	-0,154	-0,184	-0,099	-0,151
	Gray-Level Variance	0,127	0,083	-0,156	,203*	,214*	0,183	,200*	0,139	-0,075	-0,053	-,306**
	Run-Length Variance	-0,012	0,137	-0,027	0,150	0,060	0,033	0,017	0,157	0,043	0,037	-0,128
GLSZM	Small Zone Emphasis	,214*	-0,111	-0,132	-0,014	,238*	,244*	,241*	-0,043	-,232*	-0,047	-0,017
	Large Zone Emphasis	-,350**	0,005	0,191	-0,139	-,350**	-,369**	-,403**	-0,003	,296**	0,096	0,056
	Gray-Level Nonuniformity	-0,150	0,140	0,068	0,090	-0,089	-0,060	-0,133	0,157	0,150	0,117	0,084
	Zone-Size Nonuniformity	,211*	-0,112	-0,129	-0,016	,235*	,241*	,240*	-0,046	-,230*	-0,043	-0,015
	Zone Percentage	,284**	-0,056	-0,156	0,068	,288**	,296**	,311**	-0,023	-,246*	-0,087	-0,029
	Low Gray-Level Zone Emphasis	-,307**	-0,052	0,05	-0,129	-,269**	-,226*	-,340**	0,127	,288**	0,026	0,16
	High Gray-Level Zone Emphasis	0,164	-0,094	-0,036	-0,062	0,163	0,116	0,192	-0,16	-0,169	-0,106	-0,134
	Small Zone Low Gray-Level Zone Emphasis	-,252*	-0,049	0,007	-0,097	-,244*	-,198*	-,305**	0,16	,255**	0,006	0,18
	Small Zone High Gray-Level Zone Emphasis	0,169	-0,093	-0,041	-0,055	0,166	0,125	,200*	-0,158	-0,167	-0,104	-0,121
	Large Zone Low Gray-Level Zone Emphasis	-0,109	0,016	0,104	-0,036	-0,185	-0,166	-,200*	-0,021	0,132	0,04	0,035
	Large Zone High Gray-Level Zone Emphasis	0,045	-0,122	0,045	-0,148	-0,006	-0,085	0,009	-0,165	-0,16	-0,021	-0,150
	Grey-Level Variance	0,151	0,012	-0,152	0,114	0,233*	0,248*	,312**	0,049	-,211*	-0,112	-0,176
	Zone-Size Variance	0,008	0,070	-0,131	0,149	0,116	0,151	0,193	0,148	-0,120	-0,069	-0,034
NGTDM	Coarseness	0,17	0,078	-0,018	0,087	0,053	0,049	0,108	0,131	-0,174	-0,014	-0,136
	Contrast	0,021	-0,081	-0,06	-0,039	0,054	0,125	0,074	-0,001	-0,004	-0,007	0,028
	Busyness	-0,168	-0,025	0,042	-0,054	-0,108	-0,094	-0,176	-0,043	,201*	0,084	0,178
	Complexity	0,074	-0,114	-0,041	-0,081	0,126	0,121	0,14	-0,093	-0,113	-0,060	-0,035
	Strength	0,078	-0,075	0,014	-0,099	0,028	0,006	0,067	-0,029	-0,175	-0,029	-0,071

Abbreviations: BMI: body mass index; MS: muscle strength; MT: muscle thickness; SFT: subcutaneous fat thickness; OPQoL: Older´s People Quality of Life; AU: arbitrary anits; IHF: Intensity Histogram Features; GLCM: Gray-Level Co-occurrence Matrix; GLRLM: Gray-Level run-Length Matrix; GLSZM: Gray-Level Size Zone Matrix; NGTDM: Neighborhood Gray-Tone Difference Matrix.

Rho of Spearman used for the statistical analysis

* The correlation is significant at the 0.05 level (bilateral).

** The correlation is significant at the 0.01 level (bilateral).

Table 8.10.3 Axial Vastus Intermedius Textures Features Correlations with Baseline Characteristics (n = 101)

	Texture Feature	Age (years)	Weight (kg)	Height (m)	BMI (kg/m²)	Gait Speed (s)	Frailty Criteria	Frailty Phenotype	SFT (cm)	MT (cm)	MS (kg)	OPQoL (A.U.)
IHF	Variance	,150*	-,180**	-0,067	-,177**	0,072	-0,022	0,066	-0,073	-,296**	-0,012	-0,012
	Skewness	-,320**	,152*	,151*	0,064	-,272**	-,216**	-,320**	0,013	,419**	0,008	0,065
	Kurtosis	-,300**	,179**	0,113	0,112	-,235**	-,171*	-,273**	0,044	,406**	0,013	0,056
GLCM	Energy	-,412**	,144*	,169*	0,019	-,398**	-,382**	-,461**	0,043	,511**	0,052	0,117
	Contrast	,175*	-0,075	0,058	-0,082	,163*	0,074	,156*	-,158*	-,231**	-0,070	0,005
	Entropy	,386**	-,148*	-0,09	-0,071	,349**	,286**	,384**	-0,107	-,507**	-0,070	-0,086
	Homogeneity	-,366**	0,122	0,124	0,027	-,360**	-,313**	-,393**	0,022	,468**	0,061	0,076
	Correlation	,207**	-,147*	-0,001	-,164*	0,123	0,08	,181*	-,261**	-,333**	-0,065	-0,037
	Sum Average	,418**	-,155*	-0,1	-0,085	,389**	,343**	,452**	-,147*	-,534**	-0,063	-0,114
	Variance	,264**	-0,13	0,045	-,150*	,200**	0,096	,200**	-,274**	-,370**	-0,079	-0,026
	Dissimilarity	,273**	-0,107	-0,01	-0,07	,258**	,171*	,261**	-0,097	-,373**	-0,050	-0,014
	Auto-Correlation	,403**	-,155*	-0,071	-0,106	,361**	,301**	,413**	-,178**	-,515**	-0,071	-0,108
GLRLM	Short Run Emphasis	,358**	-,138*	-0,11	-0,053	,342**	,279**	,368**	-0,052	-,468**	-0,060	-0,066
	Long Run Emphasis	-,372**	0,11	,178**	-0,01	-,386**	-,379**	-,431**	-0,03	,441**	0,047	0,101
	Gray-Level Nonuniformity	-,374**	,145*	0,04	0,112	-,307**	-,223**	-,348**	,202**	,502**	0,062	0,081
	Run Length Nonuniformity	,357**	-,134*	-0,107	-0,053	,338**	,274**	,365**	-0,054	-,465**	-0,053	-0,067
	Run Percentage	,388**	-0,118	-,168*	0	,383**	,362**	,437**	0	-,478**	-0,052	-0,09
	Low Gray-Level Run Emphasis	-,424**	0,100	,145*	-0,008	-,427**	-,405**	-,504**	0,025	,487**	0,063	0,113
	High Gray-Level Run Emphasis	,376**	-,158*	-0,04	-0,12	,328**	,255**	,378**	-,210**	-,478**	-0,067	-0,103
	Short Run Low Gray-Level	-,421**	0,088	0,118	-0,005	-,425**	-,385**	-,508**	0,06	,489**	0,063	,138*
	Short Run High Gray-Level	,374**	-,158*	-0,041	-0,121	,329**	,256**	,378**	-,212**	-,473**	-0,066	-0,103
	Long Run Low Gray-Level	-,381**	0,092	,176*	-0,018	-,391**	-,393**	-,446**	-0,042	,423**	0,063	0,101
	Long Run High Gray-Level	,380**	-,144*	-0,051	-0,104	,341**	,277**	,406**	-,210**	-,494**	-0,067	-0,118
	Gray-Level Variance	,389**	-0,124	-,166*	-0,019	,391**	,383**	,455**	-0,001	-,453**	-0,057	-0,103
	Run-Length Variance	0,123	0,003	-,176*	0,093	,153*	,221**	,171*	,211**	-0,068	0,01	-0,014
GLSZM	Small Zone Emphasis	0,071	-0,079	0,108	-,139*	0,079	-0,035	0,012	-,209**	-0,098	-0,059	-0,045
	Large Zone Emphasis	-,368**	0,113	,184**	-0,013	-,374**	-,369**	-,426**	-0,055	,436**	0,048	0,095
	Gray-Level Nonuniformity	-,356**	,138*	0,015	0,123	-,291**	-,189*	-,321**	,229**	,468**	0,072	0,069
	Zone-Size Nonuniformity	0,070	-0,080	0,107	-,138*	0,078	-0,035	0,012	-,208**	-0,098	-0,06	-0,045
	Zone Percentage	,363**	-,137*	-0,113	-0,046	,349**	,292**	,377**	-0,056	-,469**	-0,065	-0,066
	Low Gray-Level Zone Emphasis	-,422**	0,120	0,112	0,024	-,423**	-,388**	-,508**	0,086	,507**	0,058	,147*
	High Gray-Level Zone Emphasis	,369**	-,154*	-0,028	-0,123	,319**	,247**	,370**	-,227**	-,469**	-0,072	-0,102
	Small Zone Low Gray-Level Zone Emphasis	-,433**	0,127	0,133	0,027	-,418**	-,406**	-,519**	0,085	,525**	0,058	,140*
	Small Zone High Gray-Level Zone Emphasis	,359**	-,151*	-0,02	-0,125	,310**	,232**	,355**	-,240**	-,446**	-0,069	-0,094
	Large Zone Low Gray-Level Zone Emphasis	-,359**	0,099	,180**	-0,012	-,365**	-,359**	-,418**	-0,063	,405**	0,059	0,086
	Large Zone High Gray-Level Zone Emphasis	0,057	-0,054	0,071	-0,109	0,043	0,049	0,104	-,247**	-0,132	-0,072	-,174*
	Grey-Level Variance	,372**	-0,104	-,145*	0,006	,358**	,354**	,429**	0,023	-,437**	-0,054	-0,102
	Zone-Size Variance	0,002	0,054	-0,091	0,097	0,022	0,103	0,102	,142*	0,05	-0,021	-0,134
NGTDM	Coarseness	,245**	0,004	-0,105	0,075	,265**	,252**	,325**	0,017	-,323**	-0,053	-,146*
	Contrast	,200**	-0,081	0,054	-0,09	,145*	0,038	0,119	-0,128	-,310**	-0,034	0,041
	Busyness	-,397**	0,096	0,113	0,023	-,387**	-,348**	-,453**	0,104	,494**	0,064	0,135
	Complexity	,290**	-0,123	0,007	-0,111	,238**	,167*	,258**	-,200**	-,393**	-0,073	-0,032
	Strength	0,109	-0,052	0,085	-0,103	0,086	0,047	0,114	-,289**	-,147*	-0,106	-0,075

Abbreviations: BMI: body mass index; MS: muscle strength; MT: muscle thickness; SFT: subcutaneous fat thickness; OPQoL: Older´s People Quality of Life; AU: arbitrary anits; IHF: Intensity Histogram Features; GLCM: Gray-Level Co-occurrence Matrix; GLRLM: Gray-Level run-Length Matrix; GLSZM: Gray-Level Size Zone Matrix; NGTDM: Neighborhood Gray-Tone Difference Matrix.

Rho of Spearman used for the statistical analysis

* The correlation is significant at the 0.05 level (bilateral).

** The correlation is significant at the 0.01 level (bilateral).

Table 8.10.4 Sagittal Vastus Intermedius Textures Features Correlations with Baseline Characteristics (n = 101)

	Texture Feature	Age (years)	Weight (kg)	Height (m)	BMI (kg/m²)	Gait Speed (s)	Frailty Criteria	Frailty Phenotype	SFT (cm)	MT (cm)	MS (kg)	OPQoL (A.U.)
IHF	Variance	0,172	-,252*	0,017	-,306**	,221*	0,183	0,183	-,218*	-,347**	-0,142	-0,139
	Skewness	-,536**	0,158	,205*	0,033	-,458**	-,367**	-,499**	0,003	,673**	-0,005	0,171
	Kurtosis	-,473**	,206*	0,153	0,132	-,407**	-,341**	-,457**	0,076	,640**	0,045	0,193
GLCM	Energy	-,495**	,247*	0,158	0,146	-,518**	-,402**	-,505**	0,116	,781**	-0,012	0,179
	Contrast	0,158	-,277**	0,063	-,309**	,242*	0,138	0,178	-,279**	-,467**	-0,129	-0,026
	Entropy	,443**	-,274**	-0,093	-,212*	,459**	,342**	,455**	-,219*	-,736**	-0,077	-0,123
	Homogeneity	-,437**	,275**	0,096	,207*	-,453**	-,349**	-,443**	0,153	,747**	0,055	0,097
	Correlation	,249*	-0,102	-0,114	-0,081	0,189	0,093	,210*	-,273**	-0,182	-0,0990	-0,082
	Sum Average	,497**	-,283**	-0,150	-0,191	,522**	,386**	,509**	-,223*	-,766**	-0,048	-0,152
	Variance	,248*	-,257**	0,038	-,301**	,310**	0,170	,265**	-,402**	-,501**	-0,168	-0,067
	Dissimilarity	,276**	-,293**	0,006	-,292**	,322**	,230*	,295**	-,249*	-,598**	-0,126	-0,049
	Auto-Correlation	,456**	-,292**	-0,113	-,231*	,486**	,349**	,469**	-,276**	-,732**	-0,070	-0,132
GLRLM	Short Run Emphasis	,439**	-,283**	-0,096	-,219*	,458**	,341**	,442**	-0,179	-,742**	-0,079	-0,095
	Long Run Emphasis	-,477**	,235*	0,141	0,141	-,522**	-,416**	-,509**	0,091	,760**	-0,025	0,158
	Gray-Level Nonuniformity	-,449**	,261**	0,084	,215*	-,456**	-,304**	-,435**	,295**	,691**	0,118	0,116
	Run Length Nonuniformity	,429**	-,286**	-0,092	-,224*	,452**	,331**	,433**	-0,185	-,738**	-0,079	-0,093
	Run Percentage	,470**	-,251*	-0,13	-0,163	,493**	,394**	,488**	-0,112	-,769**	-0,014	-0,137
	Low Gray-Level Run Emphasis	-,510**	,201*	0,152	0,086	-,543**	-,431**	-,552**	0,099	,752**	-0,025	0,16
	High Gray-Level Run Emphasis	,423**	-,286**	-0,079	-,246*	,468**	,320**	,441**	-,312**	-,698**	-0,074	-0,119
	Short Run Low Gray-Level	-,502**	0,194	0,143	0,083	-,536**	-,411**	-,543**	0,117	,748**	-0,026	0,162
	Short Run High Gray-Level	,419**	-,288**	-0,075	-,249*	,464**	,316**	,436**	-,317**	-,693**	-0,078	-0,118
	Long Run Low Gray-Level	-,486**	0,182	0,137	0,091	-,512**	-,413**	-,506**	0,018	,698**	-0,028	0,146
	Long Run High Gray-Level	,437**	-,296**	-0,103	-,241*	,473**	,327**	,447**	-,299**	-,712**	-0,070	-0,141
	Gray-Level Variance	,516**	-0,180	-0,116	-0,105	,529**	,418**	,543**	-0,094	-,727**	0,026	-0,14
	Run-Length Variance	,227*	0,089	-0,084	0,152	0,192	,201*	,265**	,277**	-,221*	0,164	-0,005
GLSZM	Small Zone Emphasis	0,126	-0,189	0,156	-,283**	0,187	0,061	0,113	-,370**	-,332**	-0,092	-0,012
	Large Zone Emphasis	-,464**	,243*	0,159	0,131	-,530**	-,424**	-,510**	0,069	,757**	-0,024	0,177
	Gray-Level Nonuniformity	-,415**	,273**	0,049	,254*	-,429**	-,268**	-,402**	,336**	,655**	0,126	0,097
	Zone-Size Nonuniformity	0,125	-0,19	0,158	-,285**	0,185	0,059	0,111	-,370**	-,331**	-0,094	-0,012
	Zone Percentage	,442**	-,277**	-0,085	-,221*	,457**	,345**	,441**	-,200*	-,724**	-0,072	-0,092
	Low Gray-Level Zone Emphasis	-,512**	,228*	0,143	0,124	-,540**	-,411**	-,545**	0,16	,767**	-0,009	0,158
	High Gray-Level Zone Emphasis	,418**	-,289**	-0,077	-,248*	,466**	,313**	,434**	-,323**	-,688**	-0,076	-0,12
	Small Zone Low Gray-Level Zone Emphasis	-,515**	,228*	0,15	0,121	-,534**	-,413**	-,543**	0,153	,771**	-0,011	0,165
	Small Zone High Gray-Level Zone Emphasis	,400**	-,288**	-0,059	-,258**	,448**	,295**	,415**	-,338**	-,674**	-0,076	-0,107
	Large Zone Low Gray-Level Zone Emphasis	-,463**	0,180	0,137	0,089	-,492**	-,410**	-,501**	0	,684**	-0,021	0,164
	Large Zone High Gray-Level Zone Emphasis	0,090	-0,078	-0,069	-0,052	0,100	0,007	0,117	-,214*	-0,179	0,137	-0,092
	Grey-Level Variance	,492**	-,236*	-0,161	-0,126	,553**	,454**	,543**	-0,084	-,759**	0,026	-0,181
	Zone-Size Variance	0,184	-0,033	-0,068	0,039	,196*	0,185	,238*	0,08	-,220*	,242*	-0,145
NGTDM	Coarseness	,332**	-0,036	-0,113	0,048	,340**	,261**	,360**	0,026	-,469**	-0,039	-0,089
	Contrast	0,157	-,240*	0,059	-,290**	,212*	0,136	0,17	-,268**	-,409**	-,207*	-0,023
	Busyness	-,490**	,228*	0,157	0,13	-,518**	-,412**	-,532**	0,167	,730**	0,020	0,147
	Complexity	,273**	-,294**	-0,006	-,296**	,354**	,235*	,305**	-,323**	-,576**	-0,136	-0,073
	Strength	0,127	-,206*	0,061	-,269**	,243*	0,156	,220*	-,367**	-,325**	-0,147	-0,029

Abbreviations: BMI: body mass index; MS: muscle strength; MT: muscle thickness; SFT: subcutaneous fat thickness; OPQoL: Older´s People Quality of Life; AU: arbitrary anits; IHF: Intensity Histogram Features; GLCM: Gray-Level Co-occurrence Matrix; GLRLM: Gray-Level run-Length Matrix; GLSZM: Gray-Level Size Zone Matrix; NGTDM: Neighborhood Gray-Tone Difference Matrix.

Rho of Spearman used for the statistical analysis

* The correlation is significant at the 0.05 level (bilateral).

** The correlation is significant at the 0.01 level (bilateral).

8.11 ANNEX 11: CORRELATIONS OF TEXTURE FEATURES WITH ASSOCIETED DISEASES, RISK FACTORS, VARIABLES ASSOCIETED WITH FRAILTY, AND DEATH

Table 8.11.1 Axial Rectus Femoris Textures Features Correlations with Associated Diseases, Risk Factors, variables associated with frailty, and death (n = 101)

	Texture Feature	Hypertension	Hyperlipidemia	DM	COPD	Hearing Impairment	Visual Impairment	Parkinson Disease	Previous Stroke	Congestive Heart Failure	Heart Disease	Myocardial Infarction	Renal Disease	Previous Cancer	Artritis/Osteo arthitis	Anxiety/Depression	Previous Fracture	Liver Disease	Dementia/Memory Loss	Connective Tissue Disease	Hemiplagia	Neoplasm	Leukemia	Solid Metastasis	Peripheral Vascular Disease	CCI	Estimated Survival	Smoker	Falls	Obesity	# of Visits to PC	# of Visits to ED	# of Hospitalizations	Death
IHF	Variance	-0,031	-0,025	-0,048	-0,035	,188*	0,021	0,045	0,127	-0,068	0,158	,195*	0,005	0,042	0,068	-0,001	-0,086	0,127	0,121	-0,049	0,132	0,083	-0,052	0,076	-0,020	0,014	0,072	0,124	0,149	-0,092	-0,064	0,038	0,088	,194*
	Skewness	-0,027	-0,138	0,049	0,052	-0,146	-,215**	-0,028	-,179*	-0,058	-0,117	-,190*	-,161*	-0,058	-0,108	-0,109	0,035	-0,121	-0,047	,199*	-0,101	-0,086	-0,034	0,011	-0,051	-,155*	,161*	0,017	-0,157	0,003	0,026	0,047	-0,037	-,247**
	Kurtosis	0,012	-0,037	0,079	0,056	-,190*	-,189*	-0,017	-,173*	-0,028	-,168*	-,230**	-0,094	-0,063	-0,099	-0,082	0,022	-0,121	-0,094	,194*	-0,124	-0,108	-0,002	-0,020	-0,007	-0,104	0,067	-0,065	-,175*	0,023	0,028	0,028	-0,071	-,272**
GLCM	Energy	0,099	0,049	-0,015	0,016	-,198*	-0,120	-0,059	-,177*	-0,004	-,167*	-,166*	-0,061	-0,088	-0,064	-0,103	0,000	-0,127	-0,152	0,090	-0,135	-0,107	-0,044	-0,087	-0,007	-0,093	0,049	-0,110	-,217**	-0,032	-0,052	-0,057	-0,077	-,241**
	Contrast	-0,131	-0,155	0,025	-0,021	0,148	-0,049	0,042	0,067	-0,056	0,042	0,015	-0,095	0,036	-0,066	0,018	0,033	0,096	0,140	0,048	0,062	0,007	0,032	0,110	-0,061	-0,061	0,098	0,135	0,080	0,006	-0,001	0,083	0,011	0,049
	Entropy	-0,118	-0,096	0,006	-0,021	,196*	0,060	0,042	0,156	-0,056	0,138	0,105	0,009	0,070	0,031	0,072	-0,001	0,124	,174*	-0,036	0,132	0,069	0,042	0,113	-0,036	0,036	0,008	0,127	,199*	0,013	0,022	0,089	0,048	,168*
	Homogeneity	0,156	0,134	0,001	0,033	-,182*	-0,016	-0,014	-0,103	-0,032	-0,107	-0,071	-0,007	-0,039	0,008	-0,046	-0,072	-0,121	-0,141	0,033	-0,099	-0,054	-0,042	-0,090	-0,007	-0,030	-0,004	-0,135	-,162*	-0,047	-0,017	-0,042	0,008	-,164*
	Correlation	,227**	0,151	-0,072	-0,059	0,068	0,077	-0,017	0,134	-0,102	0,041	0,054	0,124	0,035	,167*	0,059	-0,105	0,011	0,000	-0,062	0,124	0,050	-0,018	-0,051	0,002	0,071	-0,036	-0,107	0,118	-0,046	-0,006	-0,023	0,094	0,051
	Sum Average	-0,072	-0,017	0,010	0,002	,198*	0,139	0,062	,189*	-0,080	0,113	,192*	0,070	0,070	0,094	0,120	-0,042	0,132	,164*	-0,072	0,135	0,100	0,052	0,090	-0,033	0,129	-0,064	0,101	,222**	0,000	0,041	0,065	0,075	,227**
	Variance	-0,024	-0,066	-0,021	-0,035	,196*	0,031	0,020	0,141	-0,136	0,109	0,110	-0,022	0,066	0,071	0,057	-0,035	0,110	,169*	0,016	0,138	0,047	0,008	0,087	-0,067	-0,011	0,070	0,124	,194*	-0,020	0,005	0,118	0,082	0,109
	Dissimilarity	-0,152	-0,156	0,012	-0,031	,164*	-0,036	0,031	0,087	-0,038	0,054	0,029	-0,071	0,049	-0,055	0,032	0,043	0,107	0,142	0,031	0,068	0,021	0,044	0,104	-0,038	-0,031	0,071	0,138	0,100	0,015	0,012	0,073	0,006	0,085
	Auto-Correlation	-0,059	-0,026	-0,001	-0,012	,198*	0,126	0,056	,183*	-0,104	0,115	,176*	0,059	0,085	0,094	0,109	-0,048	0,132	,174*	-0,051	0,135	0,096	0,048	0,093	-0,031	0,109	-0,047	0,101	,220**	-0,009	0,035	0,074	0,081	,202*
GLRLM	Short Run Emphasis	-0,160	-0,120	0,005	-0,023	,180*	0,048	0,014	0,114	0,088	0,136	0,110	0,032	0,045	0,001	0,048	0,061	0,115	0,147	-0,062	0,104	0,096	0,050	0,093	0,038	0,058	-0,017	0,138	,163*	0,042	0,030	0,028	0,004	,206*
	Long Run Emphasis	,179*	0,113	0,040	0,028	-,176*	-0,081	0,003	-0,090	-0,082	-0,132	-0,097	-0,081	-0,018	0,011	-0,056	-0,098	-0,118	-0,152	0,054	-0,096	-0,077	-0,038	-0,082	-0,052	-0,081	0,052	-0,110	-,180*	-0,086	-0,059	-0,022	-0,030	-,202*
	Gray-Level Nonuniformity	0,027	0,023	-0,005	0,023	-,194*	-0,107	-0,053	-,169*	0,098	-,169*	-0,157	-0,038	-0,082	-0,099	-0,095	0,056	-0,127	-0,160	0,103	-0,141	-0,081	-0,028	-0,084	0,034	-0,061	0,004	-0,101	-,230**	-0,010	-0,018	-0,096	-0,105	-,197*
	Run Length Nonuniformity	-0,156	-0,121	0,009	-0,022	,180*	0,047	0,023	0,120	0,086	0,136	0,113	0,029	0,048	0,001	0,046	0,058	0,115	0,145	-0,062	0,107	0,099	0,050	0,093	0,033	0,057	-0,016	0,138	,164*	0,040	0,026	0,026	0,003	,208*
	Run Percentage	-,169*	-0,121	-0,016	-0,025	,178*	0,067	0,006	0,103	0,088	0,140	0,097	0,054	0,029	-0,006	0,052	0,082	0,115	0,155	-0,056	0,101	0,089	0,046	0,087	0,047	0,075	-0,041	0,127	,171*	0,063	0,047	0,023	0,014	,201*
	Low Gray-Level Run Emphasis	0,119	-0,066	0,011	-0,109	-,178*	-0,145	-0,141	-,223**	-0,052	-0,026	-,232**	-0,064	-0,149	0,068	-,172*	0,032	-0,082	-0,125	0,064	-0,104	-0,130	-0,054	-0,048	-0,008	-,167*	0,098	-0,059	-,188*	-0,020	-,145*	0,007	-0,026	-,230**
	High Gray-Level Run Emphasis	-0,064	-0,036	0,001	-0,012	,198*	0,119	0,059	,181*	-0,104	0,115	,172*	0,051	0,082	0,091	0,107	-0,049	0,132	,176*	-0,046	0,135	0,091	0,046	0,093	-0,036	0,100	-0,038	0,104	,221**	-0,012	0,035	0,079	0,074	,200*
	Short Run Low Gray-Level	0,092	-0,074	-0,021	-0,089	-,180*	-0,140	-0,138	-,224**	-0,040	-0,045	-,250**	-0,053	-0,149	0,034	-,175*	0,046	-0,076	-0,114	0,069	-0,104	-,169*	-0,062	-0,053	-0,008	-,190*	0,110	-0,031	-,180*	-0,012	-,162*	-0,015	-0,046	-,233**
	Short Run High Gray-Level	-0,071	-0,032	0,002	-0,009	,198*	0,119	0,062	,183*	-0,100	0,111	,167*	0,053	0,088	0,084	0,104	-0,048	0,132	,176*	-0,046	0,135	0,097	0,046	0,099	-0,031	0,101	-0,040	0,104	,220**	-0,012	0,032	0,078	0,070	,194*
	Long Run Low Gray-Level	0,124	0,142	0,118	-0,048	-0,074	-,165*	0,090	-0,061	-0,022	-0,129	0,097	-0,077	0,014	0,046	-0,016	-0,109	-0,132	-0,068	-0,013	-0,079	0,091	-0,052	0,017	-0,082	-0,015	0,035	-0,087	-,175*	-0,095	-0,018	-0,012	-0,023	-0,013
	Long Run High Gray-Level	-0,027	-0,008	0,001	-0,006	,194*	0,130	0,065	,197*	-0,118	0,109	,180*	0,053	0,089	0,118	0,119	-0,060	0,124	,165*	-0,046	0,141	0,082	0,050	0,087	-0,043	0,104	-0,038	0,096	,215**	-0,017	0,029	0,079	0,091	,193*
	Gray-Level Variance	-0,076	-0,001	-0,040	-0,069	,184*	,194*	-0,008	0,066	0,042	0,108	0,146	,172*	0,022	0,001	0,109	0,070	0,121	0,129	-0,117	0,017	0,132	0,124	0,113	0,056	,194**	-,143*	-0,011	,209*	0,008	0,116	0,037	0,066	,230**
	Run-Length Variance	-0,064	-0,056	-0,050	-0,048	-0,036	0,056	-0,096	-,187*	0,086	0,034	-0,001	0,135	-0,078	-0,125	-0,001	0,123	-0,039	-0,013	-0,018	-0,124	0,049	0,100	0,082	0,034	0,122	-0,108	-0,113	-0,051	-0,004	0,087	-0,035	0,020	0,071
GLSZM	Small Zone Emphasis	-0,155	-,162*	0,019	-0,033	,174*	-0,012	0,008	0,094	0,036	0,090	0,056	0,001	0,023	-0,019	0,023	0,033	0,113	0,158	-0,011	0,118	0,067	0,042	0,099	0,000	0,020	0,029	0,135	0,159	0,050	0,000	0,057	-0,028	0,155
	Large Zone Emphasis	,190*	0,113	0,065	0,029	-,166*	-0,098	0,011	-0,084	-0,064	-0,134	-0,081	-0,079	-0,018	0,007	-0,061	-0,115	-0,118	-0,143	0,051	-0,082	-0,061	-0,050	-0,079	-0,061	-0,077	0,056	-0,113	-,166*	-0,078	-0,062	-0,014	-0,048	-,194*
	Gray-Level Nonuniformity	0,010	0,040	0,017	0,023	-,194*	-0,078	-0,051	-,169*	0,118	-0,146	-0,149	-0,019	-0,080	-0,098	-0,074	0,059	-0,121	-,164*	0,054	-0,141	-0,064	-0,022	-0,087	0,065	-0,035	-0,027	-0,107	-,226**	0,005	-0,020	-0,102	-0,101	-,163*
	Zone-Size Nonuniformity	-0,154	-,162*	0,021	-0,033	,172*	-0,011	0,008	0,093	0,034	0,089	0,054	0,000	0,023	-0,020	0,024	0,033	0,113	0,157	-0,011	0,118	0,068	0,044	0,099	-0,002	0,020	0,029	0,135	0,158	0,050	-0,001	0,056	-0,027	0,155
	Zone Percentage	-,181*	-0,135	-0,013	-0,031	,178*	0,034	0,003	0,091	0,080	0,122	0,089	0,037	0,021	-0,006	0,041	0,070	0,115	,162*	-0,044	0,101	0,088	0,042	0,090	0,033	0,052	-0,014	0,135	,175*	0,072	0,018	0,033	-0,006	,190*
	Low Gray-Level Zone Emphasis	0,116	-0,039	-0,045	-0,092	-,190*	-0,120	-0,121	-,217**	-0,022	-0,058	-,232**	-0,052	-0,125	0,037	-,175*	0,026	-0,087	-,178*	0,062	-0,110	-0,159	-0,098	-0,065	0,008	-,186*	0,112	-0,070	-,186*	-0,017	-,157*	-0,039	-0,072	-,243**
	High Gray-Level Zone Emphasis	-0,067	-0,031	0,001	-0,009	,198*	0,113	0,059	,180*	-0,106	0,102	,168*	0,046	0,079	0,083	0,103	-0,049	0,132	,180*	-0,038	0,135	0,093	0,048	0,096	-0,043	0,097	-0,036	0,104	,218**	-0,014	0,035	0,083	0,075	,189*
	Small Zone Low Gray-Level Zone Emphasis	0,099	-0,048	-0,059	-0,102	-,190*	-0,138	-0,124	-,236**	-0,010	-0,054	-,236**	-0,064	-0,125	0,017	-0,154	0,048	-0,070	-,176*	0,049	-0,127	-,161*	-0,104	-0,076	0,007	-,205**	0,134	-0,053	-,185*	-0,018	-,151*	-0,033	-0,086	-,236**
	Small Zone High Gray-Level Zone Emphasis	-0,080	-0,039	0,006	-0,008	,198*	0,103	0,065	,180*	-0,102	0,102	,162*	0,053	0,085	0,068	0,093	-0,044	0,132	,175*	-0,031	0,135	0,094	0,050	0,099	-0,041	0,103	-0,040	0,104	,221**	-0,013	0,038	0,086	0,078	,190*
	Large Zone Low Gray-Level Zone Emphasis	0,151	,162*	0,085	-0,021	0,030	-0,145	0,096	-0,013	-0,024	-0,127	0,153	-0,069	0,018	0,068	0,052	-0,108	-0,099	0,034	-0,084	-0,070	0,114	-0,016	-0,008	-0,087	0,022	0,023	-0,076	-0,059	-0,084	0,076	0,031	0,011	0,042
	Large Zone High Gray-Level Zone Emphasis	,173*	0,094	-0,004	0,018	,164*	0,154	0,068	,217**	-0,138	0,078	0,147	0,061	0,082	,179*	0,124	-0,123	0,084	0,097	-0,031	0,138	0,050	0,062	0,039	-0,065	0,112	-0,061	-0,042	,167*	-0,050	0,010	0,073	0,113	0,116
	Grey-Level Variance	-,191*	-0,089	-0,121	-0,053	0,140	,180*	-0,056	0,087	-0,022	0,114	0,052	0,152	0,018	-0,021	0,061	,167*	0,124	0,081	-0,007	0,084	0,035	0,094	0,079	0,083	0,090	-0,098	0,082	0,107	0,012	0,058	-0,012	0,106	,174*
	Zone-Size Variance	-,175*	-0,137	-0,078	-0,036	-0,098	0,107	-0,101	-0,120	0,012	0,020	-0,129	0,081	-0,042	-0,127	-0,013	,230**	0,079	-0,082	0,085	-0,082	-0,034	0,046	0,008	0,100	0,012	-0,080	0,006	-0,122	0,018	0,018	-0,059	0,062	-0,041
NGTDM	Coarseness	-0,048	0,005	-0,070	-0,019	0,026	0,097	0,056	-0,023	0,026	0,078	0,098	0,100	0,060	-0,084	0,120	0,117	0,053	0,060	-0,034	0,051	0,005	0,066	0,082	0,101	0,029	0,003	0,099	-0,009	-0,091	-0,033	0,069	0,006	0,156
	Contrast	-0,101	-0,114	-0,053	-0,058	,192*	-0,041	0,008	0,073	-0,076	0,091	0,015	-0,077	0,028	-0,006	0,008	0,010	0,127	0,108	-0,007	0,076	-0,021	0,008	0,079	-0,046	-0,115	0,136	0,138	0,132	0,018	-0,073	0,082	0,018	0,069
	Busyness	0,044	-0,010	0,042	0,016	-0,158	-0,142	-0,068	-0,133	0,022	-0,099	-0,154	-0,118	-0,076	-0,032	-0,133	-0,045	-0,118	-0,145	0,071	-0,121	-0,074	-0,076	-0,090	-0,065	-0,118	0,067	-0,110	-0,140	0,060	-0,032	-0,096	-0,042	-,222**
	Complexity	-0,093	-0,125	-0,016	-0,042	,194*	0,013	0,020	0,127	-0,104	0,074	0,060	-0,026	0,052	0,027	0,059	0,019	0,129	,164*	0,039	0,121	0,038	0,052	0,101	-0,057	-0,005	0,051	0,129	,177*	0,003	0,020	0,111	0,048	0,106
	Strength	-0,035	-0,057	-0,060	-0,032	0,130	0,016	0,059	0,074	-0,068	0,073	0,125	0,057	0,079	0,004	0,108	0,046	0,093	0,148	0,016	0,115	0,033	0,072	0,096	0,034	0,008	0,062	0,132	0,091	-0,084	0,033	0,127	0,050	,161*

Abbreviations : DM: Diabetes Mellitus; COPD: Chronic Obstructive Pulmonary Disease; CCI: Charlson Comorbidity Index; #: number; PC: primary care; ED: emergency department; IHF: Intensity Histogram Features; GLCM: Gray-Level Co-occurrence Matrix; GLRLM: Gray-Level run-Length Matrix; GLSZM: Gray-Level Size Zone Matrix; NGTDM: Neighborhood Gray-Tone Difference Matrix.

Tau B of Kendal used for the statistical analysis.

* The correlation is significant at the 0.05 level (bilateral).

** The correlation is significant at the 0.01 level (bilateral).

Table 8.11.2 Sagital Rectus Femoris Textures Features Correlations with Associated Diseases, Risk Factors, variables associated with frailty, and death (n = 101)

	Texture Features	Hypertension	Hyperlipidemia	DM	COPD	Hearing Impairment	Visual Impairment	Parkinson Disease	Previous Stroke	Congestive Heart Failure	Heart Disease	Myocardial Infarction	Renal Disease	Previous Cancer	Artritis/Osteo arthitis	Anxiety/Depression	Previous Fracture	Liver Disease	Dementia/Memory Loss	Connective Tissue Disease	Hemiplagia	Neoplasm	Leukemia	Solid Metastasis	Peripheral Vascular Disease	CCI	Estimated Survival	Smoker	Falls	Obesity	# of Visits to PC	# of Visits to ED	# of Hospitalizations	Death
IHF	Variance	0,030	-0,018	-0,103	-0,021	0,156	0,101	0,020	0,087	-0,026	0,098	0,060	-0,109	0,123	0,157	0,058	0,061	0,068	0,094	0,138	-0,003	0,127	0,072	-0,107	0,044	-0,005	0,062	0,132	-0,010	-0,031	0,077	0,040	0,100	0,107
	Skewness	-0,073	-0,118	0,124	0,029	-0,124	-,165*	-0,025	-0,104	-0,070	-0,136	-0,094	-0,104	-,166*	-,179*	-0,121	-0,093	-0,132	0,023	0,102	0,017	-0,021	0,030	0,028	-0,133	-0,072	0,049	0,020	-0,104	-0,028	0,059	0,059	-0,002	-0,140
	Kurtosis	-0,057	-0,078	0,127	-0,001	-,168*	-0,158	-0,068	-0,129	-0,052	-0,151	-0,134	-0,026	-,181*	-,199*	-0,133	-0,101	-0,138	-0,029	0,084	0,020	-0,060	-0,002	0,053	-0,118	-0,061	0,012	-0,048	-0,094	0,005	-0,005	0,024	-0,027	-0,158
GLCM	Energy	0,073	-0,034	0,062	-0,062	-,198*	-0,071	-0,090	-,200*	-0,110	-0,099	-0,082	-0,023	-,170*	-0,130	-0,154	-0,101	-0,129	-0,104	0,034	-0,079	-0,106	0,068	-0,008	-0,082	-0,061	-0,015	-0,141	-0,114	-0,017	-0,064	0,018	0,063	-0,117
	Contrast	-,164*	-0,056	-0,076	0,066	,194*	-0,048	0,104	0,109	0,042	0,035	0,008	-0,093	0,085	0,064	0,092	0,086	0,124	0,159	0,090	-0,048	0,019	-0,010	-0,045	-0,029	-0,061	0,105	0,141	0,046	0,010	0,091	0,039	-0,092	-0,022
	Entropy	-0,107	-0,026	-0,071	0,058	,196*	0,018	0,090	,171*	0,076	0,080	0,054	-0,032	0,136	0,119	0,130	0,100	0,127	0,140	0,018	0,048	0,082	-0,034	-0,023	0,034	0,018	0,049	0,141	0,089	0,012	0,086	0,002	-0,056	0,071
	Homogeneity	0,096	0,011	0,057	-0,068	-,198*	-0,014	-0,118	-,176*	-0,144	-0,072	-0,067	0,004	-0,136	-0,080	-0,131	-0,124	-0,121	-0,124	0,000	-0,028	-0,057	0,070	0,053	-0,057	-0,004	-0,047	-0,141	-0,085	0,000	-0,087	0,016	0,101	-0,073
	Correlation	0,071	-0,019	-0,003	-0,051	-0,146	0,082	-0,138	-0,070	-0,142	0,024	-0,065	0,030	-0,031	0,101	0,024	-0,046	-0,006	-0,074	0,033	0,107	0,064	0,024	0,068	0,036	0,112	-0,060	-0,042	0,019	-0,055	-0,020	0,029	0,138	0,015
	Sum Average	-0,079	-0,026	-0,127	0,058	,196*	0,064	0,008	0,140	0,046	0,109	0,083	-0,004	0,109	0,154	0,087	0,078	0,138	0,110	0,007	0,079	0,062	-0,008	0,011	0,033	0,051	0,008	0,138	0,137	0,020	0,065	-0,022	-0,033	0,127
	Variance	-0,097	-0,054	-0,065	0,033	,184*	-0,024	0,028	0,107	-0,040	0,046	0,004	-0,107	0,075	0,123	0,095	0,068	0,129	0,127	0,110	0,042	0,069	0,000	-0,011	-0,026	-0,030	0,097	0,141	0,083	-0,001	0,090	0,045	-0,009	0,008
	Dissimilarity	-0,140	-0,036	-0,069	0,069	,196*	-0,041	0,118	0,134	0,086	0,043	0,035	-0,070	0,110	0,068	0,107	0,089	0,127	0,150	0,067	-0,037	0,034	-0,018	-0,059	0,002	-0,042	0,094	0,141	0,041	0,003	0,093	0,027	-0,098	0,011
	Auto-Correlation	-0,089	-0,026	-0,131	0,052	,196*	0,047	0,006	0,133	0,038	0,103	0,071	-0,026	0,106	0,149	0,086	0,078	0,138	0,116	0,021	0,070	0,065	-0,004	0,008	0,028	0,036	0,021	0,138	0,128	0,010	0,070	-0,002	-0,023	0,113
GLRLM	Short Run Emphasis	-0,079	0,021	-0,048	0,068	,198*	0,046	0,118	,207*	0,152	0,074	0,080	0,025	0,150	0,075	0,142	0,125	0,110	0,125	-0,030	0,065	0,093	-0,052	-0,051	0,085	0,054	0,003	0,138	0,090	0,001	0,100	-0,037	-0,080	0,121
	Long Run Emphasis	0,102	0,021	0,058	-0,066	-,196*	-0,072	-0,113	-,190*	-0,152	-0,090	-0,078	-0,026	-0,123	-0,061	-0,100	-0,124	-0,118	-0,114	0,016	-0,082	-0,085	0,082	0,020	-0,093	-0,072	0,016	-0,132	-0,099	-0,032	-0,068	0,039	0,094	-0,115
	Gray-Level Nonuniformity	0,067	-0,001	0,078	-0,046	-,194*	-0,045	-0,048	-0,159	-0,048	-0,111	-0,064	0,021	-0,146	-0,149	-0,134	-0,082	-0,138	-0,131	-0,002	-0,070	-0,096	0,036	-0,017	-0,074	-0,059	-0,014	-0,141	-0,110	-0,036	-0,059	-0,014	0,014	-0,088
	Run Length Nonuniformity	-0,076	0,022	-0,049	0,066	,198*	0,045	0,118	,209*	0,152	0,073	0,081	0,025	0,152	0,075	0,143	0,125	0,110	0,127	-0,030	0,065	0,094	-0,052	-0,051	0,085	0,057	0,004	0,138	0,089	0,000	0,100	-0,039	-0,078	0,123
	Run Percentage	-0,082	0,000	-0,051	0,065	,198*	0,058	0,113	,207*	0,148	0,084	0,079	0,028	0,140	0,080	0,131	0,118	0,115	0,121	-0,028	0,084	0,090	-0,060	-0,037	0,087	0,063	-0,003	0,135	0,104	0,017	0,090	-0,030	-0,081	0,124
	Low Gray-Level Run Emphasis	0,136	0,009	0,134	-0,062	-0,092	-0,071	0,068	-0,111	-0,102	-0,070	-0,039	-,172*	-0,096	-0,101	-0,074	-0,109	-0,039	-0,079	-0,020	-0,087	0,013	-0,004	0,039	-0,074	-0,127	0,107	-0,093	-,182*	-0,042	-0,091	0,019	0,069	-0,146
	High Gray-Level Run Emphasis	-0,090	-0,034	-0,130	0,052	,196*	0,042	0,008	0,133	0,034	0,095	0,065	-0,036	0,103	0,140	0,094	0,074	0,138	0,125	0,031	0,068	0,063	0,002	0,006	0,021	0,033	0,023	0,138	0,123	0,013	0,076	0,000	-0,019	0,109
	Short Run Low Gray-Level	0,142	0,032	0,132	-0,046	-0,054	-0,045	0,096	-0,093	-0,074	-0,054	0,002	-,202*	-0,076	-0,117	-0,070	-0,092	-0,031	-0,081	-0,023	-0,093	0,034	-0,018	0,034	-0,044	-0,119	0,100	-0,070	-,182*	-0,042	-0,091	0,016	0,067	-0,130
	Short Run High Gray-Level	-0,090	-0,036	-0,126	0,052	,196*	0,039	0,014	0,136	0,042	0,094	0,067	-0,038	0,103	0,140	0,095	0,074	0,138	0,127	0,033	0,068	0,063	0,000	0,000	0,020	0,032	0,025	0,138	0,121	0,013	0,076	-0,002	-0,023	0,108
	Long Run Low Gray-Level	-0,018	-0,074	0,063	-0,035	-0,116	-0,108	-0,087	-0,081	-0,148	-0,108	-0,132	0,049	-0,092	0,047	0,072	-0,136	-0,132	-0,086	-0,054	0,025	-0,065	0,100	-0,062	-0,111	-,160*	0,138	-0,070	-0,004	-0,046	-0,075	0,046	0,044	0,028
	Long Run High Gray-Level	-0,089	-0,037	-0,140	0,038	,196*	0,043	-0,034	0,117	0,008	0,091	0,061	-0,045	0,079	0,158	0,077	0,065	0,138	0,119	0,028	0,076	0,067	0,016	0,017	-0,008	0,031	0,028	0,138	0,134	0,006	0,076	0,007	-0,013	0,111
	Gray-Level Variance	-0,046	-0,004	-,192*	0,073	0,038	0,037	0,000	0,134	0,116	0,040	0,055	0,029	0,136	0,047	-0,033	-0,007	0,129	0,038	0,000	0,087	-,195*	-0,070	-0,093	0,093	0,057	-0,074	0,023	-0,006	-0,006	-0,018	-0,082	-,178*	0,036
	Run-Length Variance	0,059	0,011	0,001	0,026	-0,146	-0,009	0,011	-0,046	0,058	-0,089	0,012	0,069	0,005	-0,144	-,160*	-0,086	-0,082	-0,035	0,056	-0,014	-,278**	-0,020	-0,110	0,047	0,039	-0,111	-0,135	-,164*	-0,027	-0,041	-0,017	-0,130	-0,084
GLSZM	Small Zone Emphasis	-0,111	-0,044	-0,063	0,073	,198*	-0,004	0,107	,170*	0,140	0,052	0,056	-0,014	0,106	0,071	0,134	0,110	0,115	0,148	0,031	0,051	0,058	-0,072	-0,042	0,041	0,011	0,047	0,138	0,059	-0,001	0,083	-0,008	-0,107	0,078
	Large Zone Emphasis	0,098	0,013	0,062	-0,066	-,198*	-0,073	-0,115	-,204*	-0,158	-0,090	-0,095	-0,027	-0,133	-0,059	-0,082	-0,123	-0,121	-0,119	0,018	-0,082	-0,083	0,074	0,020	-0,095	-0,091	0,037	-0,129	-0,112	-0,028	-0,084	0,059	0,088	-0,122
	Gray-Level Nonuniformity	0,072	0,016	0,076	-0,039	-,190*	-0,021	-0,037	-0,143	-0,010	-0,078	-0,034	0,061	-0,122	-0,134	-0,115	-0,076	-0,135	-0,135	-0,043	-0,068	-0,098	0,024	-0,028	-0,051	-0,032	-0,037	-0,141	-0,092	-0,031	-0,065	-0,010	0,007	-0,059
	Zone-Size Nonuniformity	-0,114	-0,046	-0,063	0,073	,198*	-0,004	0,107	,170*	0,140	0,053	0,056	-0,016	0,107	0,072	0,133	0,109	0,115	0,148	0,033	0,048	0,058	-0,072	-0,042	0,041	0,010	0,048	0,138	0,058	0,000	0,085	-0,007	-0,108	0,077
	Zone Percentage	-0,095	-0,024	-0,052	0,065	,198*	0,044	0,107	,190*	0,144	0,078	0,064	0,014	0,123	0,084	0,134	0,110	0,115	0,127	-0,015	0,082	0,079	-0,080	-0,037	0,079	0,036	0,028	0,138	0,087	0,014	0,076	-0,020	-0,096	0,107
	Low Gray-Level Zone Emphasis	0,137	0,036	0,134	-0,082	-0,114	-0,047	0,039	-0,134	-0,050	-0,084	-0,067	-0,144	-0,100	-0,111	-0,088	-0,104	-0,048	-0,099	0,007	-0,084	0,014	-0,040	0,053	-0,008	-0,099	0,067	-0,101	-,194*	-0,018	-0,108	0,018	0,035	-,174*
	High Gray-Level Zone Emphasis	-0,092	-0,040	-0,124	0,055	,194*	0,032	0,008	0,127	0,028	0,096	0,056	-0,043	0,103	0,134	0,087	0,069	0,138	0,129	0,043	0,062	0,054	0,000	0,003	0,010	0,026	0,033	0,138	0,118	0,019	0,078	0,004	-0,024	0,092
	Small Zone Low Gray-Level Zone Emphasis	0,113	0,045	0,139	-0,095	-0,134	-0,041	0,045	-0,137	-0,020	-0,067	-0,082	-0,110	-0,099	-0,108	-0,046	-0,089	-0,070	-0,098	-0,018	-0,087	0,033	-0,028	0,034	0,034	-0,093	0,056	-0,104	-,184*	-0,014	-0,087	0,034	0,040	-0,154
	Small Zone High Gray-Level Zone Emphasis	-0,102	-0,039	-0,118	0,058	,194*	0,025	0,017	0,127	0,034	0,091	0,059	-0,041	0,097	0,131	0,090	0,071	0,138	0,128	0,053	0,059	0,054	-0,016	-0,003	0,003	0,018	0,038	0,141	0,117	0,014	0,073	-0,001	-0,034	0,090
	Large Zone Low Gray-Level Zone Emphasis	-0,036	-0,036	0,042	-0,015	-0,110	-0,023	-0,115	-0,091	-0,080	-0,064	-0,067	0,123	-0,060	0,062	0,090	-0,094	-0,129	-0,115	-0,051	-0,006	-0,022	0,060	-0,096	-0,015	-0,095	0,090	-0,051	0,032	-0,033	-0,092	0,061	0,056	0,059
	Large Zone High Gray-Level Zone Emphasis	0,001	0,042	-0,132	0,021	,176*	0,070	-0,115	0,061	-0,106	0,048	0,025	-0,007	0,016	0,157	0,040	0,018	0,101	0,081	0,011	0,090	0,088	0,036	0,028	-0,059	0,039	0,033	0,090	0,128	-0,031	0,043	0,038	0,047	0,091
	Grey-Level Variance	-0,096	-0,086	-0,064	0,032	0,056	0,016	0,118	0,156	0,112	0,136	0,022	-0,100	0,133	0,026	-0,006	0,056	0,141	0,085	0,003	0,025	-0,066	0,040	-0,017	0,007	0,007	-0,020	0,068	0,018	0,006	0,059	-0,087	-0,108	0,015
	Zone-Size Variance	-0,010	-0,082	0,085	-0,056	-0,154	-0,024	0,132	0,024	0,074	0,022	-0,037	-0,101	0,066	-,178*	-0,116	0,030	0,084	-0,047	0,007	-0,059	-,165*	0,086	-0,034	-0,026	-0,024	-0,066	-0,127	-0,119	0,008	0,001	-0,108	-0,073	-0,124
NGTDM	Coarseness	0,080	0,040	-0,110	-0,100	0,028	0,034	-0,039	-0,033	-0,072	0,022	0,065	0,044	0,060	-0,108	0,012	0,067	0,056	0,055	0,064	0,065	-0,099	0,012	-0,115	0,034	0,005	0,016	0,096	-0,125	-0,068	-0,030	0,039	0,020	0,089
	Contrast	-0,122	-0,045	-0,057	0,036	,194*	-0,050	0,104	0,096	0,048	0,075	0,005	-0,086	0,090	0,123	0,134	0,084	0,129	0,131	0,023	-0,065	0,029	-0,032	-0,056	0,007	-0,074	0,122	0,141	0,045	0,014	0,048	0,046	-0,058	-0,029
	Busyness	0,038	0,042	,211**	0,053	-0,142	-0,026	0,090	-0,049	0,040	-0,064	-0,058	-0,010	-0,055	-0,035	-0,011	-0,065	-0,135	-0,076	-0,057	-0,107	0,075	-0,002	0,093	-0,018	0,011	-0,027	-0,129	-0,022	0,026	-0,012	-0,002	0,019	-0,122
	Complexity	-0,140	-0,068	-0,093	0,063	,196*	-0,030	0,076	0,106	0,010	0,063	0,015	-0,083	0,079	0,124	0,098	0,076	0,132	0,134	0,089	-0,008	0,041	0,006	-0,039	-0,034	-0,049	0,098	0,141	0,087	-0,004	0,092	0,040	-0,053	0,013
	Strength	-0,047	-0,094	-0,113	-0,065	0,104	-0,082	-0,048	-0,004	-0,126	0,018	0,009	-0,095	0,028	-0,022	0,005	0,032	0,115	0,089	,169*	0,065	-0,076	0,036	-0,115	-0,057	-0,085	0,104	0,138	-0,066	-0,063	0,059	0,073	0,015	0,035

Abbreviations: DM: Diabetes Mellitus; COPD: Chronic Obstructive Pulmonary Disease; CCI: Charlson Comorbidity Index; #: number; PC: primary care; ED: emergency department; IHF: Intensity Histogram Features; GLCM: Gray-Level Co-occurrence Matrix; GLRLM: Gray-Level run-Length Matrix; GLSZM: Gray-Level Size Zone Matrix; NGTDM: Neighborhood Gray-Tone Difference Matrix.

Tau B of Kendal used for the statistical analysis.

* The correlation is significant at the 0.05 level (bilateral).

** The correlation is significant at the 0.01 level (bilateral).

Table 8.11.3 Axial Vastus Intermedius Textures Features Correlations with Associated Diseases, Risk Factors, variables associated with frailty, and death (n = 101)

	Texture Features	Hypertension	Hyperlipidemia	DM	COPD	Hearing Impairment	Visual Impairment	Parkinson Disease	Previous Stroke	Congestive Heart Failure	Heart Disease	Myocardial Infarction	Renal Disease	Previous Cancer	Artritis/Osteo arthritis	Anxiety/Depression	Previous Fracture	Liver Disease	Dementia/Memory Loss	Connective Tissue Disease	Hemiplagia	Neoplasm	Leukemia	Solid Metastasis	Peripheral Vascular Disease	CCI	Estimated Survival	Smoker	Falls	Obesity	# of Visits to PC	# of Visits to ED	# of Hospitalizations	Death
IHF	Variance	-0,071	0,055	0,015	-0,070	0,034	0,103	-0,082	-0,024	-0,058	0,029	0,010	-0,057	0,110	-0,046	0,070	-0,008	-0,062	0,076	-0,005	-0,048	,190*	,184*	0,076	0,026	0,115	-0,100	0,138	-0,021	-0,127	0,087	-0,017	0,128	,165*
	Skewness	0,057	0,029	-0,002	-0,046	-0,062	-0,065	-0,090	-0,157	-0,034	-0,090	-0,089	0,019	-0,070	0,000	-0,066	-0,048	-0,003	-,199*	0,098	-0,023	-,161*	-0,106	-0,070	0,083	-,193**	0,141	-0,107	-0,054	-0,022	-0,074	-0,026	-,172*	-,186*
	Kurtosis	0,070	0,022	-0,011	-0,025	-0,058	-0,080	-0,076	-0,123	-0,022	-0,075	-0,079	0,039	-0,086	0,005	-0,092	-0,038	-0,008	-,171*	0,085	0,000	-,182*	-,164*	-0,087	0,069	-,194**	,149*	-0,127	-0,048	0,031	-0,092	-0,032	-,194*	-,203*
GLCM	Energy	-0,007	-0,114	0,010	-0,123	-,180*	-0,081	-0,076	-,210*	-0,066	-0,107	-,187*	-0,097	-0,154	0,054	0,025	-0,076	-0,056	-,182*	0,090	-0,110	-0,143	-0,076	0,025	0,062	-,206**	0,124	-0,076	-0,128	0,101	-0,107	-0,044	-0,103	-,296**
	Contrast	-0,047	0,145	-0,090	0,066	,168*	0,049	-0,006	0,107	0,024	0,059	0,134	0,121	0,110	0,035	-0,005	0,050	0,087	0,032	0,079	0,104	0,062	0,078	0,084	0,029	0,056	-0,030	0,110	0,057	-,174*	0,029	0,032	0,084	,258**
	Entropy	-0,033	0,145	-0,010	0,119	,172*	0,060	0,079	,206*	0,042	0,083	,188*	0,117	,167*	-0,058	-0,002	0,066	0,048	0,157	-0,064	0,115	0,126	0,118	0,023	-0,041	,188*	-0,120	0,087	0,113	-0,127	0,108	0,023	0,114	,309**
	Homogeneity	0,018	-0,142	0,051	-0,116	-,180*	-0,056	-0,039	-,169*	-0,074	-0,114	-0,145	-0,116	-0,143	0,035	0,028	-0,069	-0,118	-0,140	0,069	-0,090	-0,104	-0,102	0,006	0,011	-,183*	0,126	-0,087	-0,100	0,120	-0,095	-0,034	-0,099	-,281**
	Correlation	-0,098	0,008	0,106	0,086	-0,042	0,073	0,099	0,096	-0,086	-0,013	0,118	-0,045	0,117	-0,059	0,115	-0,008	-0,099	0,116	-0,033	0,003	0,125	0,150	0,031	-0,082	0,115	-0,089	0,056	0,046	0,008	,147*	0,007	,164*	0,109
	Sum Average	-0,024	0,129	-0,003	0,146	,186*	0,059	0,104	,226**	0,060	0,104	,219**	0,101	,193*	-0,054	0,035	0,049	0,014	,174*	-0,080	0,121	0,133	0,112	0,008	-0,034	,196**	-0,112	0,096	0,104	-0,122	0,120	0,045	0,129	,344**
	Variance	-0,084	0,116	0,013	0,086	0,136	0,077	0,065	0,147	-0,036	-0,006	,189*	0,079	,162*	-0,034	0,054	0,021	-0,028	0,119	0,025	0,087	0,095	0,152	0,070	-0,025	0,119	-0,067	0,110	0,067	-0,110	0,111	0,020	0,131	,287**
	Dissimilarity	-0,054	0,147	-0,070	0,093	,172*	0,062	0,017	0,140	0,040	0,094	0,142	0,124	0,132	-0,002	-0,018	0,063	0,101	0,072	0,021	0,096	0,092	0,102	0,056	0,020	0,120	-0,080	0,101	0,077	-0,155	0,061	0,019	0,083	,282**
	Auto-Correlation	-0,041	0,132	-0,002	0,139	0,160	0,062	0,101	,219*	0,044	0,097	,224**	0,101	,190*	-0,052	0,049	0,042	0,003	,169*	-0,062	0,124	0,125	0,124	0,008	-0,034	,175*	-0,096	0,104	0,101	-0,124	0,113	0,042	0,123	,349**
GLRLM	Short Run Emphasis	-0,015	0,145	-0,051	0,107	,174*	0,080	0,028	,176*	0,074	0,126	0,154	0,130	0,152	-0,019	-0,003	0,063	0,110	0,123	-0,062	0,104	0,113	0,122	0,006	0,015	,180*	-0,122	0,110	0,078	-0,137	0,083	0,006	0,104	,309**
	Long Run Emphasis	-0,019	-0,108	0,015	-0,105	-,170*	-0,046	-0,053	-0,146	-0,086	-0,125	-0,145	-0,091	-0,106	0,068	0,052	-0,091	-0,121	-0,149	0,085	-0,099	-0,104	-0,054	0,042	0,038	-,170*	0,104	-0,059	-0,103	0,086	-0,074	-0,033	-0,087	-,258**
	Gray-Level Nonuniformity	0,071	-0,104	-0,001	-0,116	-0,156	-0,076	-0,084	-,204*	-0,008	-0,050	-,219**	-0,082	-,173*	0,022	-0,063	-0,024	0,020	-,182*	0,051	-0,110	-0,146	-,162*	-0,053	0,051	-,174*	0,100	-0,107	-0,090	0,111	-0,133	-0,019	-0,123	-,338**
	Run Length Nonuniformity	-0,012	0,145	-0,053	0,106	,174*	0,081	0,025	,176*	0,072	0,126	0,156	0,131	0,154	-0,008	-0,001	0,060	0,110	0,118	-0,061	0,104	0,112	0,122	0,006	0,015	,179*	-0,122	0,110	0,077	-0,137	0,084	0,004	0,104	,313**
	Run Percentage	0,000	0,126	-0,025	0,112	,172*	0,047	0,045	,171*	0,088	0,126	0,150	0,114	0,133	-0,060	-0,046	0,078	0,115	0,153	-0,080	0,101	0,103	0,080	-0,031	-0,021	,188*	-0,129	0,082	0,100	-0,105	0,093	0,024	0,086	,274**
	Low Gray-Level Run Emphasis	-0,012	-0,094	-0,006	-,196*	-0,118	-0,015	-0,141	-,196*	-0,114	-0,112	-,169*	-0,056	-0,154	0,046	-0,012	-0,102	-0,034	-,185*	0,100	-0,118	-0,076	-0,058	0,028	0,011	-,198**	0,116	-0,096	-0,092	0,084	-0,108	-0,028	-0,103	-,258**
	High Gray-Level Run Emphasis	-0,042	0,134	-0,006	0,137	0,158	0,064	0,096	,214**	0,028	0,080	,218**	0,098	,193*	-0,035	0,059	0,032	-0,003	,163*	-0,044	0,124	0,110	0,124	0,014	-0,038	,156*	-0,081	0,121	0,089	-0,130	0,109	0,043	0,117	,348**
	Short Run Low Gray-Level	-0,005	-0,103	-0,006	-,218**	-0,108	-0,016	-0,138	-,211**	-0,104	-0,121	-,173*	-0,065	-,179*	0,031	-0,029	-0,102	-0,023	-,181*	0,102	-0,121	-0,067	-0,056	0,025	0,013	-,188*	0,111	-0,118	-0,095	0,104	-0,126	-0,032	-0,100	-,264**
	Short Run High Gray-Level	-0,040	0,138	-0,009	0,139	0,158	0,065	0,096	,214**	0,030	0,081	,219**	0,098	,194*	-0,034	0,061	0,033	-0,003	0,157	-0,041	0,124	0,110	0,122	0,014	-0,038	,156*	-0,080	0,121	0,089	-0,133	0,108	0,044	0,117	,349**
	Long Run Low Gray-Level	-0,024	-0,102	0,009	-0,143	-0,122	0,007	-0,138	-,167*	-0,104	-0,091	-0,131	-0,047	-0,113	0,054	0,047	-0,097	-0,068	-,174*	0,098	-0,101	-0,045	-0,020	0,045	0,020	-,178*	0,108	-0,051	-0,082	0,059	-0,054	-0,011	-0,070	-,204*
	Long Run High Gray-Level	-0,029	0,138	-0,002	0,157	0,160	0,068	0,104	,223**	0,034	0,071	,230**	0,099	,190*	-0,026	0,057	0,034	-0,011	,166*	-0,071	0,124	0,116	0,126	0,011	-0,044	,158*	-0,078	0,124	0,092	-0,123	0,121	0,031	0,119	,348**
	Gray-Level Variance	-0,008	0,090	-0,046	0,092	0,138	0,042	0,076	0,144	0,092	0,150	,169*	0,077	0,125	-0,061	0,009	0,100	0,048	,191*	-0,095	0,082	0,085	0,046	-0,025	-0,036	,164*	-0,093	0,073	0,073	-0,074	0,067	0,041	0,123	,255**
	Run-Length Variance	0,037	0,040	0,002	-0,045	0,026	-0,046	0,014	-0,023	0,106	0,129	0,001	0,008	-0,035	-0,119	-0,088	0,120	0,076	0,081	-0,094	-0,025	-0,025	-0,096	-0,084	-0,010	0,048	-0,030	-0,053	0,022	0,058	-0,038	0,019	0,024	-0,022
GLSZM	Small Zone Emphasis	-0,003	0,055	-0,113	0,012	0,142	-0,012	-0,042	0,056	-0,008	0,001	0,120	0,094	0,092	0,072	0,030	-0,054	0,087	0,009	0,074	0,059	0,052	0,114	0,014	0,013	-0,012	0,032	0,115	-0,003	-,180*	0,051	0,055	0,047	,233**
	Large Zone Emphasis	-0,024	-0,122	0,013	-0,119	-,170*	-0,060	-0,059	-0,134	-0,094	-0,111	-0,126	-0,083	-0,089	0,061	0,043	-0,104	-0,115	-0,150	0,077	-0,099	-0,109	-0,058	0,042	0,036	-,165*	0,100	-0,065	-0,086	0,079	-0,056	-0,021	-0,073	-,248**
	Gray-Level Nonuniformity	0,080	-0,108	-0,012	-0,109	-0,146	-0,065	-0,084	-,187*	0,000	-0,040	-,214**	-0,081	-,174*	0,025	-0,069	-0,015	0,025	-,177*	0,031	-0,104	-0,119	-,162*	-0,053	0,044	-,161*	0,090	-0,110	-0,083	0,113	-0,128	-0,025	-0,120	-,331**
	Zone-Size Nonuniformity	-0,004	0,055	-0,113	0,012	0,142	-0,012	-0,042	0,057	-0,008	0,002	0,118	0,095	0,093	0,072	0,030	-0,054	0,087	0,010	0,074	0,059	0,050	0,114	0,014	0,015	-0,012	0,032	0,115	-0,003	-,180*	0,051	0,054	0,045	,231**
	Zone Percentage	-0,026	0,126	-0,045	0,102	,174*	0,056	0,039	,169*	0,066	0,126	0,157	0,116	0,146	-0,039	-0,018	0,056	0,121	0,135	-0,053	0,101	0,114	0,118	0,011	-0,002	,178*	-0,124	0,093	0,086	-0,130	0,083	0,023	0,107	,299**
	Low Gray-Level Zone Emphasis	0,000	-0,099	0,011	-,203*	-0,110	-0,017	-0,127	-,226**	-0,104	-0,143	-,204*	-0,099	-,196*	0,034	-0,032	-0,094	-0,014	-,170*	0,094	-0,129	-0,077	-0,076	0,025	0,010	-,193**	0,110	-0,124	-0,126	0,123	-,140*	-0,041	-0,118	-,306**
	High Gray-Level Zone Emphasis	-0,048	0,132	-0,006	0,136	0,154	0,062	0,096	,210*	0,026	0,075	,218**	0,097	,190*	-0,044	0,061	0,031	-0,008	,166*	-0,028	0,124	0,108	0,122	0,023	-0,043	,151*	-0,076	0,118	0,090	-0,133	0,109	0,046	0,118	,345**
	Small Zone Low Gray-Level Zone Emphasis	-0,005	-0,103	-0,009	-,193*	-0,110	-0,029	-0,132	-,220**	-0,106	-0,139	-,201*	-0,095	-,190*	0,047	-0,038	-0,097	-0,011	-,189*	0,097	-0,129	-0,097	-0,072	0,025	0,008	-,201**	0,112	-0,099	-0,119	0,111	-,138*	-0,051	-0,126	-,301**
	Small Zone High Gray-Level Zone Emphasis	-0,051	0,132	-0,008	0,135	0,152	0,058	0,093	,203*	0,026	0,078	,215**	0,100	,190*	-0,046	0,059	0,023	-0,003	0,157	-0,011	0,121	0,098	0,124	0,023	-0,038	,148*	-0,078	0,118	0,090	-0,137	0,101	0,054	0,114	,339**
	Large Zone Low Gray-Level Zone Emphasis	-0,006	-0,114	0,012	-0,139	-0,140	0,002	-0,124	-0,150	-0,098	-0,094	-0,121	-0,037	-0,100	0,046	0,056	-0,083	-0,115	-,178*	0,089	-0,076	-0,033	-0,030	0,042	0,020	-,166*	0,107	-0,062	-0,073	0,055	-0,047	0,008	-0,051	-,196*
	Large Zone High Gray-Level Zone Emphasis	0,114	0,105	0,037	0,160	0,034	-0,018	0,093	0,117	-0,034	-0,095	,181*	0,035	0,126	-0,005	0,078	-0,081	-0,110	0,013	-0,108	0,082	0,042	0,048	-0,048	-0,074	-0,003	0,071	0,124	-0,028	-0,081	0,089	0,066	-0,007	,173*
	Grey-Level Variance	0,005	0,155	-0,019	0,146	0,158	0,069	0,084	0,139	0,096	0,118	0,125	0,073	0,102	-0,067	0,000	0,111	0,062	0,153	-0,056	0,099	0,098	0,052	-0,037	-0,039	,155*	-0,090	0,087	0,078	-0,078	0,056	0,027	0,073	,248**
	Zone-Size Variance	0,094	,187*	-0,059	0,103	0,048	-0,024	0,031	-0,003	0,076	0,012	-0,039	0,036	0,015	-0,066	0,026	0,068	0,082	-0,040	0,010	0,008	-0,086	-0,072	-0,115	-0,029	-0,053	0,062	0,099	-0,035	-0,040	-0,042	0,062	-0,144	0,021
NGTDM	Coarseness	-0,072	0,107	0,006	0,119	0,028	0,080	0,093	0,033	0,038	0,069	0,105	-0,039	0,119	-,211*	0,009	0,124	-0,087	0,148	-0,026	-0,034	0,035	0,028	0,059	-0,061	0,089	-0,076	0,127	-0,095	-0,086	0,005	-0,014	0,043	0,117
	Contrast	-0,092	0,092	-0,060	0,018	0,134	0,123	-0,014	0,064	-0,046	0,012	0,144	0,073	0,106	0,052	0,031	0,052	0,056	0,050	0,031	0,020	0,116	,174*	0,090	0,010	0,091	-0,064	0,101	0,015	-0,132	0,075	0,006	0,140	,271**
	Busyness	0,034	-0,128	-0,003	-0,156	-0,114	-0,050	-0,115	-,161*	-0,074	-0,111	-,196*	-0,065	-,176*	0,116	-0,009	-0,084	0,011	-,198*	0,076	-0,070	-0,092	-0,094	-0,023	0,041	-,182*	0,126	-0,104	-0,031	0,123	-0,089	-0,009	-0,088	-,276**
	Complexity	-0,064	,163*	-0,013	0,102	0,154	0,058	0,051	0,154	0,014	0,070	,176*	0,120	,166*	-0,058	0,006	0,049	0,053	0,089	-0,003	0,101	0,090	0,114	0,039	0,007	0,118	-0,078	0,104	0,087	-0,145	0,074	0,017	0,095	,288**
	Strength	-0,067	0,156	-0,025	0,086	0,068	0,035	0,076	0,026	-0,034	-0,026	0,153	0,037	0,160	-0,139	0,062	0,026	-0,104	0,054	0,080	-0,003	-0,021	0,058	0,051	-0,015	-0,010	0,009	0,127	-0,064	-,189*	0,023	0,015	0,017	,176*

Abbreviations: DM: Diabetes Mellitus; COPD: Chronic Obstructive Pulmonary Disease; CCI: Charlson Comorbidity Index; #: number; PC: primary care; ED: emergency department; IHF: Intensity Histogram Features; GLCM: Gray-Level Co-occurrence Matrix; GLRLM: Gray-Level Run-Length Matrix; GLSZM: Gray-Level Size Zone Matrix; NGTDM: Neighborhood Gray-Tone Difference Matrix.

Tau B of Kendal used for the statistical analysis.

* The correlation is significant at the 0.05 level (bilateral).

** The correlation is significant at the 0.01 level (bilateral).

Table 8.11.4 Sagital Vastus Intermidius Textures Features Correlations with Associeted Diseases, Risk Factors, variables associated with frailty and death (n = 101)

	Texture Features	Hypertension	Hyperlipidemia	DM	COPD	Hearing Impairment	Visual Impairment	Parkinson Disease	Previous Stroke	Congestive Heart Failure	Heart Disease	Myocardial Infarction	Renal Disease	Previous Cancer	Artritis/Osteo arthitis	Anxiety/Depression	Previous Fracture	Liver Disease	Dementia/Memory Loss	Connective Tissue Disease	Hemiplagia	Neoplasm	Leukemia	Solid Metastasis	Peripheral Vascular Disease	CCI	Estimated Survival	Smoker	Falls	Obesity	# of Visits to PC	# of Visits to ED	# of Hospitalizations	Death
IHF	Variance	0,036	0,042	-0,103	-0,009	,176*	0,096	0,062	0,151	-0,062	-0,043	,192*	-0,016	0,123	,165*	0,022	-,172*	-0,059	0,039	0,074	0,087	0,152	,186*	-0,003	0,010	0,091	-0,039	-0,065	0,001	-0,116	,144*	0,055	,166*	,297**
	Skewness	0,011	-0,008	0,093	0,076	-0,114	-0,117	-0,017	-0,156	-0,096	-0,142	-,197*	-0,110	-0,021	-0,086	-0,041	-0,029	0,059	-,214**	0,113	-0,070	-0,158	-0,134	0,096	0,015	-,245**	,185*	0,101	-0,012	-0,010	-,185**	-0,026	-0,133	-,356**
	Kurtosis	-0,015	-0,024	0,127	0,082	-,184*	-0,134	-0,020	-,186*	-0,036	-0,099	-,216**	-0,090	-0,046	-0,125	-0,022	0,030	0,037	-,186*	0,077	-0,096	-,181*	-,162*	0,093	0,028	-,222**	,155*	0,104	-0,035	0,028	-,190**	-0,040	-,170*	-,366**
GLCM	Energy	0,050	-0,083	0,105	-0,052	-,192*	-0,042	-0,090	-,244**	-0,074	-0,095	-,213**	-0,119	-0,147	0,011	-0,053	-0,048	-0,028	-,223**	0,051	-0,135	-0,078	-0,158	0,101	0,031	-,178*	0,119	0,039	-0,081	0,109	-,164*	-0,007	-0,088	-,326**
	Contrast	-0,095	0,012	-0,103	0,069	,168*	-0,016	0,076	,186*	0,022	-0,027	0,159	0,040	0,133	0,034	-0,039	-0,043	0,006	0,068	,172*	0,129	0,085	0,064	0,056	0,065	0,002	0,025	0,034	0,042	-,214**	0,073	0,011	0,033	,180*
	Entropy	-0,063	0,068	-0,087	0,063	,190*	0,059	0,087	,233**	0,052	0,064	,219**	0,102	0,154	-0,008	0,030	0,014	0,028	,184*	0,059	0,135	0,111	0,144	-0,070	0,031	,162*	-0,115	-0,023	0,080	-0,134	,162*	0,004	0,116	,306**
	Homogeneity	0,071	-0,054	0,096	-0,065	-,188*	-0,040	-0,087	-,230**	-0,066	-0,054	-,215**	-0,090	-0,125	0,022	-0,008	-0,029	-0,065	-,164*	-0,053	-0,132	-0,094	-0,114	0,082	-0,011	-0,142	0,102	-0,006	-0,058	0,147	-,148*	0,016	-0,101	-,288**
	Correlation	0,007	0,028	0,022	-0,035	0,002	0,089	-0,020	0,073	-0,030	0,106	-0,010	0,047	0,072	0,085	0,007	-0,056	-0,014	0,106	-0,098	-0,006	0,143	0,106	0,025	-0,008	,157*	-,145*	-0,113	0,068	0,018	0,116	0,015	,202**	0,076
	Sum Average	-0,054	0,055	-0,076	0,042	,182*	0,064	0,084	,223**	0,088	0,128	,216**	0,110	0,143	-0,011	0,036	0,023	0,011	,232**	-0,011	0,121	0,151	0,160	-0,059	0,007	,198**	-0,134	-0,031	0,066	-0,100	,163*	0,013	0,132	,349**
	Variance	-0,078	0,044	-0,065	0,038	,192*	0,053	0,059	,199*	-0,016	0,004	,192*	0,069	0,152	0,029	-0,017	-0,071	-0,008	0,131	0,125	0,127	0,141	,168*	0,048	0,056	0,101	-0,067	-0,028	0,082	-0,125	0,127	0,027	0,137	,255*
	Dissimilarity	-0,082	0,028	-0,098	0,072	,174*	0,015	0,079	,199*	0,042	0,000	,189*	0,059	0,125	0,002	-0,024	-0,008	0,028	0,111	0,154	0,132	0,102	0,086	0,000	0,057	0,062	-0,032	0,023	0,044	-,187*	0,102	0,000	0,069	,231**
	Auto-Correlation	-0,056	0,050	-0,079	0,035	,186*	0,064	0,079	,223**	0,072	0,110	,215**	0,112	0,146	0,000	0,024	0,005	-0,003	,222**	0,010	0,124	0,153	,166*	-0,042	0,013	,180*	-0,121	-0,034	0,073	-0,111	,155*	0,015	0,137	,340**
GLRLM	Short Run Emphasis	-0,056	0,050	-0,089	0,062	,188*	0,049	0,087	,234**	0,078	0,064	,221**	0,087	0,139	-0,005	0,005	0,019	0,070	0,156	0,026	0,132	0,131	0,124	-0,042	0,038	,146*	-0,106	0,006	0,066	-0,150	,148*	-0,028	0,106	,305*
	Long Run Emphasis	0,063	-0,067	0,097	-0,066	-,174*	-0,012	-0,096	-,226**	-0,082	-0,079	-,205*	-0,106	-0,130	0,064	-0,007	-0,057	-0,093	-,198*	0,038	-0,132	-0,054	-0,116	0,104	0,061	-,164*	0,122	0,020	-0,053	0,102	-0,126	0,020	-0,065	-,290**
	Gray-Level Nonuniformity	0,044	-0,065	0,050	-0,028	-,192*	-0,081	-0,079	-,227**	-0,034	-0,065	-,222**	-0,112	-0,160	-0,026	-0,036	0,012	0,023	-,203*	-0,021	-0,124	-,167*	-,180*	0,017	-0,041	-,187*	0,124	0,053	-0,087	0,111	-,165*	-0,009	-0,137	-,326**
	Run Length Nonuniformity	-0,055	0,046	-0,090	0,062	,188*	0,049	0,084	,233**	0,078	0,062	,219**	0,085	0,137	-0,001	0,004	0,018	0,068	0,153	0,031	0,132	0,132	0,122	-0,037	0,039	0,142	-0,104	0,008	0,063	-0,152	,145*	-0,026	0,107	,302**
	Run Percentage	-0,063	0,067	-0,103	0,059	,188*	0,034	0,093	,237**	0,090	0,078	,214**	0,105	0,136	-0,034	0,021	0,055	0,087	,192*	-0,020	0,132	0,078	0,120	-0,099	-0,007	,160*	-0,121	-0,020	0,059	-0,120	,145*	-0,018	0,081	,297**
	Low Gray-Level Run Emphasis	0,031	-0,031	0,038	-0,072	-0,124	-0,062	-0,118	-,206*	-0,122	-0,113	-,184*	-0,100	-0,117	0,087	-0,012	-0,094	-0,039	-,233**	0,053	-0,124	-0,117	-0,074	0,084	0,049	-,227**	,153*	0,014	-0,006	0,051	-0,127	0,011	-0,079	-,285**
	High Gray-Level Run Emphasis	-0,051	0,054	-0,080	0,039	,186*	0,058	0,082	,226**	0,060	0,102	,213**	0,106	0,150	0,015	0,022	-0,011	-0,006	,209*	0,021	0,127	0,157	,164*	-0,014	0,011	,165*	-0,110	-0,028	0,076	-0,116	,145*	0,018	0,132	,334**
	Short Run Low Gray-Level	0,037	-0,019	0,050	-0,058	-0,128	-0,057	-0,101	-,200*	-0,118	-0,118	-,173*	-0,098	-0,102	0,070	-0,016	-0,092	-0,034	-,239**	0,051	-0,124	-0,117	-0,080	0,068	0,054	-,219**	,147*	0,017	-0,014	0,064	-0,124	0,005	-0,079	-,282**
	Short Run High Gray-Level	-0,052	0,054	-0,084	0,039	,188*	0,056	0,082	,227**	0,060	0,100	,214**	0,105	0,150	0,019	0,022	-0,014	-0,006	,206*	0,030	0,127	0,156	,162*	-0,014	0,015	,163*	-0,107	-0,028	0,076	-0,122	,147*	0,020	0,131	,332**
	Long Run Low Gray-Level	0,043	-0,023	0,023	-0,089	-0,100	-0,023	-0,141	-,176*	-0,124	-0,061	-,194*	-0,085	-0,139	0,119	0,012	-0,124	-0,107	-,204*	0,049	-0,068	-0,067	-0,058	0,104	0,056	-,217**	,152*	0,006	0,008	0,028	-,138*	0,017	-0,071	-,239**
	Long Run High Gray-Level	-0,040	0,060	-0,072	0,041	,184*	0,062	0,084	,227**	0,068	0,106	,203*	0,106	0,150	0,005	0,025	-0,010	-0,008	,224**	0,008	0,124	0,160	,168*	-0,037	0,010	,172*	-0,111	-0,031	0,064	-0,096	,152*	0,022	0,126	,334**
	Gray-Level Variance	-0,063	0,003	-0,060	0,043	0,130	0,031	0,110	0,139	0,102	0,138	,177*	0,081	0,088	-0,070	-0,014	0,054	0,045	,219**	-0,034	0,042	0,084	0,082	-0,093	-0,075	,169*	-0,110	-0,056	0,027	-0,043	,150*	-0,006	0,060	,294**
	Run-Length Variance	-0,067	-0,005	0,009	0,041	-0,082	-0,063	0,059	-0,051	0,056	0,042	-0,025	0,032	-0,033	-0,125	-0,043	0,125	0,121	0,051	-0,043	-0,068	-0,131	-0,058	-0,132	-0,098	0,048	-0,047	-0,045	-0,046	0,104	0,049	-0,067	-0,085	-0,012
GLSZM	Small Zone Emphasis	-0,016	0,002	-0,114	0,036	,184*	-0,026	0,068	,190*	-0,012	-0,012	,169*	0,035	0,110	0,113	-0,019	-0,094	0,011	0,057	0,110	0,124	0,102	0,088	0,076	0,036	0,017	0,012	0,053	0,046	-,214**	0,054	-0,021	0,041	,194*
	Large Zone Emphasis	0,063	-0,072	0,096	-0,063	-,168*	-0,021	-0,093	-,223**	-0,102	-0,084	-,194*	-0,099	-0,133	0,077	0,005	-0,060	-0,090	-,182*	0,026	-0,129	-0,059	-0,094	0,118	0,059	-,152*	0,107	0,037	-0,053	0,086	-0,119	0,013	-0,045	-,283**
	Gray-Level Nonuniformity	0,051	-0,066	0,050	-0,032	-,192*	-0,073	-0,079	-,226**	-0,024	-0,049	-,221**	-0,102	-,170*	-0,027	-0,025	0,026	0,031	-,186*	-0,059	-0,121	-,165*	-,182*	0,003	-0,049	-,173*	0,110	0,045	-0,089	0,118	-,159*	-0,010	-0,147	-,310**
	Zone-Size Nonuniformity	-0,016	0,000	-0,114	0,036	,184*	-0,026	0,068	,189*	-0,012	-0,012	,168*	0,032	0,109	0,112	-0,020	-0,094	0,011	0,058	0,112	0,124	0,102	0,088	0,076	0,036	0,015	0,014	0,053	0,046	-,214**	0,053	-0,019	0,041	,193*
	Zone Percentage	-0,069	0,039	-0,089	0,063	,188*	0,040	0,090	,229**	0,062	0,070	,218**	0,087	0,130	-0,015	-0,001	0,015	0,070	,166*	0,033	0,132	0,104	0,114	-0,068	0,016	0,144	-0,108	0,000	0,060	-0,151	0,136	-0,025	0,102	,290**
	Low Gray-Level Zone Emphasis	0,024	-0,030	0,067	-0,052	-0,146	-0,060	-0,099	-,207*	-0,122	-0,129	-,189*	-0,113	-0,105	0,044	-0,029	-0,083	-0,020	-,257**	0,044	-0,124	-0,139	-0,098	0,065	0,033	-,221**	,146*	0,023	-0,028	0,074	-0,136	-0,003	-0,090	-,301**
	High Gray-Level Zone Emphasis	-0,059	0,054	-0,079	0,039	,188*	0,055	0,082	,226**	0,058	0,096	,214**	0,105	0,150	0,015	0,023	-0,013	-0,011	,205*	0,028	0,127	0,160	,164*	-0,008	0,010	,164*	-0,109	-0,031	0,077	-0,115	,145*	0,020	0,134	,332**
	Small Zone Low Gray-Level Zo	0,038	-0,031	0,070	-0,046	-0,148	-0,056	-0,087	-,201*	-0,124	-0,134	-,185*	-0,120	-0,097	0,046	-0,025	-0,074	-0,008	-,258**	0,043	-0,124	-0,140	-0,104	0,073	0,038	-,221**	,147*	0,028	-0,036	0,067	-0,136	-0,011	-0,084	-,307**
	Small Zone High Gray-Level Z	-0,060	0,050	-0,082	0,041	,188*	0,054	0,082	,227**	0,054	0,084	,214**	0,097	0,153	0,018	0,018	-0,023	-0,011	,196*	0,051	0,127	0,154	0,158	-0,006	0,015	,153*	-0,100	-0,023	0,076	-0,129	,141*	0,017	0,133	,323**
	Large Zone Low Gray-Level Zo	0,047	-0,019	0,028	-0,100	-0,094	-0,019	-0,135	-,170*	-0,120	-0,070	-,173*	-0,078	-0,149	0,125	0,018	-0,125	-0,132	-,173*	0,025	-0,076	-0,046	-0,044	0,118	0,034	-,192**	0,139	0,023	0,001	0,027	-,138*	0,014	-0,047	-,213**
	Large Zone High Gray-Level Z	,183*	,164*	-0,067	-0,004	0,124	0,025	0,020	0,123	0,024	0,010	0,061	0,125	0,099	0,033	0,056	-0,020	-0,104	0,124	-,162*	0,068	0,116	0,096	0,099	-0,038	0,113	-0,032	-0,011	-0,014	-0,010	0,093	-0,027	0,035	,162*
	Grey-Level Variance	-0,050	0,036	-0,085	0,060	0,144	0,025	0,099	,200*	0,114	0,127	,184*	0,075	0,125	-0,085	-0,016	0,072	0,042	,180*	-0,020	0,121	0,075	0,082	-0,115	-0,061	,147*	-0,090	-0,045	0,028	-0,081	0,131	-0,005	0,044	,288**
	Zone-Size Variance	0,096	0,099	-0,043	0,058	-0,014	-0,064	0,070	0,060	0,088	0,074	0,035	0,032	0,046	-0,125	-0,060	0,088	0,090	-0,009	-0,092	0,056	-0,099	-0,040	-0,118	-0,111	-0,007	0,008	-0,011	-0,033	-0,008	0,012	-0,043	-0,106	0,068
NGTDM	Coarseness	-0,119	0,081	-0,075	-0,026	0,058	0,122	0,113	0,010	0,034	0,101	0,136	0,105	0,110	-0,052	0,036	,195*	-0,039	,163*	0,067	-0,079	0,025	,172*	-0,124	0,059	0,141	-,147*	-0,104	0,051	-0,023	0,016	0,035	0,123	,202*
	Contrast	-0,067	-0,001	-0,083	0,035	,178*	0,020	0,034	0,160	-0,026	-0,058	,188*	0,043	0,132	0,068	-0,026	-0,064	0,020	0,046	0,154	0,121	0,115	0,128	0,076	0,085	0,032	-0,010	-0,008	0,060	-,187*	0,113	0,031	0,083	,219**
	Busyness	0,076	-0,070	0,092	-0,043	-,170*	-0,083	-0,113	-,171*	-0,088	-0,144	-,216**	-0,122	-0,150	0,017	-0,047	-0,094	-0,003	-,236**	-0,003	-0,042	-0,115	-,170*	0,096	-0,025	-,196**	,151*	0,045	-0,062	0,100	-0,132	0,001	-0,132	-,347**
	Complexity	-0,089	0,048	-0,067	0,085	,186*	0,025	0,087	,214**	0,020	0,022	,197*	0,058	,167*	-0,002	-0,024	-0,033	0,051	0,120	0,125	0,129	0,118	0,130	0,014	0,052	0,090	-0,053	0,020	0,063	-0,156	0,110	0,019	0,109	,257**
	Strength	-0,098	0,069	-0,106	0,046	,162*	0,033	0,115	0,107	-0,042	0,060	0,157	0,053	0,154	0,008	-0,012	-0,003	-0,003	0,100	,169*	0,014	0,022	0,154	-0,053	0,067	0,002	-0,004	-0,020	0,078	-0,137	0,030	0,028	0,107	,212**

Abbreviations : DM: Diabetes Mellitus; COPD: Chronic Obstructive Pulmonary Disease; CCI: Charlson Comorbidity Index; #: number; PC: primary care; ED: emergency department; IHF: Intensity Histogram Features; GLCM: Gray-Level Co-occurrence Matrix; GLRLM: Gray-Level run-Length Matrix; GLSZM: Gray-Level Size Zone Matrix; NGTDM: Neighborhood Gray-Tone Difference Matrix.

Tau B of Kendal used for the statistical analysis.

* The correlation is significant at the 0.05 level (bilateral).

** The correlation is significant at the 0.01 level (bilateral).